MATHEMATICAL MODELLING OF GROWTH AND METABOLISM IN ANAEROBIC MICROBES

A thesis presented in partial fulfilment of the requirements for the degree of

Doctor of Philosophy

in

Mathematics

at Massey University, Palmerston North,

New Zealand.

Brandon Connor Jones

2025

Contents

1 Introduction **3**

1.1 Modelling Microbes 3

1.2 This Work - an Outline 4

2 Single Substrate Models **7**

2.1 Introduction to Microbes 7

2.2 Introduction to Modelling Microbial Growth 10

2.3 Existing Single Substrate Models 11

2.3.1 Monod (Empirical) 14

2.3.2 Jin and Bethke (Empirical and Thermodynamics Hybrid) 19

2.3.3 Modified Haldane (Enzyme Kinetics) 20

2.3.4 DLQB (Statistical Mechanics) 27

2.3.5 Rates Comparisons 29

3 A Model that Optimises ΔG_{ATP} **36**

3.1 ΔG_{ATP} in Current Models 37

3.2 Biology of ΔG_{ATP} 38

3.3 The Data 40

3.4 An Optimised Rate 46

3.4.1 q_{ATP} 50

3.4.2 Continuity of the Derivative of q_{ATP} 52

3.4.3 A Choice of r 54

3.5 Results . . . 56

4 Validation **62**

4.1 Batch Culture with Negligible Thermodynamic Inhibition . . . 63

4.2 Batch Culture with Thermodynamic Inhibition . . . 70

4.3 Continuous Culture with Thermodynamic Inhibition . . . 75

5 Multiple Rate-Limiting Substrates **99**

5.1 Introduction and Empirical Rates . . . 99

5.2 Enzyme Kinetic Models . . . 105

5.3 Black Box Mechanism . . . 106

5.4 Ordered Ternary Mechanism . . . 108

5.4.1 Using an Expansion . . . 112

5.5 Random Ternary Mechanism . . . 115

5.5.1 A Simple Quasi-Steady-State Assumption . . . 117

5.5.2 A Michaelis-Menten-Type Approach . . . 118

5.5.3 A Partially Irreversible Consideration . . . 123

5.5.4 Variations to the Random Ternary Mechanism . . . 123

5.6 Confluence Mechanism . . . 127

5.6.1 A Simple Quasi-Steady-State Assumption . . . 131

5.6.2 A Biological Assumption . . . 132

5.6.3 A Strong Quasi-Steady-State Assumption . . . 134

5.7 Statistical Mechanics . . . 139

5.8 Summary . . . 141

6 Conclusions **143**

6.1 Introduction . . . 143

6.2 Chapter 2 . . . 143

6.3 Chapter 3 . . . 145

6.4 Chapter 4 . . . 148

6.5 Chapter 5 149
6.6 Future Work 151

A Limits of ΔG_{ATP} **153**

B ATP Yields **155**

B.1 ATP Yields used for the Dataset in Chapter 3 155
B.2 Argument for $\eta = 3.3\,\mathrm{mol_{ATP}}\,\mathrm{mol}^{-1}_{\mathrm{substrate}}$ for *Geobacter sulfurreducens* 160
B.3 ATP Yields for the Reactions in Chapter 4 161

C Additions for Chapter 4 **162**

C.1 Malonate and Crotonate Data 162
C.2 Initial Conditions for Malonate 162
C.3 ΔH_f^o and S_f^o for Crotonate 164

D Dataset Conditions and Assumptions **165**

D.1 Microbes in the Dataset 165
D.2 Conditions and Assumptions 170

Bibliography **193**

List of Tables

2.1 Typical rate values for different time scales 24

3.1 L2 norms for each choice of ΔG_{ATP} for the S_{min} data and the K_{app} data. 46
3.2 Parameter values for methane reaction 57

4.1 Standard enthalpies of formation and entropies of formation for substances in the malonate reaction. 66
4.2 Standard Gibbs free energy of formation and enthalpy of formation values for substances in crotonate fermentation. 73
4.3 Standard enthalpy of formation and entropy of formation values for substances in glutamate fermentation. 77

C.1 Data for the dataset shown in Figure 1(a) of Janssen [73]. 162
C.2 Data for the dataset shown in Figure 1(b) of Janssen [73]. 163
C.3 Data for the dataset shown in Figure 1(c) of Janssen [73]. 163
C.4 Data for the dataset shown in Figure 1 of Wallrabenstein and Schink [177]. . . . 164
C.5 Data used to estimate standard enthalpy and entropy of formation for crotonate 164

List of Figures

2.1 Simplified scheme of microbial metabolism. 9

2.2 Plot of idealised experimental data with non-dimensionalised units. 14

2.3 Shapes of three empirical rates. 16

2.4 Comparison of the shape of the Monod, Modified Haldane, and DLQB rates showing high substrate concentration behaviour. 29

2.5 Comparison of the shape of the Monod, Modified Haldane, and DLQB rates showing low substrate concentration behaviour. 30

3.1 Plot showing the difference in threshold concentration at different ΔG_{ATP} values. 40

3.2 Plot of the $S_{\min}$ data comparing $1/Q$ for each experiment to $\exp\left(\left(\Delta G_T^o + \eta \Delta G_{\mathrm{ATP}}\right)/RT\right)$ with three different values of ΔG_{ATP}. 42

3.3 Plot of the K_{app} data comparing $1/Q$ for each experiment to $\exp\left(\left(\Delta G_T^o + \eta \Delta G_{\mathrm{ATP}}\right)/RT\right)$ with three different values of ΔG_{ATP}. 43

3.4 Rescaled version of Figure 3.3, ignoring the large outlier. 44

3.5 Plot of the K_{app} data showing the effect of using $\eta = 3.3\,\mathrm{mol_{ATP}\,mol^{-1}_{substrate}}$ for the *Geobacter sulfurreducens* reaction. 45

3.6 A typical optimal curve. 52

3.7 The value of ΔG_{ATP} that maximises $r_L \cdot q_{\max} \frac{S-\zeta\nu}{K_{\mathrm{Lynch}}+S+\zeta\nu}$ 56

3.8 Plot of the $S_{\min}$ data comparing the measured and calculated value of S for each experiment. 58

3.9 Plot of the K_{app} data comparing the measured and calculated value of S for each experiment. 59

3.10 Combination of both Figures 3.8 and 3.9. 60

4.1 Plot of strain 16mal1 growing with malonate. 63
4.2 Plot of strain NHI868 growing with malonate. 64
4.3 Plot of strain NCTC7427 growing with malonate. 65
4.4 Plot of ΔG_T and θ at each measurement time point using data for strain 16mal1 from Figure 4.1 and Table C.1. 66
4.5 Plot of ΔG_T and θ at each measurement time point using data for strain NHI868 from Figure 4.2 and Table C.2. 67
4.6 Plot of ΔG_T and θ at each measurement time point using data for strain NCTC7427 from Figure 4.3 and Table C.3. 68
4.7 Plot of concentrations during simulation of malonate fermentation. 69
4.8 Plot of θ and optimised ΔG_{ATP} during simulation of malonate fermentation. . . 70
4.9 Plot of growth of strain DM-3 on crotonate with substrate and product concentrations over time. 71
4.10 Plot of ΔG_T and θ at each measurement time point using data from Figure 4.9 and Table C.4. 72
4.11 Plot of concentrations during simulation of crotonate fermentation. 74
4.12 Plot of θ and optimised ΔG_{ATP} during simulation of crotonate fermentation. . . 75
4.13 Plot of concentrations during simulation of strain DKglu16 fermenting glutamate at $\alpha = 0.1\,\mathrm{day}^{-1}$. 80
4.14 Plot of θ and optimised ΔG_{ATP} during simulation of strain DKglu16 fermenting glutamate at $\alpha = 0.1\,\mathrm{day}^{-1}$. 80
4.15 Plot of concentrations during simulation of strain DKglu26 fermenting glutamate at $\alpha = 0.1\,\mathrm{day}^{-1}$. 82
4.16 Plot of θ and optimised ΔG_{ATP} during simulation of strain DKglu26 fermenting glutamate at $\alpha = 0.1\,\mathrm{day}^{-1}$. 82
4.17 Plot of the steady state glutamate and biomass concentrations at different values of α for strains DKglu16 and DKglu26. 84

4.18 Plot of the steady state glutamate and biomass concentrations at different values of α for strains DKglu16 and DKglu26 with maintenance included. 85
4.19 Plot of the steady state glutamate and biomass concentrations at different values of α, between 0.6 and 0.8, for strains DKglu16 and DKglu26 with maintenance included. 85
4.20 Plot of substrate, product, and cell concentrations during simulation of competition with $\alpha = 0.1\,\mathrm{day}^{-1}$. 87
4.21 Plot of optimised ΔG_{ATP} for each microbe during simulation of competition with $\alpha = 0.1\,\mathrm{day}^{-1}$. 87
4.22 Plot of Figures 4.20 and 4.21 extended to show longer time span. 88
4.23 Plot of the steady-state glutamate and biomass concentrations at different values of α for DKglu16 and DKglu26 in competition with each other. 89
4.24 Plot of the steady-state glutamate and biomass concentrations at different values of α for DKglu16 and DKglu26 in competition with each other and with maintenance included. 90
4.25 Plot of the steady-state glutamate and biomass concentrations at different values of α for DKglu16 and DKglu26 in competition with each other, with maintenance included, and considering the relative sizes of the two microbes. 91

5.1 Four simplified schemes of microbial metabolism. 101
5.2 Simplified scheme for microbial metabolism where both of the two substrates A and B are required at a fixed stoichiometry to produce ATP. 102

Abstract

The growth rates of microbes can be thermodynamically limited by unfavourable ratios of energy substrates and end products. This thesis explored and expanded mathematical models that apply to a broad range of anaerobic microbes with different metabolisms, especially at low substrate to product ratios.

The rates considered here fall into four categories based on how they are derived. *Prima facie* these rates are unrelated; however, for large concentrations of substrate they are in agreement. A new term based on the properties of the ATP synthase enzyme was added to a model derived from the Briggs-Haldane rate to allow the microbe to vary the energy required to produce ATP (ΔG_{ATP}) at low substrate concentrations. Experimental data were used to show that different values of ΔG_{ATP} were better suited for predicting K_{app} and S_{min}, substrate concentration values corresponding to half-maximal growth rate and growth shutoff, respectively. This term allowed growth to continue in challenging thermodynamic conditions by optimising ΔG_{ATP} to maximise the growth rate. When ΔG_{ATP} was considered variable between biologically relevant limits, the model predicted the measured K_{app} and S_{min} values from the dataset.

Results from the model were compared with experimental data reported at multiple times as growth occurs. The results agreed qualitatively for batch cultures with and without thermodynamic inhibition. The model produced results that were consistent with experimental data for a continuous culture for two strains of microbe. In addition, it was adapted for modelling direct competition between the two strains which compete for the same energy substrate. Modelling this competition identified conditions for stable coexistence, a result that has yet to be shown analytically.

Different approaches for modelling metabolisms where multiple substrates are simultaneously required to produce ATP were explored, with a focus on four variations of an analogy between microbes and enzymes. This analysis identified several rates that may have applications in different situations, and also identified a derivation for a widely-used empirical rate as a special case. An extension of a rate based on statistical mechanics to multiple substrates also showed promise.

Acknowledgements

Firstly, I thank my supervisors: Tammy Lynch, Bruce van Brunt, and Peter Janssen. Your insights into mathematical modelling, microbes, and a great deal of other topics helped me to understand this field. Our regular discussions enabled me to clearly communicate about it. Your encouragement made sure that I stayed on the right track and finished the work.

I thank Massey University for the Doctoral Scholarship that I benefitted from during my study. I also thank the Mathematics Department at Massey University for the role that each of the staff played in growing my knowledge of mathematics and my passion for the subject. I am grateful to have learned from you and for the employment that I benefitted from during my study.

Finally, I thank my wife and the rest of my family and friends for your love, support, and encouragement. I would not be where I am without you.

Nomenclature

A	Concentration of rate-limiting substrate
B	Concentration of rate-limiting substrate
C_i	Concentration of enzyme complex with substrate i
E	Concentration of enzyme
E_T	Total concentration of enzyme in any form
K_{app}	Substrate concentration at half-maximal growth rate
K_{eq}	Equilibrium constant
K_H	Constant in Modified Haldane rate
K_M	Monod constant
k_i	Reaction rate for enzyme reaction
m	Cellular maintenance requirement
P	Concentration of product
Q	Reaction quotient
q	Rate of substrate metabolism
q_D	Desmond-Le Quéméner and Bouchez rate
q_H	Modified Haldane rate
q_J	Jin and Bethke rate
q_M	Monod rate
q_{max}	Maximum rate of substrate metabolism
R	Ideal gas constant
r	Penalty function term in Optimised rate
S	Concentration of rate-limiting substrate
S_{min}	Threshold substrate concentration
S^o	Standard entropy
T	Temperature
X	Concentration of the microbe
Y	Cell yield factor

α	Flow rate in continuous culture
γ	Quotient of product concentration and equilibrium constant
ΔG_{ATP}	Energy required to produce ATP
ΔG_T	Gibbs free energy change for a reaction
ΔG_T^o	Gibbs free energy change for a reaction at standard conditions
ΔH_f^o	Standard enthalpy of formation
η	Yield of ATP per substrate transformed
θ	Thermodynamic inhibition factor in Modified Haldane rate
Λ	Desmond-Le Quéméner and Bouchez rate constant

Chapter 1

Introduction

1.1 Modelling Microbes

Bacteria and *Archaea* are two of the three major domains of life, the third being *Eukarya*, containing animals, plants, fungi, and protozoa [140]. Bacteria and archaea, which we will collectively call **microbes**, are characterised by generally being single-celled organisms with cell dimensions of the order of 1-2 μm. There is an enormous species diversity in both of these microbial groups [104], and understanding how they compete, cooperate, and otherwise interact in the often highly species-diverse ecosystems they inhabit is challenging [146]. Models based on the behaviour of microbial cells can be used to describe and explore the growth (and decay) of populations of a microbial species, along with species interactions. In this work, we focus on models with substrate concentration limiting the microbial growth rate. We will use the term **substrate** to refer to a compound(s) that a microbe takes up from its environment and transforms to harness some of the Gibbs free energy change from that transformation for its maintenance and growth.

Mathematical models that capture the population dynamics of microbes, species interactions, and the impact of substrate and product concentrations are motivated by practical interests in addition to academic study. Microbe population dynamics play a key role in many problems including, for example: methane emissions from methanogens in environments like the rumen; fermentation processes to produce high value chemicals; anaerobic water purification

for wastewater treatment and biogas production; and understanding the human gastrointestinal tract. Experiments to understand microbes in their natural settings can be time-consuming, difficult, and expensive. From a purely practical standpoint, a model might provide enough information to avoid the need to perform the experiment, or to identify how the experiment should be focused in order to maximise the utility of the results while minimising the time, difficulty, and cost. More "academic interests" include, for example, the effects of thermodynamic inhibition on microbial growth. The concentration of products, as well as reactants, contribute to the environment that a microbe is in and can influence how quickly reactions take place, inhibiting the reaction rate when product concentration is high, even if reactant concentration is also high. Clearly, the practical and academic interests have a considerable overlap.

There are different approaches to modelling microbes. One approach is the agent-based modelling explored by Nagarajan *et al.* in their review [130]. Here, each member of a population is individually modelled interacting with their local environment. At the other extreme is the dynamical system approach such as that by Gonze *et al.* [56], where entire populations are considered together. The approach that we will take is between these two. We make two fundamental assumptions: there is a huge population of any single microbial species, with individual cells at different stages of their growth cycle, so we can treat it as a continuum, and there is a uniformity to the environment resulting in homogeneity. Obviously the second assumption does not always hold, but these assumptions will allow us to consider what happens at the scale of a single cell without modelling every individual.

1.2 This Work - an Outline

The main goal of this work is to produce a mathematical model that is applicable to multiple microbial populations with a range of different metabolisms, to identify the limits of validity of the model using data found in the literature, and to identify avenues for further model development. The model should use parameters that have a predictable physical basis to allow demonstration of its usefulness for predicting outcomes.

In Chapter 2 we review existing mathematical models of microbial growth. We separate the

growth rates used in these models into four categories based on how they are derived. These categories are:

1. Empirical;
2. Hybrid of empirical with thermodynamic considerations;
3. Enzyme kinetics analogues; and
4. Statistical mechanics.

The derivation of these rates is briefly discussed and then the rates are compared and some new connections between them are described .

The existing rates have strengths and the merit of simplicity, but more is known about the biology of microbes that could be incorporated into the model. In Chapter 3 we seek a model that balances mathematical tractability with key biological ideas. We thus turn our attention to the development of a model that incorporates additional biological information. We then compare the new model against some existing ones. To do this, we surveyed literature and collated a dataset of 107 experiments. This dataset is then used to test the relevance of including the additional biologically-motivated terms. We use the dataset to motivate the inclusion of the new term, and then explore some properties that this term should have, which then will aid us in choosing the most suitable form for that term. We also use the dataset to assess how well our new rate can predict the substrate concentration for each experiment.

A feature of the above dataset is that, in each experiment, data were recorded for at least one of two scenarios, *viz.*, when the substrate concentration is at a threshold value (i.e., the concentration below which the microbe can no longer grow) or when the concentration results in half of the maximal growth rate. In Chapter 4 we turn our attention to examples that illustrate the efficacy of the new model for microbes using different metabolic reactions where experimental data are available. We start with a batch culture that has negligible thermodynamic inhibition and compare the experimental results to the results of our simulations. We next compare experimental data and results from our model for a batch culture with thermodynamic inhibition. Finally, we consider a continuous culture example with thermodynamic inhibition. This last

example is a more realistic experimental analogy to nature and applications, so it is an important benchmark for the model. This example includes two strains of microbe utilising different fermentation pathways which allows us to explore competition and coexistence, in addition to comparing the results of our simulation to the reported experimental results.

The models considered in Chapters 2, 3, and 4 involved microbial growth limited by a single substrate. Growth rates limited by multiple substrates are also of interest and a target of any model would be its adaptability to microbial growth with multiple limiting substrates. In Chapter 5 we look at different approaches for modelling this situation, with a focus on the case where the multiple substrates are simultaneously required to produce ATP. Any extensions to multiple limiting substrate models require a deeper knowledge of how the microbe utilises the substrates. For example, does it need substrate A before substrate B to produce ATP? Can the microbe "harvest" substrate A and store it whilst trying to acquire substrate B? It turns out that even for two substrates there are many possible extensions. We begin this Chapter with a brief exploration of empirical rates that have been used or suggested for multiple rate-limiting substrates. We then consider a variety of possible extensions to enzyme kinetic models, exploiting the analogy between microbes and enzymes. Finally, we consider how a rate derived from statistical mechanics could be extended to multiple rate-limiting substrates and we discuss some links between the different rates and mechanisms. A summary of results and suggestions for future work is provided in Chapter 6.

Chapter 2

Single Substrate Models

2.1 Introduction to Microbes

Bacteria and *Archaea* are two of the three major domains of life, the third being *Eukarya*, containing animals, plants, fungi, and protozoa [140]. Bacteria and archaea, which we will collectively call microbes, are characterised by generally being single-celled organisms with cell dimensions of the order of 1-2 μm. There is an enormous species diversity in both of these microbial groups [104], and understanding how they compete, cooperate, and otherwise interact in the often highly species-diverse ecosystems they inhabit is challenging [146]. Models describing the behaviour of microbial cells can be used to describe and explore the growth of populations of a microbial species, and so help us to better understand communities that consist of multiple co-existing populations.

We will use the term "substrate" to refer to a compound that a microbe takes up from its environment and transforms to harness some of the Gibbs free energy change from that transformation for its maintenance and growth. Microbes usually take up substrates from their environment using transporter proteins in the cell envelope, although a few substrates can diffuse across the cell envelope. The substrate is transformed through a series of steps, catalysed by multiple enzymes [4], in a sequence that is called a metabolic pathway. The final products are then secreted or diffuse from the cell. There is an enormous diversity of metabolic pathways [83] and, since most microbes have not been studied ([104], [146]), the potential for novel metabolisms

is large.

Microbial growth proceeds from the transformation of substrate to product, with temporary capture in the form of ATP of some of the Gibbs free energy associated with the transformation, at a yield of ATP per substrate transformed (η) that is determined by the pathway and the total amount of Gibbs free energy available. That ATP is then broken down again and the energy released is used to do useful work in the cell. That work may be cell maintenance or the synthesis of new cell material. Although ATP is sometimes thought of as an energy-carrying molecule, in reality the utility for coupling ATP to drive metabolism comes from maintaining the ratio of ATP and its breakdown products (ADP and inorganic phosphates) away from chemical equilibrium. A simplified scheme of microbial metabolism is shown in Figure 2.1. The amount of ATP used for cellular maintenance functions (m) by a live cell can be assumed to be non-zero [174] and depends on the physical conditions of the cell's environment, which result in physiological stresses on the cell [60], as well as ATP requirements for normal cell homeostasis and regulation of its general metabolism. If the energy available for ATP synthesis exceeds that required for cell maintenance, that excess can be used to produce more cell material. The way that the cell uses ATP for growth depends on the substrate and other available nutrients and is described as a cell yield factor Y. This yield is often expressed as cell matter produced per unit of substrate, but here we express it as cell matter produced per ATP, remembering that the amount of ATP per substrate transformed is η. As new cell matter is produced, the cell increases in size (usually in length) until it divides into two daughter cells.

Product accumulation can reduce the rate of substrate transformation, and this effect is thought to be due to less favourable reaction thermodynamics. Examples include the activity of hydrogen-forming fermentative microbes being inhibited by hydrogen accumulation [152], acetate slowing the metabolism of acetate-forming bacteria [144], and methane inhibiting the activity of methane-forming methanogens [31].

If a microbe metabolises substrate to product so that the concentration of substrate decreases and the product concentrations increase, at some point the thermodynamics are no longer favourable, and metabolism halts. The substrate concentration when metabolism ceases

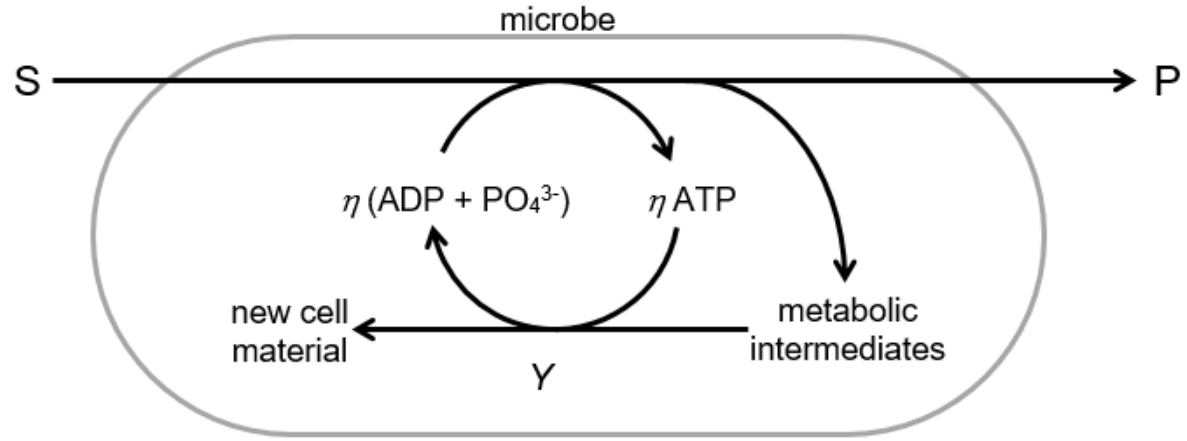

Figure 2.1: Simplified scheme of microbial metabolism. Substrate, S, is taken up from the external environment and transformed to product, P, through metabolic pathways. The microbe harnesses part of the Gibbs free energy change of that transformation by forming adenosine triphosphate (ATP) from adenosine diphosphate (ADP) and either free phosphate (PO_4^{3-}) in the cell or phosphate from phosphate-containing metabolic intermediates in its metabolic pathways. The ratio of ATP molecules formed per substrate molecule is η. That ATP is used for cellular maintenance (not shown) and to provide the energy for synthesis of new cell material from a subset of metabolic intermediates at a cell yield per ATP (Y). Other constituents of cell material can also be taken up from the external environment (not shown).

is termed a threshold, $S_{\min}$, and these have been experimentally demonstrated for different microbes and substrates, e.g., for ethanol [170], glutamate [132], acetate [122], and hydrogen [36]. Lynch *et al.* showed how different values of η can result in different $S_{\min}$ for microbes with otherwise identical substrates and products, and growing under identical conditions [108]. The differences in η result from differences in the metabolic pathways transforming substrates to products. This is because increasing η, while increasing ATP, decreases the magnitude of the net Gibbs free energy change associated with the transformation of substrate to product due to the energy required for ATP formation. However, even when working with the same strain of the same species, different authors report different $S_{\min}$ values. These are likely the result of using different experimental set-ups resulting in different concentrations of other components in the reaction beyond the substrate, so producing different thermodynamic effects. For example, $S_{\min}$ values for hydrogen of 1.1×10^{-8}, 2.3×10^{-8}, and 6.9×10^{-8} M have been reported for *Methanospirillum hungatei* strain JF-1 (cf. [36], [106], [155]). More examples are included in the dataset we used in Chapter 3.

2.2 Introduction to Modelling Microbial Growth

A wide range of mathematical models for microbial growth can be found in the literature. The basic form of many of these models is

$$\frac{dS}{dt} = -qX, \tag{2.1}$$

$$\frac{dX}{dt} = \phi qX, \tag{2.2}$$

where S is the concentration of the growth limiting substrate, X is the concentration of the microbe, ϕ is a factor that accounts for how quickly the microbe can grow compared to the substrate consumption, and q is the rate of substrate metabolism (the reaction rate). It should be noted that these models consider a single growth-rate limiting substrate only. Other substrates needed for growth, whether needed for ATP production or for cell synthesis, are assumed to be in plentiful supply and are not considered in the models. Multiple species models are of the form

$$\frac{dS}{dt} = -\sum_{i=1}^{n} q_i X_i, \tag{2.3}$$

$$\frac{dX_i}{dt} = \phi_i q_i X_i, \tag{2.4}$$

where X_i are the concentrations of the n different species of microbes and ϕ_i and q_i are the ϕ and q corresponding to their respective species. There are often other terms included in these models such as a passage rate through the system and the rate of substrate formation or introduction into the system, but it is the reaction rate q that is the main distinguishing feature of a given model. The reaction rate is an element of all models but there are many different forms, each with their own justification. In forming our model a primary consideration is that the rate used has a robust theoretical basis for the presence and position of each term. The parameters should have biological significance and be experimentally measureable. The model should: be generalisable to a number of applications; explicitly include thermodynamic inhibition; have a non-zero threshold substrate concentration; and be able to be extended to include multiple

rate-limiting substrates.

We first consider the case where there is a single rate-limiting substrate. That substrate is usually the energy yielding substrate for growth that is considered to drive ATP formation and is usually present in the environment at concentrations that limit the rate of metabolism. However, it is possible that other substrates, like electron acceptors, are also rate-limiting. Therefore, we will go on to explore ways to incorporate multiple rate-limiting substrates. The rates proposed for microbial growth fall into four categories based on how they were derived. These categories are:

1. Empirical;
2. Hybrid of empirical with thermodynamic considerations;
3. Enzyme kinetics analogues; and
4. Statistical mechanics.

Investigating these different approaches provides a broad understanding of how microbial growth has previously been modelled. To easily identify the rates, we have given each of them a name taken from one or two of the authors who were involved in modelling the rate, while noting that these rates have been widely used and other authors have also contributed.

2.3 Existing Single Substrate Models

The Monod model [125] captures all of the features of microbial growth described earlier, in a pair of parameters. In practice, the Monod model is fitted to experimental data, and the parameters $q_{\max}$ and K_M describe the curve that is fitted. The theoretical interpretation for the maximum growth rate, $q_{\max}$, is relatively simple to understand since we know it contains η and Y. The original Monod model used a parameter describing population growth, $\mu_{\max}$, which implicitly contains η, Y, the maximum rate of substrate transformation, $q_{\max}$, and also the cell maintenance component of metabolism, m. In contrast, K_M is a term that is fitted to the data but its biological significance is unclear ([91], [102]). The Monod model has been adapted to

include maintenance as an explicit term and other modifications have been made to include substrate thresholds, $S_{\min}$, and product inhibition [143].

A different approach is to model substrate transformation by the cell and then describe the growth of the cell based on an ATP or Gibbs free energy budget. This is the approach used by Lynch *et al.* [108] and Desmond-Le Quéméner and Bouchez [39] (among others, e.g., Kleerebezem and Van Loosdrecht [89]). The rate of substrate transformation to product is described using non-linear saturation kinetics with a maximum rate of substrate transformation $q_{\max}$ and the rate of ATP formation described using the ATP to substrate stoichiometric parameter η. The ATP is then partitioned into use for maintenance (at an ATP requirement per unit of time) and growth using the residual ATP after the maintenance requirement has been met. The yield parameter Y can be used to convert ATP to cell material and thereby the growth rate of the cell can be calculated [179]. In this case, the $q_{\max}$ and K terms contain neither the yield nor maintenance parameters. If thermodynamic control is also added to the model, then $q_{\max}$ and K do not depend on contributions from thresholds and product inhibition. Instead, thresholds and product inhibition emerge from this new model [108]. The K term reflects other features of microbial metabolism, including substrate encounter frequency and capture efficiencies, which are more easily comprehended. If we assume that substrate encounter frequency is similar for simple dissolved molecules and for cells of similar size [13], and that evolution has optimised capture efficiencies on the assumption that organisms with less-than-optimal capture efficiencies would be uncompetitive and go extinct, we may be able to generalise a value of K without needing to determine this parameter for every microbe, substrate, and set of environmental conditions. This general K value seems particularly applicable for anaerobes because the influence of the thermodynamic terms is greater than that of the K term. This will be elaborated on in a later chapter. Parameters such as the ATP yield per substrate (η) have a profound effect on the growth competitiveness of different species [108], and such models allow exploration of the effects of end products under thermodynamic limitation, differing Y, and increases in m such as when stresses are increased.

We first present the modelled growth rates for the four main categories of models together, to allow easy comparison of the equation forms and different parameters. We then elaborate on

these rates individually. In all the rates we use S as the concentration of the energy-yielding substrate and normalise $q_{\max}$, the maximum rate, to 1, which non-dimensionalises the rates for easier comparison.

1. The **Monod** rate is
$$q_M(S) = \frac{S}{K_M + S}, \tag{2.5}$$
where K_M is a positive constant that depends on the organism.

2. The **Jin and Bethke** rate is
$$q_J(S) = \frac{S}{K_J + S} F_T, \tag{2.6}$$
where K_J is a positive constant that depends on the organism and F_T is a thermodynamic potential factor that depends on the temperature and the thermodynamic driving force (which is determined by the prevailing concentrations of substrates and products).

3. The **Modified Haldane** rate is
$$q_H(S) = \begin{cases} \frac{S(1-\theta)}{K_H + S(1+\theta)} & \text{if} \quad \theta \leq 1 \\ 0 & \text{if} \quad \theta > 1, \end{cases} \tag{2.7}$$
where K_H is a positive constant that depends on the organism and θ is a thermodynamic inhibition factor that depends on the temperature and the prevailing concentrations of substrates and products.

4. The **Desmond-Le Quéméner and Bouchez** rate, hereinafter referred to as the **DLQB** rate, is
$$q_D(S) = e^{-\Lambda/S}, \tag{2.8}$$
where Λ is a positive constant that depends on the organism, the temperature, and the concentrations of substrates and products.

We now look at each of these rates in more detail and discuss the underlying models and their shortcomings before comparing the rates and possible extensions to multiple substrates.

2.3.1 Monod (Empirical)

Several growth rates based on fitting to experimental data have been proposed as models of microbial growth with one growth-limiting substrate. Figure 2.2 shows a plot of what some

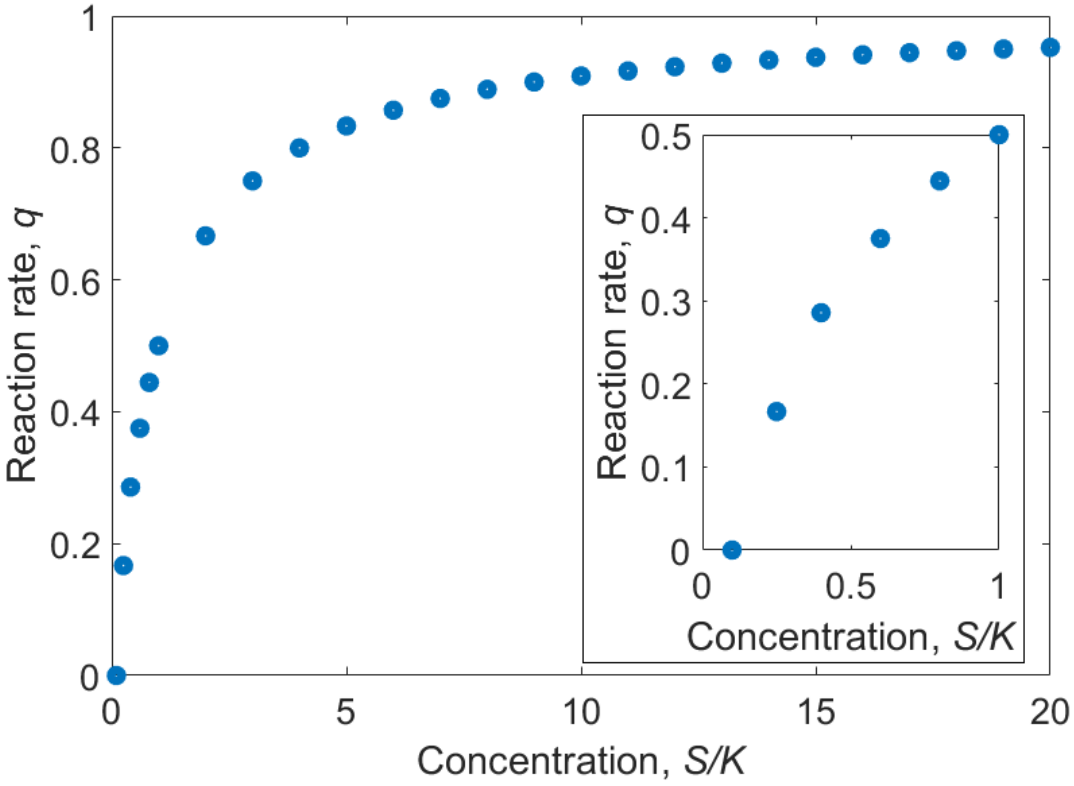

Figure 2.2: Plot of idealised experimental data with non-dimensionalised units.

idealised experimental measurements could look like. The values have been synthesised for this plot with the intention of showing the shape that has been seen by microbiologists since Monod. Here, the rate q is the non-dimensional rate, which is the quotient of the rate and the maximum rate, so its maximum value is 1. This shows an asymptotic approach to $q_{\max}$ after a steep initial increase at low concentration, with the inset showing that reaction rate is 0 at some non-zero concentration.

Bader [6] notes that the empirical rates are based, in general, on one of three types. In dimensionless form these are:

1. **Monod**

$$q = \frac{z}{1+z};$$

2. **Blackman**

$$q = \begin{cases} \frac{z}{2} & \text{if } z < 2 \\ 1 & \text{if } z \geq 2; \end{cases}$$

3. **Exponential**

$$q = 1 - 2^{-z}.$$

Here,

$$z = \frac{S}{K}.$$

The earliest rate is perhaps that given by Blackman [17] in 1905. Monod [124], [125] proposed his rate in 1942. The three rates are depicted in Figure 2.3. Again, the measurements shown on the graph are intended to be indicative of the shape seen by microbiologists but they are not actual data. The graph shows that the Monod rate approaches the asymptote $q = 1$ much slower than the other rates. Bader [6] refers to this speed at which the rates approach the asymptote as the saturation rate. Full saturation is when the addition of more substrate does not increase the rate. Of the three rates, only the Blackman rate reaches full saturation. He notes that:

> The Blackman and exponential models generally give a better fit to experimental data; primarily because they both saturate faster than the Monod model. Most data fall between the Blackman and exponential models...

Nonetheless, it is the Monod model that is most widely used. Bader further remarks

> The Monod model is also a simple and continuous algebraic relationship which lends itself readily to theoretical analysis. Of the three models, the Monod model generally represents the worst fit to experimental data.

Concerning the Blackman and exponential models, Bader explains

> Both of these models are not frequently used because of the [derivative] discontinuity

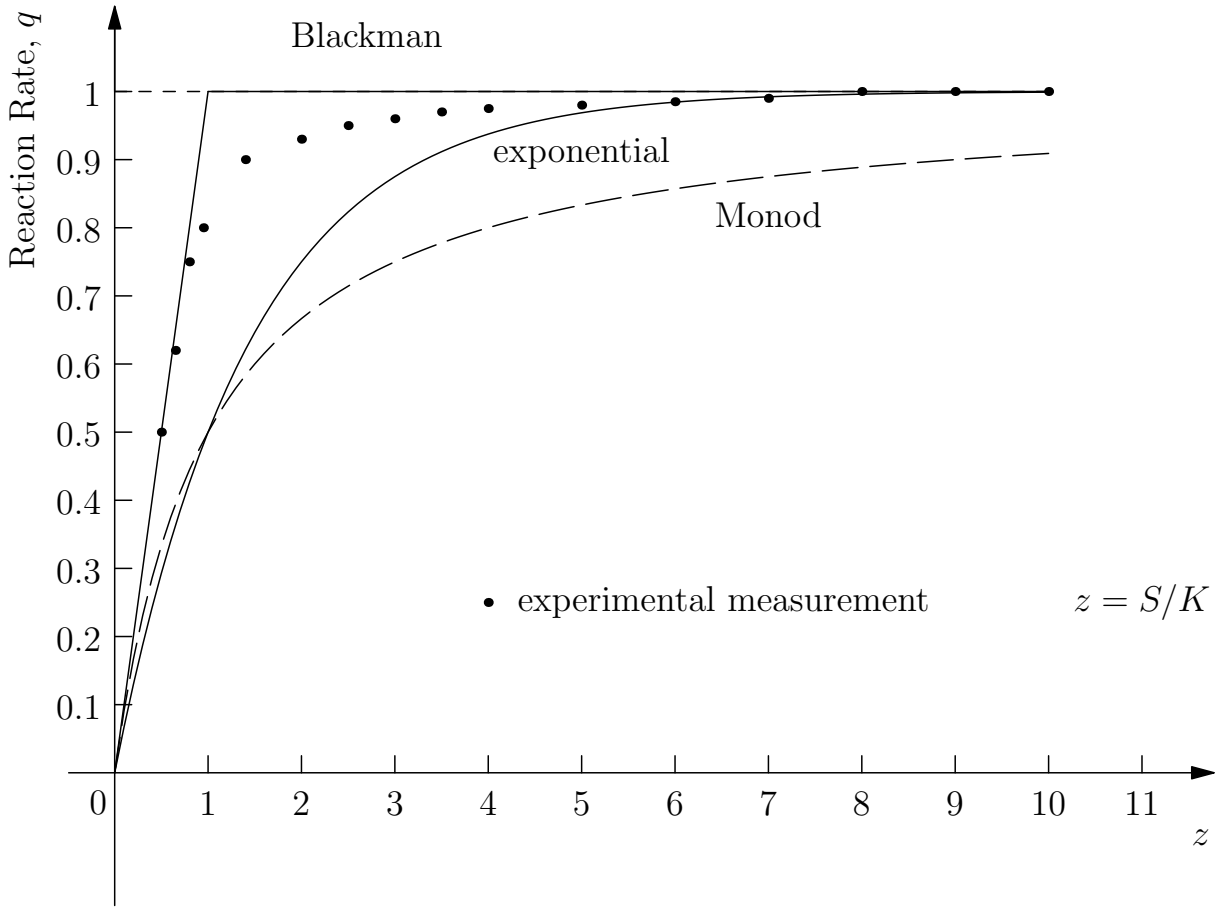

Figure 2.3: Shapes of three empirical rates.

in the Blackman model and the exponential term in the exponential model. These lead to mathematical complexities which one frequently would prefer to avoid.

Dabes *et al.* [37] discuss and compare the three rates in more detail. They also show that the rates are connected through a three parameter model and make a case for the Blackman model under certain circumstances.

The Monod model is certainly the most widely used model for microbial growth that is limited by a single substrate. This model has attracted the interest of many researchers who attempt to find a deeper understanding of the rate beyond simply a curve fit to data. Liu [102] gives an overview of various theoretical approaches to derive the Monod rate. Approaches include straightforward biological models [14], analogies with enzyme kinetics (discussed in the next section), thermodynamics [101], [103], mass transport [119] and statistical quantum mechanics

[171]. The variety of approaches leading to the Monod rate is partially a consequence of various rates from related applications that are functionally identical. In particular, the Monod rate is formally the same as the Michaelis-Menten rate from enzyme kinetics. In addition, this rate is also functionally the same as the Langmuir adsorption rate, which is derived in chemical kinetics, thermodynamics, and also in statistical mechanics (cf. [48], [185]). As noted by Bader [6], the Monod rate has the advantage of simplicity; moreover, it has the advantage that a number of related processes have rates with the same functional form, which allows one to use analogies to guide refinements and modifications to the basic model.

The rates discussed in this section are empirical in character, though this is somewhat hidden in the non-dimensional form in which they are presented. The empirical character emerges from the parameter K in the variable z. The constant K is the same for the three models. It must be determined from experimental data, and this prompts the ticklish question of what K means/measures. Here, we will refer to K as the *Monod constant*.

The Monod constant is elusive. Monod himself maintained that the rate was empirical in character, being determined by the substrate concentration that results in the growth rate being half of the maximum rate, and that the interpretation of K in terms of, say, the Michaelis-Menten constant is meaningless (cf. Liu [102]). In fact, measurements of the Monod constant seem to vary considerably with experimental conditions for (at least) *Escherichia coli*. Liu [102] remarks that

> So far, the large variation in values of the Monod constant has been extensively reported in the literature. The data available for *Escherichia coli* growing with glucose show that values of the Monod constant varied over more than three orders of magnitude for different *E. coli* strains [91]. There is no conclusive explanation of such a large variation in the Monod constant. In the past half century, the Monod equation has been regarded as a mathematical analog of the Michaelis–Menten equation for an enzyme-catalyzed reaction, but it is empirical. In this regard, Monod [125] noted that there is no relationship between the Monod constant and the Michaelis–Menten constant.

Certainly a weakness in the three rates discussed is the nature of K. Roughly speaking K seems

to depend strongly on the conditions under which the experiment was performed. This suggests that the "constant" K, in fact, depends on temperature, inhibition caused by other substrates and products, and other thermodynamic quantities. Liu [102] concludes:

> In my opinion, the Monod equation would only have numerical meaning for microbial growth, but might not have biological basis other than a regression-based mathematical formula. Obviously, on the journey to understanding the Monod equation, we are making progress, but we are not yet close to the truth even after more than a half-century of intensive research efforts.

Yet other shortcomings of the these rates are:

1. They all predict a non-zero growth rate for any positive concentration. We know that there is no growth below a certain concentration of substrate because not enough ATP can be formed if S is too small. This is known as the threshold, $S_{\min}$, and has been measured experimentally to be non-zero in many organisms (e.g., [36], [122], [132], [170]).

2. As noted by Bader [6] the rates (except Blackman) never reach full saturation. Using Monod or exponential rates, the rate will always increase towards the asymptote $q = 1$ as S is increased. In practice, there should be a concentration greater than which the organism cannot grow any faster, i.e., finite S saturation.

It is the first shortcoming that indicates the need for terms that reflect the thermodynamic restrictions on growth.

The Monod model is flexible and can be adapted to many scenarios: it forms a foundation upon which more sophisticated models can be built. It cannot be applied generically to all situations, but it can often be adjusted to meet with specific requirements. For example, Moser [127] proposed the rate

$$q = \frac{z^n}{1 + z^n}.$$

This rate was subsequently derived from statistical mechanics [171], where the parameter n corresponds to the number of binding sites. The rate also appears as the Hill-Langmuir equation [54].

Yet another variation is the rate proposed by Contois [35]

$$q = \frac{z}{1+z},$$

where

$$z = \frac{S}{K_C X},$$

X is the population density of the microbe, and K_C is a Monod-like constant. These variants have spawned a number of related rates adapted to particular conditions. The reader is referred to Gerber and Span [53] for a more comprehensive account.

The Monod rate is empirical, and this makes it difficult to generalise, to incorporate, for example, the effects of thermodynamics. Nonetheless, this rate is widely known and used: it is the "industry standard". The other rates that we discuss are related to the Monod rate, at least in functional dependence.

2.3.2 Jin and Bethke (Empirical and Thermodynamics Hybrid)

The Jin and Bethke rate [79] is regarded as a "hybrid" rate because it incorporates thermodynamic effects, but such terms are multiplicatively appended to empirical parts. Jin and Bethke first considered the dissolution and precipitation of a mineral and developed the form of the thermodynamic potential factor, F_T, to apply to microbial growth.

$$F_T = 1 - \exp\left(\frac{\Delta G + \Delta G_M}{\chi R T}\right), \tag{2.9}$$

where ΔG and ΔG_M are the Gibbs free energy changes of the substrate to product reaction and of the hydrolysis of ATP, respectively, χ is the average stoichiometric number which represents the number of times the rate-determining step occurs for each turnover of the full reaction, R is the ideal gas constant ($R = 0.00831446\,\mathrm{kJ\,K^{-1}\,mol^{-1}}$), and T is the temperature. They considered some empirical rate laws (0-order, 1^{st}-order, logistic, logarithmic, Monod) and chose

to base their model on the Monod rate. Recall that the Jin and Bethke rate is

$$q_J(S) = \frac{S}{K_J + S} F_T.$$

The rate they derived came from appending the thermodynamic potential factor "in a way that honors the requirement of thermodynamic consistency" [79]. No explanation is given for why the thermodynamic potential factor should be appended to what is otherwise the Monod rate and so we regard it as a 'hybrid' that uses an empirical relation (Monod) along with a factor derived from thermodynamic principles. The rate provides a better fit to data than the Monod rate and it has been implemented by van Lingen *et al.* [176] to model microbial metabolism in the anaerobic rumen environment.

2.3.3 Modified Haldane (Enzyme Kinetics)

In contrast to the Monod rate, the Modified Haldane rate comes from enzyme kinetics. We call the rate shown in Eq. (2.7) the Modified Haldane rate as it starts with the rate from the work Briggs and Haldane [22], it was adapted to microbial growth by Hoh and Cord-Ruwisch [67], and was refined by Lynch *et al.* [108]. There is a formal similarity between the Monod rate and the Michaelis-Menten rate. The latter is an early result from enzyme kinetics and it is unsurprising that this theory can be used on models for microbial growth. The Haldane rate is imported directly from the work of Briggs and Haldane [22] on enzyme kinetics. In the derivation of q_H we will see that the thermodynamic terms emerge as a consequence of the system of differential equations, arising from the assumption of mass action, that model the chemical reactions. Significantly, the Briggs-Haldane theory includes Michaelis-Menten kinetics as a special case, but there are notable differences in the assumptions leading to the functional form for this rate. The Michaelis-Menten rate was published in 1913 [120]; the Haldane rate was published in 1925 [22]. Both rates are widely used in enzyme kinetics. The Michaelis-Menten rate is now derived using the Briggs-Haldane approach along with their interpretation of the Michaelis-Menten constant.

Modelling microbial growth through an analogy with enzyme kinetics provides a promising

framework for generalisations to more complicated scenarios, including multiple limiting substrates, multiple products, and substrates that inhibit growth. It is thus worth a look at the derivation of q_H in detail. Before we do this, however, it is helpful to comment on the analogy itself. How can we use enzyme kinetics to model microbial growth?

An enzyme is a protein that acts as a catalyst in the conversion of substrate to product. Enzymes are produced by living organisms and they accelerate chemical reactions. A microbe contains many copies of many different enzymes catalysing metabolic reactions; however, in the analogy we regard the microbe itself as a single enzyme. The resulting model is thus simplified substantially because the need for a detailed knowledge and analysis of the enzyme kinetics within the microbe is avoided, yet the model itself captures the role of the microbe as a catalytic entity that facilitates the conversion of an energy-yielding substrate to a product.

Reactions involving enzymes are typically characterised by:

1. The concentration of the enzyme is small compared to that of the substrate.
2. The enzyme complex is formed rapidly compared to the formation of the product.
3. The enzyme is not altered by the reaction in that, after the product formation, it is available for further reaction with substrate. There is no loss or gain of enzymes in the reaction.

Microbes viewed as catalysts analogous to enzymes arguably satisfy these characteristics for many models.

The differential equations that model reactions involving enzymes (like most chemical reactions) are based on the law of mass action. At the heart of the Briggs-Haldane approach, however, is an assumption known as the "quasi-steady-state assumption" (QSSA) that reflects the rapidity at which enzymes complex with reactants (characteristic 2). A partial justification for this is the assumption that the enzymes are present in small concentrations compared to the substrate (characteristic 1). We will see that the QSSA yields to a conservation law for enzymes (characteristic 3). The mathematical foundations of the assumption have been studied extensively. It is beyond the scope of this work to give a complete account of the QSSA and its ramifications, but the reader can consult Murray [129] for a biologically-relevant account of

the assumption. We note that the assumption was introduced by Briggs and Haldane in 1925 [22] and thereafter used extensively in enzyme kinetics. It was more than 50 years after their work was published that the assumption drew the attention of mathematicians (e.g., [150], [159], [160]). There is now extensive mathematical literature concerning this assumption, its limitations, and its extensions. For examples: Schnell and Maini [154] have studied the validity of the QSSA under certain conditions when the concentration of the enzyme is large; the QSSA has been adapted for stochastic versions of enzyme kinetics [2], [84]; and the "use and abuse" of the QSSA has been discussed [47].

The QSSA in enzyme kinetics requires two time scales. The fast scale tracks the speed at which a catalyst forms a complex with a reactant; the slower scale reflects the speed at which the product is formed. Pursuing the analogy to microbes, we require yet another time scale for the reproduction of the organsim. It is important to recognise the need for this slow scale because, for enzyme kinetics, the QSSA implies the conservation of the enzyme. If a microbe is regarded as an enzyme, then its number will be conserved under the QSSA. We are reminded here that we seek a model for microbial growth/decay. The answer is that there is yet another, still slower time scale. In this analogy we thus juggle three time scales:

1. the **fast scale** that reflects the rate at which enzymes interact with substrate;

2. the **intermediate scale** which concerns the speed that products are formed by the reaction, and;

3. the **slow scale** that models the speed at which a microbe reproduces.

Roughly speaking, although the QSSA predicts a conservation of enzyme (in our case a microbe), it can be argued that microbes reproduce on a time scale much slower than the rate at which products are formed.

Typical measurements support the assumption of three distinct time scales. Let E, S, C_S, and P denote the concentrations of enzyme, substrate, enzyme complexed with substrate, and product respectively. We consider the following reaction:

$$\mathrm{E} + \mathrm{S} \underset{\mathrm{k_2}}{\overset{\mathrm{k_1}}{\rightleftharpoons}} \mathrm{C_S} \underset{\mathrm{k_4}}{\overset{\mathrm{k_3}}{\rightleftharpoons}} \mathrm{E} + \mathrm{P}, \tag{2.10}$$

where the k_j denote reaction rates, and compare typical rates of substrate binding and transformation to product. This is followed by determining a typical number for the specific growth rate of a microbe. We first estimate the "fast rate", i.e., the rate of substrate binding to the enzyme.

Fersht [46] tabulated association rate constants for enzyme-substrate interaction, k_1. These are in the range 10^6 to $10^8\,\mathrm{s}^{-1}(\mathrm{mol\,L}^{-1})^{-1}$. Let us use a value of $10^7\,\mathrm{s}^{-1}(\mathrm{mol\,L}^{-1})^{-1}$. Intracellular concentrations of enzyme substrates in the bacterium *Escherichia coli*, tabulated by Bennett *et al.* [12], were in the range of 1.3×10^{-7} to $9.7\times10^{-2}\,\mathrm{mol\,L}^{-1}$, with a median value of $2.4\times10^{-4}\,\mathrm{mol\,L}^{-1}$. Assuming first-order reaction kinetics, the rate of substrate binding to the enzyme can be calculated from $k_1\times S$, which yields $(2.4\times10^{-4}\,\mathrm{mol\,L}^{-1})\times(10^7\,\mathrm{s}^{-1}(\mathrm{mol\,L}^{-1})^{-1}) = 2.4\times10^3\,\mathrm{s}^{-1}$.

We now consider the rate of substrate to product transformations by an enzyme. This rate is denoted in the literature by k_{cat}. In terms of Eq. (2.10) we have $k_{\mathrm{cat}} = k_3 \times P$. Bar-Even [9] summarised k_{cat} values for 1942 purified enzymes and calculated a median $k_{\mathrm{cat}} = 13.7\,\mathrm{s}^{-1}$. We note that the estimated k_{cat} values for enzymes in cells of *Escherichia coli* were in good agreement for those determined for purified enzymes [38].

We now consider the time scale for a microbe to grow and divide to form two daughter microbes. *Escherichia coli* has a doubling time, t_d, of 21 to 150 min under optimal conditions, depending on the growth substrate [186]. Doubling times for other microbes are 28 min to over 13 h (cf. [140]). For a microbe growing rapidly with a doubling time of 20 min, the specific growth rate, μ, can be calculated (cf. [143]) from

$$\mu = \frac{\ln 2}{t_d}$$

as approximately $6\times10^{-4}\,\mathrm{s}^{-1}$. The rates for the three time scales are summarised in Table 2.1. Finally, in this enzyme kinetics analogy model, the crucial assumption is made that the rate of change of the microbe concentration is proportional to the rate of change of the product concentration.

A key feature of the Briggs-Haldane approach is that it allows a reaction from product

Table 2.1: Typical rate values for different time scales

time scale	rate	typical value
Fast	$k_1 S$	$2.4 \times 10^3\,\mathrm{s}^{-1}$
Intermediate	$k_3 P$	$13.7\,\mathrm{s}^{-1}$
Slow	μ	$6 \times 10^{-4}\,\mathrm{s}^{-1}$

back to substrate. This, in turn, opens the door for thermodynamic feedback. The Briggs and Haldane derivation concerns only enzyme kinetics, but through the above analogy their work was adapted for microbial growth by Hoh and Cord-Ruwisch [67]. In this manner it is possible to "import" the thermodynamic terms from enzyme kinetics for microbial growth. The rate was further adapted by Lynch *et al.* [108] to include directly the effects of ATP conservation in the thermodynamic feedback, providing a formal description for different ATP yields (η) found in microbes with the same overall metabolism.

Returning to Eq. (2.10) we now derive an expression for the rate of change of product concentration P.

Assuming the law of mass action, the rates of change of the concentrations are given by the differential equations:

$$\frac{dE}{dt} = -k_1 ES + k_2 C_S + k_3 C_S - k_4 EP, \tag{2.11}$$

$$\frac{dS}{dt} = -k_1 ES + k_2 C_S, \tag{2.12}$$

$$\frac{dC_S}{dt} = k_1 ES - k_2 C_S - k_3 C_S + k_4 EP, \tag{2.13}$$

$$\frac{dP}{dt} = k_3 C_S - k_4 EP. \tag{2.14}$$

Adding Eqs. (2.11) and (2.13) gives the conservation law $\frac{d}{dt}(E + C_S) = 0$. Let $E + C_S = E_T$, where E_T is a constant that denotes the total amount of enzyme. The assumption that $E \ll S$ is made, meaning that the enzyme is present in "catalytic amounts" and a quasi-steady-state is established very quickly. This quasi-steady-state assumption (QSSA) amounts to the relations

$$\frac{dE}{dt} = \frac{dC_S}{dt} = 0,$$

i.e.,

$$k_1 ES - k_2 C_S - k_3 C_S + k_4 EP = 0. \tag{2.15}$$

We now seek an expression for $\frac{dP}{dt}$ that involves only S and P. The enzyme conservation law and the QSSA can be used to achieve this. First, since $C_S = E_T - E$, Eq. (2.15) implies

$$E = \frac{(k_2 + k_3)E_T}{(k_2 + k_3) + k_1 S + k_4 P}. \tag{2.16}$$

Note that Eq. (2.16) has only the variables, S and P. Substituting $E_T - E$ for C_S in Eq. (2.14) gives

$$\frac{dP}{dt} = k_3 E_T - (k_3 + k_4 P)E$$

which, after replacing E using Eq. (2.16), becomes

$$\begin{aligned} \frac{dP}{dt} &= k_3 E_T - \frac{(k_3 + k_4 P)(k_2 + k_3)E_T}{(k_2 + k_3) + k_1 S + k_4 P}, \\ &= E_T \left(k_3 - \frac{k_3 + k_4 P}{1 + \frac{k_1 S}{k_2 + k_3} + \frac{k_4 P}{k_2 + k_3}} \right). \end{aligned} \tag{2.17}$$

We thus have

$$\frac{dP}{dt} = E_T \left(k_3 - \frac{k_3 + k_4 P}{1 + \frac{S}{K_S} + \frac{P}{K_P}} \right), \tag{2.18}$$

where K_S and K_P are defined as

$$K_S = \frac{k_2 + k_3}{k_1}, \tag{2.19}$$

and

$$K_P = \frac{k_2 + k_3}{k_4}. \tag{2.20}$$

Defining the maximum forward reaction rate and maximum backward reaction rate as $v_f = E_T k_3$

and $v_b = E_T k_2$, respectively, Eq. (2.18) gives

$$\begin{aligned}\frac{dP}{dt} &= \frac{E_T\left(k_3\frac{S}{K_S} - k_2\frac{P}{K_P}\right)}{1+\frac{S}{K_S}+\frac{P}{K_P}},\\ &= \frac{v_f\frac{S}{K_S} - v_b\frac{P}{K_P}}{1+\frac{S}{K_S}+\frac{P}{K_P}}.\end{aligned} \tag{2.21}$$

At equilibrium $\frac{dP}{dt} = 0$; hence,

$$\frac{v_f}{K_S}S_{\text{eq}} - \frac{v_b}{K_P}P_{\text{eq}} = 0$$

and

$$\frac{P_{\text{eq}}}{S_{\text{eq}}} = \frac{v_f K_P}{v_b K_S} = K_{\text{eq}}. \tag{2.22}$$

Equation (2.22) is the Haldane relation. Substituting this relation into Eq. (2.18) gives

$$\begin{aligned}\frac{dP}{dt} &= \frac{\frac{v_b}{K_P}\left(SK_{\text{eq}} - P\right)}{1+\frac{1}{K_P}\left(S\frac{K_P}{K_S}+P\right)},\\ &= \frac{v_b\left(SK_{\text{eq}} - P\right)}{K_P + \frac{v_b}{v_f}SK_{\text{eq}} + P},\\ &= \frac{v_b S\left(1-\frac{P}{SK_{\text{eq}}}\right)}{\frac{K_P}{K_{\text{eq}}} + S\left(\frac{v_b}{v_f}+\frac{P}{SK_{\text{eq}}}\right)},\\ &= \frac{v_f S\left(1-\frac{P}{SK_{\text{eq}}}\right)}{\frac{v_f}{v_b}\frac{K_P}{K_{\text{eq}}} + S\left(1+\frac{v_f}{v_b}\frac{P}{SK_{\text{eq}}}\right)};\end{aligned}$$

therefore,

$$\frac{dP}{dt} = \frac{v_f S\left(1-\theta\right)}{K_S + S\left(1+\frac{v_f}{v_b}\theta\right)}, \tag{2.23}$$

where

$$\theta = \frac{Q}{K_{\text{eq}}} = \frac{P}{SK_{\text{eq}}} = \frac{P}{S}\frac{S_{\text{eq}}}{P_{\text{eq}}}, \tag{2.24}$$

and $\frac{v_f}{v_b} = \frac{k_3}{k_2}$ is the ratio of the maximum forward reaction rate and the maximum backward reaction rate. It is assumed by Hoh and Cord-Ruwisch [67] (and by Lynch *et al.* [108]) that these rates are equal (i.e., $v_f = v_b$ or $k_3 = k_2$), and this gives the final form of the rate (Eq. (2.7)), where K_S is renamed K_H for clarity when comparing to other rates. Note that Q is

the reaction quotient and K_{eq} is the equilibrium constant (the result of calculating the reaction quotient using the equilibrium concentrations). The reaction quotient for the general reaction $a\text{A} + b\text{B} \rightleftharpoons c\text{C} + d\text{D}$ is $\frac{[\text{C}]^c[\text{D}]^d}{[\text{A}]^a[\text{B}]^b}$ where a, b, c, and d are the stoichiometric coefficients of the respective species and the concentrations are taken in the prevailing conditions.

A special case is when the reaction from the complex to the product is irreversible, i.e., $k_4 = 0$, so that the reaction is

$$\text{E} + \text{S} \underset{\text{k}_2}{\overset{\text{k}_1}{\rightleftharpoons}} \text{C}_\text{S} \overset{\text{k}_3}{\rightharpoonup} \text{E} + \text{P}, \tag{2.25}$$

In this case Eq. (2.17), using K_S as defined in Eq. (2.19), is

$$\frac{dP}{dt} = \frac{v_f \frac{S}{K_S}}{1 + \frac{S}{K_S}} = \frac{v_f S}{K_S + S}. \tag{2.26}$$

Eq. (2.26) is the Michaelis-Menten rate. We thus see that the Michaelis-Menten rate is a special case of the Modified Haldane rate. It should be noted, however, that the original derivation of the Michaelis-Menten rate differed from that of Briggs and Haldane in that they did not use the QSSA. Instead, they used the more restrictive assumption that $k_1, k_2 \gg k_3$, and this leads to an interpretation of the constant K_S as

$$K_S = \frac{k_2}{k_1}.$$

The interpretation and history of the Michaelis-Menten rate and constant are discussed in depth by Johnson [80]. An English translation of the original paper [120] is provided by Johnson and Goody [81].

2.3.4 DLQB (Statistical Mechanics)

The DLQB rate was developed by Desmond-Le Quéméner and Bouchez [39] using statistical mechanics and has since been used to model the growth of methanogenic microbes [128]. An outline of the derivation is given here.

The derivation deals with three systems:

1. Σ is the whole system, comprised of n elementary volumes (or statistical units) where

$n = V_{\text{tot}}/V_{\text{harv}}$, V_{tot} is the total volume, and V_{harv} is the volume that each individual microbe can access to harvest the substrate: V_{harv} is a volume of environment per cell and can be seen as a term related to substrate concentration;

2. Σ' is the subsystem comprised of the N statistical units that contain microbes; and

3. R is the reservoir, the $n-N$ statistical units that do not contain microbes, i.e., $R = \Sigma - \Sigma'$.

It is assumed that Σ has much larger volume than Σ'. Considering the canonical ensemble of microstates that each consist of a distribution of substrate molecules in Σ' gives a Boltzmann distribution. Using the partition function and Stirling's approximation they determine the proportion of microbes that have enough substrate within their statistical unit to trigger division to be

$$\frac{N^{\ddagger}}{N} = \exp\left(\frac{-v}{V_{\text{harv}} \cdot S}\right), \tag{2.27}$$

where $N^{\ddagger}$ is the number of statistical units containing microbes that have enough substrate within their elementary volume to trigger division and v is the threshold number of substrate molecules. They then showed that Eq. (2.27) can be interpreted as a rate. Gibbs energy methods derived earlier by Kleerebezem and van Loosdrecht [89] are modified and used to estimate v as

$$v = \frac{E_M + E_{\text{dis}}}{E_{\text{cat}}}. \tag{2.28}$$

Here, E_M is the energy captured in the biomass if it were to be assembled from its constituent components and E_{dis} is the energy dissipated during biomass formation. The sum $E_M + E_{\text{dis}}$ is a constant for a microbe on a certain substrate and gives the amount of energy required per mole of produced cell matter. E_{cat} is the negative of the Gibbs free energy change associated with the conversion of substrate to product. If the Gibbs free energy change is not negative then E_{cat} is set to zero, which halts metabolism when the forward reaction is thermodynamically unfavourable, ensuring the microbe doesn't degrade itself and its products back to substrate. This shows that v can be interpreted as the ratio of energy captured to energy available. The ratio

$$\frac{v}{V_{\text{harv}}} = \frac{E_M + E_{\text{dis}}}{E_{\text{cat}} \cdot V_{\text{harv}}} = \Lambda,$$

returns the rate to the form shown in Eq. (2.8).

2.3.5 Rates Comparisons

The four rates we have presented come from different sources ranging from pure empirical (Monod), enzyme kinetics (Modified Haldane), and statistical mechanics (DLQB). Despite their different origins, there are connection among these rates. In this section we establish these connections.

We note first that the Monod rate is of the same form as the Michaelis-Menten rate, and the connection between this rate and the Modified Haldane rate has already been discussed. In addition, it is clear that q_M can be readily recovered from q_J as the special case $F_T = 1$, and from q_H as the special case $\theta = 0$. In other words, the Monod rate, q_M, corresponds formally to q_J and q_H with the thermodynamic influence neutralised. A link between the Monod rate and the DLQB rate is less obvious and will be given below. We now look at comparisons of the rates q_J, q_H, and q_D.

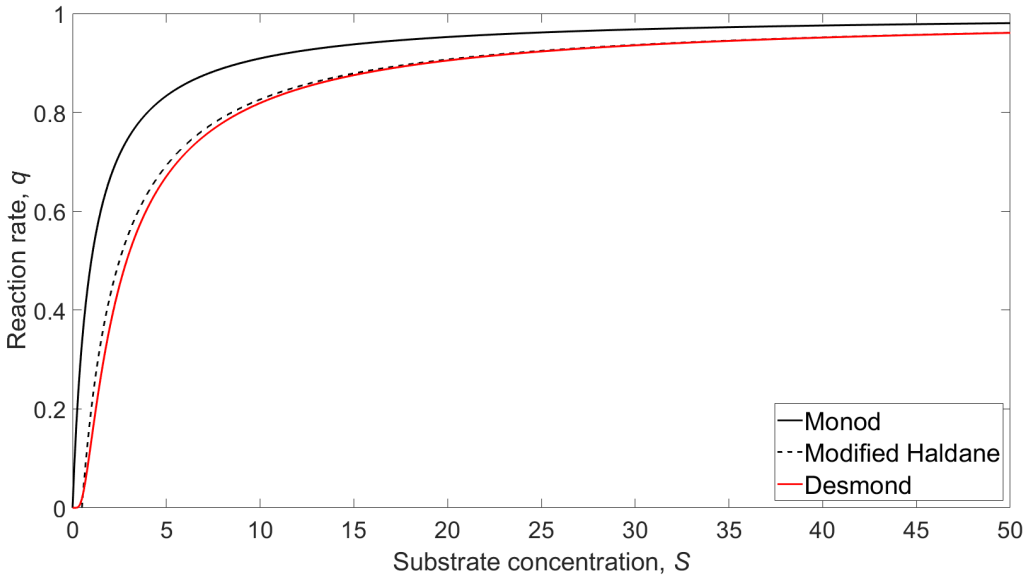

Figure 2.4: Comparison of the shape of the Monod, Modified Haldane, and DLQB rates showing high substrate concentration behaviour.

Figure 2.4 illustrates the typical shapes of the Monod, Modified Haldane, and DLQB rates and the similar behaviour of the rates at high substrate concentration. Figure 2.5 highlights the

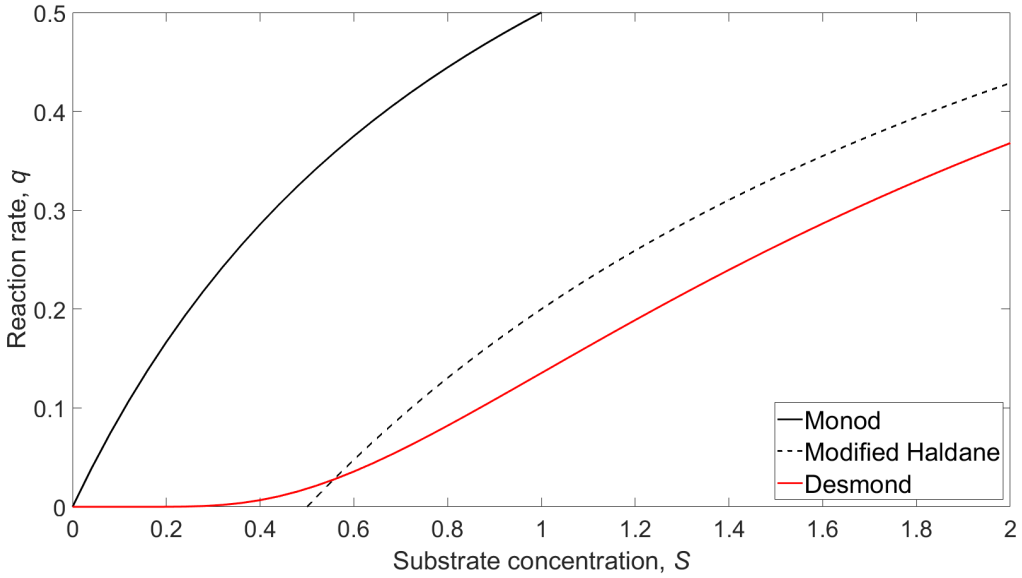

Figure 2.5: Comparison of the shape of the Monod, Modified Haldane, and DLQB rates showing low substrate concentration behaviour.

significant differences between the rates at low substrate concentration. The Jin and Bethke rate was not included as its functional similarity to the Modified Haldane rate would mean that its inclusion would provide no further insight. As these plots are intended to show the typical shape of the rates, the product concentration was held constant while the substrate concentration was varied in making these plots.

Modified Haldane and Jin & Bethke

The rates q_H and q_J share the feature of an explicit thermodynamic term that can produce a reaction shutdown. They both predict non-zero threshold values, $S_{\min}$. If the thermodynamics in Eq. (2.9) are repackaged as $F_T = 1 - \theta$ (a move similar to that done by Jin and Bethke when comparing their thermodynamic potential factor to the thermodynamic terms of Hoh and Cord-Ruwisch [79]), then Eq. (2.6) is

$$q_J = \frac{S(1-\theta)}{K_J + S}. \tag{2.29}$$

Now, θ is given by Eq. (2.24) so that if K_J is defined as $K_J = K_{JH} + C$, where $\gamma = S\theta = P\frac{S_{\text{eq}}}{P_{\text{eq}}}$, then q_J can be expressed in the form

$$q_J = \frac{S(1-\theta)}{K_{JH} + \gamma + S} = \frac{S(1-\theta)}{K_{JH} + S(1+\theta)}, \tag{2.30}$$

which is the same form as the Modified Haldane rate. In this sense, the Jin and Bethke rate does not provide a rate form distinct from the Modified Haldane rate. The identification of q_J with q_H is deceptively simple: it must be remembered that $K_{JH} = K_J - \gamma$, and γ depends on the product concentration, which is generally not constant. This means that K_{JH} is not, in general, constant, in contrast with K_J which is a constant in q_J. Jin and Bethke derived a thermodynamic term and appended it to the Monod rate q_M. This means that $K_M = K_J$. In this limited sense, Jin and Bethke's rate can be considered a "hybrid" that uses a thermodynamic term derived from basic principles and a rate that is empirical.

The above connection between the rates is superficial and unsatisfactory because of the product dependence of K_{JH}. A deeper connection between the rates can be seen by going back to the equations from enzyme kinetics but using the Michaelis-Menten assumption instead of the QSSA. Unlike the derivation of the Michaelis-Menten rate, we let the reaction for the product be reversible. Like the Michaelis-Menten derivation, however, we make the assumption that the rates which complex the substrate dominate the product formation rates, i.e.,

$$k_1, k_2 \gg k_3, k_4.$$

In this case, Eq. (2.15) can be replaced by

$$k_1 ES - k_2 C_S = 0, \tag{2.31}$$

and since $E_T = E + C_S$, this implies

$$E = \frac{E_T K}{K + S}, \tag{2.32}$$

where $K = k_2/k_1$ is the Michaelis-Menten constant. Eqs. (2.14), (2.31), and (2.32) imply

$$\frac{dP}{dt} = \frac{E_T k_3 S\,(1-\theta)}{K+S},$$

where the thermodynamic term θ is

$$\theta = \frac{k_4}{k_3} K \frac{P}{S}. \tag{2.33}$$

Ignoring the multiplicative constant $E_T k_3$, we get the rate

$$q = \frac{S\,(1-\theta)}{K+S}, \tag{2.34}$$

which is q_J when we identify the Michaelis-Menten constant with the Monod constant and F_T with $1-\theta$. Note that if we had used the assumption that the only "slow rate" is k_3, i.e.,

$$k_1, k_2, k_4 \gg k_3,$$

then we would still get a rate of the form in Eq. (2.34) with K replaced by the Modified Haldane constant K_S given by Eq. (2.19).

Modified Haldane and DLQB

The DLQB rate is functionally very different from the other rates. Nonetheless, Figure 2.4 indicates that the graph of q_D is very close to q_H for values of S away from zero. Figure 2.5 illustrates the different graph shapes near $S = 0$. The rates q_D and q_H depend on S in very different ways and this indicates that connections are most likely through a limiting case. Before we look at a limiting case, we note the biological parameters needed for q_H and q_D. The Modified Haldane rate requires finding a value of K_H in order to use the rate. This is the half-saturation constant for a microbe growing without thermodynamic inhibition. It assumes all compounds needed for growth other than the substrate of interest are in plentiful supply and the products are in low concentration. A value for this must be measured experimentally, but once it has been measured the value can be used for modelling any organism with length of about $1-2\,\mu$m. In contrast, the DLQB model requires estimating a value for V_{harv}, which is needed to calculate

Λ. This is the volume that a microbial cell can access to harvest substrate.

Regarding q_D and q_H as functions of S, it is clear that for any choice of positive constants Λ, K_H, and γ

$$\lim_{S\to\infty} q_D(S) = \lim_{S\to\infty} q_H(S) = 1, \tag{2.35}$$

which means the rates are asymptotic to the line $q = 1$. This can be seen in Figure 2.4 as the DLQB and Modified Haldane rates clearly approach $q = 1$ asymptotically. For values of S that are large compared to Λ and K_H, the Modified Haldane and DLQB rate converge but the choices of constants have an effect on the rate of this convergence. We show, plainly speaking, that the rate of convergence is fastest if $\Lambda = K_H$.

The Taylor series for the exponential is

$$e^x = 1 + x + \frac{1}{2!}x^2 + \frac{1}{3!}x^3 + \dots,$$

so that

$$q_D(S) = e^{-\Lambda/S} = \frac{1}{e^{\Lambda/S}} = \frac{1}{1 + \frac{\Lambda}{S} + \frac{1}{2!}\left(\frac{\Lambda}{S}\right)^2 + \dots}. \tag{2.36}$$

Using Eqs. (2.7) and (2.24), the Modified Haldane rate (when $\gamma \le S$, so $\theta \le 1$) can be expressed as

$$q_H = \frac{1 - \frac{\gamma}{S}}{1 + \frac{K_H+\gamma}{\gamma}}. \tag{2.37}$$

In general,

$$|q_H(S) - q_D(S)| = O\left(\frac{1}{S}\right) \tag{2.38}$$

as $S \to \infty$. We seek a relationship among Λ, K_H, and γ such that

$$|q_H(S) - q_D(S)| = O\left(\frac{1}{S^2}\right) \tag{2.39}$$

as $S \to \infty$. Eqs. (2.36) and (2.37) imply

$$q_H - q_D = \frac{1}{\left(1 + \frac{K_H+\gamma}{\gamma}\right)\exp\frac{\Lambda}{S}}\left(\left(1 - \frac{\gamma}{S}\right)\left(1 + \frac{\Lambda}{S} + \left(\frac{\Lambda}{S}\right)^2\frac{1}{2!} + \dots\right) - \left(1 + \frac{K_H+\gamma}{S}\right)\right). \tag{2.40}$$

The $O(\frac{1}{S})$ terms of $q_H - q_D$ in Eq. (2.40) must cancel in order to satisfy Eq. (2.39), and this leads to

$$\frac{\Lambda - \gamma}{S} - \frac{K_H + \gamma}{S} = 0, \tag{2.41}$$

consequently,

$$\Lambda = K_H + 2\gamma. \tag{2.42}$$

Given the values of K_H and γ, the value of Λ determined by Eq. (2.42) brings the two rates very close under the assumption that $\frac{\Lambda}{S} \ll 1$ (or $S \gg \Lambda$). Note that Λ is determined uniquely by Eq. (2.39).

A link between the DLQB rate and the Monod rate can be made by noting that an $O\left(\frac{1}{S}\right)$ approximation of q_D from Eq. (2.36) has the same form as the Monod rate with Λ in place of K_M and again relying on the assumption that $S \gg \Lambda$. In fact, Desmond-Le Quéméner and Bouchez [39] identified Λ with K_M. No explanation for this identification was given, but certainly they compared their results with Monod using $K_M = \Lambda$.

Recall that the DLQB rate is

$$q_D = \exp\left(-\frac{\Lambda}{S}\right),$$

where

$$\Lambda = \frac{E_{\text{dis}} + E_M}{E_{\text{cat}} V_{\text{harv}}}.$$

Prima facie is appears that q_D does not have a positive threshold. Indeed, Desmond-Le Quéméner and Bouchez [39] interpret the flattening of the rate curve for small concentrations as an "apparent threshold". Desmond-Le Quéméner and Bouchez [39] and others [128] regard Λ as a positive constant for specific microbes. The zero threshold comes from the relation $q_D \to 0$ as $S \to 0$. In fact, with a careful definition of the rate, it is straightforward to incorporate a positive threshold without changing the model.

The thermodynamic term in q_D is E_{cat}. This term corresponds to the chemical energy available for the microbe as a result of the conversion of substrate to product: E_{cat} is thus the negative of the change in Gibbs free energy associated with the reaction. We can therefore express E_{cat} in the same terms used for the thermodynamic parameter in the Modified Haldane

rate. specifically,

$$E_{\text{cat}} = \begin{cases} -RT \ln \frac{Q}{K_{\text{eq}}}, & \text{if } 0 < Q < K_{\text{eq}} \\ 0 & \text{otherwise.} \end{cases}, \tag{2.43}$$

where Q and K_{eq} are the reaction quotient and equilibrium constant, as described earlier. Let

$$\Psi = \frac{E_{\text{dis}} + E_M}{V_{\text{harv}}},$$

and define q_D as follows:

$$q_D = \begin{cases} \exp\left(-\frac{\Psi}{E_{\text{cat}} S}\right), & \text{if } E_{\text{cat}} S > 0 \\ 0, & \text{if } E_{\text{cat}} S = 0. \end{cases}$$

This definition is not arbitrary: it is the only way to define q_D so that the rate is continuous at $E_{\text{cat}} S = 0$. Noting that the thermodynamic parameter in the Modified Haldane rate is $\theta = Q/K_{\text{eq}}$, we can write

$$q_D = \begin{cases} \exp\left(-\frac{\Psi}{SRT \ln \theta}\right), & \text{if } S \ln \theta < 0 \\ 0, & \text{if } S \ln \theta = 0. \end{cases}$$

It is evident under the above definition that q_H and q_D have precisely the same thresholds for the same thermodynamic reasons. In Figures 2.4 and 2.5 we held E_{cat} constant but if we allowed E_{cat} to vary, the curve for the DLQB rate would move across and reach the x-axis in the same place as the Modified Haldane rate. As $\theta \to 1$ we see that $q_H \to 0$ and $q_D \to 0$ (the common positive threshold). A fundamental difference in the rates is when $\theta \to 0$. For the Modified Haldane rate, q_H takes the form of the Monod rate. In contrast, $\ln \theta \to -\infty$ as $\theta \to 0^+$ so that $q_D \to 1$. Small values of θ can occur, for instance, when P is small but S is not. Consider, for example the case where $S = K_H$ and P is nearly zero. Then, $q_H \approx 1/2$, but $q_D \approx 1$.

In this chapter we have explored the rates from these different existing models and derived some new links between them. We will next consider a new rate before using some experimental data from literature to validate and illustrate the use of the single substrate models.

Chapter 3

A Model that Optimises ΔG_{ATP}

We seek a model that balances mathematical tractability with key biological ideas. It should reflect these ideas, apply to a range of microbes, and still be simple enough to test against existing data and be used for predictions. The single substrate rates that were discussed in the previous chapter, particularly the Modified Haldane and DLQB (shown in Eqs. (2.7) and (2.8) respectively), have strengths, but there is more known about the biology that can be incorporated into a model. Knowledge of the ATP generating process in the cell membrane offers a means by which the Gibbs free energy requirement for ATP synthesis can be varied in an understandable way, with implications for the rate of ATP synthesis. The ATP synthase is a multi-subunit enzyme that rotates on an axis perpendicular to a microbial cell's membrane. A gradient of ions is maintained across the membrane and each time an ion, driven by that gradient, crosses the membrane through the ATP synthase, the rotor turns one step. The total number of steps required for a full turn is determined by the number of proteins in the c-ring (between 8 and 15), and one full turn results in the synthesis of three molecules of ATP from three ADP and three phosphate ions [117]. Miller *et al.* [121] present a model where the rate of ATP synthesis by the membrane-bound ATP synthase is regulated by the size of the gradient across the membrane (from outside the cell to inside), measured as the proton motive force (or sodium motive force for organisms that use sodium ions rather than protons). There is a minimum proton motive force, below which the rotor cannot turn [121] and there is a maximum rate, which is associated with a proton motive force above which the rate of ATP synthesis cannot be increased any further

[41] [121]. This range of proton motive force and the accompanying relation of the rate of rotation of the ATP synthase can be interpreted as the thermodynamic potential of the proton motive force driving the rotor. Out of thermodynamic considerations, there is also an equal but opposite energy requirement to replenish the gradient, and that energy requirement will be largest at the maximum gradient and smallest at the minimum gradient. It is understood that gradient replenishment and gradient depletion occur simultaneously as the cell metabolises its energy substrate (replenishment) and uses the gradient for functions including ATP synthesis (depletion). Thus, as the proton motive force falls, less energy is required to export each proton across the membrane, but the rate of ATP synthesis will be lower. This consideration now allows us to propose a model where, as the thermodynamics of an energy-yielding metabolic reaction that generates ATP become thermodynamically unfavourable, the cell lowers the membrane potential to allow continued proton motive force replenishment, but with the penalty of a lower rate of ATP synthesis as the ATP synthase turns more slowly with reduced proton motive force. We further propose that a microbe will maximise the rate of ATP synthesis by optimising the proton motive force. This is the model we explore in this chapter.

In this chapter we use a dataset collated from the literature to justify the need for a model to incorporate this additional biological information. We then develop a model that incorporates this additional biological knowledge. Finally, we compare the performance of this new model against the experimental data. Although the DLQB rate shows promise for extensions, we will focus on modifying the Modified Haldane rate.

3.1 ΔG_{ATP} in Current Models

The Gibbs free energy change for a reaction, ΔG_T^*, can be expressed as

$$\Delta G_T^* = RT \ln \left(Q/K_{\mathrm{eq}}\right) = \Delta G_T^o + RT \ln Q \tag{3.1}$$

where ΔG_T^o is the Gibbs free energy change at standard conditions (which may be known using, for example, tabulated standard enthalpy and entropy values). The net Gibbs free energy change

for the reaction coupled to ATP formation, ΔG_T, can instead be found using

$$\Delta G_T = \Delta G_T^o + RT \ln Q + \eta \Delta G_{\mathrm{ATP}} \tag{3.2}$$

where η is the number of moles of ATP produced per mole of substrate consumed, and ΔG_{ATP} is the energy required to form a mole of ATP. This form of ΔG_T is defined by Lynch *et al.* [108]. The novelty for this version of ΔG_T is the addition of the term $\eta \Delta G_{\mathrm{ATP}}$, which accounts for the energy required for the microbe to produce ATP. We note that earlier work, including that of Hoh and Cord-Ruwisch [67], does not include the energy required to produce ATP.

The thermodynamic inhibition term in the Modified Haldane rate, θ, was given in Chapter 2 as $\theta = \frac{Q}{K_{\mathrm{eq}}}$. By including the ATP term from Eq. (3.2), Lynch *et al.* [108] obtain

$$\theta = \exp\left(\Delta G_T / RT\right) = Q \exp \frac{\Delta G_T^o + \eta \Delta G_{\mathrm{ATP}}}{RT}. \tag{3.3}$$

The form of θ in Eq. (3.3) is useful for modelling of the Modified Haldane rate because ΔG_T^o is a constant for a particular reaction and η is a constant for a particular metabolic pathway, while a fixed value of ΔG_{ATP} can be chosen. While a fixed value may be justified over a wide range of substrate concentrations; we have proposed (above) that organisms can change their ΔG_{ATP} under near-threshold conditions, allowing them to continue to generate ATP by maintaining $\Delta G_{\mathrm{ATP}} < \Delta G_T^*$. In the Lynch *et al.* [108] model this ΔG_{ATP} term was considered constant. We will see that the ΔG_{ATP} term can take values between about 55 kJ $\mathrm{mol}_{\mathrm{ATP}}^{-1}$ and 75 kJ $\mathrm{mol}_{\mathrm{ATP}}^{-1}$. It is this behaviour that we build into a model.

3.2 Biology of ΔG_{ATP}

The term η is the number of moles of ATP formed per mole of the energy-yielding substrate that is transformed. In more detail, it is the number of ATP (adenosine triphosphate) formed from ADP (adenosine diphosphate) in conjunction with the energy-yielding reaction in the microbe. The ATP can be formed either by substrate level phosphorylation or by an ATP synthase coupled to a transmembrane gradient of H^+ or Na^+.

Transmembrane gradients of H^+ or Na^+ that are generated during substrate transformations are harnessed by membrane-inserted ATP synthases to produce ATP in many anaerobes. ATP that is generated in the cell can also be converted to transmembrane gradients that can be used to drive uptake or other reactions. The value of ΔG_{ATP} must be the same as the energy used to drive the number of protons required to generate one ATP via a membrane-inserted ATP synthase. ATP synthases have different stoichiometries, with a complete cycle of the rotational component of an ATP synthase generating 3 ATP and requiring between 8 and 15 ions (H^+ or Na^+) [117]. The number of ions required for a full rotation of the ATP synthase appears to be the same within an organism but can vary between organisms [117]. Miller *et al.* [121] showed that ATP synthases that require more ions for a full rotation have a smaller driving force (membrane potenial, Δp) for the transport of one ion with the net result that the total amount of energy required for a full rotation (and, hence, ΔG_{ATP}) is about the same, regardless of the number of ions required to generate one ATP. The model by Miller *et al.* also predicts a minimum ΔG_{ATP}, $\Delta G_{\mathrm{ATPmin}}$, below which Δp is insufficient for rotation of the ATP synthase and a maximum ΔG_{ATP}, $\Delta G_{\mathrm{ATPmax}}$, corresponding to a Δp where the ATP synthesis is maximal. We use $\Delta G_{\mathrm{ATPmin}} = 55\,\mathrm{kJ\,mol}_{\mathrm{ATP}}^{-1}$ and $\Delta G_{\mathrm{ATPmax}} = 75\,\mathrm{kJ\,mol}_{\mathrm{ATP}}^{-1}$ as the limits on ΔG_{ATP} while recognising that a range of similar values are used elsewhere. The justification for these values is given in Appendix A.

When the supply of substrate is plentiful, the growth rate according to the Modified Haldane rate is maximised if we use $\Delta G_{\mathrm{ATP}} = 75\,\mathrm{kJ\,mol}_{\mathrm{ATP}}^{-1}$ and the ATP synthase is forming ATP at its maximum rate. This was the value used by Lynch *et al.* [108]. Conversely, when the substrate concentration is close to the threshold, so $\eta\Delta G_{\mathrm{ATP}}$ is close to the Gibbs free energy change, the growth rate would be higher if a smaller value of ΔG_{ATP} was used. As the value of ΔG_{ATP} decreases, the threshold also decreases and growth, or survival, is possible in conditions that would not be possible with ΔG_{ATP} fixed at the high value. This behaviour is exhibited in Figure 3.1. The figure was produced using *Desulfovibrio vulgaris* growing with H_2 and SO_4^{2-}. The basic energetics and growth conditions are in Appendices B and D (M008 and C052, respectively). The same ATP yield per H_2, environmental conditions, and reactant and product concentrations were used for all calculations, except that the energy substrate H_2 and ΔG_{ATP} were varied.

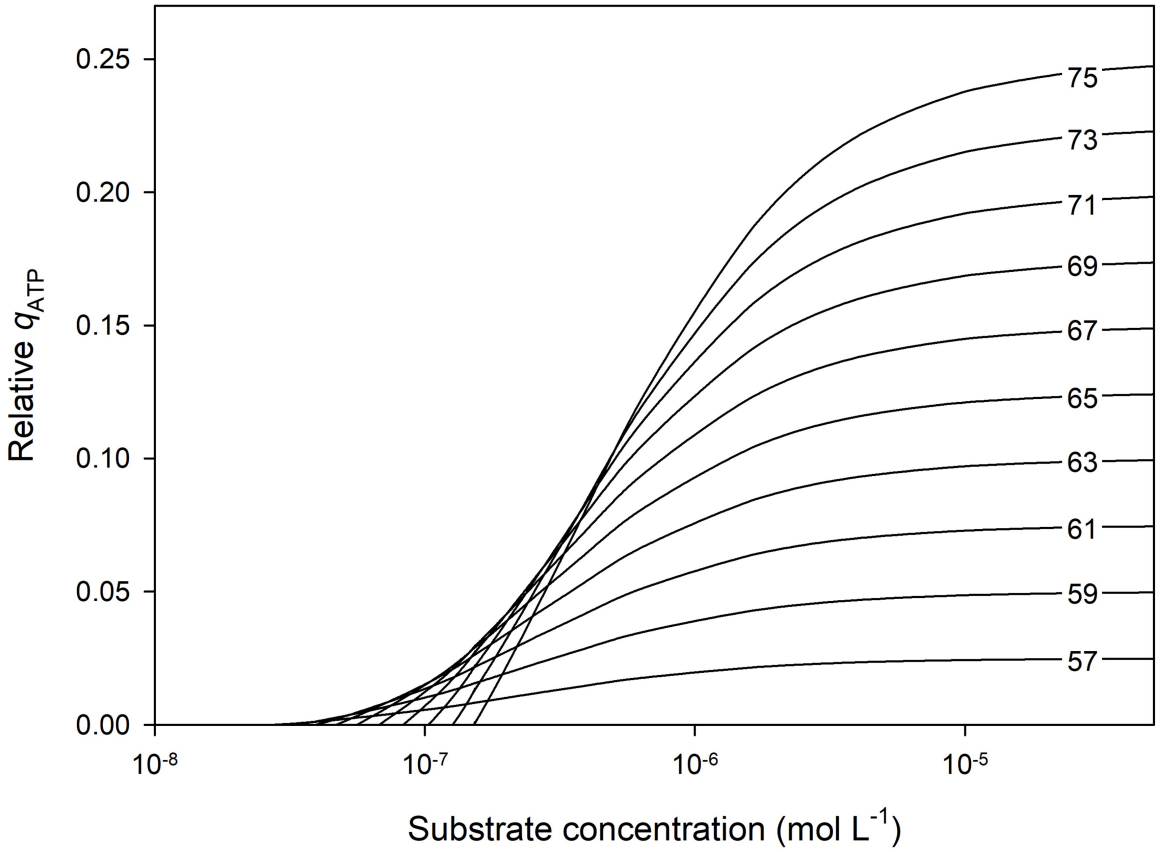

Figure 3.1: Plot showing the difference in threshold concentration at different ΔG_{ATP} values while other values (including product concentrations) are held constant.

3.3 The Data

We collated a dataset to test the relevance of the variable ΔG_{ATP} in the new rate against what has been measured experimentally. With a focus on experiments that included anaerobes, literature was surveyed to verify whether the required information was present in the paper or could be found (e.g., in supplementary material or through references to prevailing experimental conditions in other papers). The required information included concentrations of substrates and products, pH, and temperature. We concentrated on papers that reported S_{min} and K_{app} values. Dissolved concentrations of gases were calculated from gaseous partial pressures using tabulated Ostwald coefficients [184] with corrections for temperature [10], along with using the pH and dissociation constants for carbon dioxide. Papers in which not

enough information was provided were not included and we were left with a dataset of 107 experiments that we used to investigate how well the model predicts the values of $S_{\min}$ or K_{app}, compared to their experimentally-determined values. The dataset can be found in Appendix D. We split the dataset into two groups based on whether the measurements were for $S_{\min}$ (73 experiments) or K_{app} (34 experiments). In Figures 3.2 and 3.3 we plot the reciprocal of the reaction quotient calculated from the reported prevailing conditions for each experiment against $\exp\left((\Delta G_T^o + \eta \Delta G_{\mathrm{ATP}})/RT\right)$ for three values of ΔG_{ATP}. The first value of ΔG_{ATP} is $0\,\mathrm{kJ\,mol_{ATP}^{-1}}$, which removes the energetic cost of making ATP from the calculation, leaving it in the form of earlier models such as that of Hoh and Cord-Ruwisch [67]. The other two values of ΔG_{ATP} used are $55\,\mathrm{kJ\,mol_{ATP}^{-1}}$ and $75\,\mathrm{kJ\,mol_{ATP}^{-1}}$, corresponding to the approximate minimum and maximum values described earlier.

Eq. (3.3) implies

$$\exp \frac{\Delta G_T^o + \eta \Delta G_{\mathrm{ATP}}}{RT} = \frac{\theta}{Q}.$$

By plotting the experiment values for $1/Q$ against the model calculated values for $\exp \frac{\Delta G_T^o + \eta \Delta G_{\mathrm{ATP}}}{RT}$ we can easily identify the line corresponding to $\theta = 1$ ($y = x$ in Figures 3.2 and 3.3). A value that is on this line corresponds to shutdown due to thermodynamic inhibition. For the $S_{\min}$ data, values should ideally lie on the line because the concentrations were recorded at the threshold. In contrast, the K_{app} data has concentrations that were recorded when the reaction rate was at half of its maximum value, which is non-zero, so we do not expect the K_{app} data to fall on the line. Instead, we expect it to be slightly below the line, which corresponds to maximising the rate without reaching thermodynamic shutdown. The value of ΔG_{ATP} affects the position of a point and can determine whether it is above, below, or on the line. If the optimal value of ΔG_{ATP} is different for the $S_{\min}$ and K_{app} data, which are two fundamentally different situations for the microbe to be in, it suggests that a rate where ΔG_{ATP} is variable is an improvement.

The $S_{\min}$ data is given in Figure 3.2. We can see that ignoring the energy cost to produce ATP ($\Delta G_{ATP} = 0$) estimates values that are noticeably further from the centre line ($\theta = 1$) than either of the other ΔG_{ATP} values. This shows a benefit of the Lynch *et al.* rate compared to the Hoh and Cord-Ruwisch rate, regardless of the choice for the value of ΔG_{ATP}. Using

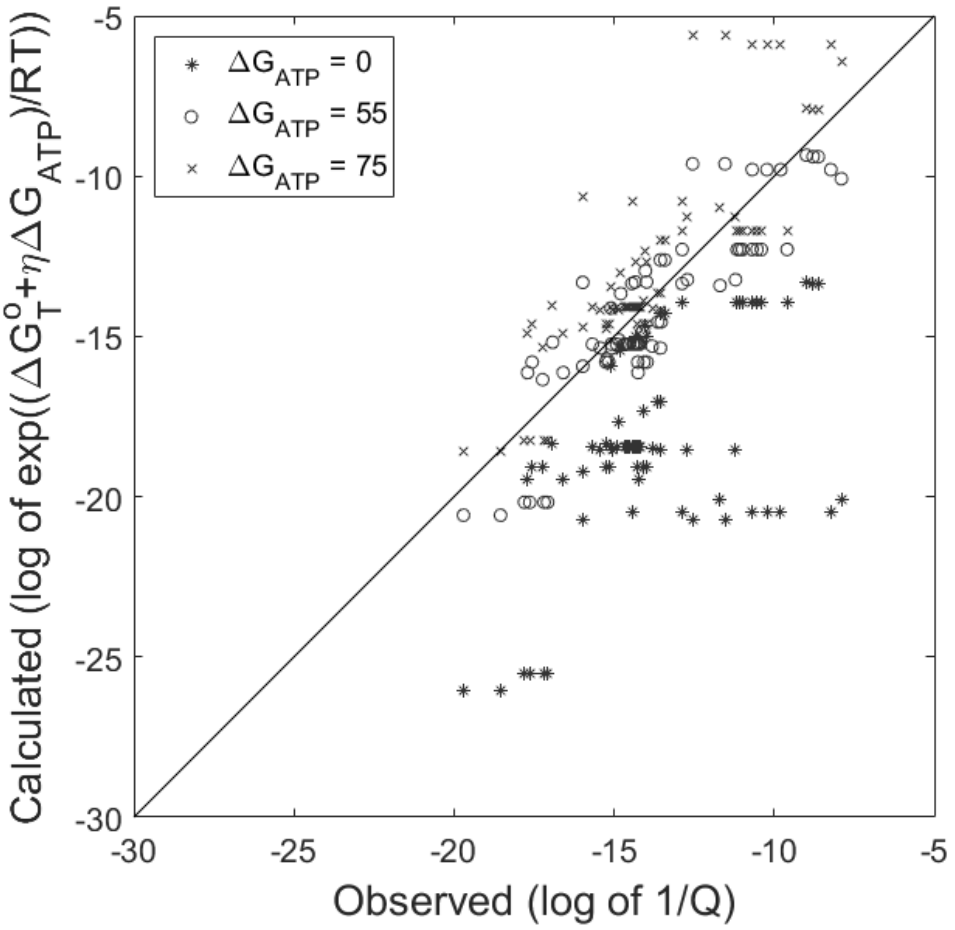

Figure 3.2: Plot of the $S_{\min}$ data comparing $1/Q$ for each experiment to $\exp\left(\left(\Delta G_T^o + \eta \Delta G_{\mathrm{ATP}}\right)/RT\right)$ with three different values of ΔG_{ATP}.

$\Delta G_{\mathrm{ATP}} = 75\,\mathrm{kJ\,mol}_{\mathrm{ATP}}^{-1}$ tends to over-correct and, on average, the calculations using $\Delta G_{\mathrm{ATP}} = 55\,\mathrm{kJ\,mol}_{\mathrm{ATP}}^{-1}$ tend to be closer to the line. This observation is quantified more formally by using the L2 norm to measure the departure from the line. These norm values are shown in Table 3.1. Here, the norm value for $\Delta G_{\mathrm{ATP}} = 0\,\mathrm{kJ\,mol}_{\mathrm{ATP}}^{-1}$ is much larger than the norm values for the other two, further reinforcing the benefit of using the Lynch *et al.* rate compared to the rate of Hoh and Cord-Ruwisch. Note also that the value for $55\,\mathrm{kJ\,mol}_{\mathrm{ATP}}^{-1}$ is smaller than that for $75\,\mathrm{kJ\,mol}_{\mathrm{ATP}}^{-1}$. Note that this figure presents log transformed data, as do others later in the chapter. While this does have the effect of reducing the apparent scale of differences from the centre line or from other data points which decreases the apparent size of outliers, it also shows the trend far more readily and allows us to use the whole dataset without the figures being

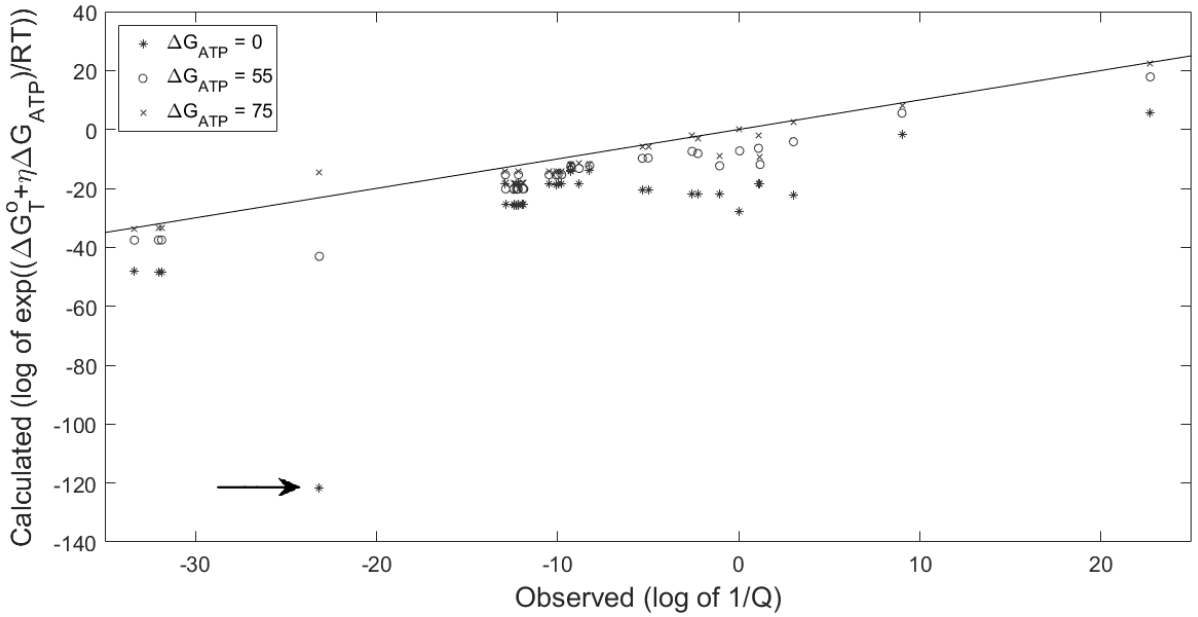

Figure 3.3: Plot of the K_{app} data comparing $1/Q$ for each experiment to $\exp\left(\left(\Delta G_T^o + \eta \Delta G_{\mathrm{ATP}}\right)/RT\right)$ with three different values of ΔG_{ATP}. The outlier discussed in the text is marked with an arrow.

dominated by a small number of extreme points.

Figure 3.3 shows the results when estimating K_{app} data. Figure 3.4 increases readability by ignoring the large outlier at about (-23,-121) when setting the axes. As for the S_{min} data, the points corresponding to $\Delta G_{\mathrm{ATP}} = 0\,\mathrm{kJ\,mol}_{\mathrm{ATP}}^{-1}$ are clearly further from the line than those for the other values of ΔG_{ATP}. Note that the points for $\Delta G_{\mathrm{ATP}} = 75\,\mathrm{kJ\,mol}_{\mathrm{ATP}}^{-1}$ are the closest, with many points lying very close to the line. The L2 norm values in Table 3.1 quantify these observations. One might question the impact of the outlier on the relative values for the L2 norms. Table 3.1 lists the norm values with the outlier excluded. We note that although this exclusion certainly reduces the L2 norm for $\Delta G_{\mathrm{ATP}} = 0\,\mathrm{kJ\,mol}_{\mathrm{ATP}}^{-1}$, the hierarchy is preserved and this value is still much larger than the others. The large difference between the norm value for $\Delta G_{\mathrm{ATP}} = 0\,\mathrm{kJ\,mol}_{\mathrm{ATP}}^{-1}$ and the norm values for the other two again highlights the improvement in using a rate that has an $\eta \Delta G_{\mathrm{ATP}}$ term compared to one without such a term.

We can also use least squares methods to find which value of ΔG_{ATP} would put the trend line as close as possible to $y = x$ ($\theta = 1$) for each portion of the dataset. For the S_{min} data this value is approximately $58.8\,\mathrm{kJ\,mol}_{\mathrm{ATP}}^{-1}$ and for the K_{app} data it is approximately $74.6\,\mathrm{kJ\,mol}_{\mathrm{ATP}}^{-1}$.

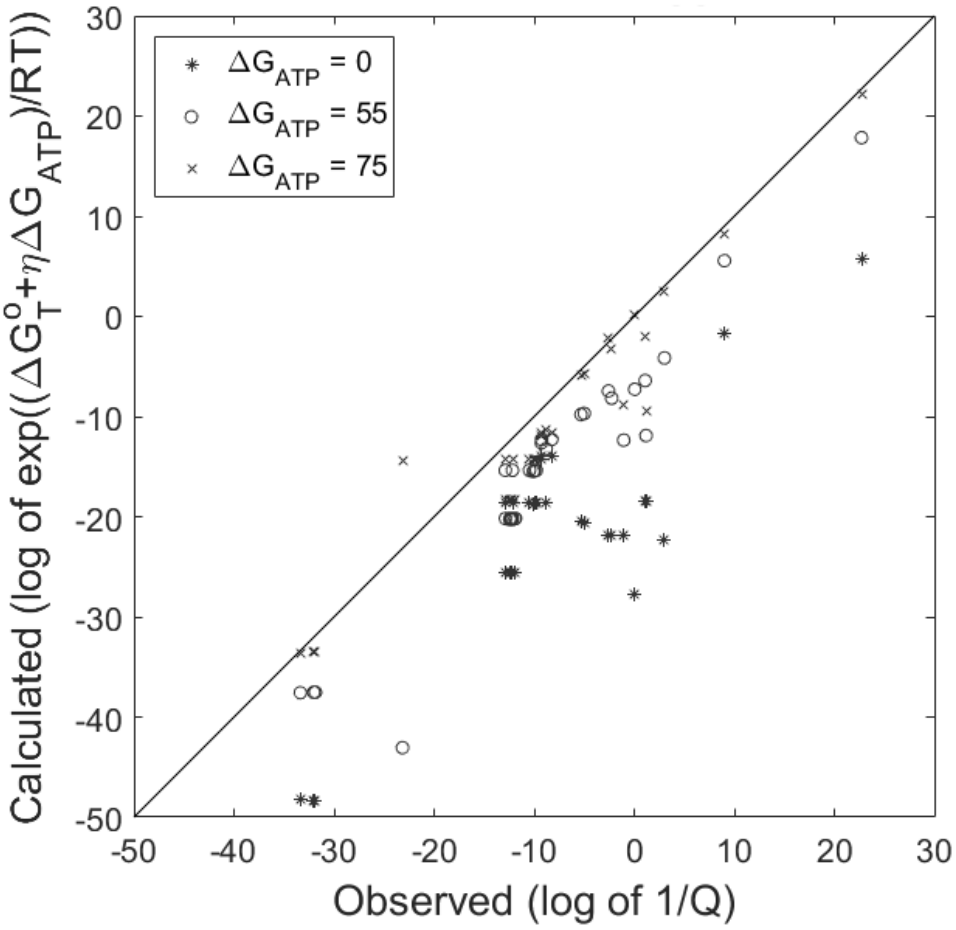

Figure 3.4: Rescaled version of Figure 3.3, ignoring the large outlier.

Further refinement of ΔG_{ATP} values may be possible using such datasets.

We pause here to focus on the experiment containing the outlier in Figure 3.3 (due to the size of the outlier when $\Delta G_{\mathrm{ATP}} = 0\,\mathrm{kJ\,mol^{-1}_{ATP}}$ and as it has the only point that lies clearly above the line, doing so by a large margin). The microbe in question is *Geobacter sulfurreducens* growing on acetate and fumarate. This is the only experiment in the dataset using this proposed metabolism. The value of η that it used was $3.6\,\mathrm{mol_{ATP}\,mol^{-1}_{substrate}}$. The explanation for the choice for this value of η is given in Appendix B. The size of the outlier above the line for $\Delta G_{\mathrm{ATP}} = 75\,\mathrm{kJ\,mol^{-1}}$ prompted us to return to the biological assumptions that had been made and check if any of them should be reconsidered. Upon further investigation we make the argument that $\eta = 3.3\,\mathrm{mol_{ATP}\,mol^{-1}_{substrate}}$ for this microbe, with justification for this new value

in Appendix B.2. In Figure 3.5 we see the effect of changing η from 3.6 to 3.3 for this microbe is that the predicted value of $\exp\left(\left(\Delta G_T^o + \eta \Delta G_{\mathrm{ATP}}\right)/RT\right)$ using $\Delta G_{\mathrm{ATP}} = 75\,\mathrm{kJ\,mol}_{\mathrm{ATP}}^{-1}$ lands very close to the line $y = x$. The proximity to the line $y = x$ suggests this process produces 3.3 ATP, rather than 3.6, per substrate consumed. Note that this new value of η was suggested based on reconsidering the biological assumptions and then replotting the figure using the new value, resulting in a figure that provided support for the reasoning that led to the new value of $3.3\,\mathrm{mol}_{\mathrm{ATP}}\,\mathrm{mol}_{\mathrm{substrate}}^{-1}$. The model predicts values that are generally a good fit for the data, and prompts us to use the model to test our assumptions. In this case it led to us suggesting a different value for η for *Geobacter sulfurreducens* growing on acetate and fumarate. Hereafter we will use $\eta = 3.3\,\mathrm{mol}_{\mathrm{ATP}}\,\mathrm{mol}_{\mathrm{substrate}}^{-1}$ for the *Geobacter sulfurreducens* reaction. This revised

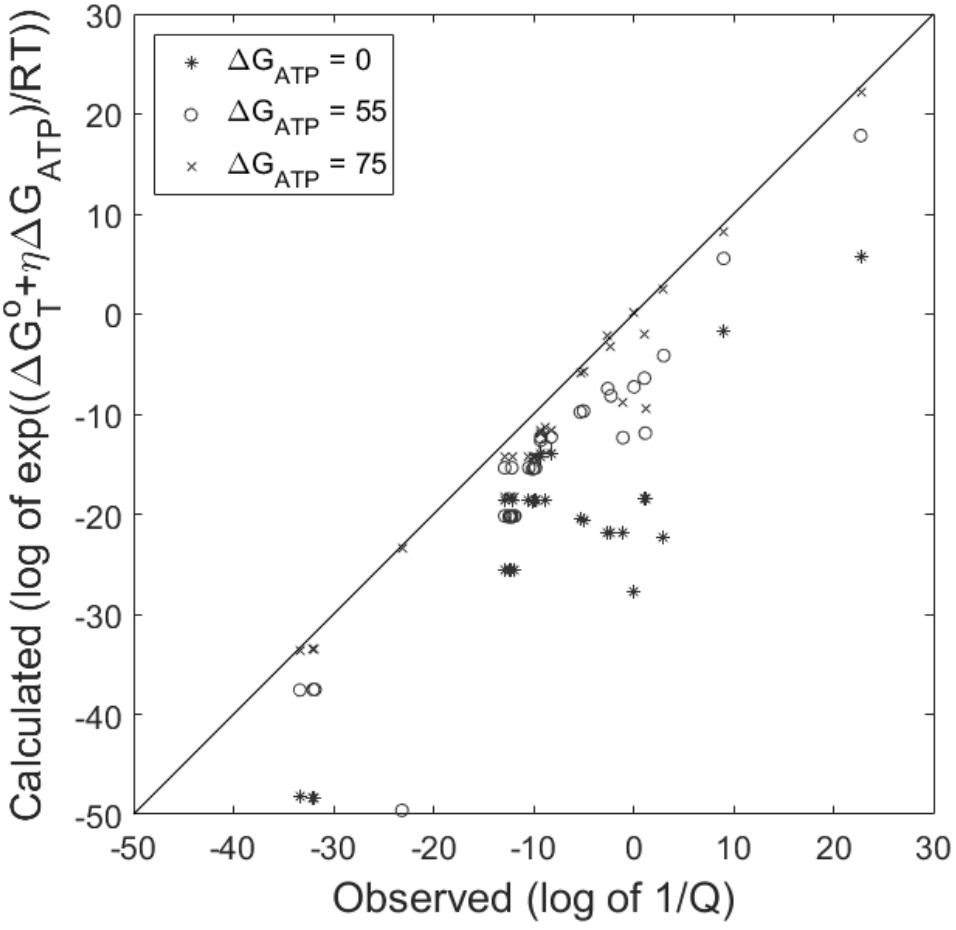

Figure 3.5: Plot of the K_{app} data showing the effect of using $\eta = 3.3\,\mathrm{mol}_{\mathrm{ATP}}\,\mathrm{mol}_{\mathrm{substrate}}^{-1}$ for the *Geobacter sulfurreducens* reaction.

value results in the least squares method for the K_{app} data giving a value of $79.4\,\text{kJ mol}_{\text{ATP}}^{-1}$, rather than the original value of $74.6\,\text{kJ mol}_{\text{ATP}}^{-1}$. We choose to continue using $55\,\text{kJ mol}_{\text{ATP}}^{-1}$ and $75\,\text{kJ mol}_{\text{ATP}}^{-1}$ for the limits on ΔG_{ATP} throughout the rest of our work, noting that available literature values bracket these. We note here that a use of the model could be to estimate η values from data and so to help verify metabolic schemes.

When the concentration is near the threshold, the model supported by the data indicates the best fit is for $\Delta G_{\text{ATP}} = 58.8\,\text{kJ mol}_{\text{ATP}}^{-1}$. In contrast, the best fit for the K_{app} data is $\Delta G_{ATP} = 79.4\,\text{kJ mol}_{\text{ATP}}^{-1}$. Given the size of the data set, this difference in ΔG_{ATP} values supports the claim that the value of ΔG_{ATP} is not constant over the range of substrate concentrations that a microbe could encounter (e.g., S_{min} vs K_{app}). This observation motivates the development of a model for the growth rate that incorporates a variable ΔG_{ATP}. We now investigate a potential avenue for how such changes in ΔG_{ATP} could be incorporated into the rate.

Table 3.1: L2 norms for each choice of ΔG_{ATP} for the S_{min} data and the K_{app} data.

ΔG_{ATP}	$0\,\text{kJ mol}_{\text{ATP}}^{-1}$	$55\,\text{kJ mol}_{\text{ATP}}^{-1}$	$75\,\text{kJ mol}_{\text{ATP}}^{-1}$	n
S_{min}	45.2017	11.8218	16.6230	73
K_{app} (with $\eta = 3.6$)	129.9335	42.2114	25.7717	34
K_{app} (without outlier)	84.7846	37.2261	24.2707	34
K_{app} (with $\eta = 3.3$)	129.9335	45.6642	24.2721	34

3.4 An Optimised Rate

In Section 3.3 it was argued that a microbe could respond to challenging conditions, such as near threshold substrate concentrations, by reducing its ΔG_{ATP} requirement. There is a minimum ΔG_{ATP} value below which the microbe cannot reproduce and a maximum ΔG_{ATP} value above which the ATP synthesis rate is not further increased. In this section we model a rate that reflects these conditions. In particular, we require:

1. The rate is positive provided that $\Delta G_{\text{ATP}} > \Delta G_{\text{ATPmin}}$ where ΔG_{ATPmin} is a given minimum energy at or below which the rate is zero.

2. There is a maximum ΔG_{ATP}, ΔG_{ATPmax}, that the microbe can use. Additional energy beyond this value only impacts the rate through the other thermodynamic term θ.

3. For a given substrate concentration, the microbe will use the value of ΔG_{ATP} that maximises the rate.

The term ΔG_{ATP} is now considered a variable; hence, the thermodynamic term in the Modified Haldane rate, Eq. (2.7), is written

$$\theta(\Delta G_{\mathrm{ATP}}, S) = \frac{\Upsilon}{S} \exp\left(\frac{\eta \Delta G_{\mathrm{ATP}}}{RT}\right)$$

where Υ is positive, has the same dimensions as S, and does not depend on ΔG_{ATP}. We introduce the non-dimensional variables

$$\sigma = \sigma(\Delta G_{\mathrm{ATP}}) = \frac{\eta \Delta G_{\mathrm{ATP}}}{RT}$$

and

$$\nu = \nu\left(\Delta G_{\mathrm{ATP}}\right) = \exp\left(\sigma\right),$$

defining $\sigma_0 = \sigma(\Delta G_{\mathrm{ATPmin}})$ and $\sigma_1 = \sigma(\Delta G_{\mathrm{ATPmax}})$, as well as with $\nu_0 = \nu\left(\Delta G_{\mathrm{ATPmin}}\right)$ and $\nu_1 = \nu\left(\Delta G_{\mathrm{ATPmax}}\right)$. The same extrema will be captured by ν as by ΔG_{ATP} as ν is a strictly increasing function of ΔG_{ATP}. We also introduce the non-dimensional variable

$$u = \frac{S}{\Upsilon},$$

and the non-dimensional constant

$$\kappa = \frac{K_H}{\Upsilon}.$$

In terms of these new quantities, we have $\theta = \nu/u$ and a non-dimensional growth rate q_{ND} given by

$$q_{ND}(\nu, u) = \frac{u - \nu}{\kappa + u + \nu} \tag{3.4}$$

when $u \geq \nu$ and 0 otherwise. If u has a fixed value, q_{ND} decreases as ν increases and so the optimal value of ν that would maximise q_{ND} is always ν_0. If we used q_{ND} for the model described in assumptions 1-3, the microbe would always adjust the value of ΔG_{ATP} to the minimum but

we have assumed the rate to be zero at this value of ΔG_{ATP} in assumption 1. Thus, we are motivated to introduce a "penalty function", $r(\nu)$, that does not increase the rate for $\nu > \nu_1$ ($\Delta G_{\mathrm{ATP}} > \Delta G_{\mathrm{ATPmax}}$), and gives a zero rate for $\nu < \nu_0$ ($\Delta G_{\mathrm{ATP}} < \Delta G_{\mathrm{ATPmin}}$). The simplest way to achieve this is to define the rate $q(\nu, u) = r(\nu)\, q_{ND}(\nu, u)$. Here, we assume r has the following properties:

1. $0 \leq r(\nu) \leq 1$
2. $$r(\nu) = \begin{cases} 0 & \text{if } \nu \leq \nu_0 \\ 1 & \text{if } \nu \geq \nu_1, \end{cases}$$
3. $r(\nu)$ is continuous on $[\nu_0, \nu_1]$ and differentiable on (ν_0, ν_1) with $r'(\nu) > 0$ for all $\nu \in (\nu_0, \nu_1)$, and
4. r is dimensionless.

Together, the first three properties imply that r is monotonic strictly increasing and that $0 < r(\nu) < 1$ for $\nu \in (\nu_0, \nu_1)$. We define the rate q in term of u and ν as

$$q(\nu, u) = \frac{r(\nu)\,(u - \nu)}{\kappa + u + \nu}. \tag{3.5}$$

The rate q has two thermodynamic 'brakes', the zeros of q, that represent two distinct mechanisms. One zero occurs when $u = \nu$ and models the thermodynamic inhibition caused by the presence of products (this is the case $\theta = 1$ in the Modified Haldane rate). The other zero occurs due to r when $\nu = \nu_0$, capturing the assumption that the rate is zero when there is not enough energy available to form ATP even when $\Delta G_{\mathrm{ATP}} = \Delta G_{\mathrm{ATPmin}}$. For any u, $q(\nu_0, u) = 0$ and $q(u, u) = 0$ and

$$0 < q(\nu, u) < 1 \tag{3.6}$$

for $\nu_0 < \nu < u$. This means that for any fixed value of $u > \nu_0$ there exists $\hat{\nu} \in (\nu_0, u)$ such that q achieves its global maximum at $(\hat{\nu}, u)$. We only optimise on ν when q is a function of ν and u because the microbe can "control" its ΔG_{ATP} response but it cannot control the environment (u).

Note that if $\nu > \nu_1$, $r = 1$ so $q(\nu, u) = q_{ND}(\nu, u)$, and

$$\frac{\partial q_{ND}}{\partial \nu} < 0. \tag{3.7}$$

Now q is continuous for $\nu \geq \nu_0$ and Eq. (3.7) implies that for a fixed value of u, a global maximum will be attained and it cannot be attained for $\nu > \nu_1$. This implies that the global maximum must be attained in $(\nu_0, \nu_1]$.

Suppose that $\hat{\nu} \in (\nu_0, \nu_1)$, then

$$\frac{\partial}{\partial \nu} q(\hat{\nu}, u) = 0. \tag{3.8}$$

We have

$$\frac{\partial}{\partial \nu} q(\nu, u) = \left(\frac{r'(\nu)}{r(\nu)} - \frac{\kappa + 2u}{(u - \nu)(\kappa + u + \nu)} \right) q(\nu, u),$$

and Eqs. (3.6) and (3.8), imply that

$$\frac{r'(\nu)}{r(\nu)} - \frac{\kappa + 2u}{(u - \nu)(\kappa + u + \nu)} = 0. \tag{3.9}$$

Let

$$b(\nu) = \frac{r(\nu)}{r'(\nu)}. \tag{3.10}$$

Then Eq. (3.9) can be recast as

$$u^2 + u\left(\kappa - 2b(\nu)\right) - \left(b(\nu)\kappa + \nu\kappa + \nu^2\right) = 0. \tag{3.11}$$

Now u must be non-negative, hence,

$$u(\nu) = \frac{1}{2}\left(2b(\nu) - \kappa + \sqrt{\left(2b(\nu) - \kappa\right)^2 + 4\left(b(\nu)\kappa + \nu\kappa + \nu^2\right)} \right). \tag{3.12}$$

Eq. (3.12) shows that given any $\nu \in (\nu_0, \nu_1)$ there is exactly one value of u that maximises the rate. This is an implicit relation for $\hat{\nu}$. We would prefer to know if, given a value of u, there is a unique value of ν that maximises the rate. We note that if r is such that $u'(\nu) > 0$ then there

will be a unique ν that maximises the rate for a fixed value of u. We have

$$u'(\nu) = b'(\nu) + \frac{\kappa + 2\nu + 2b(\nu)b'(\nu)}{\sqrt{(2b(\nu) - \kappa)^2 + 4\left(b(\nu)\kappa + \nu\kappa + \nu^2\right)}}. \tag{3.13}$$

The condition is satisfied if, for example, $r''(\nu) \leq 0$ for $\nu \in (\nu_0, \nu_1)$ because

$$b'(\nu) = \left(\frac{r(\nu)}{r'(\nu)}\right)' = 1 - b(\nu)\frac{r''(\nu)}{r'(\nu)},$$

so that $b'(\nu) > 0$ and hence $u'(\nu) > 0$ by Eq. (3.13).

Theorem 1 *Let q be defined as in Eq. (3.5), where r has the properties 1-4. For a fixed value of u, there is a $\hat{\nu} \in (\nu_0, \nu_1]$ at which q assumes its global maximum. If the maximum occurs in (ν_0, ν_1), then Eq. (3.8) is satisfied and thus $\hat{\nu}$ is a solution to Eq. (3.12). A sufficient (but not necessary) condition for Eq. (3.12) to have a unique solution, $\hat{\nu}$, is*

$$r''(\nu) \leq 0, \tag{3.14}$$

for all $\nu \in (\nu_0, \nu_1)$. If the maximum occurs at ν_1 then the above inequality also ensures that the global maximum occurs only at ν_1.

We note that any property of r that ensures $u'(\nu) > 0$ will lead to a unique maximum location. This condition is not necessary for uniqueness and certainly the condition in Eq. (3.14) is not necessary.

3.4.1 q_{ATP}

The rate q_{ATP} is non-dimensional and is defined for a given u as

$$q_{\mathrm{ATP}}(u) = \max_{\nu \in (\nu_0, \nu_1]} q(\nu, u) \tag{3.15}$$

with q given in Eq. (3.5). There are two cases to consider: $\hat{\nu} \in (\nu_0, \nu_1)$ or $\hat{\nu} = \nu_1$.

If the maximum occurs at some $\hat{\nu} \in (\nu_0, \nu_1)$ then Eq. (3.9) is satisfied at $\hat{\nu}$ and yields

$$q(\hat{\nu}, u) = r'(\hat{\nu})(u - \hat{\nu}) - r(\hat{\nu}).$$

Eq. (3.12) shows that $\hat{\nu}$ depends on the choice of u, so that if we regard u now as variable, then $\hat{\nu} = \nu(u)$, and

$$q_{\mathrm{ATP}}(u) = r'(\hat{\nu}(u))(u - \hat{\nu}(u)) - r(\hat{\nu}(u)),$$

where $'$ still denotes $d/d\nu$. We let κ_{app} denote the value of u that produces $q_{\mathrm{ATP}}(u) = 1/2$, the non-dimensional K-apparent. In this case where the maximum occurs in the interior, the value of κ_{app} is given implicitly as the solution $u = \kappa_{\mathrm{app}}$ to

$$\frac{1}{2} = r'(\hat{\nu}(u))(u - \hat{\nu}(u)) - r(\hat{\nu}(u)).$$

If the maximum occurs at the endpoint ν_1, then $r(\nu_1) = 1$, so that

$$q_{\mathrm{ATP}}(u) = \frac{u - \nu_1}{\kappa + u + \nu_1},$$

and

$$\kappa_{\mathrm{app}} = \kappa + 3\nu_1$$

which is effectively the case studied for the Modified Haldane rate discussed in Chapter 2.

Eq. (3.12) defines a curve $u = u(\hat{\nu})$ for $\hat{\nu} \in [\nu_0, \nu_1]$ that represents, for a given value of u near the threshold, the ATP requirement $\hat{\nu}$ of the microbe for a maximal rate. We call this curve the *optimal curve*. Assuming that $u'(\hat{\nu}) > 0$, we can use the inverse function theorem to get (at least in theory) $\hat{\nu}$ as a function of u. This is what was assumed implicitly in the calculations for q_{ATP} and κ_{app}. Under this assumption, the optimal curve has a positive slope and increases from $u(\nu_0) = \nu_0$ to $u(\nu_1)$. The optimal curve lies above the line defined by $u = \nu$, which is where the rate is zero, intersecting only at the point (ν_0, u_0). Figure 3.6 depicts a typical optimal curve with non-dimensional variables, recall that $\sigma = \frac{\eta \Delta G_{\mathrm{ATP}}}{RT}$ and $u = \frac{S}{\Upsilon}$. The point (ν_0, u_0) corresponds to the threshold ($u > u_0 = \nu_0$ for a positive rate); the other endpoint $(\nu_1, u(\nu_1))$ is

the point at which the rate q_{ATP} is maximised by ν_1 for all values of $u \geq u(\nu_1)$.

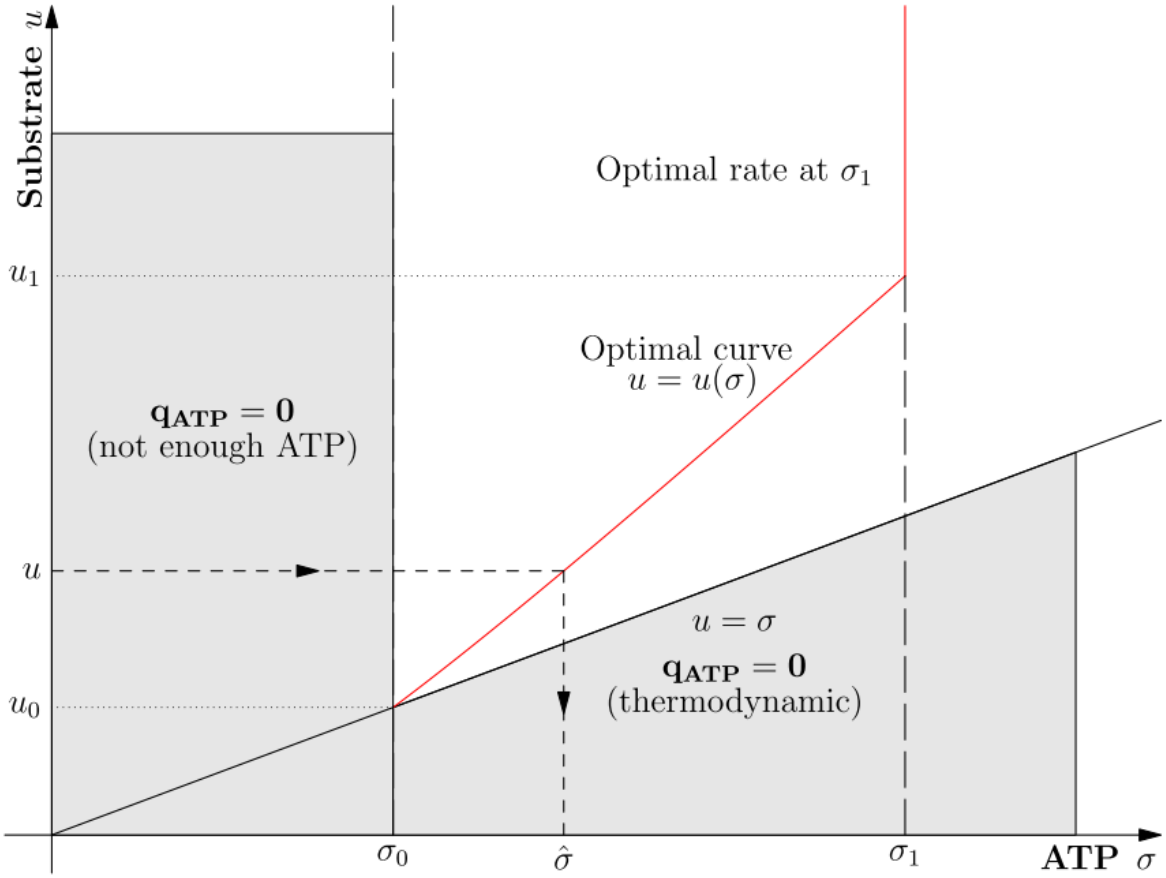

Figure 3.6: A typical optimal curve with non-dimensional variables, $u = u(\nu)$.

3.4.2 Continuity of the Derivative of q_{ATP}

The rate q is as given in Eq. (3.5) which we could recast as

$$q_{\mathrm{ATP}}(u) = \begin{cases} r(\nu(u))q_{ND}(\nu, u) & \text{if } u \leq u_1 \\ q_{ND}(\nu, u) & \text{if } u > u_1, \end{cases}$$

where q_{ND} is

$$q_{ND}(\nu, u) = \frac{u - \nu}{\kappa + u + \nu}$$

as in Eq. (3.4). We expect that the rate should be smooth (i.e., it should have a continuous derivative with respect to the substrate concentration). We know that

$$\frac{\partial}{\partial \nu}\left(r(\nu) q_{ND}(\nu, u)\right) = 0, \tag{3.16}$$

where $\frac{\partial}{\partial \nu}$ indicates that u is held fixed. We also know that

$$q_{\mathrm{ATP}}(u) = \frac{u - \nu_1}{\kappa + u + \nu_1},$$

for $u > u_1$, where $\nu(u_1) \equiv \nu_1$. Note that $\nu(u) \equiv \nu_1$ for all $u \geq u_1$.

Consider the derivative

$$\begin{aligned}\frac{d}{du}\left(r(\nu) q_{ND}(\nu, u)\right) &= \frac{\partial}{\partial u}\left(r(\nu) q_{ND}(\nu, u)\right) + \frac{\partial}{\partial \nu}\left(r(\nu) q_{ND}(\nu, u)\right) \nu'(u) \\ &= r(\nu) \frac{\partial}{\partial u} q_{ND}(\nu, u).\end{aligned} \tag{3.17}$$

Note that the second term vanishes due to Eq. (3.16) if $u \neq u_1$. At u_1, we have $r(\nu(u_1)) = r(\nu_1) = 1$; hence, from "below"

$$\lim_{u \to u_1^-}\left(\frac{d}{du}\left(r(\nu) q_{ND}(\nu, u)\right)\right) = \lim_{u \to u_1^-}\left(\frac{\partial}{\partial u} q_{ND}(\nu_1, u)\right)$$

and from "above"

$$\lim_{u \to u_1^+}\left(\frac{d}{du}\left(q_{ND}(\nu, u)\right)\right) = \lim_{u \to u_1^+}\left(\frac{\partial}{\partial u} q_{ND}(\nu_1, u)\right).$$

The limits agree and so the derivative is continuous at $u = u_1$, the upper limit of the substrate concentration where the penalty function affects the rate. Note that the continuity of the derivative uses only properties 1-4 for r.

3.4.3 A Choice of r

There are many choices for r because properties 1-4 are not very restrictive. In this section we choose a function r that leads to a more tractable optimisation problem. Specifically, let

$$r_L = \frac{\theta - \theta_0}{\theta_1 - \theta_0} = \frac{e^{\sigma} - e^{\sigma_0}}{e^{\sigma_1} - e^{\sigma_0}} = \frac{\nu - \nu_0}{\nu_1 - \nu_0}, \tag{3.18}$$

where

$$\theta = Q \exp \frac{\Delta G_T^o + \eta \Delta G_{\text{ATP}}}{RT},$$

as in Eq. (3.3), $\theta_1 = \theta(\Delta G_{\text{ATPmax}})$, $\theta_0 = \theta(\Delta G_{\text{ATPmin}})$, $\sigma = \frac{\eta \Delta G_{\text{ATP}}}{RT}$, and $\nu = \exp(\sigma)$.

We want to maximise

$$h(\sigma) = r_L \cdot \frac{S(1-\theta)}{K_{\text{Lynch}} + S(1+\theta)}, \tag{3.19}$$

with respect to σ. Defining $\zeta = \frac{S\theta}{\nu}$ allows us to restate Eq. (3.19) as

$$h(\sigma) = r_L \cdot \frac{S - \zeta e^{\sigma}}{K_{\text{Lynch}} + S + \zeta e^{\sigma}}. \tag{3.20}$$

Maximising Eq. (3.20) with respect to σ involves solving

$$\frac{d}{d\sigma}\left(\frac{(e^{\sigma} - \nu_0)(S - \zeta e^{\sigma})}{K_{\text{Lynch}} + S + \zeta e^{\sigma}}\right) = 0. \tag{3.21}$$

The positive solution occurs when

$$e^{\sigma} = \frac{-(K_{\text{Lynch}} + S) + \sqrt{(K_{\text{Lynch}} + S)^2 + \zeta K_{\text{Lynch}} \nu_0 + 2\zeta S \nu_0 + K_{\text{Lynch}} S + S^2}}{\zeta}. \tag{3.22}$$

So

$$\sigma = \ln\left(\frac{-(K_{\text{Lynch}} + S) + \sqrt{(K_{\text{Lynch}} + S)^2 + \zeta K_{\text{Lynch}} \nu_0 + 2\zeta S \nu_0 + K_{\text{Lynch}} S + S^2}}{\zeta}\right), \tag{3.23}$$

and

$$\Delta G_{\mathrm{ATP}} = \frac{RT \ln\left(\frac{-(K_{\mathrm{Lynch}}+S)+\sqrt{(K_{\mathrm{Lynch}}+S)^2+\zeta K_{\mathrm{Lynch}}\nu_0+2\zeta S\nu_0+K_{\mathrm{Lynch}}S+S^2}}{\zeta}\right)}{\eta} \tag{3.24}$$

For a particular set of values, if $\Delta G_{\mathrm{ATP}} \leq \Delta G_{\mathrm{ATPmin}}$, then the ATP production will shut down; if the value of $\Delta G_{\mathrm{ATP}} > \Delta G_{\mathrm{ATPmax}}$, then $\Delta G_{\mathrm{ATP}} = \Delta G_{\mathrm{ATPmax}}$. It is between these bounds that the penalty function, r_L is operating. For fixed product concentrations, we can calculate the upper and lower bounds for S where the penalty function operates (i.e., the range of S for which ΔG_{ATP} varies to maximise $r_L \cdot q_{\mathrm{ATP}}$). Rearranging Eq. (3.22) to solve for the positive value of S gives

$$S = \frac{1}{2}\left[(2\zeta\nu - 2\zeta\nu_0 - K_{\mathrm{Lynch}}) + \sqrt{(2\zeta\nu - 2\zeta\nu_0 - K_{\mathrm{Lynch}})^2 + 4(\zeta^2\nu + 2\zeta K_{\mathrm{Lynch}}\nu - \zeta K_{\mathrm{Lynch}}\nu_0)}\right]. \tag{3.25}$$

The upper and lower bounds for S where the penalty function operates can be found using Eq. (3.25) when $\nu = \nu_1$ and $\nu = \nu_0$. For example, we can find the bounds on S of the region where the penalty function optimises ΔG_{ATP} for the reaction from Lynch *et al.* (2019) [108]. This reaction is

$$[\mathrm{H_2}] + \frac{1}{4}[\mathrm{CO_2}] \rightarrow \frac{1}{4}[\mathrm{CH_4}] + \frac{1}{2}[\mathrm{H_2O}], \tag{3.26}$$

where $S = [\mathrm{H_2}]$ is the limiting substrate. The parameter values are given in Table 3.2. The bounds are calculated to be $1.37 \times 10^{-8}\,\mathrm{mol\,L^{-1}}$ and $2.86 \times 10^{-7}\,\mathrm{mol\,L^{-1}}$. This is shown in Figure 3.7.

In Section 3.3 we looked at data of two types. The "threshold data" showed that $\Delta G_{\mathrm{ATP}} = \Delta G_{\mathrm{ATPmin}}$ produces a better fit; whereas, the "K_{app} data" showed that $\Delta G_{\mathrm{ATP}} = \Delta G_{\mathrm{ATPmax}}$ is the better fit. This motivates the question about whether K_{app} occurs when $\Delta G_{\mathrm{ATP}} < \Delta G_{\mathrm{ATPmax}}$. For our choice of penalty function, r_L, we can investigate where K_{app} occurs for the reaction used by Lynch *et al.* (2019) [108] by finding $h(\sigma_1)$. Note that $r_L(\sigma_1) = 1$ so $h(\sigma_1) = \frac{S-\zeta\exp(\sigma_1)}{K_{\mathrm{Lynch}}+S+\zeta\exp(\sigma_1)}$ and so the choice of r does not appear directly in $h(\sigma_1)$ but is relevant in the calculation of S. We find that the rate is approximately 0.220, which is clearly less than 0.5. In this case K_{app} occurs when $\Delta G_{\mathrm{ATP}} = \Delta G_{\mathrm{ATPmax}}$. This is consistent with our

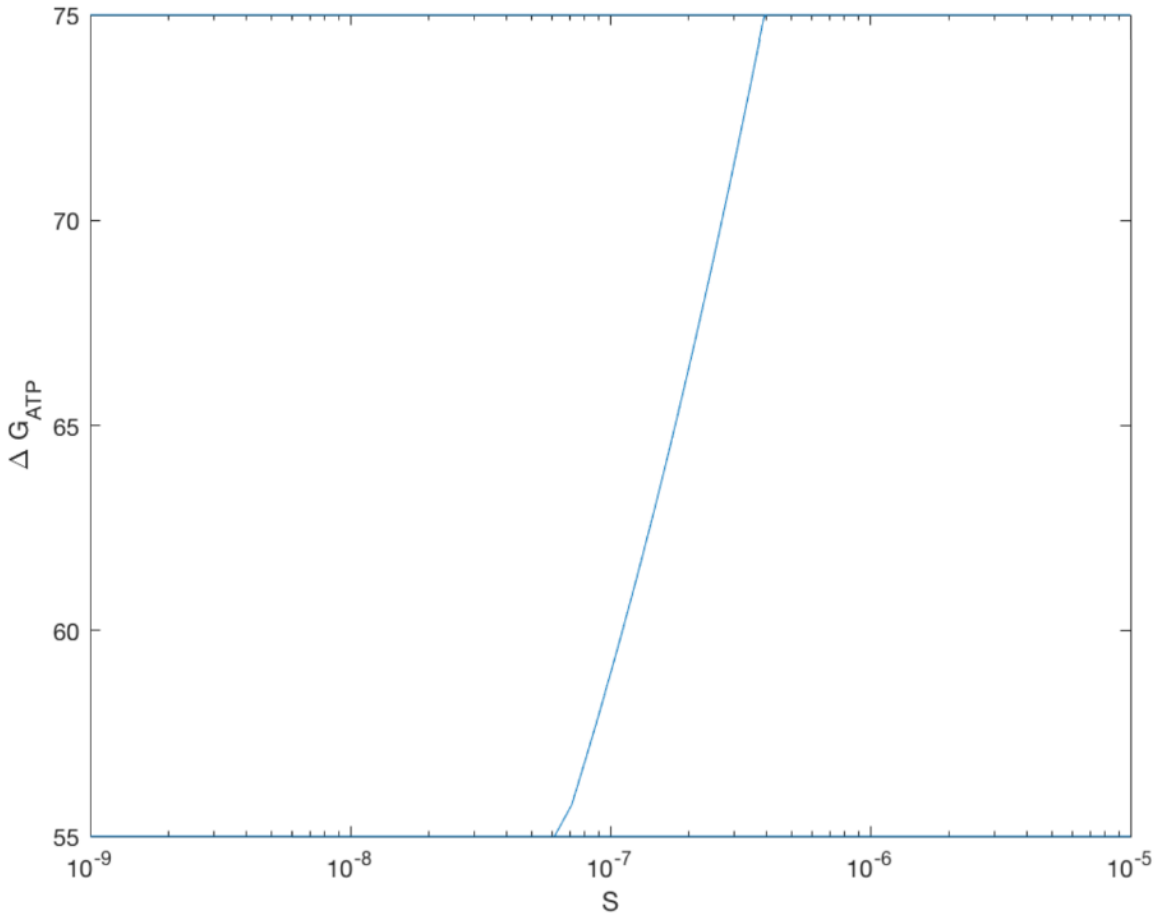

Figure 3.7: The value of ΔG_{ATP} that maximises $r_L \cdot q_{\max} \frac{S-\zeta\nu}{K_{\mathrm{Lynch}}+S+\zeta\nu}$ with parameter values taken from Lynch *et al.* [108].

results in Section 3.3.

3.5 Results

Earlier we used the dataset that we had collated in order to justify why a rate that allows ΔG_{ATP} to change seems appropriate. Now that we have explored the penalty function and selected a form which is mathematically convenient and biologically reasonable, we can use the form of the rate q to compare the substrate concentration that was reported from each experiment to what the substrate concentration would be for the reaction to be at $S_{\min}$ or K_{app}.

For the $S_{\min}$ data, we are looking for the largest substrate concentration where the rate is 0. The threshold with a fixed value of ΔG_{ATP} is lower for lower values of ΔG_{ATP}. Due

Table 3.2: Parameter values for reaction from Lynch *et al.* [108], shown here in Eq. (3.26).

Symbol	Description	Value
ΔG_T^o	Gibbs free energy change for the reaction	$-47.81\,\mathrm{kJ\,mol^{-1}}$
$[CH_4]$	Dissolved methane concentration	$3.56 \times 10^{-4}\,\mathrm{mol\,L^{-1}}$
$[CO_2]$	Dissolved carbon dioxide concentration	$5.9 \times 10^{-2}\,\mathrm{mol\,L^{-1}}$
η	ATP production per mole of substrate	$0.15\,\mathrm{mol_{ATP}\,mol^{-1}_{substrate}}$
R	Ideal gas constant	$8.314 \times 10^{-3}\,\mathrm{kJ\,mol^{-1}\,K^{-1}}$
T	Temperature	312 K
K_{Lynch}	Modified Haldane constant	$2 \times 10^{-7}\,\mathrm{mol\,L^{-1}}$

to the penalty function and the variable ΔG_{ATP}, the threshold would occur when ΔG_{ATP} is at its minimum value, i.e., $\Delta G_{ATP} = 55\,\mathrm{kJ\,mol^{-1}_{ATP}}$. Mathematically, the threshold due to thermodynamic shutdown with ΔG_{ATP} at its minimum occurs at a substrate concentration that can be found by making S the subject of the equation $\theta = 1$, i.e.,

$$S_{\mathrm{min}} = \frac{P_1^{p_1} P_2^{p_2} ... P_n^{p_n}}{S_2^{s_2} S_3^{s_3} ... S_m^{s_m}} \cdot \exp\left(\frac{\Delta G_T^o + \eta \Delta G_{\mathrm{ATPmin}}}{RT}\right) \tag{3.27}$$

for the reaction

$$S_1 + s_2 S_2 + s_3 S_3 + ... + s_m S_m \rightarrow p_1 P_1 + p_2 P_2 + ... + p_n P_n.$$

Everything in the RHS of Eq. (3.27) is known, so we calculate a theoretical value for S_{min} in the prevailing conditions and compare it to the value that was reported. The results of these calculations are shown in Figure 3.8. The data are clustered close to the line $y = x$ and the correlation coefficient between $\log(S_{\mathrm{measured}})$ and $\log(S_{\mathrm{calculated}})$ is approximately 0.9376.

For the K_{app} data, we are looking for what the substrate concentration would have to be in order for the rate to be half of its maximal value in the prevailing conditions.

$$q_{\mathrm{rel}} = \frac{q}{q_{\mathrm{max}}} = \frac{\nu - \nu_0}{\nu_1 - \nu_0} \cdot \frac{S - \zeta\nu}{K_{\mathrm{Lynch}} + S + \zeta\nu} \tag{3.28}$$

We cannot analytically solve Eq. (3.28) for S at a particular value of q_{rel} (e.g., at 0.5) due to the variable nature of ΔG_{ATP} in the ν terms. We solve this problem numerically. For each experiment: we take a range of values of ΔG_{ATP}, equally spaced between the maximum

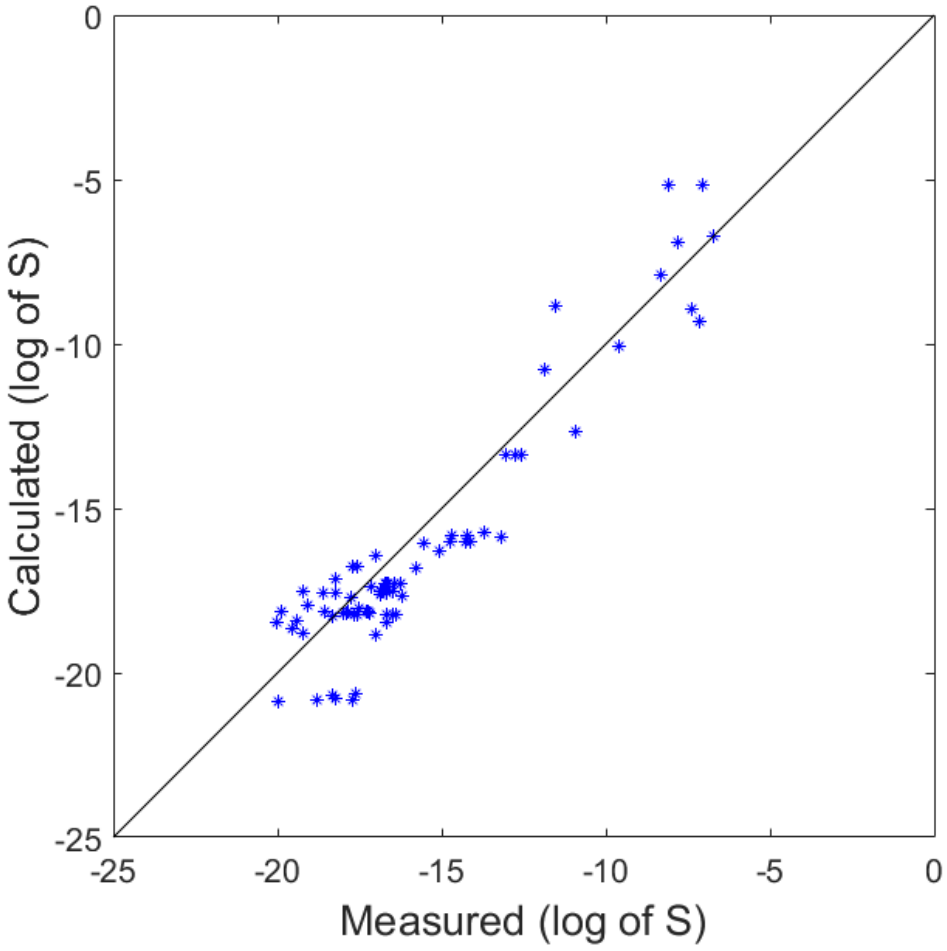

Figure 3.8: Plot of the S_{min} data showing the reported (measured) value of S in each experiment compared to the value of S calculated in the prevailing conditions according to Eq. (3.27).

and minimum values; and a range of values of S, equally spaced between multiple orders of magnitude below the reported value and multiple orders of magnitude above the reported value. We make a matrix where each entry is q_{rel} calculated in the prevailing conditions for a particular choice of ΔG_{ATP} and S. We record the largest value of q_{rel} for each value of S, along with what value of ΔG_{ATP} it corresponded to, and then find which substrate concentration gave the closest relative rate to 0.5. It was this substrate concentration that was recorded as the calculated value. Figure 3.9 shows the results of this process using 201 values of ΔG_{ATP} between $55\,\mathrm{kJ\,mol}_{\mathrm{ATP}}^{-1}$ and $75\,\mathrm{kJ\,mol}_{\mathrm{ATP}}^{-1}$ and 1000000 values of S equally spaced between four orders of magnitude below the reported value and two orders of magnitude above the reported value. Apart from one clear outlier at about $(-7.5, -14)$, the rest of the data is clustered close to the line $y = x$

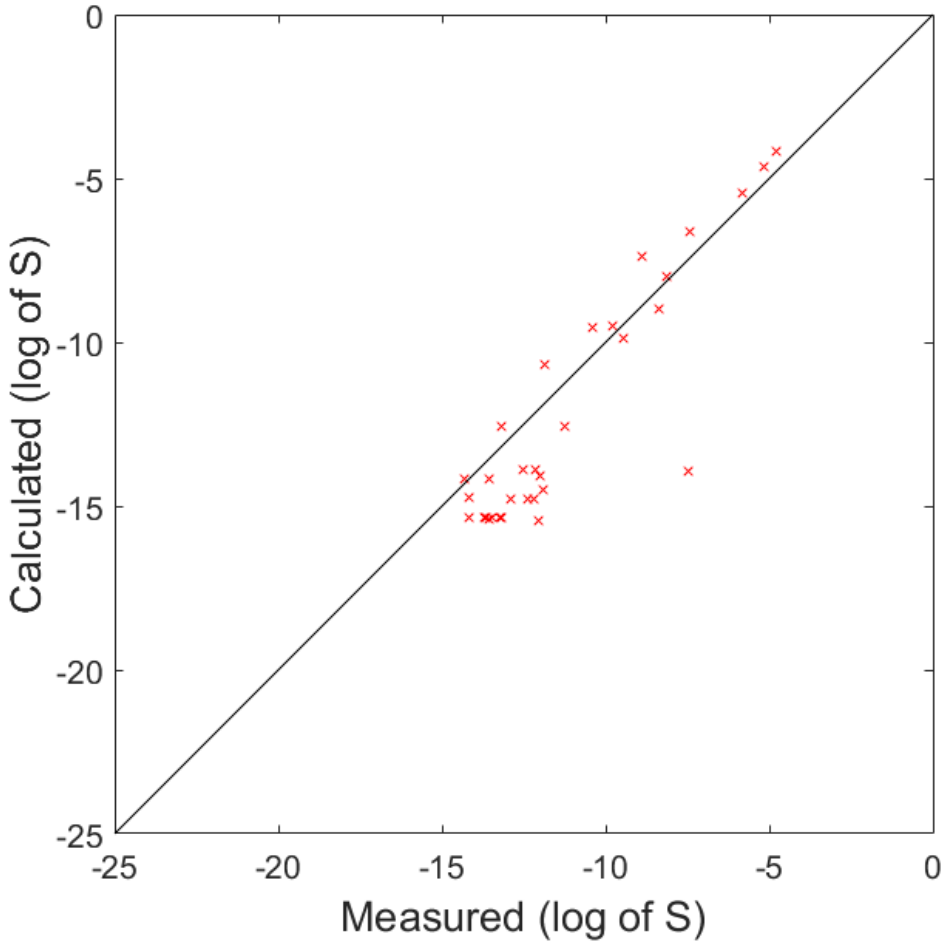

Figure 3.9: Plot of the K_{app} data showing the reported (measured) value of S in each experiment compared to the value of S calculated in the prevailing conditions according to Eq. (3.28).

and the correlation coefficient between $\log(S_{\mathrm{measured}})$ and $\log(S_{\mathrm{calculated}})$ is approximately 0.9100. As noted in the previous section, it has not yet been proven whether K_{app} occurs outside the optimisation region for a general choice of r, but it is worth noting that the method used to find the calculated substrate concentration for K_{app} determined that the optimal value of ΔG_{ATP} was $75\,\mathrm{kJ\,mol}_{\mathrm{ATP}}^{-1}$ for all 34 experiments. Given the wide variety of microbes and reactions in the 34 experiments, this result again suggests that K_{app} falls outside the region where the optimisation occurs for our choice of r_L.

As both portions of the analysis are built upon the same rate, we plot all the data together, shown in Figure 3.10. Together, the fit to the line $y = x$ appears strong and the correlation coefficient for the full dataset is approximately 0.9400. This shows that our model, with the

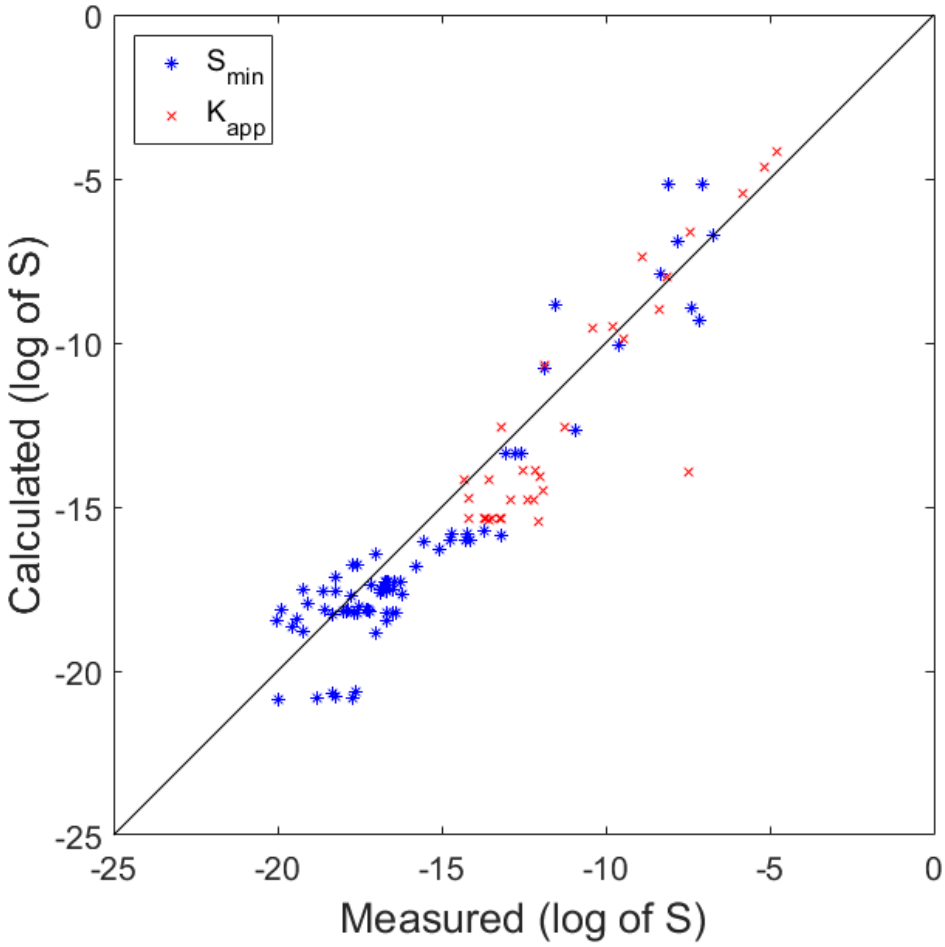

Figure 3.10: Combination of both Figures 3.8 and 3.9.

penalty function and variable ΔG_{ATP} is effective at predicting the substrate concentration for an experiment that is either at the threshold or at K_{app}.

In this chapter we have: discussed ΔG_{ATP}; used a dataset collated from literature to justify a rate having different values of ΔG_{ATP} in different situations; explored how the variable ΔG_{ATP} could appear in the rate and suggested an appropriate form; and compared the reported substrate concentrations to predicted values calculated using the rate. We acknowledge that the form for the penalty function that we used was chosen because it is mathematically convenient and biologically reasonable. The choice we made gives sensible results. A different r might be less mathematically tractable but give more biologically appropriate results. It is beyond the scope of this project to explore other possible forms and it is left as an avenue for future work. Thus

far we have only used the rate with the penalty function at particular points of a reaction (i.e., the threshold and the half-maximal growth rate). In the next chapter we investigate the performance of the rate in more dynamic examples.

Chapter 4

Validation

As noted earlier, we expect that a model should exhibit behaviour that is qualitatively the same as is seen experimentally. The model should be able to predict this behaviour before the experiment takes place or even give insights into the outcomes of experiments or into the likely outcomes of experiments that cannot (yet) be performed, rather than only being fitted to data to yield parameter values for experiments that have already been carried out. This predictive nature of the model, rather than simply being descriptive, will make it much more widely applicable. In this chapter we explore the behaviour of the optimised rate, described in Chapter 3, when used for modelling three different examples of microbes growing using different metabolic reactions where experimental data are available. We start with modelling a batch culture of a microbe using malonate as a substrate where thermodynamic inhibition was expected to have very little effect. We then consider another batch culture of a microbe growing using crotonate where thermodynamic inhibition has previously been postulated, before modelling continuous cultures for two different microbes growing with glutamate, exploring the microbes in isolation and in competition with each other. These different examples that we explore show the versatility of the model and the final example, in addition to qualitatively reproducing what had been found experimentally, allows us to make predictions about coexistence for microbes growing in competition with each other, which we wouldn't find by attempting to solve the system analytically.

4.1 Batch Culture with Negligible Thermodynamic Inhibition

We first consider a microbe growing in a batch culture using malonate according to the reaction

$$C_3H_3O_4^- \rightarrow C_2H_3O_2^- + CO_2, \tag{4.1}$$

as described by Janssen [73], where 0.3 mol of ATP is produced for each mol of malonate that is broken down into acetate and carbon dioxide, as explained in Appendix B.3. We will use the term malonate to designate $C_3H_3O_4^-$, the singly dissociated form of this dicarboxylic acid. This can also be written as Hmalonate$^-$ to denote that only one of the carboxylic acid groups is dissociated. Figures 1 (a)-(c) of Janssen [73] present data for the growth of three strains of microbes on malonate. These are repeated in Figures 4.1-4.3, where optical density is a measure of microbial biomass, and the data can be found in Tables C.1-C.3 in Appendix C.1. The

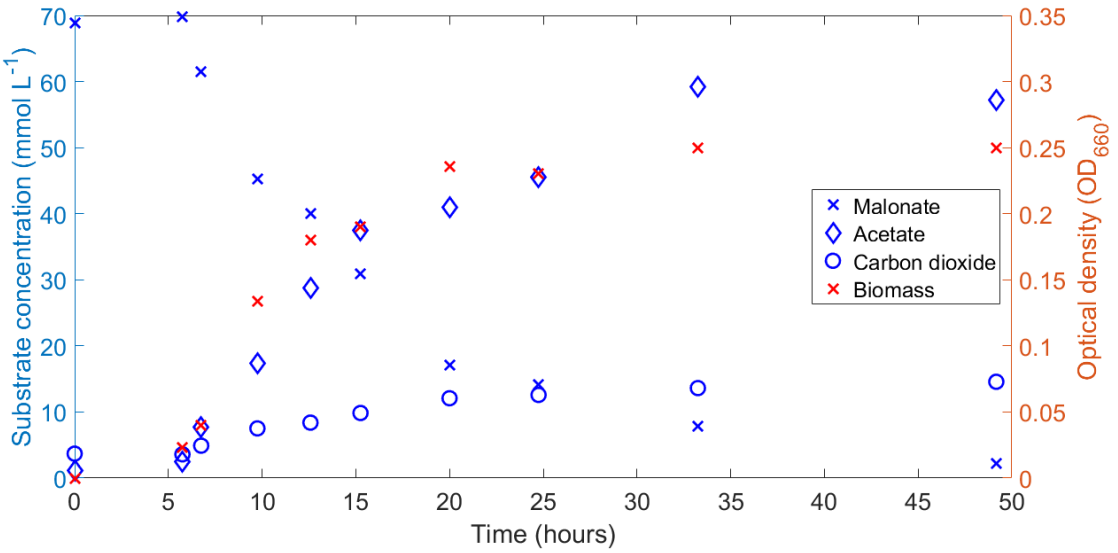

Figure 4.1: Plot of strain 16mal1 growing with malonate.

experiments were performed at a pH of 7 and a temperature of 34 °C. The concentrations of malonate and acetate were measured at various times during the experiments, and the concentration of carbon dioxide was calculated according to the method described in Appendix C.2. We use the standard enthalpies of formation (ΔH_f^o) and the standard entropies (S^o) given in Table 4.1 to calculate the standard enthalpy change (ΔH^o) and standard entropy change (ΔS^o)

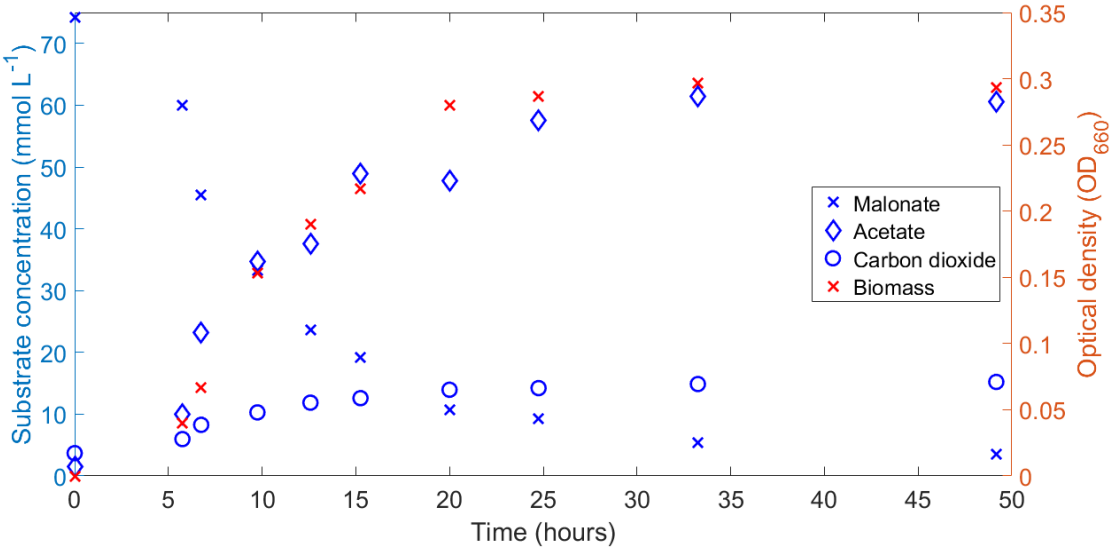

Figure 4.2: Plot of strain NHI868 growing with malonate.

for the reaction using

$$\Delta H^o = \sum_{\text{products}} \Delta H_f^o - \sum_{\text{reactants}} \Delta H_f^o$$

and

$$\Delta S^o = \sum_{\text{products}} S^o - \sum_{\text{reactants}} S^o.$$

We then calculate the Gibbs free energy change at standard conditions (ΔG_T^o) using

$$\Delta G_T^o = \Delta H^o - T\Delta S^o. \tag{4.2}$$

We find the actual Gibbs free energy change, ΔG_T, from

$$\Delta G_T = \Delta G_T^o + RT \ln Q + \eta \Delta G_{\text{ATP}} \tag{4.3}$$

where R is the ideal gas constant ($R = 0.00831446\,\text{kJ K}^{-1}\,\text{mol}^{-1}$), Q is the reaction quotient, η is the number of moles of ATP produced per mole of substrate consumed (0.3 for this reaction, as explained in Appendix B), and ΔG_{ATP} is the energy required to make a mole of ATP. We used the total concentration of malonate and acetate and assumed they were fully in the ionised forms shown in Table 4.1. The term ΔG_T is as defined in Lynch *et al.* [108]. The cost of

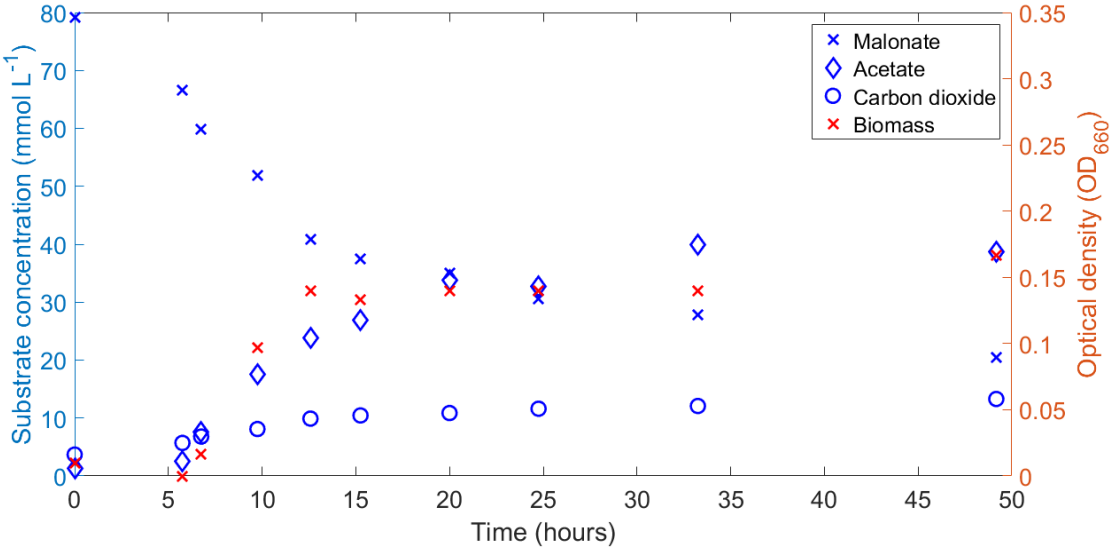

Figure 4.3: Plot of strain NCTC7427 growing with malonate.

producing ATP is not included in models such as that of Hoh and Cord-Ruwisch [67] but, when it is included, ΔG_{ATP} takes values between approximately $55\,\text{kJ mol}_{\text{ATP}}^{-1}$ and $75\,\text{kJ mol}_{\text{ATP}}^{-1}$, as explained in Chapter 3.

Note that for the general reaction

$$a\text{A} + b\text{B} \rightarrow c\text{C} + d\text{D},$$

the reaction quotient is defined as

$$Q = \frac{\text{C}^c\text{D}^d}{\text{A}^a\text{B}^b}.$$

For Reaction (4.1) this becomes

$$Q = \frac{[\text{CH}_3\text{COO}^-][\text{CO}_2]}{[\text{CH}_3\text{O}_4^-]}. \tag{4.4}$$

Recall that the thermodynamic parameter θ, introduced in Lynch *et al.* [108] is

$$\theta = \exp\left(\Delta G_T / RT\right) = Q \exp \frac{\Delta G_T^o + \eta \Delta G_{\text{ATP}}}{RT}. \tag{4.5}$$

Table 4.1: Standard enthalpies of formation and entropies of formation for substances in the malonate reaction, at 298.15 K and 1 bar.

Substance		ΔH_f^o (kJ mol^{-1})	S^o (kJ K^{-1} mol^{-1})	Reference
$CH_3O_4^-$	Hmalonate$^-$	-869.64	0.17866	[163]
CH_3COO^-	acetate$^-$	-485.8	0.0866	[30]
CO_2	carbon dioxide	-413.8	0.1176	[30]

Note also that $\theta = 1$ corresponds to complete thermodynamic shutdown and that $\theta = 0$ corresponds to no thermodynamic impact. Calculating the value of θ and ΔG_T in the prevailing conditions at each time point in the dataset gives us Figures 4.4-4.6.

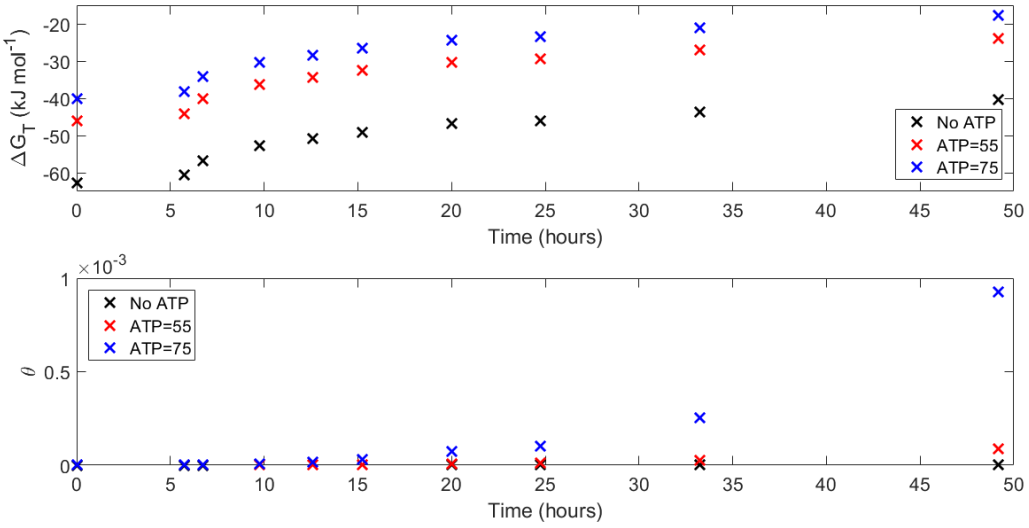

Figure 4.4: Plot of ΔG_T and θ at each measurement time point using data for strain 16mal1 from Figure 4.1 and Table C.1.

We calculated ΔG_T using $\Delta G_{\text{ATP}} = 0\,\text{kJ mol}_{\text{ATP}}^{-1}$ (as in the work of Hoh and Cord-Ruwisch, where the energy requirement to form ATP was not considered), along with $\Delta G_{\text{ATP}} = 55\,\text{kJ mol}_{\text{ATP}}^{-1}$ and $\Delta G_{\text{ATP}} = 75\,\text{kJ mol}_{\text{ATP}}^{-1}$ (the lower and upper bounds being used for the optimised rate).

Figures 4.4-4.6 show that the value of ΔG_T remains negative, regardless of the choice of value of ΔG_{ATP}. This means the reaction remains thermodynamically favourable. Note that the values of θ remain very small, less that 0.001 for each data set and much less than this value throughout most of the experiment. These results highlight that the growth of each of the three

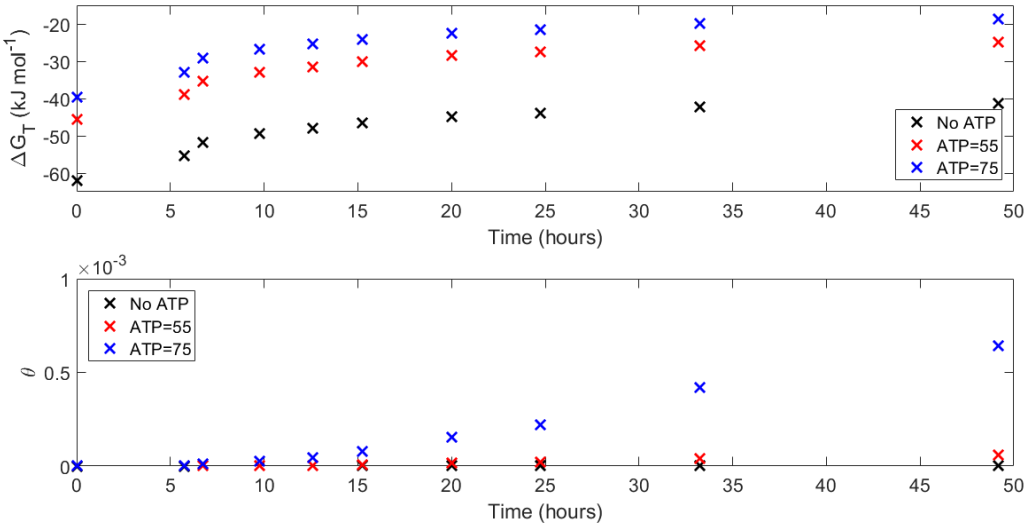

Figure 4.5: Plot of ΔG_T and θ at each measurement time point using data for strain NHI868 from Figure 4.2 and Table C.2.

strains of microbe was limited by something other than product inhibition.

The application of this model to a batch culture where there is very little or no thermodynamic inhibition until right near the end does not illustrate very well the impact of the penalty function. We can show that the model nonetheless predicts experimental outcomes that are qualitatively similar to the experimental data that were reported by Janssen [73].

The rate of malonate turnover for the Optimised rate is

$$q = r \cdot q_{\max} \frac{S\,(1-\theta)}{K + S\,(1+\theta)} \tag{4.6}$$

where θ is as defined in Eq. (4.5) and r is the penalty function term, given by

$$r = \frac{\exp\left(\eta \Delta G_{\mathrm{ATP}}/RT\right) - \exp\left(\eta \Delta G_{\mathrm{ATPmin}}/RT\right)}{\exp\left(\eta \Delta G_{\mathrm{ATPmax}}/RT\right) - \exp\left(\eta \Delta G_{\mathrm{ATPmin}}/RT\right)}. \tag{4.7}$$

Here, $\Delta G_{\mathrm{ATPmax}}$ and $\Delta G_{\mathrm{ATPmin}}$ are the upper and lower bounds for the range of values that ΔG_{ATP} can take. As explained earlier, $\Delta G_{\mathrm{ATPmax}} = 75\,\mathrm{kJ\,mol}^{-1}_{\mathrm{ATP}}$ and $\Delta G_{\mathrm{ATPmin}} = 55\,\mathrm{kJ\,mol}^{-1}_{\mathrm{ATP}}$, respectively. The so-called "penalty function" in the Optimised rate allows us to model a microbe that can modulate its metabolism to its conditions. This captures the range of

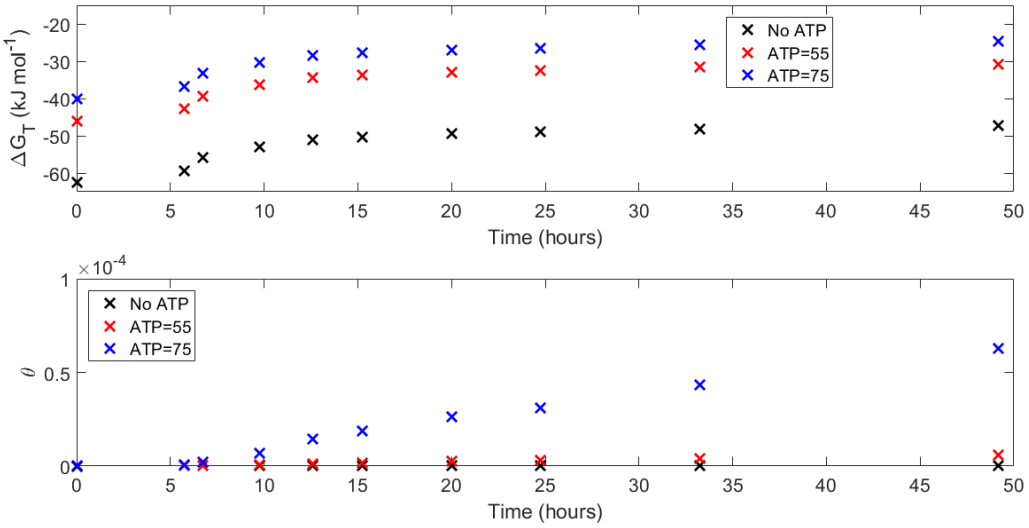

Figure 4.6: Plot of ΔG_T and θ at each measurement time point using data for strain NCTC7427 from Figure 4.3 and Table C.3.

possible ΔG_{ATP} values, maintaining q_{ATP} by reducing ΔG_{ATP} to keep $\theta < 1$ at the expense of the rate of ATP synthesis. Because ATP formation and substrate utilisation are strongly linked through metabolic feedback, this can be expressed in Eq. (4.6) as r. A more complete description of r is given in Chapter 3. For the parameters in Eq. (4.6) we use: $K = 2\times10^{-7}$ mol L^{-1}, as used by Lynch *et al.* [108] for work with hydrogen as a substrate; $q_{\max} = 7.07\times10^{-13}$ mol cell^{-1} day^{-1} as the maximum rate of substrate turnover; and $T = 307.15$ K and pH = 7.0 as in the original experiments [73].

Using the law of mass action we get the following differential equations for the rates of change of the concentrations of the species present

$$\frac{dX}{dt} = ((\eta q - m)Y)X, \tag{4.8}$$

$$\frac{d[\text{Malonate}]}{dt} = -qX, \tag{4.9}$$

$$\frac{d[\text{Acetate}]}{dt} = qX, \tag{4.10}$$

$$\frac{d[\text{CO}_2]}{dt} = qX. \tag{4.11}$$

Here: X is the concentration of microbe cells (the population expressed as cells per litre); m is

the maintenance requirement for the microbe, with units of $\mathrm{mol_{ATP}\ cell^{-1}\ day^{-1}}$ it is the amount of energy in the form of ATP required for all non-growth related cellular functions; and Y is the reproduction coefficient which we take from Lynch *et al.* [108] to be $Y = 2.36 \times 10^{13}\ \mathrm{cell\ mol_{ATP}^{-1}}$. We take the initial concentration of malonate to be $0.070\ \mathrm{mol\ L^{-1}}$, the initial concentration of acetate to be $0.0011\ \mathrm{mol\ L^{-1}}$, the initial concentration of carbon dioxide to be $0.0037\ \mathrm{mol\ L^{-1}}$, and the initial value of X to be $5 \times 10^9\ \mathrm{cells\ L^{-1}}$. The inoculum size was 1% by volume from a culture that had the maximum cell density possible from the initial malonate concentration. This allows nearly seven doublings of cell numbers to observe the behaviour of the model. We set maintenance to be $0\ \mathrm{mol_{ATP}\ cell^{-1}\ day^{-1}}$ for this simulation.

The simulation is depicted in Figure 4.7. This figure shows that the qualitative behaviour matches that recorded experimentally in Janssen's work. The obvious difference between Janssen's data [73] and Figure 4.7 is that the carbon dioxide concentration calculated from Janssen's data only increased by about 20% of the amount that acetate does, while the simulation in Figure 4.7 has the concentrations of acetate and carbon dioxide increasing at a 1:1 ratio as predicted by Eq. (4.1). This difference is because the calculated carbon dioxide produced in Janssen's experiments are in equilibrium with the gas phase. In the modelled behaviour shown in Figure 4.7, all the carbon dioxide produced is retained in the growth medium. In Figure 4.8 we plot

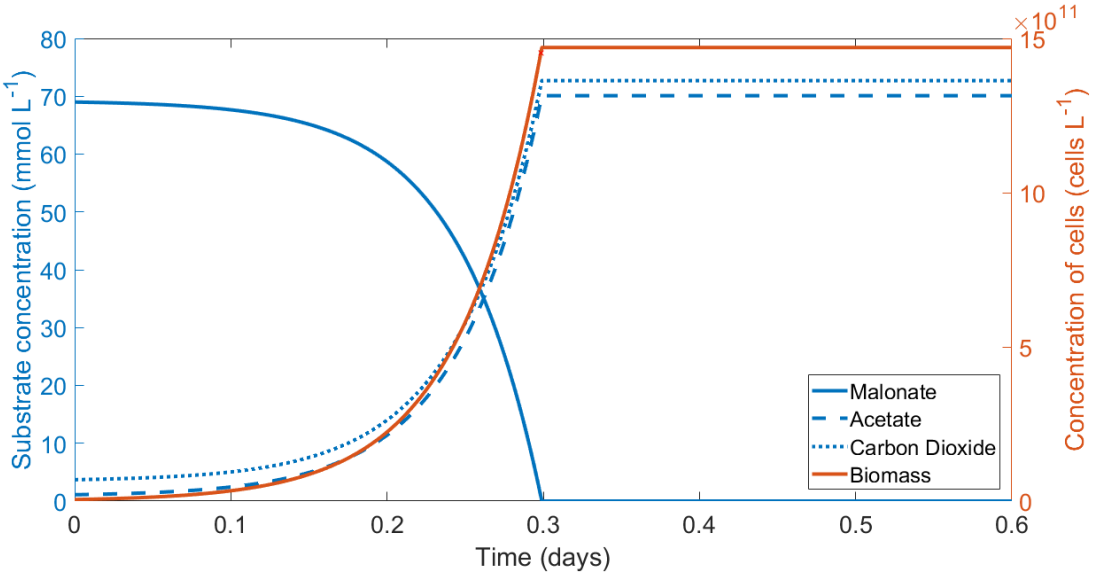

Figure 4.7: Plot of concentrations during simulation of malonate fermentation.

θ and the optimised ΔG_{ATP} over time for this simulation to see the effect of thermodynamic inhibition and the penalty function. Figure 4.8 reveals that there is very little influence either

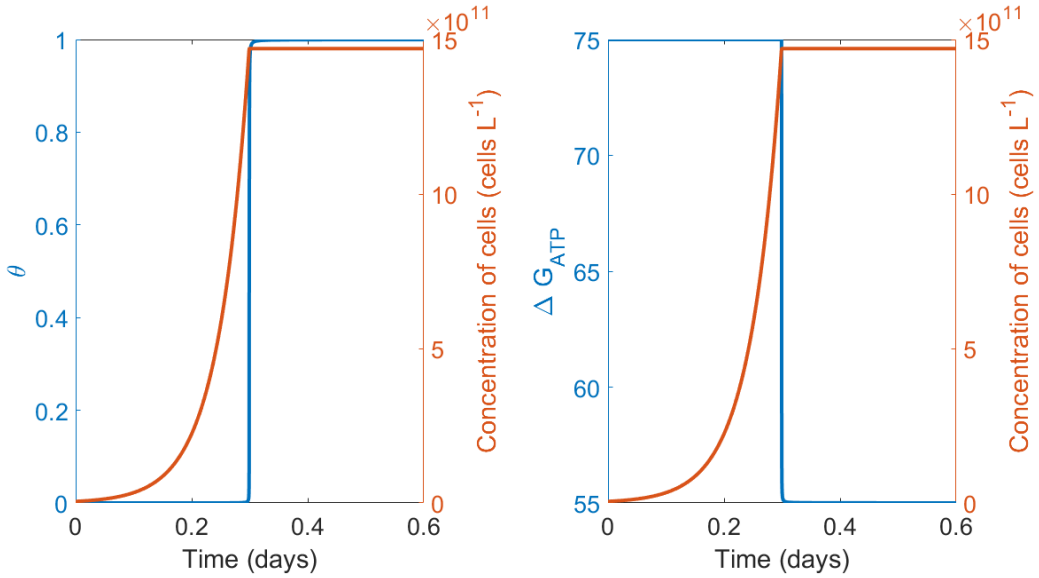

Figure 4.8: Plot of θ and optimised ΔG_{ATP} during simulation of malonate fermentation.

from the thermodynamic inhibition of θ or from ΔG_{ATP} changing away from 75 kJ $\text{mol}_{\text{ATP}}^{-1}$ until the end of the growth period for the batch culture, where the substrate has dropped from the initial value of 0.070 mol L^{-1} to less than 0.05 mmol L^{-1}. The Optimised rate is designed to cope with situations where there is thermodynamic inhibition due to the presence of products. In a batch culture like this one, the key features of the model are not utilised until the brief window at the end of the simulation. Importantly, however, the model still performs well when the inhibitory effects of products are minimal. We now consider a situation where the inhibitive effects of products are stronger.

4.2 Batch Culture with Thermodynamic Inhibition

Consider the reaction

$$\text{CH}_3(\text{CH})_2\text{COO}^- + \text{H}_2\text{O} \rightarrow \text{CH}_3\text{COO}^- + \frac{1}{2}\text{CH}_3(\text{CH}_2)_2\text{COO}^- + \frac{1}{2}\text{H}^+, \tag{4.12}$$

as presented by Wallrabenstein and Schink [177] for growth of strain DM-3 in a batch culture, breaking down crotonate into acetate and butyrate. This reaction was analysed by Jin and Bethke [79] when validating their rate. Based on the known pathway of crotonate fermentation, we estimate 0.5 mol of ATP is produced for each mol of crotonate fermented, i.e., $\eta = 0.5\,\mathrm{mol_{ATP}\ mol^{-1}_{crotonate}}$. The explanation for this is given in Appendix B.3. We estimate the prevailing concentrations of crotonate, acetate, and butyrate, along with the change in optical density as a measure of biomass, at each measurement time point from Figure 1 in Wallrabenstein and Schink [177]. No table of data was included in their work. These estimated values are given in Table C.4. Repeating what we did in Section 4.1 for microbes growing with malonate, we start with Figure 4.9, showing the data. Values for the enthalpy of formation and

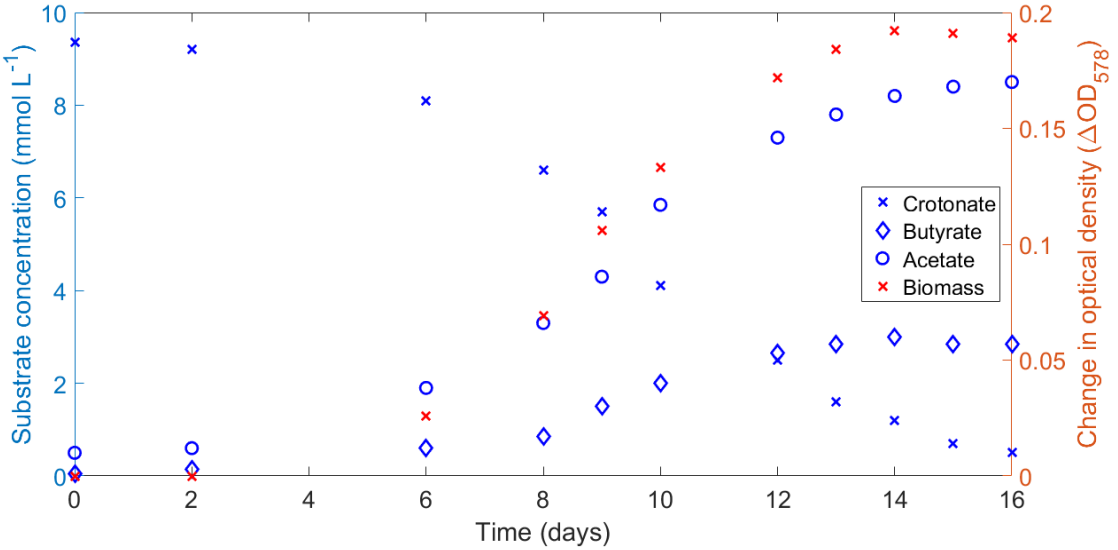

Figure 4.9: Plot of growth of strain DM-3 on crotonate with substrate and product concentrations over time.

the standard entropy for crotonate are elusive so, rather than the process we used for malonate fermentation, we use an integrated form of the Gibbs-Helmholtz equation,

$$\Delta G_{T2} \approx \frac{T_2}{T_1}\Delta G_{T1} - \Delta H\frac{T_2 - T_1}{T_1}, \tag{4.13}$$

where T is in Kelvin, to calculate ΔG_f of each species present at 28 °C, using the values in Table 4.2 for 25 °C. After calculating ΔG_f at 28 °C for each, ΔG^o_T for the reaction is

$$\Delta G^o_T = \sum_{\text{products}} \Delta G_f - \sum_{\text{reactants}} \Delta G_f,$$

which works out to $-11.723\,\text{kJ mol}^{-1}$. We then calculate ΔG_T in the prevailing conditions using Eq. (4.3), which was

$$\Delta G_T = \Delta G^o_T + RT \ln Q + \eta \Delta G_{\text{ATP}}.$$

Note that reaction quotients are normalised based on the activity of water being 1, so water does not appear in the reaction quotient reactions occuring in aqueous solutions. This means that the reaction quotient for crotonate fermentation is

$$Q = \frac{[\text{CH}_3\text{COO}^-][\text{CH}_3(\text{CH}_2)_2\text{COO}^-]^{0.5}[\text{H}^+]^{0.5}}{[\text{CH}_3(\text{CH})_2\text{COO}^-]}. \tag{4.14}$$

Plotting θ and ΔG_T in the prevailing conditions at each measurement time from the dataset

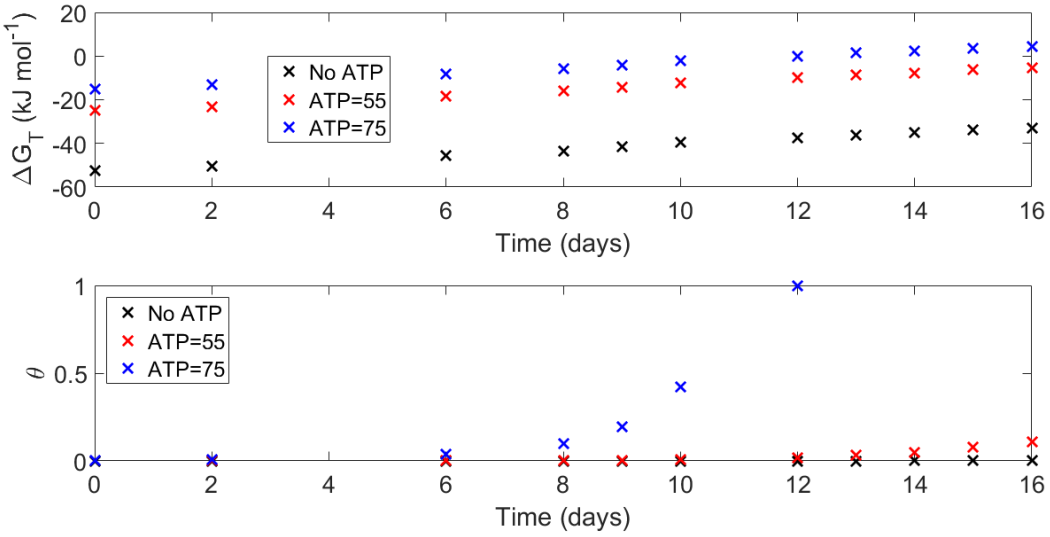

Figure 4.10: Plot of ΔG_T and θ at each measurement time point using data from Figure 4.9 and Table C.4.

gives us Figure 4.10. We see that when ΔG_{ATP} is either not included or set to $55\,\text{kJ mol}^{-1}_{\text{ATP}}$, ΔG_T is negative throughout. The value of ΔG_T is positive for the last few data points when

ΔG_{ATP} was set to $75\,\mathrm{kJ\,mol_{ATP}^{-1}}$, indicating that late in the experiment the transformation of crotonate becomes thermodynamically unfavourable at this value of ΔG_{ATP}. This is reflected in the plot showing θ: the values are much larger than they were for the duration of malonate fermentation; they stay below 2×10^{-5} without ΔG_{ATP}; they reach about 0.1 by the end of the experiment when $\Delta G_{\mathrm{ATP}} = 55\,\mathrm{kJ\,mol_{ATP}^{-1}}$; and they are very small for the first half of the experiment when $\Delta G_{\mathrm{ATP}} = 75\,\mathrm{kJ\,mol_{ATP}^{-1}}$ before increasing rapidly, reaching 1 by the last few days of the experiment. Thermodynamic inhibition is more evident than it was in the experiment with malonate, although not as strong as the Optimised rate is capable of handling. We can again run a simulation using some estimated values for parameters to show the model using the penalty function generates an output that is qualitatively similar to the experimental data reported by Wallrabenstein and Schink [177].

Table 4.2: Standard Gibbs free energy of formation and enthalpy of formation values for substances in crotonate fermentation at 298.15 K and 1 bar. ΔG_f^o for crotonate is from Thauer *et al.* [172], while ΔH_f^o is estimated based on values of similar organic acids as explained in Appendix C.3

.

Substance		ΔG_f^o (kJ mol^{-1})	ΔH_f^o (kJ mol^{-1})	Reference
$CH_3(CH)_2COO^-$	Crotonate$^-$	-277.4	-395.88	[172]
CH_3COO^-	Acetate$^-$	-376.89	-485.8	[29]
$CH_3(CH_2)_2COO^-$	Butyrate$^-$	-372.04	-535.55	[29]
H^+	Proton	0	0	[29]
H_2O	Water	-273.19	-285.84	[29]

We take q, the rate of crotonate turnover, to be given by Eq. (4.6), which was

$$q = r \cdot q_{\max} \frac{S\,(1-\theta)}{K + S\,(1+\theta)}.$$

We use: $K = 2 \times 10^{-7}\,\mathrm{mol\,L^{-1}}$, as used by Lynch *et al.* [108] for work with hydrogen as a substrate; $q_{\max} = 1.19 \times 10^{-14}\,\mathrm{mol\,cell^{-1}\,day^{-1}}$ as the maximum rate of substrate turnover calculated from data presented by Wallrabenstein and Schink [177]; and $T = 301.15\,\mathrm{K}$ and pH = 7.3.

Using the law of mass action we get the following differential equations for the rates of change

of the concentrations of the species present

$$\frac{dX}{dt} = ((\eta q - m)Y)X, \tag{4.15}$$

$$\frac{d[\text{Crotonate}]}{dt} = -qX, \tag{4.16}$$

$$\frac{d[\text{Acetate}]}{dt} = qX, \tag{4.17}$$

$$\frac{d[\text{Butyrate}]}{dt} = 0.5qX, \tag{4.18}$$

$$\frac{d[\text{H}^+]}{dt} = 0. \tag{4.19}$$

Again, these equations use: X as the concentration of microbe cells; m as the maintenance requirement for the microbe, with units of $\text{mol}_{\text{ATP}}\ \text{cell}^{-1}\ \text{day}^{-1}$; and we also import from Lynch *et al.* [108] $Y = 2.36 \times 10^{13}\ \text{cell mol}_{\text{ATP}}^{-1}$, the reproduction coefficient. We set maintenance to be $0\ \text{mol}_{\text{ATP}}\ \text{cell}^{-1}\ \text{day}^{-1}$ for this simulation. We observe in Figure 4.11 that the qualitative behaviour matches that recorded experimentally by Wallrabenstein and Schink [177] and that growth started to slow while there was still a significant amount of substrate left, rather than growth accelerating until the substrate was almost completely exhausted as was seen in the malonate example. In Figure 4.12 we plot θ and the optimised ΔG_{ATP} over time for the simulation

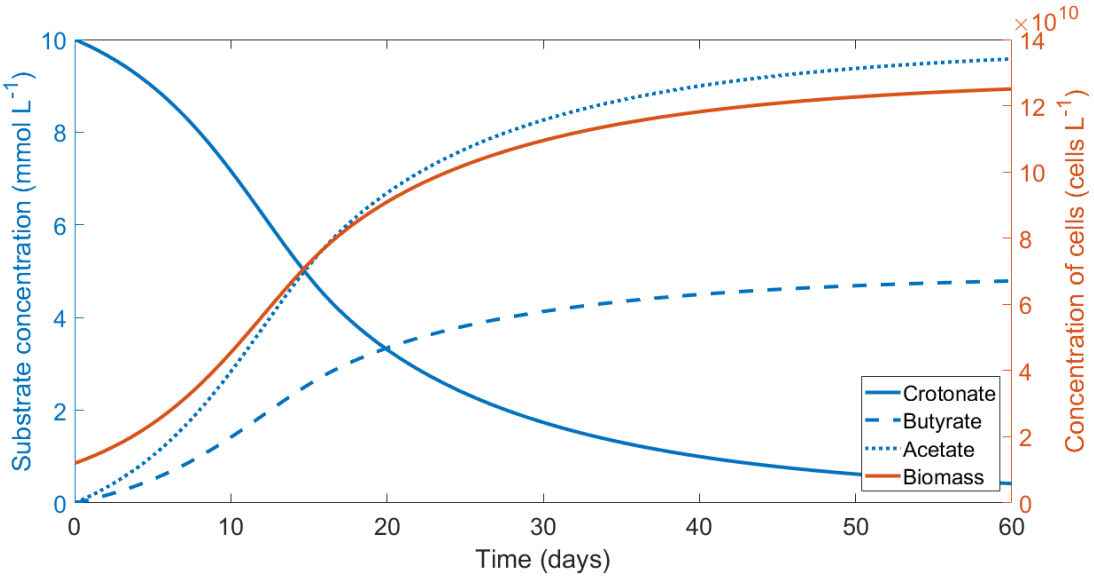

Figure 4.11: Plot of concentrations during simulation of crotonate fermentation.

to see the effect of thermodynamic inhibition and the penalty function during the simulation.

We see that both controls move considerably away from their starting values when the biomass is approximately half of its maximum value and when there is still about half of the substrate remaining. We saw in the example of malonate fermentation that the Optimised rate, which

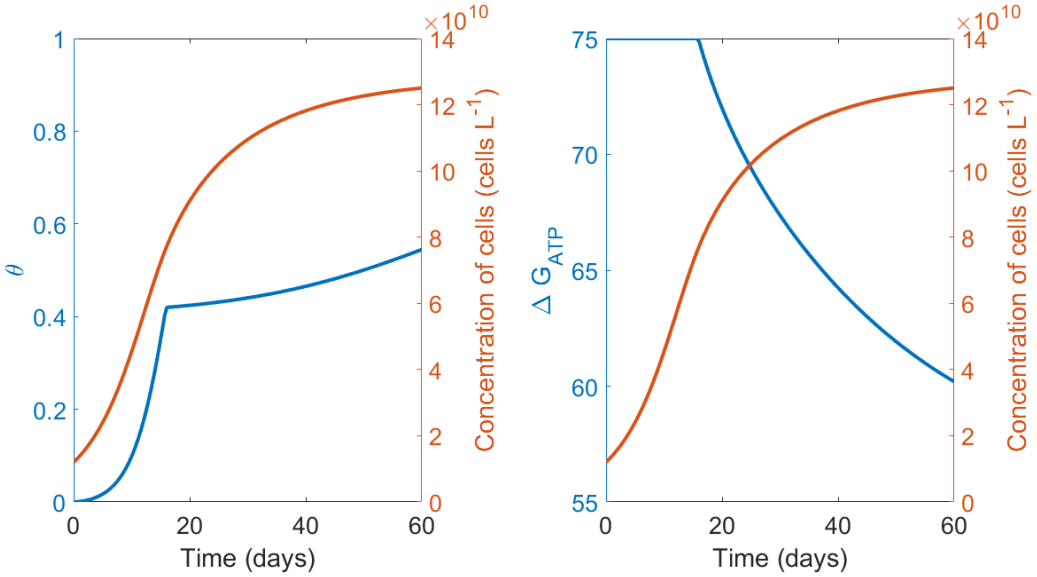

Figure 4.12: Plot of θ and optimised ΔG_{ATP} during simulation of crotonate fermentation.

is intended to model situations with thermodynamic inhibition due to the buildup of products, performs well in an example with batch cultures that have little of this inhibition until a very brief window near the end of culture growth. We now see that the function also responds to product inhibition by reducing ΔG_{ATP} to allow continued metabolism.

So our attention turns now to a continuous culture example where we can explore the behaviour of the model more fully.

4.3 Continuous Culture with Thermodynamic Inhibition

The previous sections simulated microbes growing in batch cultures with malonate and crotonate where thermodynamic limitation occurs part way through or near the end of culture growth. We now look at a continuous culture which is a more realistic representation of microbial growth in nature. Substrate concentrations tend to be low and more-or-less continuously supplied. The previous examples each only had one species of microbe present, but this example also allows us to explore the more realistic situation where there are competing species of microbe present.

Consider the following reactions which are respectively involved in the production of ATP for two strains of bacteria, DKglu16 and DKglu26 respectively, as outlined by Nanninga *et al.* [132]:

$$\text{glutamate} + \frac{4}{3}\text{H}_2\text{O} \rightarrow \frac{5}{3}\text{acetate} + \frac{1}{3}\text{propionate} + \frac{2}{3}\text{CO}_2 + \text{ammonium} \tag{4.20}$$

and

$$\text{glutamate} + \frac{6}{5}\text{H}_2\text{O} + \frac{2}{5}\text{H}^+ \rightarrow \frac{6}{5}\text{acetate} + \frac{2}{5}\text{butyrate} + \text{ammonium} + \text{CO}_2 + \frac{1}{5}\text{H}_2 \tag{4.21}$$

We can model the growth of these microbes in different continuous culture conditions, both separately or in direct competition with each other, and compare the results with those reported by Nanninga *et al.*

Before we can run simulations of the model, we need to determine the values for some chemical components in the reactions. The reaction in Eq. (4.20) produces $28/33\,\text{mol}_{\text{ATP}}$ per mole of glutamate consumed, based on net 2 ATP per 3 glutamate by substrate-level phosphorylation [131], and 2 $\{H^+/Na^+\}$ exported at the fumarate reduction step per 3 glutamate [65], and assuming 11 $\{H^+/Na^+\}$ are used per 3 ATP formed by the ATP synthase, as found in *Clostridium paradoxum* [118]. The reaction in Eq. (4.21) produces $19/20\,\text{mol}_{\text{ATP}}$ per mole of glutamate consumed, based on the scheme that has been presented by Buckel and Thauer [26] for *Clostridium tetanomorphum* which assumes 12 $\{H^+/Na^+\}$ are used to form 3 ATP at the ATP synthase. Nanninga *et al.* [132] classify DKglu26 as a member of *Clostridium cochlearium*. *C. tetanomorphum* and *C. cochlearium* are closely related [33].

Using the standard enthalpies of formation (ΔH_f^o) and the standard entropies (S^o) in Table 4.3 we calculate the standard enthalpy change (ΔH^o) and standard entropy change (ΔS^o) for the reaction using

$$\Delta H^o = \sum_{\text{products}} \Delta H_f^o - \sum_{\text{reactants}} \Delta H_f^o$$

and

$$\Delta S^o = \sum_{\text{products}} S^o - \sum_{\text{reactants}} S^o,$$

just as we did for malonate fermentation. We then calculate the Gibbs free energy change for

Table 4.3: Standard enthalpy of formation and entropy of formation values for substances in glutamate fermentation at 298.15 K and 1 bar. Conversions made from 1 cal to 4.184 J as required [126].

Substance		ΔH_f^o (kJ mol^{-1})	S^o (kJ K^{-1} mol^{-1})	Reference
$C_5H_8O_4N^-$	Glutamate	-979.68	0.18351	[5]
CH_3COO^-	Acetate	-485.8	0.0866	[30]
$CH_3CH_2COO^-$	Propionate	-513.1	0.1109	[110]
$CH_3CH_2CH_2COO^-$	Butyrate	-535.55	0.20167	[29]
H^+	Proton	0	0	[30]
H_2	Hydrogen	-4.184	0.05774	[98]
H_2O	Water	-285.8	0.0699	[30]
CO_2	Carbon dioxide	-413.8	0.1176	[30]
NH_4^+	ammonium	-132.5	0.1134	[30]

standard conditions (ΔG_T^o) using Eq. (4.2), which was

$$\Delta G_T^o = \Delta H^o - T\Delta S^o.$$

We can then find the actual Gibbs free energy change, ΔG_T, from Eq. (4.3), which was

$$\Delta G_T = \Delta G_T^o + RT \ln Q + \eta \Delta G_{\text{ATP}}.$$

As before, R is the ideal gas constant ($R = 0.00831446\,\text{kJ K}^{-1}\,\text{mol}^{-1}$), Q is the reaction quotient, η is the number of moles of ATP produced per mole of substrate consumed (28/33 and 19/20 for these reactions, as detailed above), and ΔG_{ATP} is the energy required to make a mole of ATP. Again, when the cost of producing ATP is included, ΔG_{ATP} can take values between approximately 55 kJ mol$_{\text{ATP}}^{-1}$ and 75 kJ mol$_{\text{ATP}}^{-1}$. The respective reaction quotients for the reactions in Eqs. (4.20) and (4.21) are

$$\frac{[\text{acetate}]^{5/3}[\text{propionate}]^{1/3}[\text{carbon dioxide}]^{2/3}[\text{ammonium}]}{[\text{glutamate}]} \tag{4.22}$$

and

$$\frac{[\text{acetate}]^{6/5}[\text{butyrate}]^{2/5}[\text{carbon dioxide}][\text{ammonium}][H_2]^{1/5}}{[\text{glutamate}][H^+]^{2/5}}. \tag{4.23}$$

To model the growth of these microbes in a continuous culture, we consider a fixed volume which has flow through it at some rate α. This passage rate through the system brings in nutrients at chosen concentrations and washes out a proportion of the entire contents, which is assumed to be well-mixed, to maintain the constant volume.

Again, we take q, the rate of substrate turnover for a substrate S, to be given by Eq. (4.6), which was

$$q = r \cdot q_{\max} \frac{S\,(1-\theta)}{K + S\,(1+\theta)}.$$

The forms of θ and r are given by Eqs. (4.5) and (4.7), which were

$$\theta = \exp\left(\Delta G_T / RT\right) = Q \exp \frac{\Delta G_T^o + \eta \Delta G_{\mathrm{ATP}}}{RT},$$

and

$$r = \frac{\exp\left(\eta \Delta G_{\mathrm{ATP}}/RT\right) - \exp\left(\eta \Delta G_{\mathrm{ATPmin}}/RT\right)}{\exp\left(\eta \Delta G_{\mathrm{ATPmax}}/RT\right) - \exp\left(\eta \Delta G_{\mathrm{ATPmin}}/RT\right)}.$$

We use $K = 2 \times 10^{-7}\,\mathrm{mol\,L^{-1}}$ as used by Lynch *et al.* [108] for work with hydrogen as a substrate and $q_{\max} = 3.57 \times 10^{-14}\,\mathrm{mol\,cell^{-1}\,day^{-1}}$ as the maximum substrate turnover. We assume there is a buffer keeping the pH at 6.5 (so the H^+ used in the reaction for DKglu26 will have a constant concentration) and the temperature in the culture is fixed at $T = 308.15\,\mathrm{K}$, to match the pH and temperature used by Nanninga *et al.* [132].

Initially focusing solely on strain DKglu16, we use the law of mass action to get the following differential equations for the rates of change of the concentrations of the species present:

$$\frac{dX}{dt} = ((\eta q - m)Y - \alpha)X, \tag{4.24}$$

$$\frac{d[\mathrm{Glutamate}]}{dt} = -qX - \alpha([\mathrm{Glutamate}] - [\mathrm{Glutamate}]_{\mathrm{S}}), \tag{4.25}$$

$$\frac{d[\mathrm{Acetate}]}{dt} = \frac{5}{3}qX - \alpha([\mathrm{Acetate}] - [\mathrm{Acetate}]_{\mathrm{S}}), \tag{4.26}$$

$$\frac{d[\mathrm{Propionate}]}{dt} = \frac{1}{3}qX - \alpha([\mathrm{Propionate}] - [\mathrm{Propionate}]_{\mathrm{S}}), \tag{4.27}$$

$$\frac{d[\mathrm{Ammonium}]}{dt} = qX - \alpha([\mathrm{Ammonium}] - [\mathrm{Ammonium}]_{\mathrm{S}}), \tag{4.28}$$

$$\frac{d[\mathrm{CO_2}]}{dt} = 0. \tag{4.29}$$

These equations use: X as the concentration of microbe cells; $[\text{Glutamate}]_\text{S}$ as the inflowing glutamate concentration, with the other inflowing concentrations labelled in the same way; m as the maintenance requirement for the microbe, with units of $\text{mol}_\text{ATP}\,\text{cell}^{-1}\,\text{day}^{-1}$ it is the daily amount of energy required to keep a microbe functioning; and we also import from Lynch *et al.* [108] for $Y = 2.36 \times 10^{13}\,\text{cell}\,\text{mol}_\text{ATP}^{-1}$, the reproduction coefficient.

We are assuming the concentration of carbon dioxide to be constant due to the system being a continuous culture with a gas phase. We assumed that any excess carbon dioxide produced will leave through the gas phase on a timescale much faster than the growth of the microbe (see, for example, Gibbons and Edsall [55] or Garg and Maren [52]). We use the value from the experiments reported by Nanninga *et al.* [132] to set this constant concentration of carbon dioxide to be $0.013\,\text{mol}\,\text{L}^{-1}$. For these simulations we also take $[\text{Acetate}]_\text{S}$, $[\text{Propionate}]_\text{S}$, and $[\text{Ammonium}]_\text{S}$ to be $0\,\text{mol}\,\text{L}^{-1}$ as we are not actively adding these products to the culture. We take the initial concentrations of acetate, propionate, and ammonium to be $0\,\text{mol}\,\text{L}^{-1}$ and both the initial concentration of glutamate and $[\text{Glutamate}]_\text{S}$ to be $0.010\,\text{mol}\,\text{L}^{-1}$. We set the initial value of X to $2 \times 10^9\,\text{cells}\,\text{L}^{-1}$. Nanninga *et al.* did not specify an inoculum volume. There is no universally-accepted inoculum size for liquid cultures of microbes, and a typical description is that a "small inoculum volume [is] transferred to a large volume of fresh medium" [43], so we selected 1% by volume from a culture that had the maximum cell density possible from the glutamate concentration supplied. This allows nearly seven doublings of cell numbers to observe the behaviour of the model.

We start with $m = 0\,\text{mol}_\text{ATP}\,\text{cell}^{-1}\,\text{day}^{-1}$ and run the simulation with $\alpha = 0.10\,\text{day}^{-1}$, with the concentrations shown in Figure 4.13 and the values of θ and the optimised ΔG_ATP shown in Figure 4.14. These plots look similar to Figures 4.7 and 4.8 that were produced in the simulation of malonate with the important difference of how far θ and ΔG_ATP move. In the malonate example, θ increased very quickly to very close to one and the reaction effectively ceased at the same time as ΔG_ATP dropped to almost $55\,\text{kJ}\,\text{mol}_\text{ATP}^{-1}$. In contrast, in the simulation here, with glutamate, θ only increased to about 0.43 and ΔG_ATP only decreased to about $72.3\,\text{kJ}\,\text{mol}_\text{ATP}^{-1}$ when the system reaches a steady state with the reaction rate balancing what is being washed out of the system. The value of α was selected to produce these figures but we can learn more by

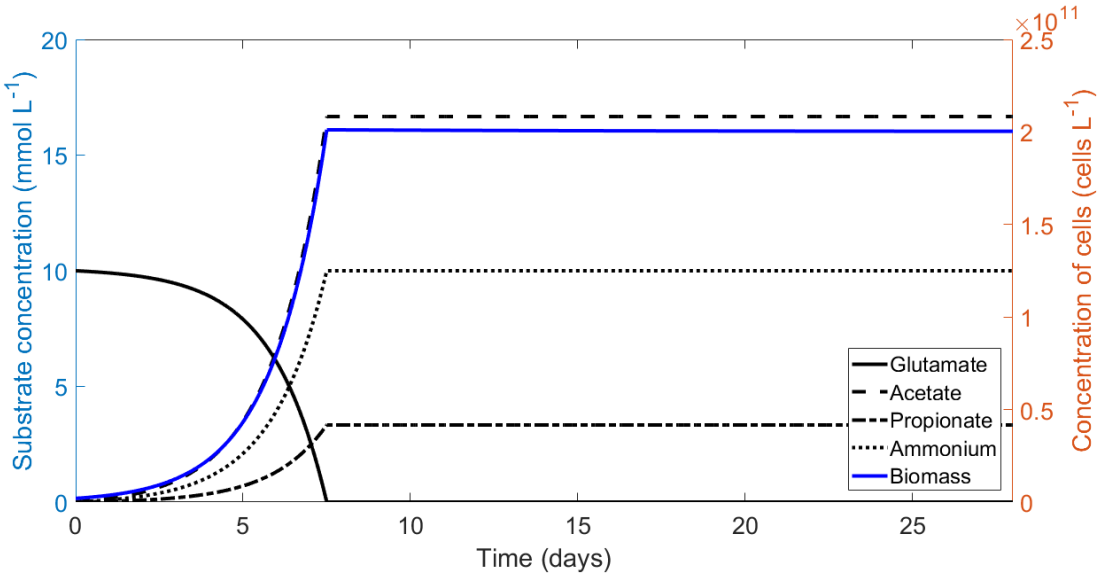

Figure 4.13: Plot of concentrations during simulation of strain DKglu16 fermenting glutamate at $\alpha = 0.1\,\text{day}^{-1}$.

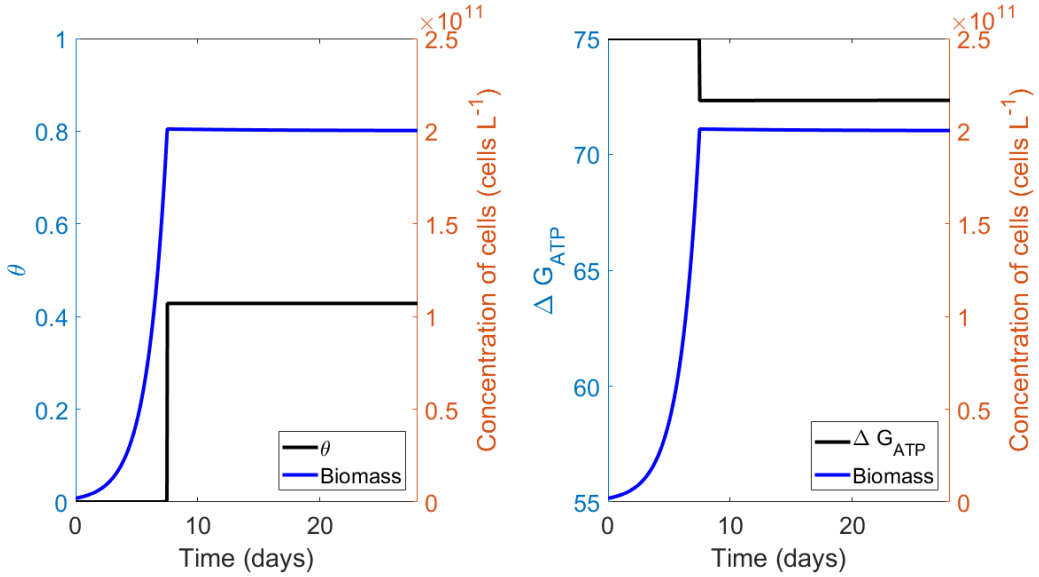

Figure 4.14: Plot of θ and optimised ΔG_{ATP} during simulation of strain DKglu16 fermenting glutamate at $\alpha = 0.1\,\text{day}^{-1}$.

using a range of values for α and comparing the resultant steady state glutamate and biomass concentrations. However, we will first focus on the other glutamate-fermenting strain, DKglu26, at the same value of α before comparing how both strains respond over a range of values of α.

Focusing solely on strain DKglu26, the equations we get from the law of mass action are:

$$\frac{dX}{dt} = ((\eta q - m)Y - \alpha)X, \tag{4.30}$$

$$\frac{d[\text{Glutamate}]}{dt} = -qX - \alpha([\text{Glutamate}] - [\text{Glutamate}]_\text{S}), \tag{4.31}$$

$$\frac{d[\text{Acetate}]}{dt} = \frac{6}{5}qX - \alpha([\text{Acetate}] - [\text{Acetate}]_\text{S}), \tag{4.32}$$

$$\frac{d[\text{Butyrate}]}{dt} = \frac{2}{5}qX - \alpha([\text{Butyrate}] - [\text{Butyrate}]_\text{S}), \tag{4.33}$$

$$\frac{d[\text{Ammonium}]}{dt} = qX - \alpha([\text{Ammonium}] - [\text{Ammonium}]_\text{S}), \tag{4.34}$$

$$\frac{d[\text{CO}_2]}{dt} = 0, \tag{4.35}$$

$$\frac{d[\text{H}^+]}{dt} = 0, \tag{4.36}$$

$$\frac{d[\text{H}_2]}{dt} = 0. \tag{4.37}$$

We again use $0.010\,\text{mol}\,\text{L}^{-1}$ for both the initial concentration of glutamate and $[\text{Glutamate}]_\text{S}$. We take the initial concentrations of acetate, butyrate, and ammonium to be $0\,\text{mol}\,\text{L}^{-1}$, as well as the values of $[\text{Acetate}]_\text{S}$, $[\text{Butyrate}]_\text{S}$, and $[\text{Ammonium}]_\text{S}$. The concentrations of carbon dioxide and protons are constant, as already explained, along with hydrogen. The concentration of hydrogen was not measured in the experiment by Nanninga *et al.* so we assume the vessel is open and the concentration of dissolved hydrogen is constant at $0.00075\,\text{mol}\,\text{L}^{-1}$. Figures 4.15 and 4.16 show the concentrations and the value of θ and the optimised ΔG_ATP for the simulation of strain DKglu26. These figures appear quite similar to those for DKglu16 but this time θ increased to about 0.42 and ΔG_ATP decreased to about $71.8\,\text{kJ}\,\text{mol}_\text{ATP}^{-1}$, the final biomass concentration is about 10% lower for strain DKglu26 than it was for strain DKglu16, and it took approximately one more day to reach the steady state. The lower biomass is a direct consequence of the smaller η for strain DKglu26.

The final glutamate concentration in the DKglu16 simulation was approximately $0.77\,\mu\text{mol}\,\text{L}^{-1}$ while in the DKglu26 simulation it was approximately $6.0\,\mu\text{mol}\,\text{L}^{-1}$. The lower value for

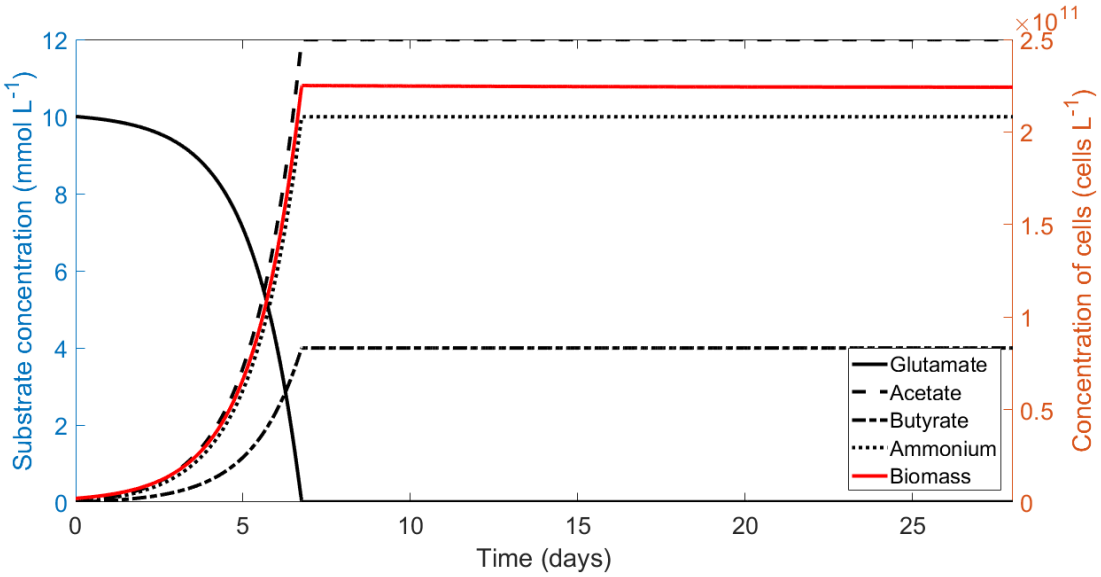

Figure 4.15: Plot of concentrations during simulation of strain DKglu26 fermenting glutamate at $\alpha = 0.1\,\mathrm{day}^{-1}$.

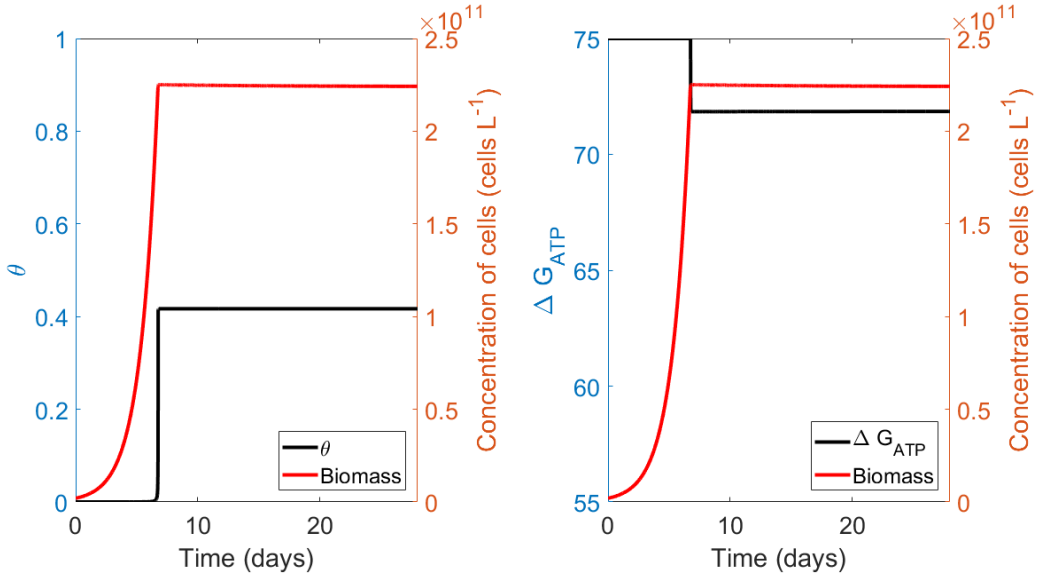

Figure 4.16: Plot of θ and optimised ΔG_{ATP} during simulation of strain DKglu26 fermenting glutamate at $\alpha = 0.1\,\mathrm{day}^{-1}$.

DKglu16 tells us that at $\alpha = 0.1\,\mathrm{day}^{-1}$ DKglu16 is able to use more of the glutamate and survive with less glutamate available, suggesting that DKglu16 would outcompete DKglu26 if the two microbes were competing for the glutamate in a combined system. At a glutamate concentration of $0.77\,\mu\mathrm{mol\,L}^{-1}$ strain DKglu26 could not grow at a rate sufficient to maintain itself for this value of α. Instead, it requires a glutamate concentration of $6.0\,\mu\mathrm{mol\,L}^{-1}$ to grow at a rate to balance cell loss at $\alpha = 0.10\,\mathrm{day}^{-1}$.

To see which microbe we expect to perform better at different values of α, we ran the simulations for strains DKglu16 and DKglu26 using values of α between 0 and 1 at intervals of 0.01. Plotting the final concentration of glutamate and the final biomass concentration each time gives Figure 4.17. The plot shows that, for low values of α, DKglu16 can survive at lower substrate concentrations than DKglu26. Therefore, we expect the substrate concentration to be reduced to this value and so expect DKglu16 to outcompete DKglu26 in the region of low α values if the two microbes were in the same culture. As α increases, we get to a point where the steady state concentration for DKglu16 exceeds the steady state concentration for DKglu26. This point is where α exceeds the maximum rate of DKglu16 and its population is washed out of the system. At values of α greater than this we expect DKglu26 to outcompete DKglu16 over the next range of values of α until a higher value of α where neither microbe can avoid being washed out of the system. Above that, the substrate concentration in the system matches the concentration being supplied by the flow. This relationship agrees qualitatively with the predictions during the discussion of competition by Nanninga *et al.* [132] based on their experimental data.

The smallest value of α that causes complete washout of the microbe is the maximum growth rate of the microbe, $\mu_{\max}$. K_{app} is the substrate concentration when the growth rate is half of its maximal value. Together, this means we can determine a value for K_{app} for each of the microbes by finding $\mu_{\max}$, halving this value, and finding the steady state glutamate concentration at that value of α. We estimate $\mu_{\max} = 0.66\,\mathrm{day}^{-1}$ and $K_{\mathrm{app}} = 2.3\,\mu\mathrm{mol\,L}^{-1}$ for DKglu16 along with $\mu_{\max} = 0.74\,\mathrm{day}^{-1}$ and $K_{\mathrm{app}} = 22\,\mu\mathrm{mol\,L}^{-1}$ for DKglu26.

The simulations so far have used $m = 0\,\mathrm{mol_{ATP}\,cell}^{-1}\,\mathrm{day}^{-1}$, but we know that the cells do have a maintenance requirement. If we use a value of $6.22 \times 10^{-16}\,\mathrm{mol_{ATP}\,cell}^{-1}\,\mathrm{day}^{-1}$ and

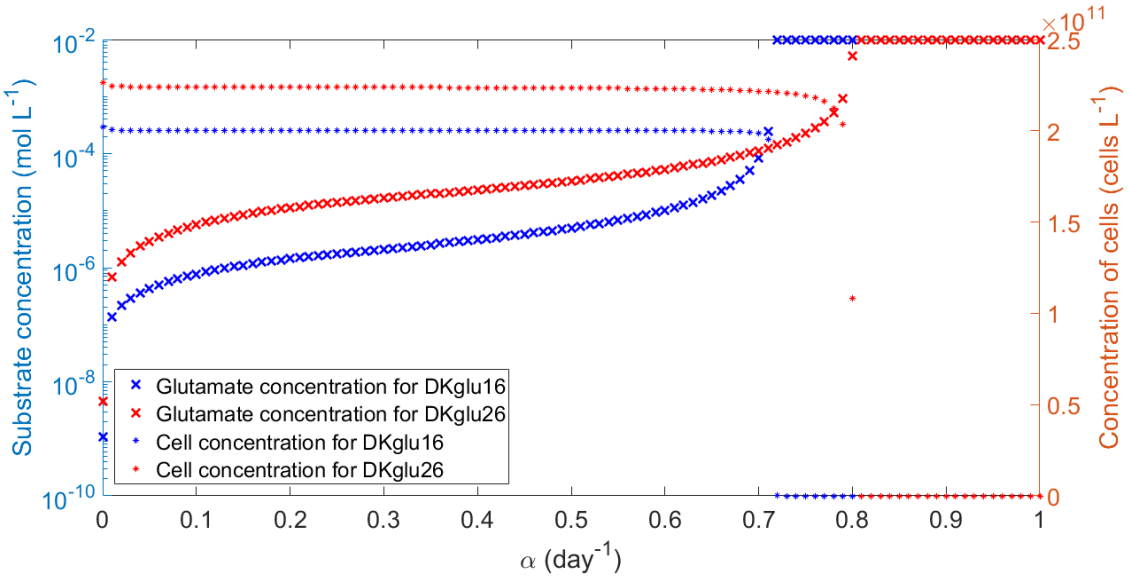

Figure 4.17: Plot of the steady state glutamate and biomass concentrations at different values of α for strains DKglu16 and DKglu26.

repeat the simulation for values of α between 0 and 1, we get Figure 4.18. At very low values of α, the steady state concentrations of DKglu16 and DKglu26 are significantly lower as the flow into the system is providing very little glutamate to maintain the population once the initial supply is consumed, reducing q and causing $\eta q - m$ to leave small amounts of ATP for cell synthesis. Beyond this early region, the plot looks very similar to Figure 4.17 but we can see that the values of α that cause DKglu16 and DKglu26 to be washed out of the system have both decreased by about 0.01. Figure 4.19 shows the same simulations as Figure 4.18 but using 100 values of α between 0.6 and 0.8 to more clearly show the detail of what is happening in the region where washout begins to dominate. Using larger values of m give a similar result: the shape stays the same but washout values of α are smaller. This means our predictions of which microbe would perform better have the same structure but the region where we expect DKglu26 to survive while DKglu16 is washed out is shifted to slightly lower values of α.

By running simulations with both microbes present in direct competition with each other, this model lets us take things a step further along the path that Nanninga *et al.* considered experimentally, and allows us to test the predictions we made from simulating the microbes growing individually. Using subscripts of 16 and 26 to refer to values for DKglu16 and DKglu26

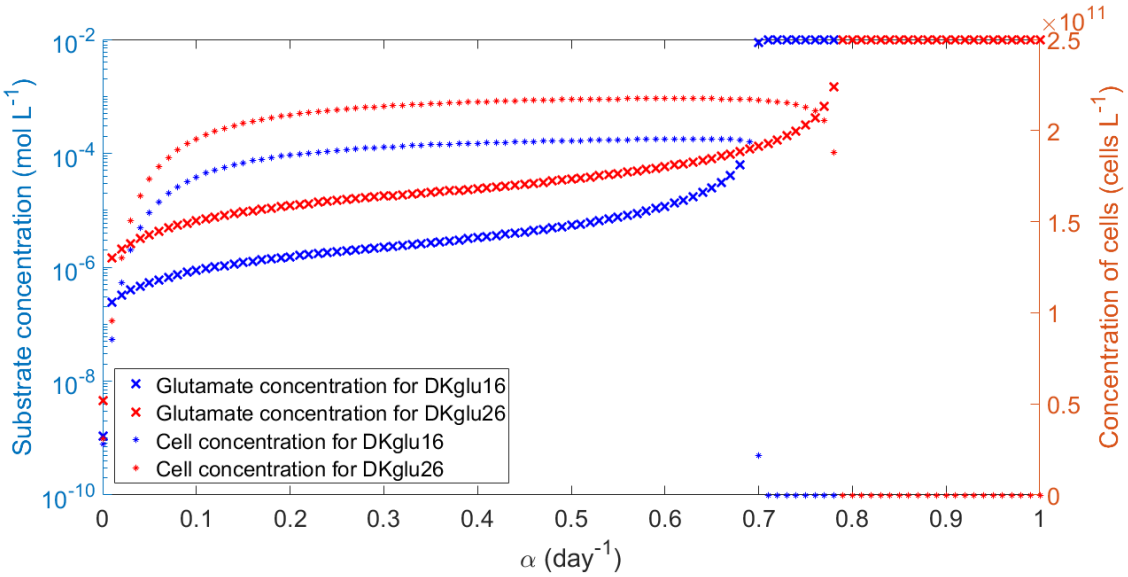

Figure 4.18: Plot of the steady state glutamate and biomass concentrations at different values of α for strains DKglu16 and DKglu26 with maintenance included.

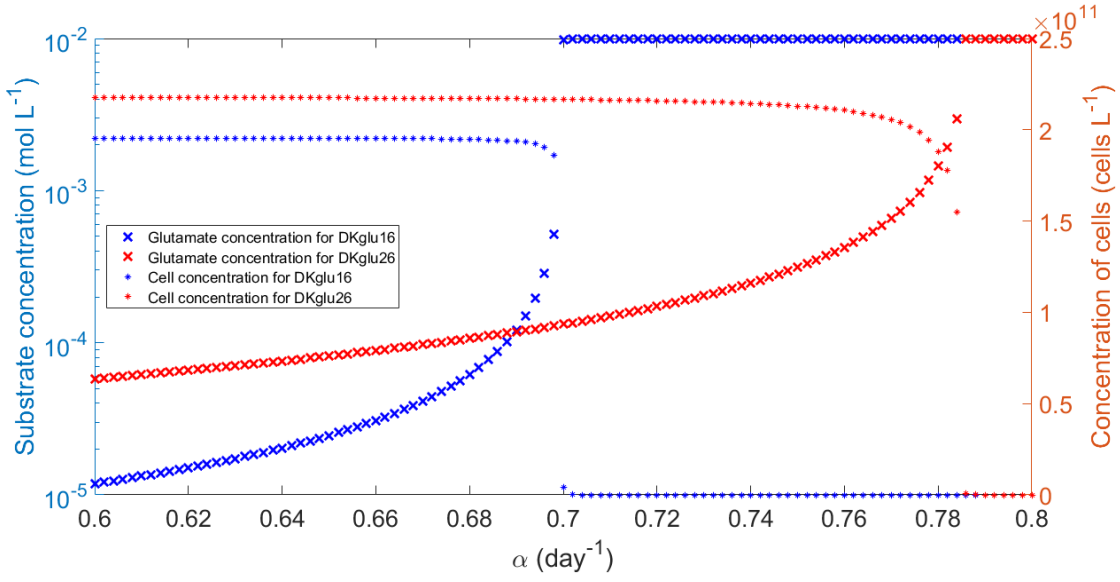

Figure 4.19: Plot of the steady state glutamate and biomass concentrations at different values of α, between 0.6 and 0.8, for strains DKglu16 and DKglu26 with maintenance included.

respectively, the equations that we get from the law of mass action are:

$$\frac{dX_{16}}{dt} = ((\eta_{16}q_{16} - m_{16})Y_{16} - \alpha)X_{16}, \tag{4.38}$$

$$\frac{dX_{26}}{dt} = ((\eta_{26}q_{26} - m_{26})Y_{26} - \alpha)X_{26}, \tag{4.39}$$

$$\frac{d[\text{Glutamate}]}{dt} = -q_{16}X_{16} - q_{26}X_{26} - \alpha[\text{Glutamate}] + 0.010\alpha, \tag{4.40}$$

$$\frac{d[\text{Acetate}]}{dt} = \frac{5}{3}q_{16}X_{16} + \frac{6}{5}q_{26}X_{26} - \alpha[\text{Acetate}], \tag{4.41}$$

$$\frac{d[\text{Propionate}]}{dt} = \frac{1}{3}q_{16}X_{16} - \alpha[\text{Propionate}], \tag{4.42}$$

$$\frac{d[\text{Butyrate}]}{dt} = \frac{2}{5}q_{26}X_{26} - \alpha[\text{Butyrate}], \tag{4.43}$$

$$\frac{d[\text{Ammonium}]}{dt} = q_{16}X_{16} + q_{26}X_{26} - \alpha[\text{Ammonium}], \tag{4.44}$$

$$\frac{d[\text{H}_2]}{dt} = 0, \tag{4.45}$$

$$\frac{d[\text{CO}_2]}{dt} = 0, \tag{4.46}$$

$$\frac{d[\text{H}^+]}{dt} = 0, \tag{4.47}$$

Note that we have already assumed that the flow into the system contains only glutamate at a concentration of $0.010\,\text{mol}\,\text{L}^{-1}$ to simplify the equations slightly.

Running the simulation first with $m = 0\,\text{mol}_{\text{ATP}}\,\text{cell}^{-1}\,\text{day}^{-1}$ and $\alpha = 0.1\,\text{day}^{-1}$ we get Figures 4.20 and 4.21 showing the concentrations of substrate and products and optimised ΔG_{ATP} over the course of 70 days. Note that the simulations were run for longer but the figures only show up to 70 days in order to allow the detail of the first 10 days to be visible while also giving a feeling for the steady state values that are being approached. Figure 4.22 shows the same simulation with a longer time span, highlighting that the quantities are reaching steady state values.

We can see that growth is initially uninhibited due to the large concentration of glutamate and DKglu26 grows faster due to having a larger value of η. After about 6 days, almost all of the glutamate has been consumed and both microbes are suddenly restricted and ΔG_{ATP} is optimised to values below 75 kJ $\text{mol}_{\text{ATP}}^{-1}$. DKglu16 is better able to cope in the low glutamate situation and continues to slowly grow while the population of DKglu26 decreases. The population

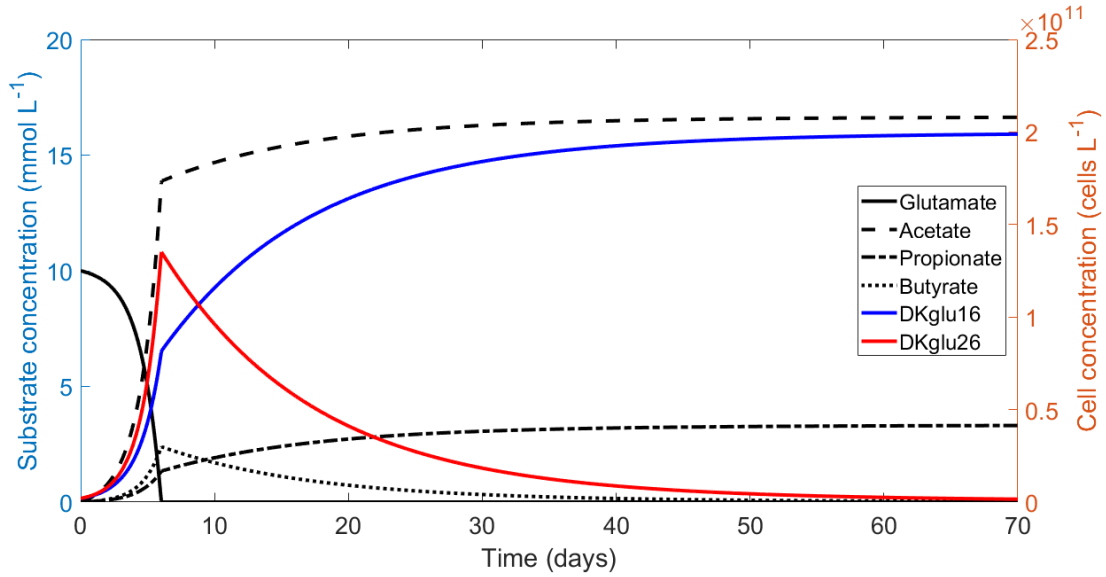

Figure 4.20: Plot of substrate, product, and cell concentrations during simulation of competition with $\alpha = 0.1$ day^{-1}.

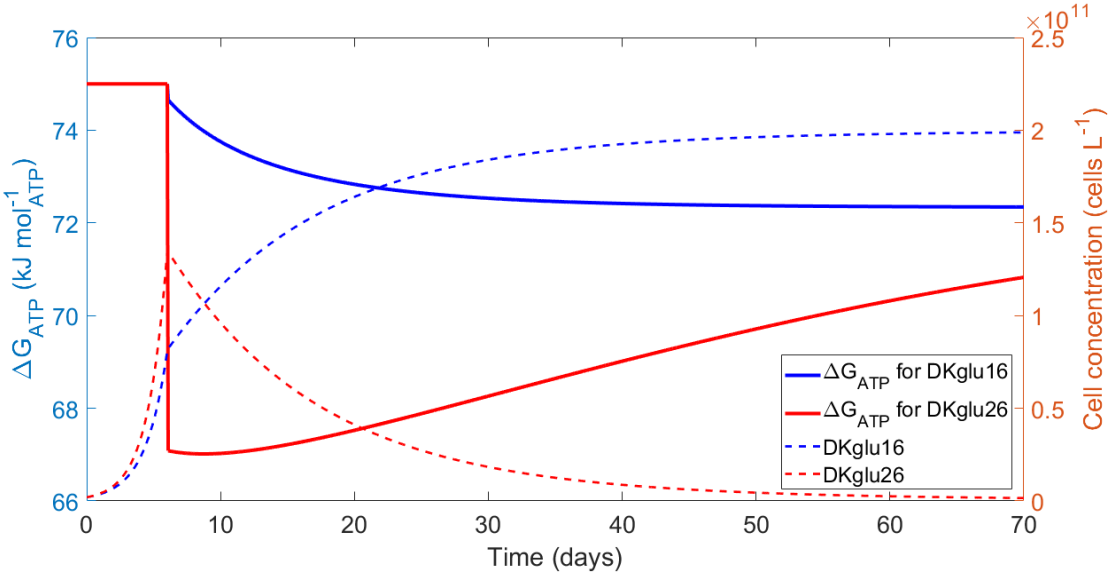

Figure 4.21: Plot of optimised ΔG_{ATP} for each microbe during simulation of competition with $\alpha = 0.1$ day^{-1}.

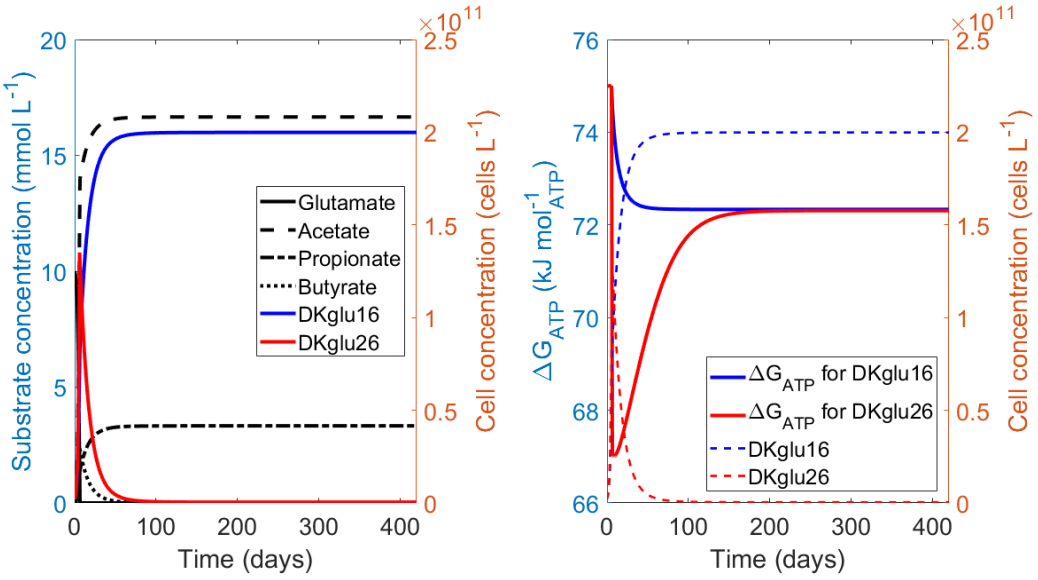

Figure 4.22: Plot of Figures 4.20 and 4.21 extended to show longer time span.

of DKglu26 reaches a steady value of about 4.0×10^8 cells L^{-1}, compared to 2.0×10^{11} cells L^{-1} for DKglu16. These concentrations suggest that the microbes can coexist for this particular set of conditions. Unfortunately Nanninga *et al.* didn't run their experiment for long enough for this coexistence to be seen. We will now consider what happens for a range of different values of α.

We start, again, with $m = 0\,\mathrm{mol_{ATP}}\,\mathrm{cell}^{-1}\,\mathrm{day}^{-1}$ and values of α between 0 and 1. The final concentration of each microbe for each value of α is shown in Figure 4.23. As predicted by the simulations for the microbes individually, we see DKglu16 dominating at low values of α before a change to a region where DKglu26 dominates at higher α. Both microbes are washed out of the system at even larger values of α. The changeover from DKglu16 dominance to DKglu26 dominance occurs in the region of α predicted when modelling the two microbes separately. We notice that the first region, where DKglu16 is dominating, both microbes coexist. DKglu16 reaches a steady state concentration of about 2.0×10^{11} cells L^{-1}, while the lowest concentration of DKglu26 in this simulation is more than 4.0×10^8 cells L^{-1} after 70 days and is still above 3.9×10^8 cells L^{-1} after the simulation runs for 420 days. This suggests stable coexistence, rather than DKglu26 slowly being eliminated. We do not see stable coexistence in the region where DKglu26 is more successful because the value of α is too large for DKglu16 to survive.

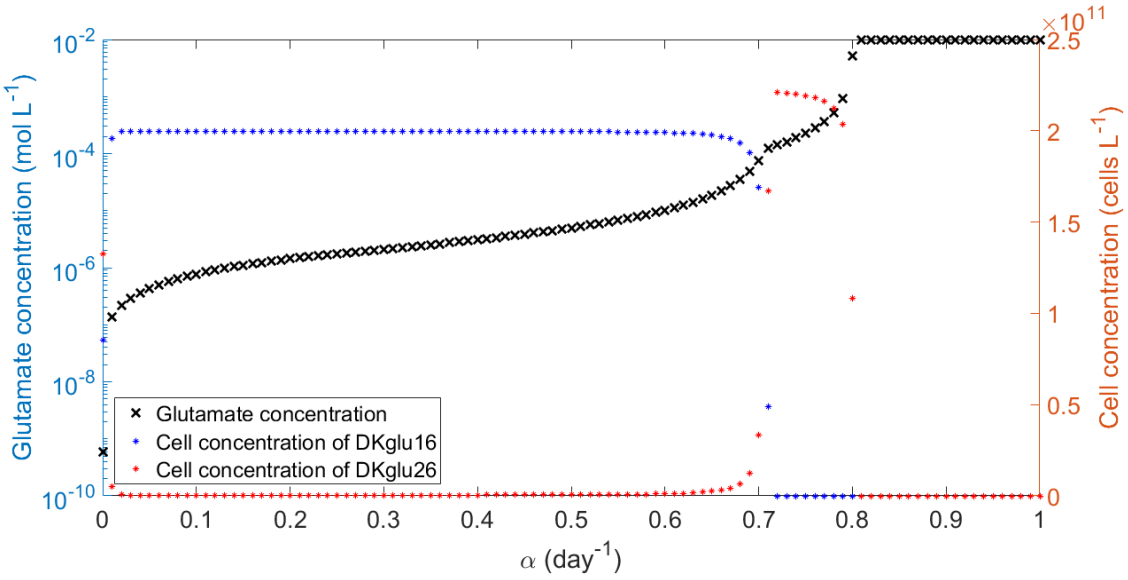

Figure 4.23: Plot of the steady-state glutamate and biomass concentrations at different values of α for DKglu16 and DKglu26 in competition with each other.

We consider now what happens if m is non-zero. The result, shown in Figure 4.24, is what we expect from the simulations where the microbes were growing separately. The crossover point where the dominant microbe changes is shifted to a smaller value of α and the value of α where both microbes are washed out also decreases, compared to the case without maintenance. As before, the simulation shown in Figure 4.24 uses 6.22×10^{-16} mol_{ATP} cell^{-1} day^{-1}, and using a larger value for m causes the same behaviour to happen at lower values of α. Once again, the lowest concentration of DKglu26 in the region where it is being outperformed by DKglu16 is about 3.8×10^8 cells L^{-1} after the simulation runs for 70 days and is still above 3.7×10^8 cells L^{-1} after the simulation runs for 420 days, suggesting again that the microbes are coexisting.

We have assumed a great deal about these two microbes, only really differentiating them by their glutamate fermentation pathways and their ATP yields, η. Included in these simplifying assumptions, we have taken Y, q_{max}, and m to be the same for both microbes. The approximate cell dimensions of DKglu16 and DKglu26 reported in Nanninga *et al.* [132] show that cells of DKglu26 have a greater volume than cells of DKglu16 by an order of magnitude. The yield, maintenance, and maximum substrate turnover are being calculated per cell and they could be affected by cell size. The model allows us to investigate the effects of setting these parameters to different values for the two microbes, increasing Y by a factor of 10 and decreasing each of

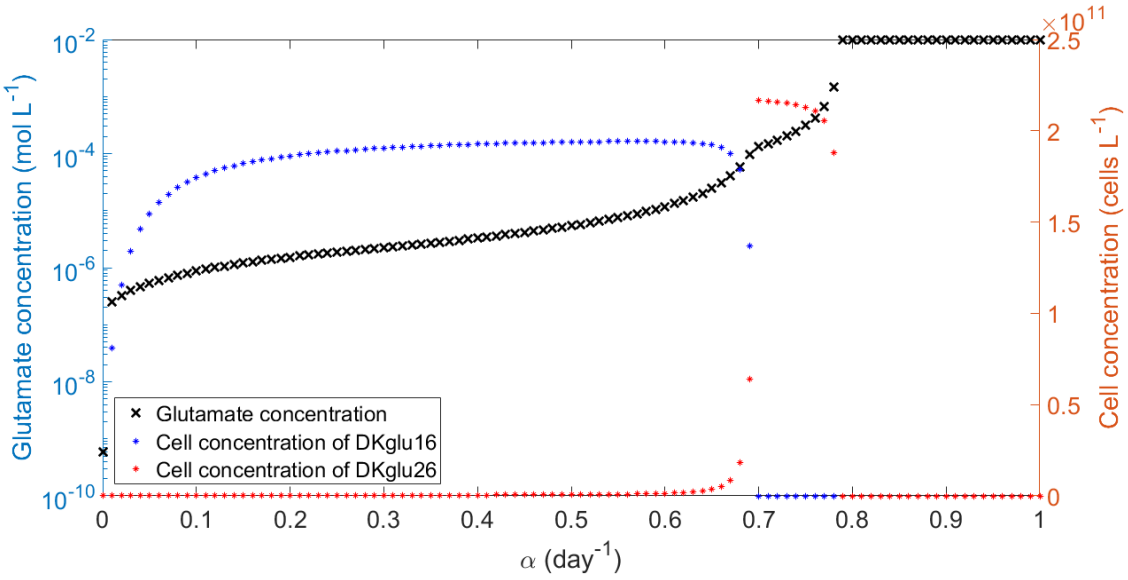

Figure 4.24: Plot of the steady-state glutamate and biomass concentrations at different values of α for DKglu16 and DKglu26 in competition with each other and with maintenance included.

$q_{\max}$ and m by a factor of 10 for DKglu16. The result of running the simulation at values of α between 0 and 1 is shown in Figure 4.25. We see that the general shape is very similar but the cell concentrations of DKglu16 have increased by a factor of about 10. The interval of values of α that cause washout of DKglu16 and allow DKglu26 to thrive starts and ends at approximately the same values of α compared when the cell dimensions are the same (Figure 4.24). Including the considerations of different cell size had no qualitative change to the growth behaviour of the microbes or how they competed with each other. This suggests that the outcomes with microbes of different sizes can be represented well by the model even if the same cell size is assumed. Thus we don't even need to know the cell volumes.

The simulations appear to show a range of values for α where the two microbes are in very different concentrations to each other, but have stable concentrations, suggesting coexistence. We can consult the differential equations to see if we could reach this conclusion analytically. Eqs. (4.38)-(4.47), the differential equations we derived from the law of mass action, must each

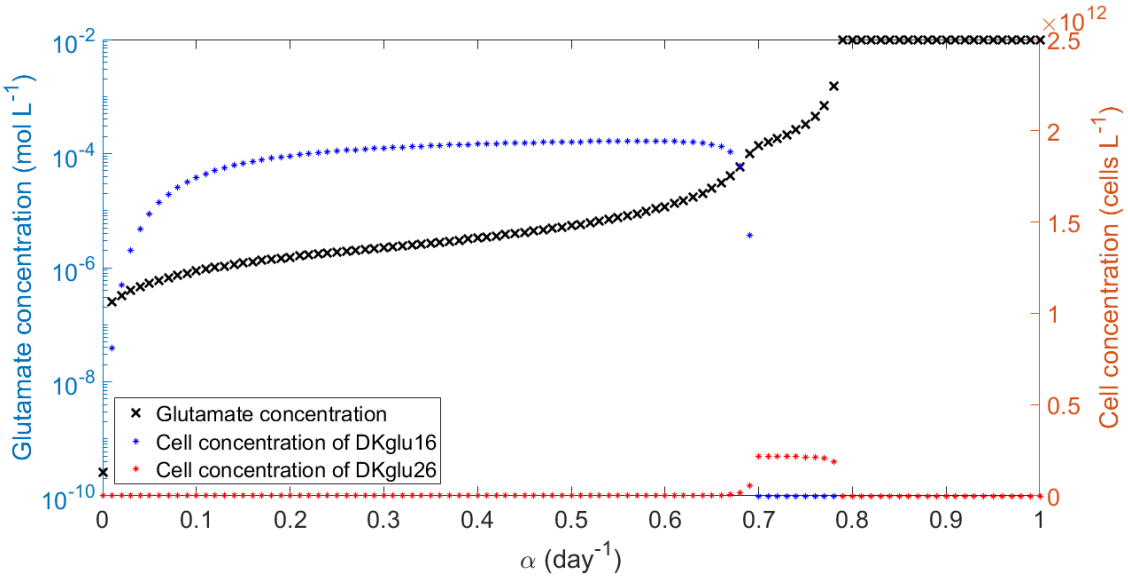

Figure 4.25: Plot of the steady-state glutamate and biomass concentrations at different values of α for DKglu16 and DKglu26 in competition with each other, with maintenance included, and considering the relative sizes of the two microbes by changing Y, q_{max}, and m as described in the text.

be equal to 0 and so we can learn something from the first seven equations. We get:

$$[\text{DKglu16}]_f = 0 \text{ or } \alpha = (\eta_{16} q_{16} - m_{16}) Y_{16}, \tag{4.48}$$

$$[\text{DKglu26}]_f = 0 \text{ or } \alpha = (\eta_{26} q_{26} - m_{26}) Y_{26}, \tag{4.49}$$

$$[\text{Glutamate}]_f = \frac{1}{100} - \frac{1}{\alpha} \left(q_{16} X_{16} + q_{26} X_{26} \right), \tag{4.50}$$

$$[\text{Acetate}]_f = \frac{1}{\alpha} \left(\frac{5}{3} q_{16} X_{16} + \frac{6}{5} q_{26} X_{26} \right), \tag{4.51}$$

$$[\text{Propionate}]_f = \frac{1}{\alpha} \left(\frac{1}{3} q_{16} X_{16} \right), \tag{4.52}$$

$$[\text{Butyrate}]_f = \frac{1}{\alpha} \left(\frac{2}{5} q_{26} X_{26} \right), \tag{4.53}$$

$$[\text{Ammonium}]_f = \frac{1}{\alpha} \left(q_{16} X_{16} + q_{26} X_{26} \right), \tag{4.54}$$

where the subscript f denotes the final concentration. To get coexistence, we assume the final concentration of both microbes is non-zero so we can rearrange the right-hand parts of Eqs.

(4.48) and (4.49) to get

$$q_{16} = \frac{1}{\eta_{16}}\left(\frac{\alpha}{Y_{16}} + m_{16}\right), \tag{4.55}$$

$$q_{26} = \frac{1}{\eta_{26}}\left(\frac{\alpha}{Y_{26}} + m_{26}\right), \tag{4.56}$$

and note that if $m_{16} = m_{26}$ and $Y_{16} = Y_{26}$ then $\eta_{16}q_{16} = \eta_{26}q_{26}$.

To make things easier to read, the final concentrations of glutamate, acetate, propionate, butyrate, carbon dioxide, ammonium, and hydrogen will be designated: G, A, P, B, C, N, and H respectively. We can find relationships between Eqs. (4.50)-(4.54) giving us

$$3P + \frac{5}{2}B - N = 0, \tag{4.57}$$

$$5P + 3B - A = 0, \tag{4.58}$$

$$N + G = \frac{1}{100}. \tag{4.59}$$

We replace the q_{16} in Eq. (4.52) using Eq. (4.55) to get

$$P = \frac{1}{\alpha}\left(\frac{1}{3}\frac{1}{\eta_{16}}\left(\frac{\alpha}{Y_{16}} + m_{16}\right)X_{16}\right), \tag{4.60}$$

$$X_{16} = \frac{3\alpha\eta_{16}}{\frac{\alpha}{Y_{16}} + m_{16}}P,$$

$$X_{16} = \frac{3\alpha\eta_{16}Y_{16}}{\alpha + m_{16}Y_{16}}P, \tag{4.61}$$

$$X_{16} - \frac{3\alpha\eta_{16}Y_{16}}{\alpha + m_{16}Y_{16}}P = 0. \tag{4.62}$$

Similarly, for q_{26} in Eq. (4.53) using Eq. (4.56), we get

$$B = \frac{1}{\alpha}\left(\frac{2}{5}\frac{1}{\eta_{26}}\left(\frac{\alpha}{Y_{26}} + m_{26}\right)X_{26}\right), \tag{4.63}$$

$$X_{26} = \frac{\frac{5}{2}\alpha\eta_{26}}{\frac{\alpha}{Y_{26}} + m_{26}}B,$$

$$X_{26} = \frac{\frac{5}{2}\alpha\eta_{26}Y_{26}}{\alpha + m_{26}Y_{26}}B, \tag{4.64}$$

$$X_{26} - \frac{\frac{5}{2}\alpha\eta_{26}Y_{26}}{\alpha + m_{26}Y_{26}}B = 0. \tag{4.65}$$

For each value of α in the coexistence region of Figure 4.24, the relationships in Eqs. (4.57)-(4.59), (4.62), and (4.65) held when using the steady state concentrations.

We have two equations for q_{16}, Eq. (4.55) along with

$$q_{16} = \frac{\nu_{16} - \nu_{16\text{min}}}{\nu_{16\text{max}} - \nu_{16\text{min}}} q_{\text{max}} \frac{G - \zeta_{16}\nu_{16}}{K_{\text{Lynch}} + G + \zeta_{16}\nu_{16}}, \tag{4.66}$$

where

$$\zeta_{16} = \frac{A^{5/3}P^{1/3}C^{2/3}N}{\exp\left(\Delta G_{T16}/RT\right)} \tag{4.67}$$

and $C = 0.013\,\text{mol}\,\text{L}^{-1}$ is a constant. For brevity, we write K_{Lynch} as K for the remainder of this section. Eqs. (4.55), (4.66), and (4.67) give

$$\left(\frac{\nu_{16} - \nu_{16\text{min}}}{\nu_{16\text{max}} - \nu_{16\text{min}}}\right) q_{\text{max}} \frac{G - \frac{A^{5/3}P^{1/3}C^{2/3}N}{\exp\left(\Delta G_{T16}/RT\right)}\nu_{16}}{K + G + \frac{A^{5/3}P^{1/3}C^{2/3}N}{\exp\left(\Delta G_{T16}/RT\right)}\nu_{16}} = \frac{1}{\eta_{16}}\left(\frac{\alpha}{Y_{16}} + m_{16}\right). \tag{4.68}$$

This becomes

$$\left(\frac{\nu_{16} - \nu_{16\text{min}}}{\nu_{16\text{max}} - \nu_{16\text{min}}}\right) q_{\text{max}}\eta_{16}Y_{16}\left(G - C^{2/3}\frac{A^{5/3}P^{1/3}N}{\exp\left(\Delta G_{T16}/RT\right)}\nu_{16}\right) = \left(\alpha + m_{16}Y_{16}\right)\left(K + G + C^{2/3}\frac{A^{5/3}P^{1/3}N}{\exp\left(\Delta G_{T16}/RT\right)}\nu_{16}\right) \tag{4.69}$$

or

$$\left[\left(\frac{\nu_{16} - \nu_{16\text{min}}}{\nu_{16\text{max}} - \nu_{16\text{min}}}\right) q_{\text{max}}\eta_{16}Y_{16} - \left(\alpha + m_{16Y_{16}}\right)\right] G - \left[\left(\frac{\nu_{16} - \nu_{16\text{min}}}{\nu_{16\text{max}} - \nu_{16\text{min}}}\right) q_{\text{max}}\eta_{16}Y_{16} + \left(\alpha + m_{16Y_{16}}\right)\right] C^{2/3}\frac{A^{5/3}P^{1/3}N\nu_{16}}{\exp\left(\Delta G_{T16}/RT\right)} = \left(\alpha + m_{16}Y_{16}\right)K. \tag{4.70}$$

This is complicated and if $\nu_{16} \neq \nu_{16\text{max}}$ (recall $\nu_{16\text{max}}$ is $\exp\left(75 \times \eta_{16}/RT\right)$ as $\Delta G_{\text{ATPmax}} = 75$) then

$$\nu_{16} = \frac{-\left(K + G\right) + \sqrt{\left(K + G\right)^2 + \zeta_{16}K\nu_{16\text{min}} + 2\zeta_{16}G\nu_{16\text{min}} + KG + G^2}}{\zeta_{16}}, \tag{4.71}$$

which increases the complexity and introduces several instances of ζ_{16} (which is equivalent to Eq. (4.67)). So, if the steady state is in a region where the penalty function is still acting, Eq. (4.70) gets significantly more unyielding (according to Eqs. (4.67) and (4.71)). If, instead, the penalty function is not acting at the steady state, Eq. (4.70) simplifies slightly with ν_{16} becoming the constant $\nu_{16\max}$ and the $\frac{\nu_{16}-\nu_{16\min}}{\nu_{16\max}-\nu_{16\min}}$ terms disappear from the coefficients of G and C.

We next repeat the process from Eqs. (4.66)-(4.71) for the analogous scenario with q_{26}. For q_{26} we have Eq. (4.56) and

$$q_{26} = \frac{\nu_{26} - \nu_{26\min}}{\nu_{26\max} - \nu_{26\min}} q_{\max} \frac{G - \zeta_{26}\nu_{26}}{K_{\text{Lynch}} + G + \zeta_{26}\nu_{26}} \tag{4.72}$$

where

$$\zeta_{26} = \frac{A^{6/5}B^{2/5}CNH^{1/5}}{10^{-pH\cdot 0.4}\exp\left(\Delta G_{T26}/RT\right)}. \tag{4.73}$$

$C = 0.013\,\text{mol}\,\text{L}^{-1}$, $H = 0.001\,\text{mol}\,\text{L}^{-1}$, and $pH = 6.5$ are constants. Eqs. (4.56), (4.72), and (4.73) give

$$\left(\frac{\nu_{26} - \nu_{26\min}}{\nu_{26\max} - \nu_{26\min}}\right) q_{\max} \frac{G - \frac{A^{6/5}B^{2/5}CNH^{1/5}}{10^{-2.6}\exp\left(\Delta G_{T26}/RT\right)}\nu_{26}}{K + G + \frac{A^{6/5}B^{2/5}CNH^{1/5}}{10^{-2.6}\exp\left(\Delta G_{T26}/RT\right)}\nu_{26}} = \frac{1}{\eta_{26}}\left(\frac{\alpha}{Y_{26}} + m_{26}\right). \tag{4.74}$$

This becomes

$$\begin{aligned}\left(\frac{\nu_{26} - \nu_{26\min}}{\nu_{26\max} - \nu_{26\min}}\right) q_{\max}\eta_{26}Y_{26}\left(G - CH^{1/5}\frac{A^{6/5}B^{2/5}N}{10^{-2.6}\exp\left(\Delta G_{T26}/RT\right)}\nu_{26}\right) \\ = (\alpha + m_{26}Y_{26})\left(K + G + CH^{1/5}\frac{A^{6/5}B^{2/5}N}{10^{-2.6}\exp\left(\Delta G_{T26}/RT\right)}\nu_{26}\right)\end{aligned} \tag{4.75}$$

or

$$\left[\left(\frac{\nu_{26}-\nu_{26\min}}{\nu_{26\max}-\nu_{26\min}}\right)q_{\max}\eta_{26}Y_{26}-(\alpha+m_{26Y_{26}})\right]G - \left[\left(\frac{\nu_{26}-\nu_{26\min}}{\nu_{26\max}-\nu_{26\min}}\right)q_{\max}\eta_{26}Y_{26}+(\alpha+m_{26Y_{26}})\right]CH^{1/5}\frac{A^{6/5}B^{2/5}N\nu_{26}}{10^{-2.6}\exp\left(\Delta G_{T26}/RT\right)} = (\alpha+m_{26}Y_{26})\,K. \quad (4.76)$$

Similar to the case with q_{16}, $\nu_{26\max}=\exp\left(75\times\eta_{26}/RT\right)$ and if $\nu_{26}\neq\nu_{26\max}$ then

$$\nu_{26}=\frac{-(K+G)+\sqrt{(K+G)^2+\zeta_{26}K\nu_{26\min}+2\zeta_{26}G\nu_{26\min}+KG+G^2}}{\zeta_{26}}. \quad (4.77)$$

So, if the penalty function is acting at the steady state, Eq. (4.76) increases in complexity (according to Eqs. (4.73) and (4.77)). Otherwise, Eq. (4.76) simplifies slightly.

Given the complexity of Eqs. (4.70) and (4.76), we consider the case without the penalty function to investigate whether or not the simplified problem is tractable. Therefore $\frac{\nu-\nu_{\min}}{\nu_{\max}-\nu_{\min}}$ is eliminated from Eqs. (4.66) and (4.72). ΔG_{ATP} is now a constant so the remaining ν's are constants (as $\nu=\exp\left(\eta\Delta G_{\mathrm{ATP}}/RT\right)$). This means that Eqs. (4.70) and (4.76) become:

$$\left[q_{\max}\eta_{16}Y_{16}-(\alpha+m_{16Y_{16}})\right]G - \left[q_{\max}\eta_{16}Y_{16}+(\alpha+m_{16Y_{16}})\right]\frac{C^{2/3}\nu_{16}}{\exp\left(\Delta G_{T16}/RT\right)}A^{5/3}P^{1/3}N = (\alpha+m_{16}Y_{16})\,K \quad (4.78)$$

and

$$\left[q_{\max}\eta_{26}Y_{26}-(\alpha+m_{26Y_{26}})\right]G - \left[q_{\max}\eta_{26}Y_{26}+(\alpha+m_{26Y_{26}})\right]\frac{CH^{1/5}\nu_{26}}{10^{-2.6}\exp\left(\Delta G_{T26}/RT\right)}A^{6/5}B^{2/5}N = (\alpha+m_{26}Y_{26})\,K. \quad (4.79)$$

We now have seven equations in seven unknowns, Eqs. (4.78) and (4.79) along with

$$3P + \frac{5}{2}B - N = 0, \tag{4.80}$$

$$5P + 3B - A = 0, \tag{4.81}$$

$$N + G = \frac{1}{100}, \tag{4.82}$$

$$X_{16} - \frac{3\alpha\eta_{16}Y_{16}}{\alpha + m_{16}Y_{16}}P = 0, \tag{4.83}$$

$$X_{26} - \frac{\frac{5}{2}\alpha\eta_{26}Y_{26}}{\alpha + m_{26}Y_{26}}B = 0. \tag{4.84}$$

We use Eq. (4.82) to get $G = \frac{1}{100} - N$, then eliminate G from (4.78) and (4.79):

$$\begin{aligned} &- \left[q_{\max}\eta_{16}Y_{16} - (\alpha + m_{16Y_{16}})\right] N \\ &\quad - \left[q_{\max}\eta_{16}Y_{16} + (\alpha + m_{16Y_{16}})\right] \frac{C^{2/3}\nu_{16}}{\exp\left(\Delta G_{T16}/RT\right)} A^{5/3}P^{1/3}N \\ &\qquad = \left(\alpha + m_{16}Y_{16}\right) K - \frac{1}{100}\left[q_{\max}\eta_{16}Y_{16} - (\alpha + m_{16Y_{16}})\right] \end{aligned} \tag{4.85}$$

and

$$\begin{aligned} &- \left[q_{\max}\eta_{26}Y_{26} - (\alpha + m_{26Y_{26}})\right] N \\ &\quad - \left[q_{\max}\eta_{26}Y_{26} + (\alpha + m_{26Y_{26}})\right] \frac{CH^{1/5}\nu_{26}}{10^{-2.6}\exp\left(\Delta G_{T26}/RT\right)} A^{6/5}B^{2/5}N \\ &\qquad = \left(\alpha + m_{26}Y_{26}\right) K - \frac{1}{100}\left[q_{\max}\eta_{26}Y_{26} - (\alpha + m_{26Y_{26}})\right]. \end{aligned} \tag{4.86}$$

Next, we replace N and A using (4.80) and (4.81), leaving equations in P and B only. We have $N = 3P + \frac{5}{2}B$ and $A = 5P + 3B$. Replacing N and A gives

$$-R_1\left(3P + \frac{5}{2}B\right) - R_2\left(5P + 3B\right)^{5/3}P^{1/3}\left(3P + \frac{5}{2}B\right) = R_3 - \frac{1}{100}R_1, \tag{4.87}$$

$$-R_4\left(3P + \frac{5}{2}B\right) - R_5\left(5P + 3B\right)^{6/5}B^{2/5}\left(3P + \frac{5}{2}B\right) = R_6 - \frac{1}{100}R_4, \tag{4.88}$$

where

$$R_1 = q_{\max}\eta_{16}Y_{16} - (\alpha + m_{16Y_{16}}), \tag{4.89}$$

$$R_2 = [q_{\max}\eta_{16}Y_{16} + (\alpha + m_{16Y_{16}})]\,\frac{C^{2/3}\nu_{16}}{\exp(\Delta G_{T16}/RT)}, \tag{4.90}$$

$$R_3 = (\alpha + m_{16}Y_{16})\,K, \tag{4.91}$$

$$R_4 = q_{\max}\eta_{26}Y_{26} - (\alpha + m_{26Y_{26}}), \tag{4.92}$$

$$R_5 = [q_{\max}\eta_{26}Y_{26} + (\alpha + m_{26Y_{26}})]\,\frac{CH^{1/5}\nu_{26}}{10^{-2.6}\exp(\Delta G_{T26}/RT)}, \tag{4.93}$$

$$R_6 = (\alpha + m_{26}Y_{26})\,K. \tag{4.94}$$

Note that $R_1 - R_6$ are all constants. Using Eqs. (4.61) and (4.64) we can see that if we could solve Eqs. (4.87) and (4.88) for P and B then the values of X_{16} and X_{26} will follow. Eqs. (4.87) and (4.88), while two equations in two unknowns, do not solve analytically, due in part to the different fractional powers on terms containing P and B. As this is the simplified version of the problem, where we eliminated the penalty function, we cannot solve the full problem analytically either. This means that only dealing with the equations analytically, there would not be coexistence apparent. The numerical simulations show evidence that the two populations are reaching non-zero steady states and this supports stable coexistence. It is known that using the Monod model, only one population can survive [69]. However, it is known, at least for special cases, that coexistence can be established analytically when thermodynamic inhibition is considered [59] [178]. The simulations we have explored provide numerical evidence for coexistence of this sort, which would not occur without the thermodynamic inhibition terms that we have (r and θ). Unfortunately, Nanninga *et al.* did not run their experiment for long enough to provide experimental support for this coexistence.

The versatility of the model has been shown through the three examples that we have explored: microbes growing on malonate, a microbe growing on crotonate, and two microbes growing on glutamate. The utility is shown, in particular, in the final example where, in addition to qualitatively reproducing what Nanninga *et al.* found experimentally for the two microbes, we are able to make predictions about the microbes growing in competition with each other

including predicting coexistence which we wouldn't find by attempting to analytically solve the system.

All of the work so far assumes that there is a single substrate limiting the reaction rate and all other reactants are present in such excess that their concentrations are effectively constant and they have no influence on the reaction rate. This is not always the case. While there can only be one reactant that limits how much of a reaction can occur, there can be multiple reactants limiting the rate of the reaction [167] [16]. We noted earlier that we would like our model to be able to be extended to include multiple rate-limiting substrates. We turn our attention to this in Chapter 5.

Chapter 5

Multiple Rate-Limiting Substrates

5.1 Introduction and Empirical Rates

The energy metabolism of most microbes is driven by the simultaneous use of at least two compounds. Sometimes one of these is water, which is normally available in excess, present at about $55\,\mathrm{mol\,L^{-1}}$ when the other substrate might be present at a concentration six orders of magnitude smaller. This is the same regime as the models discussed so far; they are for the growth of microbes where there is one rate-limiting substrate. However, sometimes multiple reactants in energy metabolism, other than water, are required and are present at similar low concentrations. A microbe growing using two compounds that are simultaneously required for ATP generation could experience conditions where both are at concentrations that, if either was considered alone, would limit the growth rate. These effects could be primarily kinetic (i.e., via Monod kinetics) or thermodynamic. A model that allows thermodynamic limitation of the rates of substrate use and ATP formation under multiple substrate limitation would be useful to explore how microbes might respond or compete. This has to be differentiated from other types of limitation also called dual substrate limitation, where a microbe could be limited for an energy substrate and a second compound not directly involved in ATP generation, e.g., for the supply of nitrogen, etc., to form cell material. Indeed, there is a large literature on dual carbon and nitrogen limitation that is not directly applicable to our question.

Dual substrate limitation for ATP formation can occur in different systems, such as during

oxygen and hydrogen use in termite guts [24], nitrification in waste water treatment [166], and in the coexistence and competition between different pathways of nitrate reduction [175]. One more detailed example is described here, of microbes in anaerobic sediments. Sulfate-reducing bacteria (SRB) mainly use substrates like acetate or hydrogen as energy sources, linking their oxidation to the reduction of sulfate to sulfide. Methanogens can also use acetate or hydrogen for methane formation, but are less competitive than SRB if sulfate concentrations are large enough [36] [107] [156]. Kuivila *et al.* [95] showed that sulfate reduction by SRB coupled to these substrates dominated in Lake Washington sediments where sulfate concentrations were about 35 to 40 μmol L^{-1}. Acetate and hydrogen concentrations were lower in those strata of the sediment, in agreement with a kinetic or threshold limitation on the use of those substrates by methanogens. Deeper in the sediments, where sulfate concentrations were lower, the acetate and hydrogen concentrations were greater, suggesting sulfate limitation for SRB but substrate concentrations that result in favourable thermodynamic conditions for methanogenic use of acetate and hydrogen. A model allowing dual substrate limitation of the energy source (hydrogen or acetate for methanogens and SRB) and sulfate (the electron acceptor for SRB) would be useful for modelling and understanding the transition from sulfate reduction to methanogenesis with increasing depth in such sediments.

For simplicity, we will assume only two substrates limiting the growth rate and let A and B denote the concentrations of these substrates. Before building a two substrate model we must remind ourselves of some potential schemes for microbial metabolism and highlight our focus. Figure 5.1 illustrates the simplified metabolism scheme for the single substrate case which was explained in more detail earlier (Figure 5.1(a)), along with three different two substrate schemes. Figure 5.1(b) illustrates a metabolism where one substrate is required in the series of reactions that result in the production of ATP and the second substrate is required in the series of reactions that result in the production of new cell material. Figure 5.1(c) illustrates a scheme where there are two different metabolisms, each of which only requires one of the substrates, that are effectively two copies of the single substrate case with alternative substrates. Figure 5.1(d) illustrates a metabolism where both substrates are required in the series of reactions that result in the production of ATP. We assume that both substrates are needed at a fixed ratio

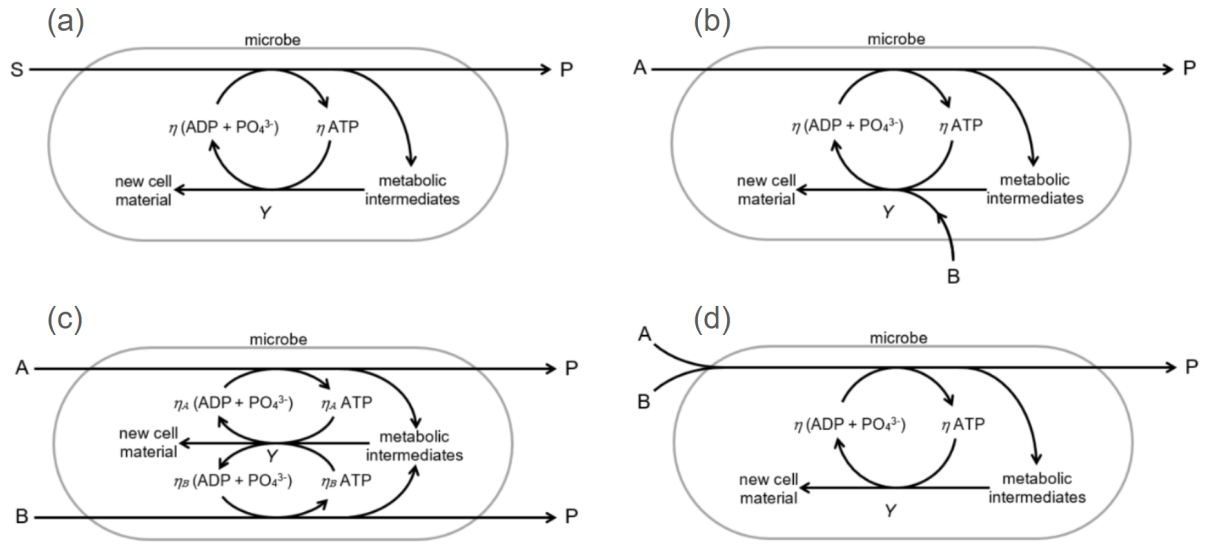

Figure 5.1: Simplified schemes for microbial metabolism. Schemes include: (a) a single substrate produces ATP, S; (b) a substrate, A, is required in producing ATP and a second substrate, B, is required in creating new cell material; (c) either of two substrates, A and B, can be used to produce ATP; and (d) both of the two substrates A and B are required to produce ATP.

determined by the metabolism of the microbe (i.e., they are not simply alternative substrates for the microbe) and, in particular, both are required in the pathway that produces ATP. The scheme of interest in this chapter is the one shown in Figure 5.1(d), repeated in Figure 5.2, whenever multiple rate-limiting substrates are considered. We have chosen to use this scheme because we are interested in thermodynamic effects on microbial ATP formation, and this model represents the case where both substrates are unconditionally required to form ATP. This is not the case for the schemes shown in Figures 5.1(b), or 5.1(c).

There are two promising avenues to pursue for models that incorporate thermodynamic feedback for microbial growth when there are multiple rate-limiting substrates. The first is the enzyme kinetics developed by Briggs and Haldane [22]. These kinetics can be generalised to multiple substrates, and a thermodynamic term will emerge as in the single substrate case. The second is the statistical mechanics approach of Desmond-Le Quéméner and Bouchez [39], which can be adapted for multiple substrates with a product of Boltzmann distributions. In both cases the obvious challenge is the identification and interpretation of the thermodynamic terms.

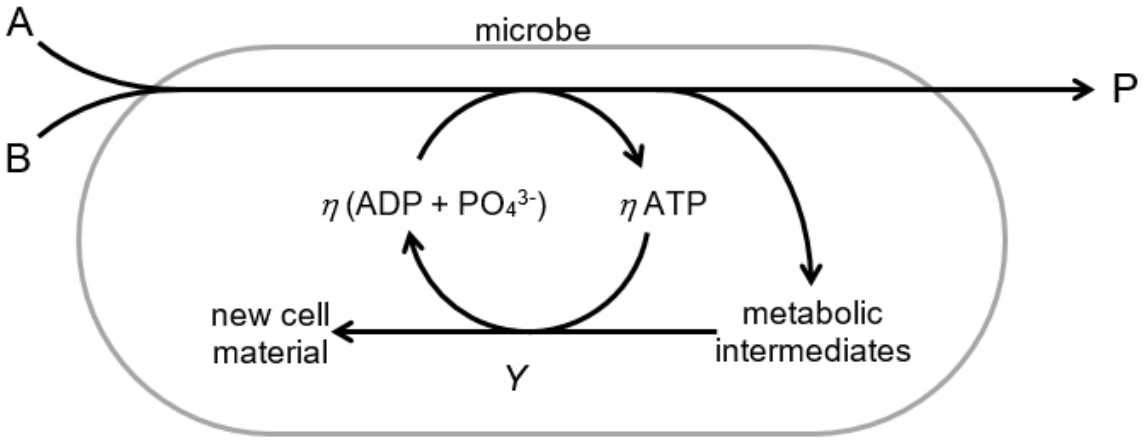

Figure 5.2: Simplified scheme for microbial metabolism where both of the two substrates A and B are required at a fixed stoichiometry to produce ATP.

Here, we concentrate on the general problem and look briefly at some empirical solutions before discussing the enzyme kinetics and statistical mechanics approaches in some detail. Some immediate questions arise concerning (among other things) any interaction between the substrates and whether the order of reaction is important. Bader [6], [7] partitions multiple substrate models into two cases, recognising that most models will be somewhere between these extremes. He describes two options that reflect the relations between the substrates and the microbe: noninteractive and interactive. In a noninteracting model, the substrates are considered separately, treating the other substrate as not limiting. In this manner we find the two rates, ignoring the other substrate. The smaller of the two rates is then used as the growth rate. For instance, if we use the Monod rates associated with A and B, we have

$$q_A = \frac{A}{K_A + A}$$
$$q_B = \frac{B}{K_B + B},$$

then the noninteractive model would give the rate

$$q_1 = \min\{q_A, q_B\}. \tag{5.1}$$

The noninteractive model, Bader argues, may be applicable for an organism that has two

separate subsystems (metabolic pathways) that consume different substrates and produce different products. The reactions are needed for reproduction, but the pathways do not require intermediates or products from the other pathway: they function independently. This is similar to the scheme schown in Figure 5.1(c). In this scenario if, say, $q_B > q_A$, then the product associated with B is produced in excess, and the growth rate is q_A. Bader [6] notes that "... it is unlikely that any two cellular subsystems would be totally independent of each other. However, the degree of interaction between certain subsystems may be rather small. In such cases, a noninteractive type of model may accurately describe the growth rate of the organism." In contrast, the interactive model is based on the premise that if both substrates are present in limiting quantities, then both must affect the growth rate. Continuing with the Monod rates, a simple interactive model would yield the so called "double Monod" rate

$$q_2 = q_A q_B. \tag{5.2}$$

Bader gives two examples where there is a strong interaction. The first involves a microbe that requires the presence of a substrate (cofactor) B to convert substrate A into a product required for growth. The second is an enzyme that requires two substrates (in linked pathways) to produce a product. This is the case of greatest interest for us, shown in Figure 5.1(d).

The double Monod rate was proposed by Megee *et al.* [116] and used subsequently by Ryder and Sinclair [148] in a model for the growth of aerobic microbes. Howell and Atkinson [68] also use this rate in a fermentation problem and consider the rate

$$q_3 = \frac{1}{1 + \frac{K_A}{A} + \frac{K_B}{B}}, \tag{5.3}$$

introduced by Bright and Appleby [23]. Mankad and Bunday [111] proposed a rate of the form

$$q_4 = W_A q_A + W_B q_B, \tag{5.4}$$

where the W_k are weight coefficients based on relative saturations, i.e.,

$$W_A = \frac{\frac{K_A}{A}}{\frac{K_A}{A} + \frac{K_B}{B}}$$
$$W_B = \frac{\frac{K_B}{B}}{\frac{K_A}{A} + \frac{K_B}{B}}.$$

A criticism of the double Monod rate raised by Mankad and Bungay [111] is that q_2 predicted rates that were too small when A and B are small, and that the problem is amplified if more limiting substrates are included in a model (more "Monod factors"). Note that

$$q_4 = q_2 \left(\frac{2K_A K_B}{K_A B + K_B A} + 1 \right),$$

so that $q_4 > q_2$. The rate q_4 was also adapted by Bungay [27] to include inhibitory terms.

The rates q_k introduced above are empirical. Generally these rates were introduced to overcome a problem with another rate, and the new rate was justified by experimental evidence. In short, a very limited amount of modelling was used to deduce these rates, and this makes it difficult to further model systems that have thermodynamic feedback directly from these rates. As with the single limiting substrate case, however, the functional form of these rates can reappear from an analogy with enzyme kinetics (much like the Monod form appears as the Michaelis-Menten rate) and statistical mechanics. We discuss these approaches in more detail in the following subsections. Here, however, we mention that Bertolazzi [14] derived these rates from a simple cell model. In fact, a general function form of the rate was derived that included q_1, q_2, and q_3 as special cases. In addition, a special case for q_4, viz.

$$\bar{q}_4 = \frac{1}{2} \left(q_A + q_B \right),$$

is also included. This model shows some promise for generalisations and it remains for it to be studied more closely. Finally, we note that Tan *et al.* [171] derived a rate related to q_4, where the weights W_A and W_B are replaced by weights based on the maximum specific growth rates. Tan *et al.* used statistical mechanics to derive this rate. There is only one substrate in this model, but there are two binding sites on an enzyme that respond to the substrate differently.

It may be possible to adapt some of their analysis for a two substrate model for microbes where the two binding sites that respond to the substrate differently in their model correspond to the two substrates in the analogy. There are promising leads, particularly in the directions of Desmond-Le Quéméner and Bouchez [39] and Bertolazzi [14], where further exploration could yield interesting results.

5.2 Enzyme Kinetic Models

The extension of the enzyme kinetic model from one to two limiting substrates, with the analogy between microbes and enzymes, is not straightforward, because there are many scenarios and this escalates the complexity. As noted, the association of the enzyme with the substrates could be interactive, noninteractive, or somewhere between the two. It may be that an enzyme can form its final complex before making a product only if A precedes B. It may be that more than one product is produced and these products appear after different stages in the reaction. Cleland [32] gives a daunting list of possibilities for just two substrates. Eventually, we want to devise a model by regarding a microbe as an enzyme, and this means that the level of information needed about interactions should not be overly detailed. Following Bader [6], we consider some simple cases that involve a ternary complex (a complex of the enzyme and two substrates) and our knowledge that we are wanting to model microbial growth will help us select mechanisms that seem appropriate. Unlike the single substrate case, it is possible that there are stoichiometric considerations. For simplicity, we will use unit coefficients. The law of mass action serves to introduce powers in the concentration variables if we have non-unit coefficients, and we can move to this level of complexity after we understand the simplest case. Unlike Bader, however, we make the enzyme to product reaction reversible in the spirit of the Briggs-Haldane approach.

There are four main mechanisms that we discuss here: the “Black Box” Mechanism, the Ordered Ternary Mechanism, the Random Ternary Mechanism, and the “Confluence” Mechanism. These mechanisms each have their own merits and will be explored in detail.

5.3 Black Box Mechanism

$$E + A + B \underset{k_2}{\overset{k_1}{\rightleftharpoons}} C_{AB} \underset{k_4}{\overset{k_3}{\rightleftharpoons}} E + P. \tag{5.6}$$

The simplest of the mechanisms that we consider, which we have dubbed the Black Box Mechanism, is shown in Eq. (5.6). We see that an enzyme complexes with two substrates, A and B, to form a ternary complex C_{AB} that can then react to form a product P. In this mechanism we are not concerned with how the substrates interact with each other. In the analogy to microbes we can think of this as the microbe taking in two substrates and transforming them through a metabolic pathway from which a product P, which is necessary for ATP formation, is formed.

Using the law of mass action, the differential equations for the concentrations of enzyme and complexes are:

$$\begin{aligned}
\frac{dE}{dt} &= -k_1 EAB + k_2 C_{AB} + k_3 C_{AB} - k_4 EP, \\
\frac{dA}{dt} &= \frac{dB}{dt} = -k_1 EAB + k_2 C_{AB}, \\
\frac{dC_{AB}}{dt} &= k_1 EAB - k_2 C_{AB} - k_3 C_{AB} + k_4 EP, \\
\frac{dP}{dt} &= k_3 C_{AB} - k_4 EP.
\end{aligned} \tag{5.7}$$

These equations are very similar to the single substrate case that lead to the Modified Haldane rate as A and B only appear together and they are in the same place that S appears in the single substrate case. Similarly, we get the conservation law $E + C_{AB} = E_T$, where E_T is the total amount of enzyme, a constant. We assume that $E \ll A, B$, meaning that the enzyme is present in catalytic amounts and a quasi-steady-state is established very quickly. This quasi-steady-state assumption amounts to the relations $\frac{dE}{dt} = \frac{dC_{AB}}{dt} = 0$, i.e.,

$$k_1 EAB - k_2 C_{AB} - k_3 C_{AB} + k_4 EP = 0. \tag{5.8}$$

We can replace C_{AB} in Eq. (5.8) and in Eq. (5.7) using $C_{AB} = E_T - E$ to get

$$E = \frac{(k_2 + k_3)\, E_T}{(k_2 + k_3) + k_1 AB + k_4 P} \tag{5.9}$$

and

$$\frac{dP}{dt} = k_3 E_T - (k_3 + k_4 P)\, E. \tag{5.10}$$

Replacing E in Eq. (5.10) using Eq. (5.9) gives

$$\begin{aligned}\frac{dP}{dt} &= E_T \left(k_3 - \frac{(k_3 + k_4 P)(k_2 + k_3)}{(k_2 + k_3) + k_1 AB + k_4 P} \right) \\ &= E_T \left(k_2 - \frac{k_3 + k_4 P}{1 + \frac{k_1 AB}{k_2 + k_3} + \frac{k_4 P}{k_2 + k_3}} \right).\end{aligned} \tag{5.11}$$

We now define the maximum forward reaction rate and maximum backward reaction rate as $v_f = k_3 E_T$ and $v_b = k_2 E_T$, respectively, and define $K_{AB} = \frac{k_2 + k_3}{k_1}$ and $K_P = \frac{k_2 + k_3}{k_4}$. Now Eq.(5.11) becomes

$$\frac{dP}{dt} = \frac{v_f \frac{AB}{K_{AB}} - v_b \frac{P}{K_P}}{1 + \frac{AB}{K_{AB}} + \frac{P}{K_P}}. \tag{5.12}$$

At equilibrium $\frac{dP}{dt} = 0$; hence,

$$\frac{v_f}{K_{AB}} A_{\text{eq}} B_{\text{eq}} - \frac{v_b}{K_P} P_{\text{eq}} = 0$$

and

$$\frac{P_{\text{eq}}}{A_{\text{eq}} B_{\text{eq}}} = \frac{v_f K_P}{v_b K_{AB}} = K_{\text{eq}}, \tag{5.13}$$

an analogue of the Haldane relation for a reaction with two rate-limiting substrates. We can use this relation in Eq. (5.12) to get

$$\begin{aligned}\frac{dP}{dt} &= \frac{v_b (AB K_{\text{eq}} - P)}{K_P + \frac{v_b}{v_f} AB K_{\text{eq}} + P}, \\ &= \frac{v_b AB \left(1 - \frac{P}{AB K_{\text{eq}}}\right)}{\frac{K_P}{K_{\text{eq}}} + AB \left(\frac{v_b}{v_f} + \frac{P}{AB K_{\text{eq}}}\right)}, \\ &= \frac{v_f AB \left(1 - \frac{P}{AB K_{\text{eq}}}\right)}{\frac{v_f}{v_b}\frac{K_P}{K_{\text{eq}}} + AB \left(1 + \frac{v_f}{v_b}\frac{P}{AB K_{\text{eq}}}\right)};\end{aligned}$$

therefore,

$$\frac{dP}{dt} = \frac{v_f AB\,(1-\theta)}{K_{AB} + AB\left(1 + \frac{v_f}{v_b}\theta\right)}, \tag{5.14}$$

where

$$\theta = \frac{P}{ABK_{\text{eq}}} = \frac{A_{\text{eq}}B_{\text{eq}}}{P_{\text{eq}}}\frac{P}{AB}.$$

The ratio $\frac{v_f}{v_b} = \frac{k_3}{k_2}$ is the ratio of the maximum forward reaction rate and the maximum backward reaction rate. In the single substrate case these rates are taken to be equal, i.e., $v_f = v_b$ or $k_3 = k_2$ (as assumed by Hoh and Cord-Ruwisch [67] and by Lynch *et al.* [108]). If this same assumption is made in the two substrate case we get a final rate for the Black Box Mechanism of

$$q_{BB} = v_f \frac{AB\,(1-\theta)}{K_{AB} + AB\,(1+\theta)}. \tag{5.15}$$

As expected from the form of Eq. (5.6) showing the mechanism, this rate has the same form as the Modified Haldane rate for a single substrate but S has been replaced by AB. This rate is relatively simple due to the uncomplicated nature of the mechanism but this means that it may be an oversimplification.

It is not necessary to assume that both substrates react simultaneously to directly form a ternary complex. What follows are explorations of mechanisms that consider pathways where the substrates react individually and binary complexes are also formed along the way.

5.4 Ordered Ternary Mechanism

$$E + A + B \underset{\text{k}_2}{\overset{\text{k}_1}{\rightleftharpoons}} C_A + B \underset{\text{k}_4}{\overset{\text{k}_3}{\rightleftharpoons}} C_{AB} \underset{\text{k}_6}{\overset{\text{k}_5}{\rightleftharpoons}} E + P. \tag{5.16}$$

The Ordered Ternary Mechanism, shown in Eq. (5.16), describes an enzyme that first complexes with substrate A to make C_A, then C_A reacts with B to form the ternary complex C_{AB}, which then forms the product P. It is worth noting immediately that this mechanism is asymmetric in A and B, and that B is not involved in the reactions corresponding to k_1 and k_2 but is shown there in order to neatly present the mechanism in a single line. In the analogy from enzyme to microbe, we can think of this mechanism as the microbe taking in two substrates that are

sequentially transformed through metabolic pathways to produce ATP and form a product P.

The law of mass action yields the following system of differential equations:

$$\begin{aligned}
\frac{dE}{dt} &= -k_1EA + k_2C_A + k_5C_{AB} - k_6EP,\\
\frac{dA}{dt} &= -k_1EA + k_2C_A,\\
\frac{dB}{dt} &= -k_3C_AB + k_4C_{AB},\\
\frac{dC_A}{dt} &= k_1EA - k_2C_A - k_3C_AB + k_4C_{AB},\\
\frac{dC_{AB}}{dt} &= k_3C_AB - k_4C_{AB} - k_5C_{AB} + k_6EP,\\
\frac{dP}{dt} &= k_5C_{AB} - k_6EP.
\end{aligned} \tag{5.17}$$

The conservation law for the total amount of enzyme is now $E_T = E + C_A + C_{AB}$. At this stage we have two options of how to proceed:

- We assume that $E \ll A, B$, meaning that the enzyme is present in catalytic amounts and a quasi-steady-state is established very quickly. This quasi-steady-state assumption amounts to the relation $\frac{dC_{AB}}{dt} = 0$, i.e.,

$$k_3C_AB - k_4C_{AB} - k_5C_{AB} + k_6EP = 0. \tag{5.18}$$

  Considering the biological side of the analogy, we can assume that $\frac{dA}{dt} = \frac{dB}{dt} = -\frac{dP}{dt}$ as the amount of A that is used up by the microbe over time must match the amount of B that is used and be equal to the amount of P that is produced to avoid build up of either complex. This is necessary because $E \ll A, B$. As Eq. (5.17) shows $\frac{dC_A}{dt} = \frac{dB}{dt} - \frac{dA}{dt}$ this means that $\frac{dC_A}{dt} = 0$. It follows that $\frac{dE}{dt} = 0$ as $\frac{dE}{dt} = -\frac{dC_{AB}}{dt} - \frac{dC_A}{dt}$.

- We assume the "fast kinetics" assumption of Michaelis and Menten, that the rates of catalyst and substrate to complex are much faster than product formation rates, i.e., $k_j \gg k_i$ for $j = 1, 2, 3, 4$ and $i = 5, 6$. This assumption implies not only $\frac{dC_A}{dt} = \frac{dC_{AB}}{dt} = \frac{dE}{dt} = 0$ but

$$\frac{dA}{dt} = \frac{dB}{dt} = 0 \tag{5.19}$$

as well.

We consider the latter assumption due to the similarity to Michaelis-Menten.

From Eq. (5.19) we get

$$k_3 C_A B = k_4 C_{AB} \tag{5.20}$$

and

$$k_1 EA = k_2 C_A. \tag{5.21}$$

Eqs. (5.20) and (5.21) can be used to replace C_A and C_{AB} in the conservation law which yields

$$\begin{aligned} E_T &= E + \frac{k_1}{k_2} EA + \frac{k_3}{k_4} C_A B \\ &= E + \frac{k_1}{k_2} EA + \frac{k_1}{k_2}\frac{k_3}{k_4} EAB \\ &= E\left(1 + \frac{k_1}{k_2} A + \frac{k_1}{k_2}\frac{k_3}{k_4} AB\right). \end{aligned} \tag{5.22}$$

This rearranges to

$$E = \frac{E_T}{1 + \frac{k_1}{k_2} A + \frac{k_1 k_3}{k_2 k_4} B} = \frac{E_T}{1 + \frac{k_1}{k_2} A \left(1 + \frac{k_3}{k_4} B\right)}. \tag{5.23}$$

Using Eqs. (5.20-5.23) we can replace C_{AB} and E in Eq. (5.17) to get

$$\begin{aligned} \frac{dP}{dt} &= \frac{\frac{k_1 k_3 k_5}{k_2 k_4} E_T AB - k_6 E_T P}{1 + \frac{k_1}{k_2} A + \frac{k_1 k_3}{k_2 k_4} AB}, \\ &= \frac{E_T\left(\frac{k_1 k_3 k_5}{k_2 k_4} AB - k_6 P\right)}{1 + \frac{k_1}{k_2} A + \frac{k_1 k_3}{k_2 k_4} AB}, \\ &= \frac{E_T \frac{k_1 k_3 k_5}{k_2 k_4} AB\left(1 - \frac{k_2 k_4 k_6 P}{k_1 k_3 k_5 AB}\right)}{1 + \frac{k_1}{k_2} A + \frac{k_1 k_3}{k_2 k_4} AB}, \\ &= \frac{v_f AB\left(1 - \frac{k_2 k_4 k_6 P}{k_1 k_3 k_5 AB}\right)}{\frac{k_2 k_4}{k_1 k_3} + \frac{k_4}{k_3} A + AB} \\ &= \frac{v_f AB\left(1 - \frac{k_6 P}{k_5 K_A K_B AB}\right)}{\frac{1}{K_A K_B} + \frac{1}{K_B} A + AB}, \end{aligned} \tag{5.24}$$

where $v_f = k_5 E_T$ is the maximum forward reaction rate, $K_A = \frac{k_1}{k_2}$ and $K_B = \frac{k_3}{k_4}$ are the ratios of the rate constants for the first and second sections of the mechanism, and If we consider

equilibrium, where $\frac{dP}{dt} = 0$, we can see the denominator of Eq. (5.24) is non-zero so we are left with

$$v_f A_{\text{eq}} B_{\text{eq}} \left(1 - \frac{k_6}{k_5 K_A K_B} \frac{P_{\text{eq}}}{A_{\text{eq}} B_{\text{eq}}}\right) = 0.$$

It follows that

$$\frac{k_5}{k_6} K_A K_B = \frac{P_{\text{eq}}}{A_{\text{eq}} B_{\text{eq}}} = K_{\text{eq}}. \tag{5.25}$$

Replacing $\frac{k_6}{k_5 K_A K_B}$ in Eq. (5.24) with $\frac{1}{K_{\text{eq}}}$ gives

$$\frac{dP}{dt} = \frac{v_f AB}{\frac{1}{K_A K_B} + \frac{1}{K_B} A + AB} \left(1 - \frac{1}{K_{\text{eq}}} \frac{P}{AB}\right). \tag{5.26}$$

We can define

$$\theta = \frac{1}{K_{\text{eq}}} \frac{P}{AB} = \frac{A_{\text{eq}} B_{\text{eq}}}{P_{\text{eq}}} \frac{P}{AB},$$

and we get the final expression for the rate:

$$q_{OTM} = v_f \frac{AB\,(1-\theta)}{\frac{1}{K_A K_B} + \frac{1}{K_B} A + AB}. \tag{5.27}$$

This form can be considered a generalisation of the Jin and Bethke rate [79], discussed in Chapter 2, to two substrates. As expected for the Ordered Ternary Mechanism, the rate is asymmetric in A and B as the denominator includes A and AB but not B. Compared to the Black Box Mechanism we also notice the lack of thermodynamic inhibition in the denominator as there is neither P nor k_6 in the denominator. The θ term in the numerator provides the thermodynamic inhibition in the rate and will produce a shutoff when the system is at equilibrium.

5.4.1 Using an Expansion

Suppose that $A(t)$ and $B(t)$ for the Ordered Ternary Mechanism are defined as:

$$A(t) = A_0 - \epsilon A_1(t), \tag{5.28a}$$

$$A'(t) = -\epsilon A_1'(t), \tag{5.28b}$$

$$B(t) = B_0 - \epsilon B_1(t), \tag{5.28c}$$

$$B'(t) = -\epsilon B_1'(t). \tag{5.28d}$$

We are considering A_0 and A_1, along with B_0 and B_1 to be of similar size and ϵ to be a small factor so that A_0 and B_0 are several orders of magnitude larger than ϵA_1 and ϵB_1, respectively. These equations correspond to the very small changes in substrate concentration that occur after the pre-steady-state period. We can use Eqs. (5.28a)-(5.28d) for an alternative method to derive the rate. The law of mass action gives

$$\frac{dE}{dt} = -k_1 EA + k_2 C_A + k_5 C_{AB} - k_6 EP = -\epsilon A_1' + P' \tag{5.29a}$$

$$\frac{dA}{dt} = -k_1 EA + k_2 C_A = -k_1 E\left(A_0 - \epsilon A_1\right) + k_2 C_A = -\epsilon A_1' \tag{5.29b}$$

$$\frac{dB}{dt} = -k_3 C_A B + k_4 C_{AB} = -k_3 C_A\left(B_0 - \epsilon B_1\right) + k_4 C_{AB} = -\epsilon B_1' \tag{5.29c}$$

$$\frac{dC_A}{dt} = k_1 EA - k_2 C_A - k_3 C_A B + k_4 C_{AB} = \epsilon\left(A_1' - B_1'\right) \tag{5.29d}$$

$$\frac{dC_{AB}}{dt} = k_3 C_A B - k_4 C_{AB} - k_5 C_{AB} + k_6 EP = \epsilon B_1' - P' \tag{5.29e}$$

$$\frac{dP}{dt} = k_5 C_{AB} - k_6 EP = P'. \tag{5.29f}$$

We can see that we still get the same conservation law, $E + C_A + C_{AB} = E_T$. Again we assume that the enzyme is present in catalytic amounts, i.e., $E \ll A, B$, and a quasi-steady-state is established very quickly. This assumption amounts to assuming $\frac{dC_{AB}}{dt} = 0$ which we can see from Eq. (5.29e) implies

$$P' = \epsilon B_1'.$$

Suppose that $\epsilon A_1' \neq \epsilon B_1'$, then either $\epsilon A_1' < \epsilon B_1'$ which results in a shortage of C_A from Eq. (5.29d) or $\epsilon A_1' > \epsilon B_1' = P'$ and there will be a shortage of E from Eq. (5.29a). In a biological setting we want to avoid either of these situations so we assume $\epsilon A_1' = \epsilon B_1'$ which implies that $\frac{dC_A}{dt} = 0$. As $\epsilon B_1' = P'$ and $\epsilon A_1' = \epsilon B_1'$ we also know that $\epsilon A_1' = P'$ so $\frac{dE}{dt} = 0$ too. Starting with Eq. (5.29b) we get a relation for C_A as follows:

$$-k_1 E\left(A_0 - \epsilon A_1\right) + k_2 C_A = -\epsilon A_1',$$

$$\begin{aligned} C_A &= \frac{k_1 E\left(A_0 - \epsilon A_1\right) - \epsilon A_1'}{k_2}, \\ &= \frac{k_1}{k_2} E A_0 - \epsilon \frac{\left(k_1 E A_1 + A_1'\right)}{k_2}. \end{aligned} \tag{5.30}$$

Similarly, starting with Eq. (5.29c) we can get a relation for C_{AB}, first including C_A and then without, as follows:

$$-k_3 C_A\left(B_0 - \epsilon B_1\right) + k_4 C_{AB} = -\epsilon B_1',$$

$$\begin{aligned} C_{AB} &= \frac{k_3 C_A\left(B_0 - \epsilon B_1\right) - \epsilon B_1'}{k_4}, \\ &= \frac{k_3}{k_4}\left(\frac{k_1}{k_2} E A_0 - \epsilon \frac{\left(k_1 E A_1 + A_1'\right)}{k_2}\right)\left(B_0 - \epsilon B_1\right) - \epsilon \frac{B_1'}{k_4}, \\ &= \frac{k_1 k_3}{k_2 k_4} E A_0 B_0 - \epsilon\left(\frac{k_1 k_3}{k_2 k_4} E A_0 B_1 + \frac{k_3}{k_2 k_4}\left(k_1 E A_1 + A_1'\right) B_0 + \frac{B_1'}{k_4}\right) + \epsilon^2 \frac{k_3}{k_2 k_4}\left(k_1 E A_1 + A_1'\right) B_1. \end{aligned} \tag{5.31}$$

Eqs. (5.30) and (5.31) we can replace C_A and C_{AB} in the conservation law to get

$$E_T = E\left(1 + \frac{k_1}{k_2} A_0 - O\left(\epsilon\right) + \frac{k_1 k_3}{k_2 k_4} A_0 B_0 - O\left(\epsilon\right) + O\left(\epsilon^2\right)\right) \tag{5.32}$$

and

$$E = \frac{E_T}{1 + \frac{k_1}{k_2} A_0 + \frac{k_1 k_3}{k_2 k_4} A_0 B_0 - O\left(\epsilon\right) + O\left(\epsilon^2\right)} \tag{5.33}$$

If we omit the $O(\epsilon)$ and $O(\epsilon^2)$ terms from Eqs. (5.31) and (5.33) we can replace C_{AB} and E in Eq. (5.29f) to get

$$\begin{aligned}
\frac{dP}{dt} &= \frac{\frac{k_1k_3k_5}{k_2k_4}E_TA_0B_0 - k_6E_TP}{1+\frac{k_1}{k_2}A_0+\frac{k_1k_3}{k_2k_4}A_0B_0}, \\
&= \frac{E_T\left(\frac{k_1k_3k_5}{k_2k_4}A_0B_0 - k_6P\right)}{1+\frac{k_1}{k_2}A_0+\frac{k_1k_3}{k_2k_4}A_0B_0}, \\
&= \frac{E_T\frac{k_1k_3k_5}{k_2k_4}A_0B_0\left(1-\frac{k_2k_4k_6P}{k_1k_3k_5A_0B_0}\right)}{1+\frac{k_1}{k_2}A_0+\frac{k_1k_3}{k_2k_4}A_0B_0}, \\
&= \frac{v_fA_0B_0\left(1-\frac{k_2k_4k_6P}{k_1k_3k_5A_0B_0}\right)}{\frac{k_2k_4}{k_1k_3}+\frac{k_4}{k_3}A_0+A_0B_0} \\
&= \frac{v_fA_0B_0\left(1-\frac{k_6P}{k_5K_AK_BA_0B_0}\right)}{\frac{1}{K_AK_B}+\frac{1}{K_B}A_0+A_0B_0},
\end{aligned} \tag{5.34}$$

where $v_f = k_5E_T$ is the maximum forward reaction rate, $K_A = \frac{k_1}{k_2}$ and $K_B = \frac{k_3}{k_4}$ are the ratios of the rate constants for the first and second sections of the mechanism, and if we consider equilibrium, where $\frac{dP}{dt} = 0$, we can see the denominator of Eq. (5.34) is non-zero so we are left with

$$v_fA_{\text{eq}}B_{\text{eq}}\left(1-\frac{k_6}{k_5K_AK_B}\frac{P_{\text{eq}}}{A_{\text{eq}}B_{\text{eq}}}\right) = 0.$$

It follows that

$$\frac{k_5}{k_6}K_AK_B = \frac{P_{\text{eq}}}{A_{\text{eq}}B_{\text{eq}}} = K_{\text{eq}}. \tag{5.35}$$

Replacing $\frac{k_6}{k_5K_AK_B}$ in Eq. (5.34) with $\frac{1}{K_{\text{eq}}}$ gives

$$\frac{dP}{dt} = \frac{v_fA_0B_0}{\frac{1}{K_AK_B}+\frac{1}{K_B}A_0+A_0B_0}\left(1-\frac{1}{K_{\text{eq}}}\frac{P}{A_0B_0}\right).$$

We can define

$$\theta = \frac{1}{K_{\text{eq}}}\frac{P}{A_0B_0} = \frac{A_{\text{eq}}B_{\text{eq}}}{P_{\text{eq}}}\frac{P}{A_0B_0},$$

and we get the final expression for the rate:

$$q_{OTM-E} = v_f \frac{A_0 B_0 (1-\theta)}{\frac{1}{K_A K_B} + \frac{1}{K_B} A_0 + A_0 B_0}. \tag{5.36}$$

This rate differs from that in Eq. (5.27) only by A and B being replaced by A_0 and B_0, respectively.

Eq. (5.16) details a specific pathway for product formation that might be applicable to enzymes, but in our analogy for microbes it might be overly complicated. A feature of the analogy is that it avoids the need for detailed information about how the microbe is using the substrate and individual reactions occurring in the microbe. If adapted for microbial growth, the rate given by Eq. (5.27) (or Eq. (5.36)) is valid under the assumption that substrate A is used before substrate B. This may sometimes be the case, but this level of detail would need to be justified in each case. We next turn our attention to the Random Ternary Mechanism, which does not rely on the knowledge of which substrate reacts first.

5.5 Random Ternary Mechanism

$$\begin{array}{ccccc} \mathrm{E} + \mathrm{A} & \underset{\mathrm{k_2}}{\overset{\mathrm{k_1}}{\rightleftharpoons}} & C_A & & \\ + & & + & & \\ \mathrm{B} & & \mathrm{B} & & \\ k_3 \Downarrow \Uparrow k_4 & & k_7 \Downarrow \Uparrow k_8 & & \\ \mathrm{C_B} + \mathrm{A} & \underset{\mathrm{k_6}}{\overset{\mathrm{k_5}}{\rightleftharpoons}} & C_{AB} & \underset{\mathrm{k_{rev}}}{\overset{\mathrm{k}_p}{\rightleftharpoons}} & E + P. \end{array} \tag{5.37}$$

Consider the Random Ternary Mechanism as shown in Eq. (5.37). This shows a mechanism with two possible routes for an enzyme to complex with the two different substrates to give the ternary complex, which can then react to give the products. The different pathways allow either binary complex, C_A or C_B, to be produced first before reacting with the other substrate to give the ternary complex, C_{AB}, with no preference for either pathway. This avoids the need to specify the order while recognising the need for both substrates. In the analogy to the microbe, this would mean the microbe can take up the substrates in either order, similar to two linked Ordered Ternary Mechanisms operating simultaneously. In Equation (5.37) this is from top left

to bottom right, going around the square either clockwise or anticlockwise. The return to a mechanism with a symmetric form with respect to A and B means that we expect the rate to be symmetric in A and B.

Using the law of mass action, the differential equations for the concentrations of enzyme and complexes are:

$$\frac{dE}{dt} = -k_1EA + k_2C_A - k_3EB + k_4C_B + k_{\mathrm{p}}C_{AB} - k_{\mathrm{rev}}EP \tag{5.38a}$$

$$\frac{dC_A}{dt} = k_1EA - k_2C_A - k_7C_AB + k_8C_{AB} \tag{5.38b}$$

$$\frac{dC_B}{dt} = k_3EB - k_4C_B - k_5C_BA + k_6C_{AB} \tag{5.38c}$$

$$\frac{dC_{AB}}{dt} = k_7C_AB - k_8C_{AB} + k_5C_BA - k_6C_{AB} - k_{\mathrm{p}}C_{AB} + k_{\mathrm{rev}}EP. \tag{5.38d}$$

These equations show that

$$E + C_A + C_B + C_{AB} = E_T \tag{5.39}$$

where E_T is a constant, the total amount of enzyme. We are interested in finding an expression for $\frac{dP}{dt}$ as this will be proportional to the growth rate of the microbe. By the law of mass action we get

$$\frac{dP}{dt} = k_{\mathrm{p}}C_{AB} - k_{\mathrm{rev}}EP. \tag{5.40}$$

We want to remove the terms involving the enzyme (C_{AB} and E) and replace them with expressions involving terms that are measurable or fixed. In order to do this we need to use a quasi-steady-state assumption (QSSA), as we did in the single substrate case and for the previous mechanisms, but exactly what the QSSA should be is not obvious.

The difficulty here comes in extending from the relative simplicity of the single substrate case to the complexity of the two substrate case. The common QSSA in the single substrate case is usually given as

$$\frac{dE}{dt} = 0$$

and since there is only one enzyme-substrate complex, C_S, by conservation of enzyme it follows

that

$$\frac{dC_S}{dt} = 0$$

also. In the single substrate case, assuming that either E or C_S is a constant implies that the other is also a constant. Which one is assumed and which is implied does not matter; the result is the same with both being constant. In the Random Ternary Mechanism there are three different complexes that form so the choice of how the QSSA should be applied is less clear.

5.5.1 A Simple Quasi-Steady-State Assumption

First we consider what we may call the "regular" QSSA. Carrying across the QSSA, as it is usually given, from the single substrate case we assume

$$\frac{dE}{dt} = \frac{dC_A}{dt} + \frac{dC_B}{dt} + \frac{dC_{AB}}{dt} = 0,$$

i.e.,

$$k_1EA - k_2C_A + k_3EB - k_4C_B - k_{\mathrm{p}}C_{AB} + k_{\mathrm{rev}}EP = 0.$$

Some progress can be made in attempting to eliminate E and C_{AB} along with C_A and C_B from Eq. (5.40) but it quickly becomes algebraically intractable. In the irreversible case ($k_{\mathrm{rev}} = 0$) an expression for C_{AB} (and so, $\frac{dP}{dt}$) is eventually reached where the numerator has terms that include E_TAB, E_TA^2B, and E_TAB^2 while the denominator includes A, B, AB, A^2, B^2, A^2B, and AB^2, as shown by Laidler and Bunting [97]. The irreversible case is the simpler case, as allowing k_{rev} to be non-zero adds more layers to the working, making it more complicated. This equation is far too unwieldy to be used with experimental data. So, next we ask how can we change the QSSA, or what other assumptions can we make, to lose some information that is not required as a trade-off to make the derivation more manageable and the equation more usable?

A slightly stronger QSSA would be if

$$\frac{dE}{dt} = \frac{dC_A}{dt} = \frac{dC_B}{dt} = \frac{dC_{AB}}{dt} = 0.$$

Here each of the enzyme-containing terms is a constant and this change allows some simplification

in the working. However, it is not enough to give us an equation that is significantly more approachable or useful.

5.5.2 A Michaelis-Menten-Type Approach

We now consider a QSSA which is more restrictive and, according to Laidler and Bunting [97], the only condition under which the rate equation can be reduced to a simple form without blocking one pathway and effectively changing the mechanism to an Ordered Ternary Mechanism. This new QSSA relies on the complexed species being in equilibrium with each other, so k_p is sufficiently small so as not to disturb this equilibrium. It can be represented as:

$$k_1 EA = k_2 C_A \tag{5.41a}$$

$$k_5 C_B A = k_6 C_{AB} \tag{5.41b}$$

$$k_3 EB = k_4 C_B \tag{5.41c}$$

$$k_7 C_A B = k_8 C_{AB} \tag{5.41d}$$

This assumption is similar to the "fast kinetics" assumption of the Michaelis-Menten derivation.

Eq. (5.41a) can be rearranged to give

$$C_A = \frac{k_1}{k_2} EA \tag{5.42}$$

which can be substituted into Eq. (5.41d) to give

$$C_{AB} = \frac{k_1 k_7}{k_2 k_8} EAB. \tag{5.43}$$

Similarly, Eq. (5.41c) can be rearranged to give

$$C_B = \frac{k_3}{k_4} EB \tag{5.44}$$

which can be substituted into Eq. (5.41b) to give

$$C_{AB} = \frac{k_3 k_5}{k_4 k_6} EAB. \tag{5.45}$$

The two expressions in Eqs. (5.43) and (5.45) for C_{AB} in terms of E, A, and B put a constraint on the values of the k's,

$$\frac{k_1 k_7}{k_2 k_8} = \frac{k_3 k_5}{k_4 k_6} = K \tag{5.46}$$

and so

$$C_{AB} = KEAB. \tag{5.47}$$

Eqs. (5.42) and (5.44) can be used to replace C_A and C_B in Eq. (5.39), leaving

$$E_T = E + \frac{k_1}{k_2} EA + \frac{k_3}{k_4} EB + C_{AB}$$

which can be rearranged to

$$E = \frac{E_T - C_{AB}}{1 + \frac{k_1}{k_2} A + \frac{k_3}{k_4} B}. \tag{5.48}$$

Eq. (5.48) can be used to replace E in Eq. (5.47) which can then be rearranged as follows:

$$\begin{aligned}
C_{AB} &= K \left(\frac{E_T - C_{AB}}{1 + \frac{k_1}{k_2} A + \frac{k_3}{k_4} B} \right) AB \\
C_{AB} + \frac{K C_{AB} AB}{1 + \frac{k_1}{k_2} A + \frac{k_3}{k_4} B} &= \frac{K E_T AB}{1 + \frac{k_1}{k_2} A + \frac{k_3}{k_4} B} \\
C_{AB} \left(1 + \frac{KAB}{1 + \frac{k_1}{k_2} A + \frac{k_3}{k_4} B} \right) &= \frac{K E_T AB}{1 + \frac{k_1}{k_2} A + \frac{k_3}{k_4} B} \\
C_{AB} &= \frac{\frac{K E_T AB}{1 + \frac{k_1}{k_2} A + \frac{k_3}{k_4} B}}{1 + \frac{KAB}{1 + \frac{k_1}{k_2} A + \frac{k_3}{k_4} B}} \\
&= \frac{K E_T AB}{1 + \frac{k_1}{k_2} A + \frac{k_3}{k_4} B + KAB} \\
&= \frac{E_T AB}{\frac{1}{K} + \frac{k_8}{k_7} A + \frac{k_6}{k_5} B + AB}.
\end{aligned} \tag{5.49}$$

Recall that the rate of change of P is given by

$$\frac{dP}{dt} = k_{\mathrm{p}} C_{AB} - k_{\mathrm{rev}} EP. \tag{5.50}$$

If we were considering the irreversible case ($k_{\mathrm{rev}} = 0$), we would be ready to proceed by replacing C_{AB} in Eq. (5.50) using Eq. (5.49). For the reversible case, we also need to be able to replace E with a term that does not contain C_{AB}, so we will first eliminate C_{AB} from our expression for E. We do this using Eq. (5.49) as follows:

$$\begin{aligned}
E &= \frac{E_T - C_{AB}}{1 + \frac{k_1}{k_2}A + \frac{k_3}{k_4}B} \\
&= \frac{E_T - \frac{E_T AB}{\frac{1}{K} + \frac{k_8}{k_7}A + \frac{k_6}{k_5}B + AB}}{1 + \frac{k_1}{k_2}A + \frac{k_3}{k_4}B} \\
&= \frac{E_T - \frac{E_T KAB}{1 + \frac{k_1}{k_2} + \frac{k_3}{k_4} + KAB}}{1 + \frac{k_1}{k_2}A + \frac{k_3}{k_4}B} \\
&= \frac{\frac{\left(1 + \frac{k_1}{k_2}A + \frac{k_3}{k_4}B + KAB\right)E_T - E_T KAB}{1 + \frac{k_1}{k_2}A + \frac{k_3}{k_4}B + KAB}}{1 + \frac{k_1}{k_2}A + \frac{k_3}{k_4}B} \\
&= \frac{\frac{\left(1 + \frac{k_1}{k_2}A + \frac{k_3}{k_4}B\right)E_T}{1 + \frac{k_1}{k_2}A + \frac{k_3}{k_4}B + KAB}}{1 + \frac{k_1}{k_2}A + \frac{k_3}{k_4}B} \\
&= \frac{E_T}{1 + \frac{k_1}{k_2}A + \frac{k_3}{k_4}B + KAB}.
\end{aligned} \tag{5.51}$$

Replacing C_{AB} using Eq. (5.49) and E using Eq. (5.51) in Eq. (5.50) gives

$$\begin{aligned}
\frac{dP}{dt} &= \frac{k_{\mathrm{p}} E_T AB}{\frac{1}{K} + \frac{k_8}{k_7}A + \frac{k_6}{k_5}B + AB} - \frac{k_{\mathrm{rev}} E_T P}{1 + \frac{k_1}{k_2}A + \frac{k_3}{k_4}B + KAB} \\
&= \frac{k_{\mathrm{p}} E_T AB}{\frac{1}{K} + \frac{k_8}{k_7}A + \frac{k_6}{k_5}B + AB} - \frac{k_{\mathrm{rev}}}{K}\frac{E_T P}{\frac{1}{K} + \frac{k_8}{k_7}A + \frac{k_6}{k_5}B + AB} \\
&= \frac{k_{\mathrm{p}} E_T AB}{\frac{1}{K} + \frac{k_8}{k_7}A + \frac{k_6}{k_5}B + AB}\left(1 - \frac{k_{\mathrm{rev}}}{k_{\mathrm{p}} K}\frac{P}{AB}\right).
\end{aligned} \tag{5.52}$$

We define $v_{max} = k_{\mathrm{p}} E_T$ and consider equilibrium, where $\frac{dP}{dt} = 0$. The denominator of Eq. (5.52)

is non-zero, so this means that at equilibrium

$$v_{\max} A_{\text{eq}} B_{\text{eq}} \left(1 - \frac{k_{\text{rev}}}{k_{\text{p}} K} \frac{P_{\text{eq}}}{A_{\text{eq}} B_{\text{eq}}}\right) = 0$$

and so

$$\frac{k_{\text{p}} K}{k_{\text{rev}}} = \frac{P_{\text{eq}}}{A_{\text{eq}} B_{\text{eq}}} = K_{\text{eq}}.$$

Replacing $\frac{k_{\text{rev}}}{k_{\text{p}} K}$ in Eq. (5.52) with $\frac{1}{K_{\text{eq}}}$ gives

$$\frac{dP}{dt} = \frac{v_{\max} AB}{\frac{1}{K} + \frac{k_8}{k_7} A + \frac{k_6}{k_5} B + AB} \left(1 - \frac{1}{K_{\text{eq}}} \frac{P}{AB}\right).$$

Again, we define

$$\theta = \frac{1}{K_{\text{eq}}} \frac{P}{AB} = \frac{A_{\text{eq}} B_{\text{eq}}}{P_{\text{eq}}} \frac{P}{AB}, \tag{5.53}$$

where $C = \frac{A_{\text{eq}} B_{\text{eq}}}{P_{\text{eq}}}$ and we get the final expression for the rate:

$$q_{RTM-MM} = v_{\max} \frac{AB\,(1 - \theta)}{\frac{1}{K} + \frac{k_8}{k_7} A + \frac{k_6}{k_5} B + AB}. \tag{5.54}$$

Note that the k's in Eq. (5.54) could be presented in other ways owing to their relationship as given in Eq. (5.46). Due to the nature of the fast kinetics assumption, the form of Eq. (5.54) is as expected with a thermodynamic shutoff in the numerator but without the thermodynamic inhibition in the denominator that appears in the Modified Haldane rate. The form of θ is as expected, with a collection of k's multiplied by the ratio of the concentration of product to substrates. If there were two products being formed, say P_1 and P_2, we would expect P in Eq. (5.53) to be replaced by $P_1 P_2$. As expected due to the symmetrical nature of the mechanism, and unlike the result for the Ordered Ternary mechanism, this rate for the Random Ternary Mechanism is symmetrical with respect to the two substrates.

This rate in Eq. (5.54), along with how θ is defined in Eq. (5.53), is a generalisation of the existing Modified Haldane rate to cope with two rate-limiting substrates, with an obvious extension to cope with multiple products if necessary. The working to get this far required similar steps to the derivation in the single substrate case but with a particularly careful choice

of the QSSA to make sure we get something both tractable and useful without giving away too much information about what is going on. This rate looks like it should be useful for modelling microbes that have their reaction rate limited by two different substrates that are both required for growth but can react in either order.

Double Monod

Suppose we take the QSSA from Section (5.5.2) and then assume either

$$\frac{k_1}{k_2} = \frac{k_5}{k_6} = K_A$$

or

$$\frac{k_3}{k_4} = \frac{k_7}{k_8} = K_B.$$

Note that from Eq. (5.46) we can see that if one of these relations between the ratio of k's is true, then the other must also be true. Then, the denominator of Eq. (5.54) can be factorised to a form with the same structure as the Double Monod rate but with a thermodynamic inhibition term included in the numerator, i.e.,

$$\frac{dP}{dt} = v_{\max} \frac{AB\,(1-\theta)}{(K_A + A)\,(K_B + B)}. \tag{5.55}$$

If we considered the irreversible case ($k_{\text{rev}} = 0$), the thermodynamic inhibition term would not be present and the rate would have the same form as the Double Monod rate.

One way of ensuring this relationship between the k's would be to replace k_5, k_6, k_7, and k_8 with αk_1, αk_2, βk_3, and βk_4 respectively, where α and β are constants. This means that the rate constants for the forward and backward reactions involving A are changed by the same factor as each other if B has already reacted and, similarly, the rate constants for the forward and backward reactions involving B are changed by the same factor as each other if A has already reacted. Such a change to the rate constants has not been explored thoroughly but it does not seem unreasonable.

We have provided here the required set of assumptions, along with a rigorous derivation, to

get to the form of a rate that matches that which has been used extensively in literature from empirical approaches. This provides a new theoretical basis for the use of rates with a Double Monod form.

5.5.3 A Partially Irreversible Consideration

We could consider a variation to the Random Ternary Mechanism where we do not allow the ternary complex to deteriorate into either binary complex (i.e., $k_6 = 0$ and $k_8 = 0$). This changes the Eqs. (5.38a)-(5.38d) to

$$\begin{aligned}
\frac{dE}{dt} &= -k_1EA + k_2C_A - k_3EB + k_4C_B + k_{\mathrm{p}}C_{AB} - k_{\mathrm{rev}}EP \\
\frac{dC_A}{dt} &= k_1EA - k_2C_A - k_7C_AB \\
\frac{dC_B}{dt} &= k_3EB - k_4C_B - k_5C_BA \\
\frac{dC_{AB}}{dt} &= k_7C_AB + k_5C_BA - k_{\mathrm{p}}C_{AB} + k_{\mathrm{rev}}EP.
\end{aligned}$$

It is still true that $E + C_A + C_B + C_{AB} = E_T$, but the QSSA of Section 5.5.2 will not work as it would force k_5 and k_7 to also be zero, meaning the ternary complex would not be formed.

Suppose we assume instead that $\frac{dE}{dt} = \frac{dC_A}{dt} = \frac{dC_B}{dt} = \frac{dC_{AB}}{dt} = 0$. The working is algebraically complicated and we get to an equation for the rate that cannot be written concisely and which contains terms such as A^2B and AB^2. The form is unwieldy and not suitable for our purposes. This agrees with Laidler and Bunting's claim that the only QSSA that will give a useful equation is the one used in Section 5.5.2.

5.5.4 Variations to the Random Ternary Mechanism

There are some variations that we may make to the structure of the Random Ternary Mechanism to slightly alter what the analogy between enzyme kinetics and microbial growth is assuming.

The most interesting of these variant mechanisms is shown in Eq. (5.57).

$$\begin{aligned} &\mathrm{E_1 + A} \underset{\mathrm{k_2}}{\overset{\mathrm{k_1}}{\rightleftharpoons}} \mathrm{C_A + B} \underset{\mathrm{k_8}}{\overset{\mathrm{k_7}}{\rightleftharpoons}} \mathrm{C_{AB1}} \underset{\mathrm{k_{rev}}}{\overset{\mathrm{k}_p}{\rightleftharpoons}} \mathrm{E_1 + P} \\ &\mathrm{E_2 + B} \underset{\mathrm{k_4}}{\overset{\mathrm{k_3}}{\rightleftharpoons}} \mathrm{C_B + A} \underset{\mathrm{k_6}}{\overset{\mathrm{k_5}}{\rightleftharpoons}} \mathrm{C_{AB2}} \underset{\mathrm{k_{rev}}}{\overset{\mathrm{k}_p}{\rightleftharpoons}} \mathrm{E_2 + P.} \end{aligned} \tag{5.57}$$

In this mechanism the enzyme is split into two groups, E_1 and E_2, which respectively react with A and B first. This is similar to the Random Ternary Mechanism but it does not allow movement between the side that involves C_A and the side that involves C_B. We are assuming that E_1 reacts all the way through to produce P and E_1 is released again, rather than E_2 being released. Similarly, E_2 reacts all the way through to produce P and E_2 again rather than releasing E_1. All of this amounts to a form very similar to a pair of linked Order Ternary Mechanism reactions. The law of mass action gives:

$$\frac{dA}{dt} = -k_1 E_1 A + k_2 C_A - k_5 C_B A + k_6 C_{AB2} \tag{5.58a}$$
$$\frac{dB}{dt} = -k_7 C_A B + k_8 C_{AB1} - k_3 E_2 B + k_4 C_B \tag{5.58b}$$
$$\frac{dE_1}{dt} = -k_1 E_1 A + k_2 C_A + k_\mathrm{p} C_{AB1} - k_\mathrm{rev} E_1 P \tag{5.58c}$$
$$\frac{dE_2}{dt} = -k_3 E_2 B + k_4 C_B + k_\mathrm{p} C_{AB2} - k_\mathrm{rev} E_2 P \tag{5.58d}$$
$$\frac{C_A}{dt} = k_1 E_1 A - k_2 C_A - k_7 C_A B + k_8 C_{AB1} \tag{5.58e}$$
$$\frac{dC_B}{dt} = k_3 E_2 B - k_4 C_B - k_5 C_B A + k_6 C_{AB2} \tag{5.58f}$$
$$\frac{dC_{AB1}}{dt} = k_7 C_A B - k_8 C_{AB1} - k_\mathrm{p} C_{AB1} + k_\mathrm{rev} E_1 P \tag{5.58g}$$
$$\frac{dC_{AB2}}{dt} = k_5 C_B A - k_6 C_{AB2} - k_\mathrm{p} C_{AB2} + k_\mathrm{rev} E_2 P \tag{5.58h}$$
$$\begin{aligned} \frac{dP}{dt} &= k_\mathrm{p} C_{AB1} - k_\mathrm{rev} E_1 P + k_\mathrm{p} C_{AB2} - k_\mathrm{rev} E_2 P \\ &= k_\mathrm{p} \left(C_{AB1} + C_{AB2} \right) - k_\mathrm{rev} \left(E_1 + E_2 \right) P. \end{aligned} \tag{5.58i}$$

We get two parts to our conservation law: $E_1 + C_A + C_{AB1} = E_{T1}$ and $E_2 + C_B + C_{AB2} = E_{T2}$. The "fast kinetics" QSSA that we used for the Random Ternary Mechanism relied on the complexed species being in equilibrium with each other, so k_p is sufficiently small to not disturb

that equilibrium. Using the same QSSA here we have:

$$k_1 E_1 A = k_2 C_A$$
$$k_5 C_B A = k_6 C_{AB2}$$
$$k_3 E_2 B = k_4 C_B$$
$$k_7 C_A B = k_8 C_{AB1},$$

which, following the working of the Random Ternary Mechanism, gives:

$$C_A = \frac{k_1}{k_2} E_1 A, \tag{5.60a}$$
$$C_{AB1} = \frac{k_1 k_7}{k_2 k_8} E_1 AB, \tag{5.60b}$$
$$C_B = \frac{k_3}{k_4} E_2 B, \tag{5.60c}$$
$$C_{AB2} = \frac{k_3 k_5}{k_4 k_6} E_2 AB. \tag{5.60d}$$

For E_1, we have

$$\begin{aligned} E_{T1} &= E_1 + C_A + C_{AB1}, \\ E_{T1} &= E_1 + \frac{k_1}{k_2} E_1 A + \frac{k_1 k_7}{k_2 k_8} E_1 AB, \\ E_1 &= \frac{E_{T1}}{1 + \frac{k_1}{k_2} A + \frac{k_1 k_7}{k_2 k_8} AB}. \end{aligned} \tag{5.61}$$

For E_2, we have

$$\begin{aligned} E_{T2} &= E_2 + C_B + C_{AB2}, \\ E_{T2} &= E_2 + \frac{k_3}{k_4} E_2 B + \frac{k_3 k_5}{k_4 k_6} E_2 AB, \\ E_2 &= \frac{E_{T2}}{1 + \frac{k_3}{k_4} B + \frac{k_3 k_5}{k_4 k_6} AB}. \end{aligned} \tag{5.62}$$

Now we use Eqs. (5.60)-(5.62) to replace E_1, C_{AB1}, E_2, and C_{AB2} in Eq. (5.58i):

$$\begin{aligned}
\frac{dP}{dt} &= k_{\mathrm{p}}\left(C_{AB1}+C_{AB2}\right)-k_{\mathrm{rev}}\left(E_1+E_2\right)P \\
&= k_{\mathrm{p}}\frac{k_1k_7}{k_2k_8}E_1AB-k_{\mathrm{rev}}E_1P+k_{\mathrm{p}}\frac{k_3k_5}{k_4k_6}E_2AB-k_{\mathrm{rev}}E_2P \\
&= E_{T1}\frac{\left(k_{\mathrm{p}}\frac{k_1k_7}{k_2k_8}AB-k_{\mathrm{rev}}P\right)}{1+\frac{k_1}{k_2}A+\frac{k_1k_7}{k_2k_8}AB}+E_{T2}\frac{\left(k_{\mathrm{p}}\frac{k_3k_5}{k_4k_6}AB-k_{\mathrm{rev}}P\right)}{1+\frac{k_3}{k_4}A+\frac{k_3k_5}{k_4k_6}AB} \\
&= k_{\mathrm{p}}E_{T1}\frac{AB\left(1-\frac{k_2k_8k_{\mathrm{rev}}P}{k_1k_7k_{\mathrm{p}}AB}\right)}{\frac{k_2k_8}{k_1k_7}+\frac{k_8}{k_7}A+AB}+k_{\mathrm{p}}E_{T2}\frac{AB\left(1-\frac{k_4k_6k_{\mathrm{rev}}P}{k_3k_5k_{\mathrm{p}}AB}\right)}{\frac{k_4k_6}{k_3k_5}+\frac{k_6}{k_5}B+AB}
\end{aligned} \tag{5.63}$$

At this stage we replace E_{T1} with p_1E_T and E_{T2} with p_2E_T where p_1 and p_2 are the respective proportions of the total enzyme that are in each group (and so $p_1+p_2=1$) and define v_f as $k_{\mathrm{p}}E_T$. These changes give

$$\frac{dP}{dt}=p_1v_f\frac{AB\left(1-\frac{k_2k_8k_{\mathrm{rev}}P}{k_1k_7k_{\mathrm{p}}AB}\right)}{\frac{k_2k_8}{k_1k_7}+\frac{k_8}{k_7}A+AB}+p_2v_f\frac{AB\left(1-\frac{k_4k_6k_{\mathrm{rev}}P}{k_3k_5k_{\mathrm{p}}AB}\right)}{\frac{k_4k_6}{k_3k_5}+\frac{k_6}{k_5}B+AB} \tag{5.64}$$

If $p_1=1$ (or $p_2=1$), the rate in Eq. (5.64) simplifies to the rate for the Ordered Ternary Mechanism. This is as expected because $p_1=1$ (or $p_2=1$) means that all of the enzyme is E_1 (or E_2) so only the first (or second) line of Eq. (5.57) can occur.

Eq. (5.64) has the sum of two non-negative terms, so if we consider equilibrium ($\frac{dP}{dt}=0$) we know that

$$p_1v_fA_{\mathrm{eq}}B_{\mathrm{eq}}\left(1-\frac{k_2k_8k_{\mathrm{rev}}P_{\mathrm{eq}}}{k_1k_7k_{\mathrm{p}}A_{\mathrm{eq}}B_{\mathrm{eq}}}\right)=0 \tag{5.65}$$

and

$$p_2v_fA_{\mathrm{eq}}B_{\mathrm{eq}}\left(1-\frac{k_4k_6k_{\mathrm{rev}}P_{\mathrm{eq}}}{k_3k_5k_{\mathrm{p}}A_{\mathrm{eq}}B_{\mathrm{eq}}}\right)=0. \tag{5.66}$$

We know that p_1 and p_2 cannot both be equal to 0 simultaneously and we have already seen that exactly one of them being equal to 0 means the mechanism simplifies to the Ordered Ternary Mechanism. If neither p_1 nor p_2 is equal to 0, Eqs. (5.65) and (5.66) give

$$\frac{k_1k_7k_{\mathrm{p}}}{k_2k_8k_{\mathrm{rev}}}=\frac{P_{\mathrm{eq}}}{A_{\mathrm{eq}}B_{\mathrm{eq}}}=K_{\mathrm{eq}}$$

and

$$\frac{k_3 k_5 k_{\mathrm{p}}}{k_4 k_6 k_{\mathrm{rev}}} = \frac{P_{\mathrm{eq}}}{A_{\mathrm{eq}} B_{\mathrm{eq}}} = K_{\mathrm{eq}}.$$

This means that

$$\frac{k_1 k_7}{k_2 k_8} = \frac{k_3 k_5}{k_4 k_6}. \tag{5.67}$$

As usual,

$$\theta = \frac{1}{K_{\mathrm{eq}}} \frac{P}{AB}$$

and we get the final expression for the rate:

$$q_{PP} = p_1 v_f \frac{AB\,(1-\theta)}{\frac{k_2 k_8}{k_1 k_7} + \frac{k_8}{k_7} A + AB} + p_2 v_f \frac{AB\,(1-\theta)}{\frac{k_4 k_6}{k_3 k_5} + \frac{k_6}{k_5} B + AB}. \tag{5.68}$$

With appropriate relabelling of p's and k's, the form of this rate is symmetrical in A and B, as expected. This has the same form as $p_1 R_1 + p_2 R_2$ where R_1 and R_2 are, respectively, the rates for the Ordered Ternary Mechanism with A reacting first and with B reacting first.

Compared to the Random Ternary Mechanism, this rate has the added complication of the proportions p_1 and p_2. It remains to be seen if the extra information built into the model is worth having the additional unknowns in the rate.

5.6 Confluence Mechanism

Another mechanism worth considering is shown in Eq. (5.69).

$$\begin{array}{lcl} \mathrm{E_A} + \mathrm{A} & \underset{\mathrm{k_2}}{\overset{\mathrm{k_1}}{\rightleftharpoons}} & \mathrm{C_A} \\ & + & \underset{\mathrm{k_6}}{\overset{\mathrm{k_5}}{\rightleftharpoons}} \quad \mathrm{C_{AB}} \quad \underset{\mathrm{k_{rev}}}{\overset{\mathrm{k_p}}{\rightleftharpoons}} \quad (\mathrm{E_A} + \mathrm{E_B}) + \mathrm{P} \\ \mathrm{E_B} + \mathrm{B} & \underset{\mathrm{k_4}}{\overset{\mathrm{k_3}}{\rightleftharpoons}} & \mathrm{C_B} \end{array} \tag{5.69}$$

In this mechanism we have two enzymes which can each react with only one of the substrates to produce a binary complex. The confluence of the two binary complexes gives another complex which can react to give the product along with returning both enzymes.

We start, as usual, by considering the law of mass action. This gives the following differential

equations for the concentrations of the species involved:

$$\frac{dA}{dt} = -k_1 E_A A + k_2 C_A \tag{5.70a}$$
$$\frac{dB}{dt} = -k_3 E_B B + k_4 C_B \tag{5.70b}$$
$$\frac{dE_A}{dt} = -k_1 E_A A + k_2 C_A + k_\mathrm{p} C_{AB} - k_\mathrm{rev} E_A E_B P \tag{5.70c}$$
$$\frac{dE_B}{dt} = -k_3 E_B B + k_4 C_B + k_\mathrm{p} C_{AB} - k_\mathrm{rev} E_A E_B P \tag{5.70d}$$
$$\frac{dC_A}{dt} = k_1 E_A A - k_2 C_A - k_5 C_A C_B + k_6 C_{AB} \tag{5.70e}$$
$$\frac{dC_B}{dt} = k_3 E_B B - k_4 C_B - k_5 C_A C_B + k_6 C_{AB} \tag{5.70f}$$
$$\frac{dC_{AB}}{dt} = k_5 C_A C_B - k_6 C_{AB} - k_\mathrm{p} C_{AB} + k_\mathrm{rev} E_A E_B P \tag{5.70g}$$
$$\frac{dP}{dt} = k_\mathrm{p} C_{AB} - k_\mathrm{rev} E_A E_B P. \tag{5.70h}$$

We can find several conservation laws by combining these differential equations. For readability, we first note that the terms in the mass action equations appear in pairs and rename the pairs as follows:

$$\begin{aligned} W &= -k_1 E_A A + k_2 C_A, \\ X &= -k_3 E_B B + k_4 C_B, \\ Y &= -k_5 C_A C_B + k_6 C_{AB}, \\ Z &= -k_\mathrm{p} C_{AB} + k_\mathrm{rev} E_A E_B P. \end{aligned} \tag{5.71}$$

Eqs. (5.70a)-(5.70h) can now be rewritten as

$$\frac{dA}{dt} = W \tag{5.72a}$$
$$\frac{dB}{dt} = X \tag{5.72b}$$
$$\frac{dE_A}{dt} = W - Z \tag{5.72c}$$
$$\frac{dE_B}{dt} = X - Z \tag{5.72d}$$
$$\frac{dC_A}{dt} = -W + Y \tag{5.72e}$$
$$\frac{dC_B}{dt} = -X + Y \tag{5.72f}$$
$$\frac{dC_{AB}}{dt} = -Y + Z \tag{5.72g}$$
$$\frac{dP}{dt} = -Z. \tag{5.72h}$$

We can see that

$$\frac{dE_A}{dt} + \frac{dC_A}{dt} + \frac{dC_{AB}}{dt} = 0$$

which means that

$$E_A + C_A + C_{AB} = E_{AT}, \tag{5.73}$$

where E_{AT} is a constant and it represents the total amount of the enzyme present, in any form, which can react with A. Similarly, we can see that

$$\frac{dE_B}{dt} + \frac{dC_B}{dt} + \frac{dC_{AB}}{dt} = 0$$

which means that

$$E_B + C_B + C_{AB} = E_{BT}, \tag{5.74}$$

where E_{BT} is a constant and it represents the total amount of the enzyme present, in any form, which can react with B. Another pair of conservation laws follow from noticing that

$$\frac{dA}{dt} + \frac{dC_A}{dt} + \frac{dC_{AB}}{dt} + P = 0,$$

which means that

$$A + C_A + C_{AB} + P = A_T, \tag{5.75}$$

and

$$\frac{dB}{dt} + \frac{dC_B}{dt} + \frac{dC_{AB}}{dt} + P = 0,$$

which means that

$$B + C_B + C_{AB} + P = B_T, \tag{5.76}$$

where A_T and B_T are constants which may be interpreted as the total amount present, in any form, of species containing or derived from substrate A and substrate B, respectively. A further pair of conservation laws follow from noticing that

$$\frac{dP}{dt} + \frac{dA}{dt} - \frac{dE_A}{dt} = 0,$$

which means that

$$P + A - E_A = N_A, \tag{5.77}$$

and

$$\frac{dP}{dt} + \frac{dB}{dt} - \frac{dE_B}{dt} = 0,$$

which means that

$$P + B - E_B = N_B, \tag{5.78}$$

where N_A and N_B are constants. Subtracting Eq. (5.73) from Eq. (5.75) and comparing to Eq. (5.77) shows that

$$N_A = A_T - E_{AT}. \tag{5.79}$$

Similarly, subtracting Eq. (5.74) from Eq. (5.76) and comparing to Eq. (5.78) shows that

$$N_B = B_T - E_{BT}. \tag{5.80}$$

We now note that while we do not have a direct interpretation of N_A and N_B, we can present

them as the difference of two other constants that we do have a better understanding of. We can interpret N_A as the difference between the total amount of A-containing material and E_A-containing material. If we start with only substrates and enzymes (no products or complexes), this means that N_A is the difference between the initial concentrations of A and E_A. The same applies to N_B, it is the difference between the total amounts of B-containing material and E_B-containing material and, if we start with only substrates and enzymes, this means that N_B is the difference between the initial concentrations of B and E_B.

We may rearrange Eqs. (5.77) and (5.78) to make E_A and E_B the subject of each and then replace E_A and E_B in Eq. (5.70h) as follows:

$$E_A = P + A - N_A, \tag{5.81}$$

$$E_B = P + B - N_B, \tag{5.82}$$

$$\frac{dP}{dt} = k_{\mathrm{p}} C_{AB} - k_{\mathrm{rev}} \left(P + A - N_A\right)\left(P + B - N_B\right) P. \tag{5.83}$$

The equation for $\frac{dP}{dt}$ now has a term that is cubic in P and it is symmetric in A and B. In order to progress further, we must make a quasi-steady-state assumption.

5.6.1 A Simple Quasi-Steady-State Assumption

We now need to determine what we should assume about the behaviour of the system. The simplest QSSA that we could make is

$$\frac{dC_{AB}}{dt} = 0, \tag{5.84}$$

which could also be stated as $Y = Z$. We can see, from either the law of mass action equations or from the conservation laws, that this means $\frac{dE_A}{dt} + \frac{dC_A}{dt} = 0$ and $\frac{dE_B}{dt} + \frac{dC_B}{dt} = 0$. These show that the sum of E_A and C_A is a constant, as is the sum of E_B and C_B. This QSSA gives us a new conservation law that we can consider,

$$C_{AB} = \tilde{C}_{AB} \tag{5.85}$$

where the tilde denotes that the value is a constant. This means that

$$\frac{dP}{dt} = k_{\mathrm{p}}\tilde{C}_{AB} - k_{\mathrm{rev}}E_A E_B P. \tag{5.86}$$

Rearranging Eq. (5.70g) gives:

$$k_5 C_A C_B - k_6 C_{AB} - k_{\mathrm{p}} C_{AB} + k_{\mathrm{rev}} E_A E_B P = 0,$$

$$\left(k_6 + k_{\mathrm{p}}\right) C_{AB} = k_5 C_A C_B + k_{\mathrm{rev}} E_A E_B P. \tag{5.87}$$

The LHS of Eq. (5.87) is a constant so we have a relation between C_A, C_B, E_A, E_B, and P (or C_A, C_B, A, B, and P if we choose to replace E_A and E_B using Eqs. (5.81) and (5.82)).

5.6.2 A Biological Assumption

If, instead of assuming Eq. (5.84), we assume that $W = X$, we get a different situation. The biological motivation for assuming $W = X$ is that we know that the amounts of C_A and C_B consumed to produce C_{AB} must match due to their 1:1 stoichiometry and so the net flux from E_A to C_A is equal to the net flux from E_B to C_B. Under this assumption, the differential equations that we get from the law of mass action clearly show that $\frac{dA}{dt} = \frac{dB}{dt}$, $\frac{dE_A}{dt} = \frac{dE_B}{dt}$, and $\frac{dC_A}{dt} = \frac{dC_B}{dt}$.

If we assume that W and X are also equal to Z, i.e., $W = X = Z$, we can take this further. The biological motivation for assuming $W = X = Z$ is the 1:1 stoichiometry in the reaction making E_A and E_B constants and meaning that the increase in P is equal to the decrease in A and B. Assuming that both W and X are also equal to Z means that $\frac{dE_A}{dt} = 0$ and $\frac{dE_B}{dt} = 0$ and that $\frac{dC_A}{dt} = \frac{dC_B}{dt} = -\frac{dC_{AB}}{dt}$.

We can introduce three new constants, which we may call N_1, N_2, and N_3, and write $A - B = N_1$, $E_A - E_B = N_2$, and $C_A - C_B = N_3$. Note that while some of the other constants must be positive, each of N_1, N_2, and N_3 may be positive or negative. Subtracting Eq. (5.78) from Eq.

(5.77) gives

$$\begin{aligned}(A - E_A) - (B - E_B) &= N_A - N_B \\ &= (A_T - E_{AT}) - (B_T - E_{BT}) \\ &= (A_T - B_T) - (E_{AT} - E_{BT})\end{aligned}$$

which we can now rewrite as $N_1 - N_2 = (A_T - B_T) - (E_{AT} - E_{BT})$.

Using Eqs. (5.77) and (5.78) we can replace E_A and E_B with $P + A - N_A$ and $P + B - N_B$ in Eq. (5.86) to get

$$\frac{dP}{dt} = k_{\mathrm{p}}\tilde{C}_{AB} - k_{\mathrm{rev}}(P + A - N_A)(P + B - N_B)P. \tag{5.88}$$

This rate contains A, B, and P but also contains five constants for which we would need to determine values.

We can get two other equations for $\frac{dP}{dt}$ by replacing either B or A. Using our definition of N_1 we can replace B from Eq. (5.88) and get

$$\begin{aligned}\frac{dP}{dt} &= k_{\mathrm{p}}\tilde{C}_{AB} - k_{\mathrm{rev}}\left(P + A - N_A\right)\left(P + (A - N_1) - N_B\right)P \\ &= k_{\mathrm{p}}\tilde{C}_{AB} - k_{\mathrm{rev}}\left(P + A - N_A\right)\left(P + A - N_4\right)P\end{aligned} \tag{5.89}$$

where $N_B + N_1 = N_4$. Similarly we could replace A from Eq. (5.88) instead and get

$$\begin{aligned}\frac{dP}{dt} &= k_{\mathrm{p}}\tilde{C}_{AB} - k_{\mathrm{rev}}\left(P + (B + N_1) - N_A\right)\left(P + B - N_B\right)P \\ &= k_{\mathrm{p}}\tilde{C}_{AB} - k_{\mathrm{rev}}\left(P + B - N_5\right)\left(P + B - N_B\right)P\end{aligned} \tag{5.90}$$

where $N_A - N_1 = N_5$. We get a relationship $N_A + N_B = N_4 + N_5$. These two rates in Eqs. (5.89) and (5.90) should be the same as the rate in Eq. (5.88).

The number of constants in the equations for $\frac{dP}{dt}$ that we have from this biological assumption makes it mathematically intractable to go further without making a stronger assumption and, if we got to a rate that we wanted to use, we would need to know values for all of the constants.

We turn our attention next to a stronger assumption.

5.6.3 A Strong Quasi-Steady-State Assumption

The strong QSSA that we could make, analogous to the one that we used for the Random Ternary Mechanism, is

$$\frac{dE_A}{dt} = \frac{dE_B}{dt} = \frac{dC_A}{dt} = \frac{dC_B}{dt} = \frac{dC_{AB}}{dt} = 0.$$

We can get this assumption by assuming either $\frac{dE_A}{dt} = \frac{dE_B}{dt} = \frac{dC_{AB}}{dt} = 0$ or $\frac{dC_A}{dt} = \frac{dC_B}{dt} = \frac{dC_{AB}}{dt} = 0$. Comparing this assumption, whichever way we make it, to the equations from the law of mass action gives us some information about W, X, Y, and Z. First, $\frac{dC_{AB}}{dt} = 0$ implies that $Y = Z$. Additionally, $\frac{dE_A}{dt} = \frac{dE_B}{dt} = 0$ implies that $W = Z$ and $X = Z$, which further implies that $W = X$. Similarly, $\frac{dC_A}{dt} = \frac{dC_B}{dt} = 0$ implies that $W = Y$ and $X = Y$, which further implies that $W = X$. Overall, this QSSA tells us that $W = X = Y = Z$ (and it does not imply that $Z = 0$). This means that the net flux over any pair of forward and backward reactions in the mechanism (one set of arrows in the mechanism diagram) is the same. This is the flow through the system of substrates A and B into product P with no net change to E_A, E_B, C_A, C_B, and C_{AB} along the way. As each of the catalytic terms is a constant we may rename them for transparency, call $C_{AB} = \tilde{C}_{AB}$ (as above), $E_A = \tilde{E}_A$, and $E_B = \tilde{E}_B$. Now we replace terms from Eq. (5.70h) and get

$$\frac{dP}{dt} = k_{\mathrm{p}}\tilde{C}_{AB} - k_{\mathrm{rev}}\tilde{E}_A\tilde{E}_B P \tag{5.91}$$

Note that k_{p}, k_{rev}, $\tilde{C}_{AB}$, $\tilde{E}_A$, and $\tilde{E}_B$ are all either rate constants or concentrations, so they are all positive constants.

If $W = X = Y = Z$ then we can see that $\frac{dP}{dt} = -\frac{dA}{dt} = -\frac{dB}{dt}$. This means we can also use

Eqs. (5.70a) and (5.70b) to get two other ways of presenting the overall reaction rate:

$$\begin{aligned}\frac{dP}{dt} &= -\frac{dA}{dt} \\ &= k_1 E_A A - k_2 C_A \\ &= k_1 \tilde{E}_A A - k_2 \tilde{C}_A \end{aligned} \tag{5.92}$$

and

$$\begin{aligned}\frac{dP}{dt} &= -\frac{dB}{dt} \\ &= k_3 E_B B - k_4 C_B \\ &= k_3 \tilde{E}_B B - k_4 \tilde{C}_B \end{aligned} \tag{5.93}$$

where $C_A = \tilde{C}_A$ and $C_B = \tilde{C}_B$. Eqs. (5.92) and (5.93) each contain the concentration of one substrate accompanying a collection of positive constants and so, along with Eq. (5.91), these differential equations can be solved analytically. Before we solve the differential equations, we combine Eqs. (5.91) and (5.92), and use $'$ to mean the derivative with respect to time, to get

$$\begin{aligned} &P' + A' = k_{\mathrm{p}} k_3 - k_{\mathrm{rev}} \tilde{E}_A \tilde{E}_B P + k_2 \tilde{C}_A - k_1 \tilde{E}_A A = 0 \\ &\left(P' + A'\right)' = -k_{\mathrm{rev}} \tilde{E}_A \tilde{E}_B P' - k_1 \tilde{E}_A A' = 0 \\ &- k_{\mathrm{rev}} \tilde{E}_A \tilde{E}_B P' + k_1 \tilde{E}_A P' = 0 \\ &\tilde{E}_A P' \left(k_1 - k_{\mathrm{rev}} \tilde{E}_B\right) = 0. \end{aligned}$$

This implies that

$$k_1 = k_{\mathrm{rev}} \tilde{E}_B$$

as $P' = 0$ only at equilibrium. We repeat this using Eqs. (5.91) and (5.93) to get:

$$\begin{aligned}
P' + B' &= k_{\mathrm{p}}k_3 - k_{\mathrm{rev}}\tilde{E}_A\tilde{E}_B P + k_4\tilde{C}_B - k_3\tilde{E}_B B = 0 \\
\left(P' + A'\right)' &= -k_{\mathrm{rev}}\tilde{E}_A\tilde{E}_B P' - k_3\tilde{E}_B B' = 0 \\
-k_{\mathrm{rev}}\tilde{E}_A\tilde{E}_B P' &+ k_3\tilde{E}_B P' = 0 \\
\tilde{E}_B P' &\left(k_3 - k_{\mathrm{rev}}\tilde{E}_A\right) = 0,
\end{aligned}$$

which implies that

$$k_3 = k_{\mathrm{rev}}\tilde{E}_A$$

for the same reason. We also note that the conservation laws from Eqs. (5.77) and (5.78) can now be restated as

$$P + A = N_A + \tilde{E}_A = \rho_A$$

and

$$P + B = N_B + \tilde{E}_B = \rho_B$$

where ρ_A and ρ_B are constants, each replacing a pair of constants.

Starting with Eq. (5.92) and solving the differential equation for A we get:

$$\begin{aligned}
\frac{dA}{dt} &= -k_1\tilde{E}_A A + k_2\tilde{C}_A \\
\frac{1}{k_2\tilde{C}_A - k_1\tilde{E}_A A}dA &= 1dt \\
\frac{-k_1\tilde{E}_A}{k_2\tilde{C}_A - k_1\tilde{E}_A A}dA &= -k_1\tilde{E}_A dt \\
\ln\left|k_2\tilde{C}_A - k_1\tilde{E}_A A\right| &= -k_1\tilde{E}_A t + a_1 \\
k_2\tilde{C}_A - k_1\tilde{E}_A A &= e^{-k_1\tilde{E}_A t + a_1} \\
A &= \frac{k_2\tilde{C}_A}{k_1\tilde{E}_A} - \frac{a_2}{k_1\tilde{E}_A}e^{-k_1\tilde{E}_A t}
\end{aligned} \tag{5.94}$$

where a_1 is the constant of integration and $a_2 = \pm e^{a_1}$ with the sign depending on the sign of

$k_2\tilde{C}_A - k_1\tilde{E}_A A$. Similarly for Eq. (5.93) we get:

$$\begin{aligned}
\frac{dB}{dt} &= -k_3\tilde{E}_B B + k_4\tilde{C}_B \\
\frac{1}{k_4\tilde{C}_B - k_3\tilde{E}_B B}dB &= 1dt \\
\frac{-k_3\tilde{E}_B}{k_4\tilde{C}_B - k_3\tilde{E}_B B}dB &= -k_3\tilde{E}_B dt \\
\ln\left(k_4\tilde{C}_B - k_3\tilde{E}_B B\right) &= -k_3\tilde{E}_B t + b_1 \\
k_4\tilde{C}_B - k_3\tilde{E}_B B &= e^{-k_3\tilde{E}_B t + b_1} \\
B &= \frac{k_4\tilde{C}_B}{k_3\tilde{E}_B} - \frac{b_2}{k_3\tilde{E}_B}e^{-k_3\tilde{E}_B t}
\end{aligned} \tag{5.95}$$

where b_1 and b_2 are as a_1 and a_2 are above. Finally, for Eq. (5.91) we get:

$$\begin{aligned}
\frac{dP}{dt} &= -k_{\text{rev}}\tilde{E}_A\tilde{E}_B P + k_{\text{p}}\tilde{C}_{AB} \\
\frac{1}{k_{\text{p}}\tilde{C}_{AB} - k_{\text{rev}}\tilde{E}_A\tilde{E}_B P}dP &= 1dt \\
\frac{-k_{\text{rev}}\tilde{E}_A\tilde{E}_B}{k_{\text{p}}\tilde{C}_{AB} - k_{\text{rev}}\tilde{E}_A\tilde{E}_B P}dP &= -k_{\text{rev}}\tilde{E}_A\tilde{E}_B dt \\
\ln\left(k_{\text{p}}\tilde{C}_{AB} - k_{\text{rev}}\tilde{E}_A\tilde{E}_B P\right) &= -k_{\text{rev}}\tilde{E}_A\tilde{E}_B t + p_1 \\
k_{\text{p}}\tilde{C}_{AB} - k_{\text{rev}}\tilde{E}_A\tilde{E}_B P &= e^{-k_{\text{rev}}\tilde{E}_A\tilde{E}_B t + p_1} \\
P &= \frac{k_{\text{p}}\tilde{C}_{AB}}{k_{\text{rev}}\tilde{E}_A\tilde{E}_B} - \frac{p_2}{k_{\text{rev}}\tilde{E}_A\tilde{E}_B}e^{-k_{\text{rev}}\tilde{E}_A\tilde{E}_B t}
\end{aligned} \tag{5.96}$$

where p_1 and p_2 are also as a_1 and a_2 are above.

To shed some light on what we have found, we consider the initial conditions and equilibrium values. Suppose $t = 0$ then

$$\begin{aligned}
A_0 &= \frac{k_2\tilde{C}_A}{k_1\tilde{E}_A} - \frac{a_2}{k_1\tilde{E}_A} \\
a_2 &= k_2\tilde{C}_A - k_1\tilde{E}_A A_0 \\
A(t) &= \frac{k_2\tilde{C}_A}{k_1\tilde{E}_A} - \frac{k_2\tilde{C}_A - k_1\tilde{E}_A A_0}{k_1\tilde{E}_A}e^{-k_1\tilde{E}_A t}.
\end{aligned}$$

Note that the only zero of Eq. (5.92) occurs when $A = \frac{k_2 \tilde{C}_A}{k_1 \tilde{E}_A}$. We let

$$A_{\text{eq}} = \frac{k_2 \tilde{C}_A}{k_1 \tilde{E}_A}.$$

Suppose $t \to \infty$ then

$$A(t) = A_{\text{eq}} - (A_{\text{eq}} - A_0)\, e^{-k_1 \tilde{E}_A t} \tag{5.97}$$

which shows that A_{eq} is a stable equilibrium. Similarly for B we get

$$\begin{aligned} b_2 &= k_4 \tilde{C}_B - k_3 \tilde{E}_B B_0 \\ B_{eq} &= \frac{k_4 \tilde{C}_B}{k_3 \tilde{E}_B} \\ B(t) &= B_{\text{eq}} - (B_{\text{eq}} - B_0)\, e^{-k_3 \tilde{E}_B t} \end{aligned} \tag{5.98}$$

and for P we get

$$\begin{aligned} p_2 &= k_{\text{p}} \tilde{C}_{AB} - k_{\text{rev}} \tilde{E}_A \tilde{E}_B P_0 \\ P_{eq} &= \frac{k_{\text{p}} \tilde{C}_{AB}}{k_{\text{rev}} \tilde{E}_A \tilde{E}_B} \\ P(t) &= P_{\text{eq}} - (P_{\text{eq}} - P_0)\, e^{-k_{\text{rev}} \tilde{E}_A \tilde{E}_B t}. \end{aligned} \tag{5.99}$$

We can see that B_{eq} and P_{eq} are also stable.

The biological assumption gave a rate that is irreconcilably different in form to any of the other rates that we have found. The cubic in P and the need for the equations in A and B to give the same results are entirely novel.

The strong QSSA allowed us to get to a point where we could analytically solve the system and get equations for $A(t)$, $B(t)$, and $P(t)$. These equations contained many constants that would need to be determined for the model to be used and it remains to be seen whether they can be effectively applied to a microbial system.

5.7 Statistical Mechanics

Having explored several enzyme kinetic mechanisms as possible ways to extend the Modified Haldane rate to multiple rate-limiting substrates, we now consider the statistical mechanics approach of Desmond-Le Quéméner and Bouchez [39] that gave the DLQB rate for a single rate-limiting substrate. Their work assumes that multiple substrates can be considered as statistically independent, which allows a much simpler expansion to multiple rate-limiting substrates when using statistical mechanics compared to using enzyme kinetics. For substrates A and B we get a rate of the form

$$q_{DD} = e^{-\Lambda_A/A} e^{-\Lambda_B/B} \tag{5.100}$$

where the Λ's are defined as for the single substrate case ($\Lambda = \frac{E_M + E_{\text{dis}}}{E_{\text{cat}} \cdot V_{\text{harv}}}$). This rate is simply the product of two single-substrate DLQB rates due to the assumption of statistically independent partition functions, which seems reasonable but more work is required for this to be fully understood.

The values of E_M, E_{dis}, and E_{cat} depend on the reaction catalysed by the microbe and on the concentrations of substrates and products in its external environment, but none of them highlight a particular substrate. This means that the values of E_M, E_{dis}, and E_{cat} will be the same for Λ_A and Λ_B. If we assume that V_{harv} is the same for both substrates, which seems to be a reasonable assumption, then $\Lambda_A = \Lambda_B$, which we will relabel as Λ, and the Double DLQB rate becomes

$$q_{DD} = e^{-\Lambda/A} e^{-\Lambda/B}. \tag{5.101}$$

It required very little work to expand the DLQB rate from a single substrate to two substrates but we are interested in how similar this equation is to some of the others that we have seen.

Considering first the Taylor series for an exponential, we have

$$\begin{aligned} e^{-\phi} &= \frac{1}{1+\phi+\frac{\phi^2}{2!}+\frac{\phi^3}{3!}+...} \\ &= \left(\frac{1}{1+\phi}\right)\left(\frac{1}{1+\frac{\left(\frac{\phi^2}{2!}+\frac{\phi^3}{3!}+...\right)}{1+\phi}}\right) \\ &= \left(\frac{1}{1+\phi}\right)\left(\frac{1}{1+\omega}\right) \\ &= \left(\frac{1}{1+\phi}\right)\left(\frac{1}{1-(-\omega)}\right) \end{aligned} \tag{5.102}$$

where

$$\omega = \frac{\left(\frac{\phi^2}{2!}+\frac{\phi^3}{3!}+...\right)}{1+\phi}.$$

Using a geometric series,

$$\frac{1}{1-(-\omega)} = 1-\omega+\omega^2-\omega^3+...$$

as long as $\omega < 1$, and so

$$e^{-\phi} = \frac{1}{1+\phi}\left(1-\omega+\omega^2-\omega^3+...\right).$$

We can see that $\omega = O(\phi^2)$, so

$$e^{-\phi} = \frac{1}{1+\phi}\left(1+O(\phi^2)\right) = \frac{1}{1+\phi}+O(\phi^2). \tag{5.103}$$

Eqs. (5.102)-(5.103) show that, in the case where $S > \Lambda$,

$$q_D = e^{\Lambda/S} = \frac{1}{1+\Lambda/S}+O\left(\left(\frac{\Lambda}{S}\right)^2\right). \tag{5.104}$$

Let $\phi_1 = \Lambda/A$ and $\phi_2 = \Lambda/B$, then

$$\begin{aligned} e^{-\phi_1}e^{-\phi_2} &= \frac{1}{1+\phi_1}\left(1+O(\phi_1^2)\right)\frac{1}{1+\phi_2}\left(1+O(\phi_2^2)\right) \\ &= \frac{1}{(1+\phi_1)(1+\phi_2)}\left(1+O(\phi_1^2+O(\phi_2^2)+O(\phi_1^2)O(\phi_2^2)\right). \end{aligned}$$

Let $\phi_k = \max\{\phi_1, \phi_2\}$, then as $\phi_k \to 0$ the Double DLQB rate will be

$$q_{DD} = \frac{1}{(1+\phi_1)(1+\phi_2)} + O(\phi_k^2)$$

which we could rewrite as

$$q_{DD} = \frac{AB}{(A+\Lambda)(B+\Lambda)} + O\left(\left(\frac{\Lambda}{S}\right)^2\right) \tag{5.105}$$

where $S = \min\{A, B\}$. This gives us a link from the Double DLQB rate to the Double Monod rate but it should be noted that some of the assumptions that were required in this derivation have not been thoroughly explored.

So far we have only considered the DLQB formulation with unit coefficients for each substrate. If we had a reaction with non-unit coefficients, it appears that these coefficients would manifest in the exponential for the corresponding substrate. For example, a reaction with a stoichiometry of one of substrate A to two of substrate B would have the form

$$q = e^{-\Lambda/A} e^{-2\Lambda/B}. \tag{5.106}$$

5.8 Summary

In this chapter we have explored several possible ways we can model situations where there are multiple rate-limiting substrates. We focused on different variations of the analogy with enzyme kinetics as we searched for an extension to the Modified Haldane rate that makes sense biologically and is mathematically tractable.

The Black Box Mechanism leads us to a rate, in Eq. (5.15), that is quite similar to the Modified Haldane rate, with S replaced by AB, but may be an oversimplification of what is happening biologically.

Using a quasi-steady-state assumption in the spirit of Michaelis-Menten, the Ordered Ternary Mechanism leads to a rate, in Eq. (5.27) that is also similar, though without an inhibitory thermodynamic term in the denominator, effectively giving a generalisation of the Jin and Bethke

rate to two substrates. The rate is asymmetric in A and B and, while it may be applicable to enzymes, the pathway may be an overly complicated for the analogy to microbes.

A strong, Michaelis-Menten-like QSSA for the Random Ternary Mechanism leads to a rate, in Eq. (5.54), that seems to be a meaningful extension of the Modified Haldane rate to two substrates. However, the required assumptions again resulted in there being no inhibitory thermodynamic term in the denominator. We have noted a particular situation where this rate can factorise to have the same form as the Double Monod rate but with the addition of a thermodynamic inhibition term in the numerator. As the Double Monod rate is a widely-used empirical rate, providing a set of assumptions and a derivation that leads to a rate of analogous form is an important contribution.

A variation of the Random Ternary Mechanism can lead us to a rate that has the form of two Ordered Ternary Mechanism rates operating in different proportions, though it is not clear whether the extra information in the model is worth additional unknowns.

The Confluence Mechanism leads us to a rate that is cubic in P and using a strong QSSA allows us to analytically solve the system for $A(t)$, $B(t)$, and $P(t)$, shown in Eqs. (5.97)-(5.99). This is novel among the mechanisms that we have investigated but it remains to be seen if this mechanism can be effectively applied in a microbial context due to the large number of constants that would need to be known.

The expansion of the DLQB rate to multiple substrates was relatively straightforward and quickly led to the rate given in Eq. (5.101). Considering the Taylor series of the exponential and a geometric series, we also found an equation, given in Eq. (5.105), that has a similar form to Double Monod. We also briefly considered how this formulation can deal with non-unit coefficients for the substrates. More work must be done to fully understand the assumptions that allowed these expansions but their simplicity is promising.

Chapter 6

Conclusions

6.1 Introduction

The goal of this thesis is to derive a mathematical model that is applicable to multiple microbial populations with a range of different metabolisms, to identify the limits of validity of the model using data found in the literature, and to identify avenues for further model development. Here, we review the extent to which these goals have been met and summarise the content and major findings in this thesis.

6.2 Chapter 2

Chapter 2 begins with a summary of existing models of microbial growth. These models are distinguished by the growth rates. We partitioned these models into four categories based on how they are derived. These categories are:

1. Empirical;
2. Hybrid of empirical with thermodynamic considerations;
3. Enzyme kinetics analogues; and
4. Statistical mechanics.

A prominent example of an empirical rate is the Monod rate. This rate is still the most widely used rate in the literature. Nonetheless, this model has its limitations, particularly its lack of end-product feedback when thermodynamic effects become important. This prompted modifications such as that by Jin and Bethke [79] that include factors in the rate that reflect the thermodynamics. This results in a hybrid rate that suffers from the lack of a solid theoretical grounding. It is here that the rates based on an analogy with enzyme kinetics come to the fore. Using Haldane's analysis, by interpreting a microbe as an analogue of an enzyme, a more rational and unified result is achieved. Here, care must be taken to recognise the relative time scales of reactions. Enzyme kinetics assume a conservation of enzyme, but microbial growth in this analogy does not fit. Here we note a much slower time scale: microbes reproduce several orders of magnitude slower than most chemical reactions, so the microbial population is effectively constant on the timescale at which the chemical reactions occur. The Modified Haldane rate comes from this analogy. The Desmond-Le Quéméner and Bouchez (DLQB) rate is derived from statistical mechanics and is fundamentally different. This rate certainly captures both the Monod type behaviour for large substrate concentrations and limiting growth behaviour for small substrate concentrations. Comparing these rates, some key observations and results in this thesis include:

1. The Monod rate corresponds formally to both the Jin and Bethke rate and the Modified Haldane rate if they have their thermodynamic influence neutralised.

2. Redefining the constant in the Jin and Bethke rate as being made up of two parts which depend on product concentration allows the rate to be written in a form that is not distinct from the Modified Haldane rate.

3. Using the enzyme kinetics analogy used for the Modified Haldane rate modified by a fast kinetics, Michaelis-Menten-like assumption, instead of the quasi-steady-state assumption, leads to a rate with the same form as that of Jin and Bethke. This highlights the similarity between the Jin and Bethke rate and the Modified Haldane rate. It provides a theoretical bases for interpreting the Jin and Bethke rate in terms of enzyme kinetics.

4. The DLQB rate contains a constant in the exponential. This constant was associated with

the Monod constant by Desmond-Le Quéméner and Bouchez [39], but, in fact, there was little formal connection identified. In this thesis it was shown, through an asymptotic expansion, as substrate concentration increases, that the constant must agree with the Monod constant.

5. The DLQB rate, as presented by the authors, did not predict a non-zero threshold. The peculiar "flick of the tail" of this rate as the substrate concentration went to zero did account, at least experimentally, for the non-zero threshold. We showed through a simple but careful interpretation of the rate that the full thermodynamic impact was contained in this rate that included a non-zero threshold.

6.3 Chapter 3

The rates discussed above have the merit of simplicity. Indeed, we have shown that for large limiting substrate concentration, these rates essentially correspond to a Monod type rate. The merit here is that the Monod rate has one "biological constant" to be determined. At this level, one need not delve into reaction rates, thermodynamic inhibitions from products etc. This is a simple and effective model in the high limiting substrate regime. The problems come when we are at small limiting substrate concentrations or environments where the concentration of products inhibits growth. In Chapter 3 we turn towards models that capture some of the thermodynamic effects of including additional biological information. The challenge was to find a model that is mathematically tractable yet applicable to low concentration scanarios where thermodynamic effects become important. Equally important was that the model should be biologically tractable in that it should contain only key biological parameters. We developed a model and compared it to some existing ones. In particular, we were interested in exploring the ΔG_{ATP} term in the Modified Haldane rate.

In the Modified Haldane rate the ΔG_{ATP} term is a constant: it is typically stated as between $55\,\mathrm{kJ\,mol}_{\mathrm{ATP}}^{-1}$ and $75\,\mathrm{kJ\,mol}_{\mathrm{ATP}}^{-1}$. However, it has been observed that the value of ΔG_{ATP} can change to allow growth in conditions where it would not be possible if ΔG_{ATP} was a fixed value. In plain terms, organisms can respond to thermodynamically challenging environments/low

substrate concentrations by lowering their ΔG_{ATP} demands. It was this behaviour that we wished to capture in the model, by allowing ΔG_{ATP} to vary within limits, with a biologically-relevant penalty in the rate of ATP formation when ΔG_{ATP} is decreased.

We collated a dataset from the literature to test the applicability of the variable ΔG_{ATP} in the new rate against experimental data. This dataset contained 107 experiments, of which 73 were experiments measuring the substrate threshold concentrations (S_{min}) and 34 were experiments measuring the substrate concentration when the growth rate is half of its maximal value (K_{app}). For each experiment we plotted the reciprocal of the reaction quotient against $\exp\left(\left(\Delta G_T^o + \eta \Delta G_{\mathrm{ATP}}\right)/RT\right)$ three times, one with each of $\Delta G_{\mathrm{ATP}} = 0\,\mathrm{kJ\,mol_{ATP}^{-1}}$, $\Delta G_{\mathrm{ATP}} = 55\,\mathrm{kJ\,mol_{ATP}^{-1}}$, and $\Delta G_{\mathrm{ATP}} = 75\,\mathrm{kJ\,mol_{ATP}^{-1}}$. The line $y = x$ in these plots corresponds to $\theta = 1$ in the Modified Haldane rate, which is shutdown due to thermodynamic inhibition. Using L2 norms to measure how far the data is from the line $y = x$ ($\theta = 1$) for each choice of ΔG_{ATP} showed that $\Delta G_{\mathrm{ATP}} = 55\,\mathrm{kJ\,mol_{ATP}^{-1}}$ was the best for S_{min} data while $\Delta G_{\mathrm{ATP}} = 75\,\mathrm{kJ\,mol_{ATP}^{-1}}$ was the best for K_{app} data. In both cases the L2 norms for $\Delta G_{\mathrm{ATP}} = 0\,\mathrm{kJ\,mol_{ATP}^{-1}}$ (corresponding to earlier forms of the Modified Haldane rate where ΔG_{ATP} is not considered) were much larger. In short, the premise that a microbe can respond to a challenging environment by reducing its ΔG_{ATP} demands is supported by the data, and changed values in the Modified Haldane rate reflect the potential for a model with variable ΔG_{ATP}.

It is of interest that there was one outlier in the K_{app} data. The size of the outlier compared to the rest of the data prompted us to return to the assumptions that had been made and check if any of them should be reconsidered. Upon further investigation, we proposed a biological argument for a different value of η (the number of moles of ATP produced per mole of substrate consumed) than the one we had been using. Using the new value for η, the outlier moved to where we expected it to be. Here, we emphasise that the parameter η was not changed to fit the model; rather, the model identified the η assumed for the microbe to be suspect. The new value of η, as derived from biological considerations, was independent of the model and yet the new value rectified the outlier problem.

The above analysis supports the value of a model that incorporates a variable ΔG_{ATP} term to capture growth behaviour in more challenging thermodynamic scenarios. It was at this stage

that we further modified the Haldane rate to deal with a variable ΔG_{ATP}. The core idea is that the microbe will optimise the ΔG_{ATP} in challenging conditions to ensure growth/survival. Guided by results in the literature, we know that there is a minimal value of ΔG_{ATP} below which growth cannot occur and that there is a maximum value of ΔG_{ATP} beyond which the microbe is unable to use any excess energy. These values are approximately 55 kJ $\mathrm{mol}_{\mathrm{ATP}}^{-1}$ and 75 kJ $\mathrm{mol}_{\mathrm{ATP}}^{-1}$ respectively. Built upon the Haldane rate, the Lynch model contains the ΔG_{ATP} term, but a direct optimisation simply leads to the choice of a maximum ΔG_{ATP} under all conditions, which is not in agreement with the analysis. We thus looked for a modification that would allow the growth rate to be non-zero in challenging thermodynamic environments. Essentially, there are two mechanisms whereby growth is precluded. The "reaction quotient", i.e., the θ in the Lynch model, is 1. In this case, in simple terms, growth has stopped because the chemical reaction has stopped. The second mechanism is that ΔG_{ATP} has decreased to its minimal value and is not sufficient for the microbe to continue ATP formation. The model we developed incorporated both these mechanisms by using the rate in the Lynch model multiplied by a "penalty function". The mathematical details of this penalty function were discussed in Chapter 3. Here, we recognise that this is doubtless a simplification and that further work is needed to refine the model. Nonetheless, this model has the decisive merit of being mathematically tractable and it does produce results in agreement with our data.

We used the new rate to predict what the substrate concentration would be at S_{min} or K_{app} for each experiment in the dataset, then compared this value to what had been reported, taking the natural log of both values. The correlation coefficient for the S_{min} data was approximately 0.94, for the K_{app} data it was approximately 0.91, and for the whole dataset together it was approximately 0.94. We noted that K_{app} occurred (i.e., the substrate concentration was equal to K_{app}) when ΔG_{ATP} was its maximal value for each of the experiments in our data. The wide variety of microbes and reactions in our dataset suggests that ΔG_{ATP} will be its maximal value at K_{app} for our choice of the "penalty function" term, but it has not yet been proved if this is the same for a general choice of the term.

6.4 Chapter 4

In Chapter 3, we focused on data that is given at either $S_{\min}$ or K_{app}. In Chapter 4 we consider examples where experimental data are available at multiple different times as microbial growth occurs. The first example is a batch culture that has negligible thermodynamic inhibition. Comparing the experimental results to those from our simulations, we showed that the model predicts outcomes that are qualitatively similar. The second example involves a batch culture that has thermodynamic inhibition; again, our model produces results that are qualitatively similar to the experimental data. The third example includes experimental data for two strains of microbe that utilise different fermentation pathways but share a substrate, allowing exploration of competition and coexistence. This example is the more common scenario of a continuous culture with thermodynamic inhibition and it is here that the model gets the opportunity to show its strength. When considering either strain individually, the results from the model agree qualitatively with experimental data. For a fixed flow rate, we predict that whichever strain has a lower steady state substrate concentration when growing individually would outcompete the other if they were in direct competition with each other. Testing a variety of values for the flow rate allowed us to predict an interval of flow rates where one strain would thrive, followed by an interval where the other strain would thrive, before the flow rate gets so high that neither strain can grow fast enough to survive.

Shifting away from comparisons with experimental data, we modelled the two strains in competition with each other to test the predictions that could be made from the simulations for the individual strains. Initially, the microbial populations are small and the amount of substrate exceeds what can be consumed. In this environment the strain with the higher growth yield grows faster. Once the substrate concentration drops enough to limit the growth rates, however, the strain that has a lower steady state substrate concentration in the individual simulations dominates. When tested with a range of flow rates, we found that one strain dominates at low flow rates; whereas the other strain dominates at higher flow rates. If the flow rate gets too high neither strain will survive. A novel result is that in the interval of low flow rates, while one strain is dominating, the other is not eliminated (as may be expected) but is instead at a steady cell

concentration about one five-hundredth of the concentration of the other strain. This provides numerical evidence that our model predicts a stable coexistence, which would not occur without thermodynamic inhibition terms. After exploring the differential equations at steady state, we determined analytical proof of this stable coexistence is, at present, elusive.

The prediction of coexistence from this model needs to be further qualified. Firstly, we note that there are no experimental results in our dataset that support (or discourage) coexistence. The data come from a continuous culture experiment, which was not run long enough for any information about coexistence. Secondly, a great deal was assumed about the two strains of microbe: they were differentiated only by their fermentation pathways and their ATP yields. Taking into account the measured cell dimensions of the two strains, we determined some of the parameters that may be affected by cell size and reduced the values of these for the strain of smaller microbe. The resulting plots of concentrations over time were consistent with the earlier simulations, with the notable difference that the cell concentrations for the smaller strain increased by a factor approximately equal to the scaling factor on the altered parameters. The results when considering the relative sizes of the strains suggest that microbes of a comparable size can be well represented by the model and, while knowledge of finer details about the microbes may give more precise results, the generic parameter values give results that are not notably different than if different cell sizes are considered. The three examples, and the last one in particular, showed the versatility of the model, qualitatively reproducing what was found experimentally and allowing predictions of coexistence to be made that remain elusive to prove analytically.

6.5 Chapter 5

In Chapter 5 we studied growth rates that are limited by multiple substrates. In particular, we focused on the situation where there are two substrates, both of which are required in the reaction pathway that produces ATP. We considered some of the many possible variations of the analogy between microbes and enzymes for two rate-limiting substrates in search of an extension to the Modified Haldane rate that makes sense biologically and is mathematically tractable. In

particular, we investigated four different mechanisms for how two substrates could complex with enzymes. These mechanisms are: the "Black Box" Mechanism; the Ordered Ternary Mechanism; the Random Ternary Mechanism; and the "Confluence" Mechanism.

The "Black Box" Mechanism involves both substrates combining with the enzyme to give a ternary complex in a single step. We derive a rate from this mechanism which is a simple extension to the Modified Haldane rate (described in detail in Chapter 2), with the substrate concentration in the Modified Haldane rate replaced by the product of the two substrate concentrations in the rate from the Black Box Mechanism.

The Ordered Ternary Mechanism involves one substrate forming a complex with the enzyme, which the other substrate then reacts with to form a ternary complex. The rate that we derive from this mechanism can be considered a generalisation of the Jin and Bethke rate to two substrates, and ordered nature of requiring one substrate before the other means the equation for the rate is not symmetrical with respect to the two substrates.

The Random Ternary Mechanism has two pathways to form the ternary complex, each with the form of the Ordered Ternary Mechanism, which avoids the problem of reaction order by allowing either reaction occur first. The extension of the quasi-steady-state assumption for this case is not obvious. We had to make assumptions while balancing detail and flexibility against a tractable model. We derived a rate that can be considered a generalisation of the Modified Haldane rate to two substrates. A prominent rate in the literature for two substrate limited growth is the Double Monod rate. This rate is an obvious generalisation of the Monod rate, but it is empirical and lacks theoretical support. We showed that this rate can be derived from our generalised Haldane rate through choices of constants. In short, the Double Monod rate is a special case.

The "Confluence" Mechanism involves the two substrates separately reacting with enzymes to form two binary complexes which then react with each other to produce a complex which includes both enzymes and both substrates. Again, the choice of the quasi-steady-state assumption is critical in allowing mathematical tractability without losing too much biological information. The system was solved, resulting in equations for the concentrations of substrates and product that were novel and irreconcilably different than any of the other rates due to the presence of a

term cubic in product concentration. The equations contained many constants that would need to be determined in order for the model to be used and it remains to be seen whether they can be effectively applied to a microbial system.

The statistical mechanics approach of Desmond-Le Quéméner and Bouchez [39] is fundamentally different from the enzyme kinetic analogy models. The assumption of statistical independence allows a much simpler extension to multiple rate-limiting substrates where the rate is the product of single substrate rates for each included substrate. Through some assumptions for the substrates we were able to show the Double DLQB rate agrees with the Double Monod rate for large substrate concentrations. The simplicity of this approach is promising and signals that more work should be done to further develop, refine, and validate this model.

6.6 Future Work

Our work suggests a number of paths for future work. These include:

1. The model developed in Chapter 3 involved the introduction of a "penalty function", allowing the model to optimise the rate by selecting a value of ΔG_{ATP} within a given range. This function was modelled based on the need for two thermodynamic brakes on growth, *viz.*, (1.) the product and substrate concentrations preclude further reaction and (2.) ΔG_{ATP} drops below the minimum threshold so that ATP formation stops. There are two avenues we identified that warrant further study:

   (a) The penalty function was simply incorporated into the rate as a coefficient. Although this approach produces satisfactory results, it lacks a more rigorous foundation. Future work would include a more in depth study of this approach or a more rigorous derivation.

   (b) Our dataset indicates that ΔG_{ATP} is maximum when K_{app} occurs. It may be possible to prove this analytically for a large class of microbes.

2. Multiple Substrate Limiting Rates.

   The complexity of models based on analogies with enzyme kinetics escalates rapidly once

two substrates are limiting the growth rate. There are a prodigious number of permutations for reactions. The choice certainly requires deeper knowledge of the reaction, which in turn means we must know a lot more about the biology. We looked at the simplest scenarios and even here were confronted with difficulties, for example, with analogues for the quasi-steady-state assumptions. This situations signals that a lot of groundwork is still needed for these models. It is recognised that different microbes might have different orders of reaction and kinetics. Indeed, the simple analogue of a microbe as an enzyme needs to be reconsidered once multiple limiting substrates are introduced. It should be kept in mind that any useful model must be mathematically tractable and contain a minimum number of species specific biological parameters.

3. The DLQB Model

   As noted, this model is very different from the models derived from analogy to enzyme kinetics. This model does have thermodynamic inhibition built-in, though it was not exploited in the literature. This model also shows perhaps the simplest way forward towards a model for several substrates limiting the growth rate. Some future work includes:

   (a) A detailed extension of this model to include thermodynamic terms similar to those found in the Lynch model.

   (b) Validation of the model using the existing dataset.

   (c) Extension of this model for multiple limiting substrates. This entails, at the simplest level, a product of Boltzmann distributions, but the interpretation needs further work.

Appendix A

Limits of ΔG_{ATP}

This section states and justifies the values of $\Delta G_{\mathrm{ATPmin}}$ and $\Delta G_{\mathrm{ATPmax}}$.

The rate of ATP synthesis by a membrane-bound ATP synthase depends on Δp, the proton motive force across the cell membrane. The ATP synthase generates ATP from ADP, and we assume that the ΔG for ATP synthesis, ΔG_{ATP}, is similar for other intracellular mechanisms of ATP formation because they all access the same intracellular pools of ATP and ADP. ATP synthesis by the ATP synthase stops at a critical minimum Δp, at which the driving force provided by Δp is no longer able to turn the molecular rotor that catalyses ATP production [121]. Similarly, we assume there is a maximum rate of synthesis, limited by the maximum catalytic rate of the ATP synthase enzyme, as demonstrated experimentally for a number of different ATP synthases [41].

Miller *et al.* [121] suggest a minimum Δp of 170 mV for the ATP synthase of the bacterium *Escherichia coli*, similar to values reported by Nicholls [134] for the mitochondrial ATP synthase. Using a conversion of $10.35\,\mathrm{mV\,kJ^{-1}}$ for H^+ translocation to generate the Δp [63] [135] [64], the minimum ΔG for H^+ translocation is $16.4\,\mathrm{kJ\,mol^{-1}}$. The ATP synthases of *E. coli* and mitochondria have 10 c-ring subunits, requiring $10\,H^+$ to turn the ring and rotor once and so generate three ATP [117]. At this minimum Δp, where ATP synthesis comes to a halt [121], ΔG_{ATP} is therefore $54.7\,\mathrm{kJ\,mol^{-1}}$. We will therefore assume a minimum $\Delta G_{\mathrm{ATP}} = 55\,\mathrm{kJ\,mol_{ATP}^{-1}}$, below which ATP synthesis is not possible.

Nicholls [134] suggests the maximum rate of ATP synthesis in mitochondria occurs when Δp

is 230 mV. Applying the same calculations as we used for the minimum ΔG_{ATP}, this yields a maximum ΔG_{ATP} of 74 kJ mol^{-1}. Even if more free energy is available, the rate of ATP synthesis by the ATP synthase cannot increase further. We will use a maximum $\Delta G_{\mathrm{ATP}} = 75\,\mathrm{kJ\,mol^{-1}_{ATP}}$. We will also assume that these maximum and minimum values also apply to Na^+ gradients.

Appendix B

ATP Yields

This appendix states and justifies the ATP yield for the microbes in the collated dataset based on the reaction they are using for growth.

B.1 ATP Yields used for the Dataset in Chapter 3

M001: *Acetobacterium carbinolicum*, 0.55 ATP per ethanol.

Ethanol + $CO_2 \rightarrow 1.5\,\text{acetate}^- + 1.5H^+$

Acetobacterium carbinolicum forms 0.55 ATP per ethanol [15], based on 10 $\{H^+/Na^+\}$ used to form 3 ATP by the ATP synthase [49] [112]. The growth yields are 4.5 to 5.9 g per mol ethanol [44] [170], which is consistent with an ATP yield of 0.43 to 0.56 per ethanol, assuming a yield of 10.5 g cell dry matter per mol ATP for anaerobes growing using acetate for biomass synthesis [168].

M002: *Acetobacterium* spp., *Sporomusa termitida*, *Acetitomaculum ruminis*, 0.075 ATP per H_2.

$H_2 + 0.5\,CO_2 \rightarrow 0.25\,\text{acetate}^- + 0.5\,H_2O + 0.25\,H^+$

These homoacetogens are assumed to translocate one $\{H^+/Na^+\}$ per acetate formed [145] [26], and use 10 $\{H^+/Na^+\}$ per 3 ATP formed by the ATP synthase [49] [112]. This yields 0.075 ATP per H_2.

M003: *Anaeromusa acidaminophila*, 0.848 ATP per glutamate$^-$.

$\text{Glutamate}^- + 1.333\,H_2O \rightarrow 1.666\,\text{acetate}^- + 0.333\,\text{propionate}^- + 0.666\,CO_2 + NH_4^+$

Anaeromusa acidaminophila forms 0.848 ATP per glutamate, based on net 2 ATP per 3 glutamate by substrate-level phosphorylation [131], and 2 $\{H^+/Na^+\}$ exported at the fumarate reduction step [65] per 3 glutamate, and assuming 11 $\{H^+/Na^+\}$ are used per 3 ATP formed by the ATP synthase like that found in *Clostridium paradoxum* [118].

M004: *Clostridium* sp. strain DKglu26, 0.95 ATP per glutamate^-.

$\text{Glutamate}^- + 1.2\,H_2O + 0.4\,H^+ \rightarrow 1.2\,\text{acetate}^- + 0.4\,\text{butyrate}^- + NH_4^+ + CO_2 + 0.2\,H_2$

Clostridium sp. strain DKglu26 forms 0.95 ATP per glutamate based on the scheme presented by Buckel and Thauer [26] for *Clostridium tetanomorphum*, which assumes 12 $\{H^+/Na^+\}$ are used to form 3 ATP at the ATP synthase. Nanninga et al. [132] classify strain DKglu26 as a member of *Clostridium cochlearium*. *C. tetanomorphum* and *C. cochlearium* are closely related [33].

M005: *Desulfobacter postgatei*, *Desulforhabdus amnigenus*, *Desulfobacca acetoxidans*, 0.5 ATP per acetate.

$\text{Acetate}^- + SO_4^{2-} + 2\,H^+ \rightarrow 2\,CO_2 + HS^- + H_2O$

This calculation assumes the metabolism postulated by Orellana [136], with one $\{H^+/Na^+\}$ used for acetate transport, 2 $\{H^+/Na^+\}$ used for SO_4^{2-} transport, 2 $\{H^+/Na^+\}$ used to drive succinate oxidation, and 10 $\{H^+/Na^+\}$ exported during sulfate reduction. Two ATP are used for SO_4^{2-} activation [100]. Acetate is oxidised via a citric acid cycle [19], with 1 ATP formed by ATP-citrate lyase from acetyl-CoA and oxaloacetate [123]. Assuming 10 $\{H^+/Na^+\}$ per 3 ATP via ATP synthase for a proteobacterium [78], this yields 0.5 ATP per acetate. *Pelobacter* spp., which are also Deltaproteobacteria, are suggested to use 10 $\{H^+/Na^+\}$ per 3 ATP [3].

M006: *Desulfobulbus propionicus*, 0.55 ATP per ethanol.

$\text{Ethanol} + 0.5\,SO_4^{2-} \rightarrow \text{acetate}^- + 0.5\,HS^- + H_2O + 0.5\,H^+$

Szewzyk and Pfennig [170] reported a growth yield of about 5.2 g per mol ethanol, or about 0.52 ATP per ethanol, assuming a yield of 10 g cell dry matter per mol ATP for anaerobes growing using acetate for biomass synthesis [168]. Szewzyk [169] calculated a maximum yield of 5.5 g per mol ethanol, or about 0.55 ATP per ethanol.

M008: *Desulfovibrio* spp., *Desulfomicrobium hypogeium*, 0.25 ATP per H_2.

$H_2 + 0.25\,SO_4^{2-} \rightarrow 0.25\,HS^- + H_2O$

It is assumed that acetate is taken up for biomass formation, since it was added to the growth medium in the studies used in this analysis. Badziong and Thauer [8] and Nethe-Jaenchen and Thauer [133] reported maximum growth yields of about 3.1 g per mol H_2. This suggests an ATP yield of 0.3 mol per mol H_2, assuming a yield of 10 g cell dry matter per mol ATP for anaerobes growing using acetate for biomass synthesis [168]. Badziong and Thauer suggest about 0.25 to 0.275 ATP per H_2.

M009: *Desulfovibrio vulgaris*, 0.3 ATP per ethanol.

$Ethanol + 0.5\,SO_4^{2-} \rightarrow acetate^- + 0.5\,HS^- + H_2O + 0.5H^+$

The growth yield was 1.5 g cell carbon per mol of ethanol [96], which is approximately 3.0 g cell dry mass per mol of ethanol, assuming that approximately 47.5% of dry mass is carbon [20]. Assuming a yield of 10 g cell dry matter per mol ATP for anaerobes growing using acetate for biomass synthesis [168], this is approximately 0.3 ATP per mol ethanol. Szewzyk and Pfennig [170] report yields for different *Desulfovibrio* spp. of 2.4 to 3.6 g per mol ethanol. Szewzyk [169] calculated a maximum yield of 3.2 g per mol ethanol.

M010: *Eubacterium limosum*, 0.1875 ATP per H_2.

$H_2 + 0.5\,CO_2 \rightarrow 0.25\,acetate^- + 0.5\,H_2O + 0.25\,H^+$

Eubacterium limosum translocates 3 $\{H^+/Na^+\}$ per acetate formed and 12 $\{H^+/Na^+\}$ are used by the ATP synthase to form 3 ATP [74]. This yields 0.75 ATP per acetate, or 0.1875 ATP per H_2. Jeong et al. also present metabolic schemes that would yield 0.25 or 0.50 ATP per acetate, i.e., 0.0625 and 0.125 ATP per H_2, respectively. Sharak Genthner and Bryant [162] reported a growth yield for *Eubacterium limosum* of 0.84 g DW per mol H_2. This suggests an ATP yield of 0.08 mol per mol H_2, assuming a yield of 10 g cell dry matter per mol ATP for anaerobes growing using acetate for biomass synthesis [168]. However, Lynd et al. [109] reported a growth yield of 1.7 g per mol H_2 for *Butyribacterium methylotrophicum*, which suggests 0.17 ATP per mol H_2. The genomes of *B. methylotrophicum* and *E. limosum* harbour very similar genes [11], suggesting that data from *B. methylotrophicum* can be used for *E. limosum*. Therefore, the largest of the three values suggested by Jeong et al. [74] is used here.

M011: *Geobacter sulfurreducens*, 3.6 ATP per acetate.

$Acetate^- + 4\,Hfumarate^- + 2\,H_2O + H^+ \rightarrow 2\,CO_2 + 4\,Hsuccinate^-$

Geobacter sulfurreducens grows by coupling the oxidation of acetate with the reduction of four fumarate to four succinate [51] [45]. The oxidation of the acetate plus one fumarate to form one succinate and two carbon dioxide is proposed to generate three reduced electron carriers via a partial citric acid cycle (NADH, NADPH, and a reduced ferredoxin [51]). If we assume CoA transfer, from the succinyl-CoA formed in that reaction, is used to activate the acetate to acetyl-CoA, this part of the reaction is ATP neutral, as suggested by Galushko and Shink [51]. The three reduced carriers are then re-oxidised by coupling to the reduction of three further fumarate molecules, yielding three more succinate molecules. This part of the metabolism is then able to pump 12 protons out of the cell, four for each succinate reduction [51], generating a proton motive force. The closely-related *Pelobacter* spp. are suggested to use the proton motive force by coupling the re-entry of 10 protons to turn the ATP synthase once and so generate 3 ATP [3]. The 12 protons thus generate 3.6 ATP for every acetate plus four fumarate metabolised.

M012: *Methanobacterium* spp., *Methanobrevibacter* spp., *Methanococcus* spp., *Methanogenium* spp., *Methanospirillum* spp., 0.15 ATP per H_2.

$H_2 + 0.25\,CO_2 \rightarrow 0.25\,CH_4 + 0.5\,H_2O$

2 $\{H^+/Na^+\}$ exported per CH_4 formed and Ehb/Ehb have anabolic roles [86]. We assume that 10 $\{H^+/Na^+\}$ are imported to rotate c-ring once to generate 3 ATP. This would result in an ATP yield of 0.15 per H_2.

M013: *Methanosaeta* spp., 0.333 ATP per acetate.

$Acetate^- + H^+ \rightarrow CH_4 + CO_2$

7 $\{H^+/Na^+\}$ are exported per acetate metabolised [182]. We assume that 9 $\{H^+/Na^+\}$ are imported to rotate c-ring once to generate 3 ATP and that 2 ATP are used for acetate activation [76] [75]. This gives net 0.333 ATP per acetate.

M014: *Methanosarcina* spp., 0.25 ATP per H_2.

$H_2 + 0.25\,CO_2 \rightarrow 0.25\,CH_4 + 0.5\,H_2O$

Methanosarcina spp. translocate 4 $\{H^+/Na^+\}$ per CH_4 formed [173]. Assuming 12 $\{H^+/Na^+\}$ are used to generate per 3 ATP by the ATP synthase [113], this yields 0.25 ATP per H_2.

M015: *Methanosarcina* spp., 0.5 ATP per acetate.

$Acetate^- + H^+ \rightarrow CH_4 + CO_2$

Welte and Deppenmeier [182] suggest 7 $\{H^+/Na^+\}$ are translocated per acetate, with one $\{H^+/Na^+\}$ used for acetate transport [181]. Twelve $\{H^+/Na^+\}$ are used to generate per 3 ATP by the ATP synthase [113]. One ATP is used for acetate activation [1]. The ATP yield is therefore 0.5 ATP per acetate.

M016: *Methanothermobacter* spp., 0.125 ATP per H_2.

$H_2 + 0.25\ CO_2 \rightarrow 0.25\ CH_4 + 0.5\ H_2O$

2 $\{H^+/Na^+\}$ exported per CH_4 formed, with Ehb and Ehb having anabolic roles [86]. 12 $\{H^+/Na^+\}$ are used to generate 3 ATP via ATP synthase [113]. This is an ATP yield of 0.125 per H_2.

M017: *Pelobacter propionicus*, 0.333 ATP per ethanol.

$Ethanol + 0.666\ CO_2 \rightarrow 0.333\ acetate^- + 0.666\ propionate^- + 0.333\ H_2O + H^+$

Schink et al. [153] suggest that ATP is only formed coupled to acetate formation via substrate level phosphorylation at acetate kinase, and not to propionate formation, i.e., expect 0.333 mol ATP per ethanol.

M018: *Propionibacterium freudenreichii*, 0.666 ATP per lactate.

$Lactate^- \rightarrow 0.333\ acetate^- + 0.666\ propionate^- + CO_2 + H_2O$

Forms one ATP at acetate kinase [57], i.e., 0.333 per lactate. Exports 2 $\{H^+/Na^+\}$ at fumarate reduction step during propionate formation [65], i.e., 1.333 per lactate. Assuming 12 $\{H^+/Na^+\}$ per 3 ATP via ATP synthase, this step yields 0.333 ATP per lactate. Net therefore of 0.666 ATP per lactate.

M019: *Veillonella parvula*, 0.633 ATP per lactate.

$Lactate^- \rightarrow 0.333\ acetate^- + 0.666\ propionate^- + CO_2 + H_2O$

Forms one ATP at acetate kinase [57], i.e., 0.333 per lactate. Exports 2 $\{H^+/Na^+\}$ at fumarate reduction step during propionate formation [65], i.e., 1.333 H+/Na+ per lactate. Exports 1 $\{H^+/Na^+\}$ at methylmalonyl-CoA decarboxylase step during propionate formation [66], i.e., 0.666 $\{H^+/Na^+\}$ per lactate. Assume one $\{H^+/Na^+\}$ for lactate uptake. Assuming 10 $\{H^+/Na^+\}$ per 3 ATP via ATP synthase, this yields 0.3 ATP per lactate. Net therefore 0.633 ATP per lactate.

M020: *Clostridium homopropionicum*, 0.44 ATP per lactate.

$\text{Lactate}^- \rightarrow 0.333\,\text{acetate}^- + 0.666\,\text{propionate}^- + CO_2 + H_2O$

Growth yield is 4.35 g per mol lactate [42]. This would be consistent with a yield of up to about 0.44 ATP per lactate, assuming a yield of 10 g cell dry matter per mol ATP for anaerobes growing using lactate for biomass synthesis [168].

B.2 Argument for $\eta = 3.3\,\text{mol}_{\text{ATP}}\,\text{mol}^{-1}_{\text{substrate}}$ for *Geobacter sulfurreducens*

Geobacter sulfurreducens grows by coupling the oxidation of acetate with the reduction of four fumarate to four succinate [51] [45]. The oxidation of the acetate plus one fumarate to form one succinate and two carbon dioxide is proposed to generate three reduced electron carriers via a partial citric acid cycle (NADH, NADPH, and a reduced ferredoxin [51]). If we assume CoA transfer, from the succinyl-CoA formed in that reaction, is used to activate the acetate to acetyl-CoA, this part of the reaction is ATP neutral, as suggested by Galushko and Shink [51]. The three reduced carriers are then re-oxidised by coupling to the reduction of three further fumarate molecules, yielding three more succinate molecules. This part of the metabolism is then able to pump 12 protons out of the cell, four for each succinate reduction [51], generating a proton motive force. The closely-related *Pelobacter* spp. are suggested to use the proton motive force by coupling the re-entry of 10 protons to turn the ATP synthase once and so generate 3 ATP [3]. The 12 protons thus generate 3.6 ATP for every acetate plus four fumarate metabolised. However, this does not consider the total metabolism. The cell needs to transport the fumarate into the cell, and this could be accomplished by harnessing fumarate import to the export of the resulting succinate using a membrane-bound antiporter. Succinate and fumarate are transported out of and into the cell, respectively, by an antiport system [28] [72]. The acetate also needs to be transported into the cell. If this is catalysed by a symporter that is driven by the co-transport of one proton, then only 11 protons remain to generate ATP via the ATP synthase, yielding 3.3 ATP per reaction instead of 3.6.

B.3 ATP Yields for the Reactions in Chapter 4

The ATP yield was estimated to be 0.3 per mole of malonate. We assume that malonate decarboxylation to acetate results in the translocation of one sodium ion or one proton for each decarboxylation [40]. These three strains are enterobacteria, which are known to use the sodium or proton motive force by coupling the re-entry of 10 ions to turn the ATP synthase once to generate 3 ATP [117]. So, one decarboxylation yields 0.3 ATP.

The ATP yield was estimated to be 0.5 per mole of crotonate. This was based on the fermentation balances for strain DM-3 reported by Wallrabenstein and Schink [177] and the enzymes reported for crotonate fermentation to the same product spectrum by *Syntrophomonas wolfei* [115] [177]. Two crotonate are first activated to two crotonyl-CoA. One mol of crotonyl-CoA is oxidised to two acetyl-CoA, and the second crotonyl-CoA is reduced to butyryl-CoA to use the electrons arising from the oxidation of the first crotonyl-CoA. The three CoA-linked acids can then form three ATP via substrate-level phosphorylation, two of which are reinvested for further crotonate activation, or two of the CoA-linked acids can directly transfer CoA to two further crotonate, leaving one to form ATP via substrate-level phosphorylation. In both schemes, there is net formation of one ATP for every two crotonate metabolised and so 0.5 ATP per crotonate.

Appendix C

Additions for Chapter 4

C.1 Malonate and Crotonate Data

This section states the data shown in Figures 1(a), 1(b), and 1(c) of Janssen [73] and estimates the data shown in Figure 1 of Wallrabenstein and Schink [177].

Table C.1: Data for the dataset shown in Figure 1(a) of Janssen [73].

Time	Biomass	Malonate	Acetate	Carbon dioxide
Hours	OD_{660}	mol L^{-1}	mol L^{-1}	mol L^{-1}
0	0.17	0.06888	0.0011	0.003696
5.75	0.1933	0.0698	0.00247	0.003591
6.75	0.21	0.06149	0.0077	0.004909
9.75	0.30444	0.04527	0.01734	0.007518
12.58	0.35	0.040	0.02881	0.00839
15.25	0.36	0.03096	0.03751	0.009848
20.00	0.40556	0.0171	0.04098	0.012082
24.75	0.40	0.01412	0.04556	0.01258
33.25	0.42	0.00789	0.05924	0.013621
49.17	0.42	0.00224	0.05717	0.014571

C.2 Initial Conditions for Malonate

The concentrations of acetate and dissolved carbon dioxide have the following origins.

The concentrations of acetate and malonate were provided by Peter Janssen from laboratory

Table C.2: Data for the dataset shown in Figure 1(b) of Janssen [73].

Time	Biomass	Malonate	Acetate	Carbon dioxide
Hours	OD_{660}	mol L^{-1}	mol L^{-1}	mol L^{-1}
0	0.2200	0.07426	0.00148	0.003696
5.75	0.2600	0.06004	0.01005	0.005966
6.75	0.28667	0.04545	0.02321	0.008279
9.75	0.37333	0.03320	0.03466	0.010285
12.58	0.4100	0.02358	0.03763	0.011861
15.25	0.43667	0.01913	0.04891	0.012594
20.00	0.5000	0.01076	0.04779	0.013955
24.75	0.50667	0.00925	0.05758	0.014222
33.25	0.51667	0.00545	0.06145	0.014878
49.17	0.51333	0.00358	0.06055	0.015222

Table C.3: Data for the dataset shown in Figure 1(c) of Janssen [73].

Time	Biomass	Malonate	Acetate	Carbon dioxide
Hours	OD_{660}	mol L^{-1}	mol L^{-1}	mol L^{-1}
0	0.2500	0.07920	0.00132	0.003696
5.75	0.2400	0.06662	0.00255	0.005708
6.75	0.25667	0.05978	0.00765	0.006801
9.75	0.33667	0.05189	0.01754	0.008105
12.58	0.3800	0.04086	0.02378	0.009896
15.25	0.37333	0.03754	0.02695	0.010445
20.00	0.3800	0.03504	0.03380	0.010864
24.75	0.3800	0.03052	0.03268	0.011607
33.25	0.3800	0.02783	0.03991	0.012076
49.17	0.40667	0.02052	0.03873	0.013289

notes made when conducting the experiments reported by Janssen [73]. The total dissolved carbon dioxide concentration was calculated as described by Blanch and Clark [18] from the amounts of $NaHCO_3$ added to the growth medium, the pH, and CO_2 production assumed to be one CO_2 per malonate degraded. The dissolved CO_2 concentration was calculated from the partial pressure of gaseous CO_2 using Henry's law and a temperature-corrected Henry's law constant for 34°C calculated from data tabulated by Sander [149], with values for further temperature corrections reported by Harned and Scholes [62] and Harned and Davis [61].

Table C.4: Data for the dataset shown in Figure 1 of Wallrabenstein and Schink [177].

Time	Biomass	Crotonate	Butyrate	Acetate
Days	OD_{578}	$mol\,L^{-1}$	$mol\,L^{-1}$	$mol\,L^{-1}$
0	0.036	0.00935	0.00005	0.0005
2	0.036	0.0092	0.00015	0.0006
6	0.062	0.0081	0.0006	0.0019
8	0.105	0.0066	0.00085	0.0033
9	0.142	0.0057	0.0015	0.0043
10	0.169	0.0041	0.002	0.00585
12	0.208	0.0025	0.00265	0.0073
13	0.220	0.0016	0.00285	0.0078
14	0.228	0.0012	0.003	0.0082
15	0.227	0.0007	0.00285	0.0084
16	0.225	0.0005	0.00285	0.0085

C.3 ΔH_f^o and S_f^o for Crotonate

Standard enthalpies and entropies of formation for straight-chain organic compounds of 1 to 8 carbons were extracted from the literature and plotted to show that these varied linearly by chain length with very similar intervals due to the introduction of a double bond. From this, a set of differences were calculated. The standard enthalpy of formation was 133.669 to 137.232 $kJ\,mol^{-1}$ more positive for the introduction of a double bond into a four-carbon chain, while the standard entropy of formation was 0.4168 to 14.2232 $J\,mol^{-1}\,K^{-1}$ for positive. The corrections were applied to the data for butyrate (four carbons, no double bonds) to calculate data for crotonate (four carbons, one double bond). The data sources used are listed in Table C.5.

Table C.5: Data used to estimate standard enthalpy and entropy of formation for crotonate

n-monocarboxylate anions (aq)	Shock and Helgeson [164]
n-monocarboxylic acids (aq)	Shock and Helgeson [164]
n-alkanes (aq)	Shock and Helgeson [164]
n-alkenes (aq)	Shock and Helgeson [164]
n-dicarboxylate mono-anions (aq)	Shock [163]
n-dicarboxylic acids (aq)	Shock [163]
fumaric acid (aq)	Chang [29]
fumarate mono-anion (aq)	Chang [29]

Appendix D

Dataset Conditions and Assumptions

This appendix lists the strains of microbe in the dataset used in Chapter 3 and states the conditions and assumptions for the dataset.

D.1 Microbes in the Dataset

Each entry lists the microbial species, the strain (if known), the code for the metabolism (see Appendix B.1), the code for the conditions, and whether the $S_{\min}$ or K_S was reported. The reference for the conditions is given in Appendix D.2.

1. *Acetitomaculum ruminis* 139B, M010, C069, $S_{\min}$.
2. *Acetitomaculum ruminis* 190A4, M010, C069, $S_{\min}$.
3. *Acetobacterium bakii* Z-4391, M002, C022, K_S.
4. *Acetobacterium carbinolicum* HP4, M002, C026, $S_{\min}$.
5. *Acetobacterium carbinolicum* HP4, M002, C026, $S_{\min}$.
6. *Acetobacterium carbinolicum* HP4, M002, C026, $S_{\min}$.
7. *Acetobacterium carbinolicum* HP4, M002, C026, $S_{\min}$.
8. *Acetobacterium carbinolicum* HP4, M002, C026, $S_{\min}$.

9. *Acetobacterium carbinolicum* W0Prop1, M002, C064, $S_{\min}$.
10. *Acetobacterium carbinolicum* WoProp1, M001, C001, K_{S}.
11. *Acetobacterium psammolithicum* CN-E, M002, C040, $S_{\min}$.
12. *Acetobacterium woodii* strain not specified, M002, C051, $S_{\min}$.
13. *Acetobacterium woodii* NZva16, M002, C072, $S_{\min}$.
14. *Acetobacterium woodii* NZva16, M002, C072, $S_{\min}$.
15. *Acetobacterium woodii* NZva16, M002, C072, $S_{\min}$.
16. *Acetobacterium woodii* NZva16, M002, C064, $S_{\min}$.
17. *Acetobacterium woodii* WB1, M002, C042, $S_{\min}$.
18. *Acetobacterium woodii* WB1, M002, C003, K_{S}.
19. *Anaeromusa acidaminophila* DKglu16, M003, C009, K_{S}.
20. *Clostridium homopropionicum* LuHBu1, M020, C073, K_{S}.
21. *Clostridium* sp. DKglu26, M004, C010, K_{S}.
22. *Desulfobacca acetoxidans* ASRB2, M005, C068, K_{S}.
23. *Desulfobacter postgatei* 2ac9, M005, C004, K_{S}.
24. *Desulfobacter postgatei* 2ac9, M005, C005, K_{S}.
25. *Desulfobulbus propionicus* Lindhorst, M006, C059, K_{S}.
26. *Desulfomicrobium hypogeium* CN-A, M008, C041, $S_{\min}$.
27. *Desulforhabdus amnigenus* ASRB1, M005, C068, K_{S}.
28. *Desulfovibrio desulfuricans* Essex 6, M008, C065, $S_{\min}$.
29. *Desulfovibrio desulfuricans* strain not specified, M008, C052, K_{S}.

30. *Desulfovibrio* sp. DG2, M008, C052, K_S.

31. *Desulfovibrio* sp. DG2, M008, C019, K_S.

32. *Desulfovibrio* sp. G-11, M008, C052, K_S.

33. *Desulfovibrio* sp. G-11, M008, C019, K_S.

34. *Desulfovibrio* sp. PS1, M008, C052, K_S.

35. *Desulfovibrio vulgaris* Madison, M008, C049, S_{min}.

36. *Desulfovibrio vulgaris* Madison, M008, C050, S_{min}.

37. *Desulfovibrio vulgaris* Madison, M008, C047, S_{min}.

38. *Desulfovibrio vulgaris* Madison, M008, C048, S_{min}.

39. *Desulfovibrio vulgaris* Marburg, M008, C039, K_S.

40. *Desulfovibrio vulgaris* Marburg, M009, C002, K_S.

41. *Desulfovibrio vulgaris* strain not specified, M008, C052, K_S.

42. *Eubacterium limosum* SA11, M010, C020, S_{min}.

43. *Geobacter sulfurreducens* PCA, M011, C029, K_S.

44. *Methanobacterium bryantii* Bab1, M012, C027, S_{min}.

45. *Methanobacterium bryantii* Bab1, M012, C027, S_{min}.

46. *Methanobacterium bryantii* Bab1, M012, C027, S_{min}.

47. *Methanobacterium bryantii* M.o.H, M012, C016, S_{min}.

48. *Methanobacterium formicicum* BRM9, M012, C063, S_{min}.

49. *Methanobacterium formicicum* JF-1, M012, C015, S_{min}.

50. *Methanobacterium formicicum* MF, M012, C066, S_{min}.

51. *Methanobacterium formicicum* strain not specified, M012, C035, $S_{\min}$.

52. *Methanobacterium* sp. YCM1, M012, C063, $S_{\min}$.

53. *Methanobrevibacter arboriphilus* AZ, M012, C066, $S_{\min}$.

54. *Methanobrevibacter arboriphilus* AZ, M012, C013, $S_{\min}$.

55. *Methanobrevibacter arboriphilus* AZ, M012, C038, K_{S}.

56. *Methanobrevibacter arboriphilus* DH1, M012, C034, K_{S}.

57. *Methanobrevibacter ruminantium* M1, M012, C063, $S_{\min}$.

58. *Methanobrevibacter smithii* PS, M012, C066, $S_{\min}$.

59. *Methanobrevibacter smithii* PS, M012, C046, K_{S}.

60. *Methanobrevibacter* sp. 10-16B, M012, C044, $S_{\min}$.

61. *Methanobrevibacter* sp. 10-18B, M012, C018, $S_{\min}$.

62. *Methanobrevibacter* sp. 229/11, M012, C063, $S_{\min}$.

63. *Methanobrevibacter* sp. AbM4, M012, C063, $S_{\min}$.

64. *Methanobrevibacter* sp. D5, M012, C063, $S_{\min}$.

65. *Methanobrevibacter* sp. RMB-1, M012, C018, $S_{\min}$.

66. *Methanobrevibacter* sp. RMB-2, M012, C018, $S_{\min}$.

67. *Methanobrevibacter* sp. RMB-3, M012, C018, $S_{\min}$.

68. *Methanobrevibacter* sp. RMB-4, M012, C018, $S_{\min}$.

69. *Methanobrevibacter* sp. SM9, M012, C063, $S_{\min}$.

70. *Methanococcus maripaludis* strain not specified, M012, C036, $S_{\min}$.

71. *Methanococcus vannielii* SB, M012, C066, $S_{\min}$.

72. *Methanogenium frigidum* Ace-2, M012, C067, $S_{\min}$.

73. *Methanosaeta soehngenii* Opfikon, M013, C032, $S_{\min}$.

74. *Methanosaeta* sp. CALS-1, M013, C024, $S_{\min}$.

75. *Methanosaeta* sp. Los Angeles River, M013, C062, $S_{\min}$.

76. *Methanosaeta* sp. VeAc9, M013, C031, $S_{\min}$.

77. *Methanosarcina barkeri* 227, M015, C060, $S_{\min}$.

78. *Methanosarcina barkeri* Fusaro, M015, C070, K_{S}.

79. *Methanosarcina barkeri* Fusaro, M015, C030, $S_{\min}$.

80. *Methanosarcina barkeri* Fusaro, M015, C033, $S_{\min}$.

81. *Methanosarcina barkeri* Fusaro, M014, C008, $S_{\min}$.

82. *Methanosarcina barkeri* Fusaro, M015, C054, K_{S}.

83. *Methanosarcina barkeri* MS, M015, C031, $S_{\min}$.

84. *Methanosarcina barkeri* MS, M014, C007, K_{S}.

85. *Methanosarcina barkeri* strain not specified, M014, C035, $S_{\min}$.

86. *Methanosarcina mazei* S-6, M015, C061, $S_{\min}$.

87. *Methanosarcina* sp. CALS-1, M015, C023, $S_{\min}$.

88. *Methanosarcina* sp. VeA23, M015, C031, $S_{\min}$.

89. *Methanospirillum hungatei* JF-1, M012, C066, $S_{\min}$.

90. *Methanospirillum hungatei* JF-1, M012, C017, $S_{\min}$.

91. *Methanospirillum hungatei* JF-1, M012, C053, K_{S}.

92. *Methanospirillum hungatei* JF-1, M012, C055, $S_{\min}$.

93. *Methanospirillum hungatei* M1h, M012, C021, $S_{\min}$.

94. *Methanospirillum* sp. PM 1, M012, C053, K_{S}.

95. *Methanospirillum* sp. PM 2, M012, C053, K_{S}.

96. *Methanothermobacter marburgensis* Marburg, M016, C028, $S_{\min}$.

97. *Methanothermobacter marburgensis* Marburg, M016, C028, $S_{\min}$.

98. *Methanothermobacter marburgensis* Marburg, M016, C028, $S_{\min}$.

99. *Methanothermobacter marburgensis* Marburg, M016, C028, $S_{\min}$.

100. *Methanothermobacter marburgensis* Marburg, M016, C014, $S_{\min}$.

101. *Methanothermobacter wolfei* strain not specified, M016, C037, $S_{\min}$.

102. *Pelobacter propionicus* KoEtOH1, M017, C012, K_{S}.

103. *Propionibacterium freudenreichii* 53-W, M018, C056, K_{S}.

104. *Sporomusa termitida* JSN-2, M002, C025, K_{S}.

105. *Sporomusa termitida* JSN-2, M002, C064, $S_{\min}$.

106. *Sporomusa termitida* JSN-2, M002, C043, $S_{\min}$.

107. *Veillonella parvula* Te3, M019, C057, K_{S}.

D.2 Conditions and Assumptions

C001: *Acetobacterium carbinolicum* WoProp1

Ethanol + CO_2 $\rightarrow$ 1.5 acetate$^-$ + 1.5 H^+

Data from Szewzyk and Pfennig [170] and Eichler and Schink [44]. K_{S} (ethanol) estimated, from continuous culture, to be 8.5×10^{-3} mol L^{-1}.

$T = 28°C$

pH = 7.1

[ethanol] varied

$[CO_2] = 4.3 \times 10^{-2}\,\mathrm{mol\,L^{-1}}$ (the gas phase contained 20% CO_2)

[acetate] $= 1.7 \times 10^{-2}\,\mathrm{mol\,L^{-1}}$

C002: *Desulfovibrio vulgaris* Marburg

$\mathrm{Ethanol} + 0.5\,SO_4^{2-} \rightarrow \mathrm{acetate^-} + 0.5\,HS^- + H_2O + 0.5\,H^+$

Data from Szewzyk and Pfennig [170]. K_S (ethanol) estimated, from continuous culture, to be $5.8 \times 10^{-6}\,\mathrm{mol\,L^{-1}}$.

$T = 28°C$

pH = 7.1

[ethanol] varied

$[SO_4^{2-}] = 1.0 \times 10^{-2}\,\mathrm{mol\,L^{-1}}$

[acetate] $= 2.0 \times 10^{-7}\,\mathrm{mol\,L^{-1}}$

$[HS^-] = 1.0 \times 10^{-3}\,\mathrm{mol\,L^{-1}}$

C003: *Acetobacterium woodii* WB1

$H_2 + 0.5\,CO_2 \rightarrow 0.25\,\mathrm{acetate^-} + 0.5\,H_2O + 0.25\,H^+$

Data from Peters *et al.* [141]. K_S (H_2) estimated, from continuous culture, to be $7.1 \times 10^{-7}\,\mathrm{mol\,L^{-1}}$.

$T = 30°C$

pH = 7.2

[H_2] varied

$[CO_2] = 5.1 \times 10^{-2}\,\mathrm{mol\,L^{-1}}$ (the gas phase contained 20% CO_2)

[acetate] $= 1.3 \times 10^{-4}\,\mathrm{mol\,L^{-1}}$

C004: *Desulfobacter postgatei* 2ac9

$\mathrm{Acetate^-} + SO_4^{2-} + 2\,H^+ \rightarrow 2\,CO_2 + HS^- + 2\,H_2O$

Data from Ingvorsen *et al.* [71]. K_S (acetate) estimated, by fitting to substrate depletion curve, to be $7.7 \times 10^{-5}\,\mathrm{mol\,L^{-1}}$.

$T = 30°C$

pH = 7.2

[acetate] varied

$[SO_4^{2-}] = 5.0 \times 10^{-2}\,\mathrm{mol\,L^{-1}}$

$[CO_2] = 7.1 \times 10^{-2}\,\mathrm{mol\,L^{-1}}$ (the gas phase contained 20% CO_2 at 1.4 atm)

$[HS^-] = 2.5 \times 10^{-4}\,\mathrm{mol\,L^{-1}}$

C005: *Desulfobacter postgatei* 2ac9

$\mathrm{Acetate^-} + SO_4^{2-} + 2\,H^+ \rightarrow 2\,CO_2 + HS^- + 2\,H_2O$

Data from Schönheit *et al.* [156]. K_S (acetate) estimated, by fitting to substrate depletion curve, to be $2.3 \times 10^{-4}\,\mathrm{mol\,L^{-1}}$.

$T = 30°C$

pH = 6.9

[acetate] varied

$[SO_4^{2-}] = 1.5 \times 10^{-2}\,\mathrm{mol\,L^{-1}}$

$[CO_2] = 2.8 \times 10^{-2}\,\mathrm{mol\,L^{-1}}$ (the gas phase contained 20% CO_2)

$[HS^-] = 4.8 \times 10^{-3}\,\mathrm{mol\,L^{-1}}$

C007: *Methanosarcina barkeri* MS

$H_2 + 0.25\,CO_2 \rightarrow 0.25\,CH_4 + 0.5\,H_2O$

Data from Robinson and Tiedje [147]. K_S (H_2) estimated, by fitting to substrate depletion curve, to be $1.3 \times 10^{-5}\,\mathrm{mol\,L^{-1}}$.

$T = 37°C$

pH = 6.7

[H_2] varied

$[CO_2] = 8.7 \times 10^{-2}\,\mathrm{mol\,L^{-1}}$ (the gas phase contained 100% CO_2)

$[CH_4] = 5.0 \times 10^{-6}\,\mathrm{mol\,L^{-1}}$

C008: *Methanosarcina barkeri* Fusaro

$H_2 + 0.25\,CO_2 \rightarrow 0.25\,CH_4 + 0.5\,H_2O$

Data from Kaster [85]. $S_{\min}$ (H_2) estimated, from substrate depletion curve, to be $1.1 \times 10^{-6}\,\mathrm{mol\,L^{-1}}$.

$T = 37°C$

pH = 7.0

[H_2] varied

$[CO_2] = 3.0 \times 10^{-2}$ mol L^{-1} (the gas phase contained 20% CO_2)

$[CH_4] = 1.3 \times 10^{-6}$ mol L^{-1}

C009: *Anaeromusa acidaminophila* DKglu16

$Glutamate^- + 1.333\ H_2O \rightarrow 1.666\ acetate^- + 0.333\ propionate^- + 0.666\ CO_2 + NH_4^+$

Data from Nanninga *et al.* [132]. K_S (glutamate) estimated, from continuous culture, to be 1.9×10^{-6} mol L^{-1}.

$T = 35°C$

pH = 6.5

[glutamate] varied

$[acetate] = 1.7 \times 10^{-2}$ mol L^{-1}

$[propionate] = 3.3 \times 10^{-3}$ mol L^{-1}

$[CO_2] = 1.3 \times 10^{-2}$ mol L^{-1} (the gas phase contained 20% CO_2)

$[NH_4^+] = 1.0 \times 10^{-2}$ mol L^{-1}

C010: *Clostridium* sp. DKglu26

$Glutamate^- + 1.2\ H_2O + 0.4\ H^+ \rightarrow 1.2\ acetate^- + 0.4\ butyrate^- + NH_4^+ + CO_2 + 0.2\ H_2$

Data from Nanninga *et al.* [132]. K_S estimated, from continuous culture, to be 7.0×10^{-6} mol L^{-1}.

$T = 35°C$

pH = 6.5

[glutamate] varied

$[acetate] = 1.2 \times 10^{-2}$ mol L^{-1}

$[butyrate] = 4.0 \times 10^{-3}$ mol L^{-1}

$[NH_4^+] = 1.0 \times 10^{-2}$ mol L^{-1}

$[CO_2] = 1.3 \times 10^{-2}$ mol L^{-1} (the gas phase contained 20% CO_2)

$[H_2] = 7.5 \times 10^{-4}$ mol L^{-1}

C012: *Pelobacter propionicus* KoEtOH1

$Ethanol + 0.666\ CO_2 \rightarrow 0.333\ acetate^- + 0.666\ propionate^- + 0.333\ H_2O + H^+$

Data from Szewzyk and Pfennig [170]. K_S (ethanol) estimated, from continuous culture, to be 5.5×10^{-5} mol L^{-1}.

$T = 28°C$

pH = 7.1

[ethanol] varied

$[CO_2] = 4.3 \times 10^{-2}$ mol L^{-1} (the gas phase contained 20% CO_2)

[acetate] = 6.6×10^{-3} mol L^{-1}

[propionate] = 1.3×10^{-2} mol L^{-1}

C013: *Methanobrevibacter arboriphilus* AZ

$H_2 + 0.25\ CO_2 \rightarrow 0.25\ CH_4 + 0.5\ H_2O$

Data from Kaster [85]. S_{min} (H_2) estimated, from substrate depletion curve, to be 5.8×10^{-8} mol L^{-1}.

$T = 37°C$

pH = 7.0

[H_2] varied

$[CO_2] = 3.0 \times 10^{-2}$ mol L^{-1} (the gas phase contained 20% CO_2)

$[CH_4] = 1.2 \times 10^{-7}$ mol L^{-1}

C014: *Methanothermobacter marburgensis* Marburg

$H_2 + 0.25\ CO_2 \rightarrow 0.25\ CH_4 + 0.5\ H_2O$

Data from Kaster [85]. S_{min} (H_2) estimated, from substrate depletion curve, to be 5.7×10^{-8} mol L^{-1}.

$T = 60°C$

pH = 7.0

[H_2] varied

$[CO_2] = 1.8 \times 10^{-2}$ mol L^{-1} (the gas phase contained 20% CO_2)

$[CH_4] = 9.2 \times 10^{-8}$ mol L^{-1}

C015: *Methanobacterium formicicum* JF-1

$H_2 + 0.25\ CO_2 \rightarrow 0.25\ CH_4 + 0.5\ H_2O$

Data from Lovley [106]. S_{min} (H_2) estimated, from substrate depletion curve, to be 4.7×10^{-8} mol L^{-1}.

$T = 39°C$

pH = 6.9

$[H_2]$ varied

$[CO_2] = 5.4 \times 10^{-2}\,\mathrm{mol\,L^{-1}}$ (the gas phase contained 20% CO_2, pressurised to 230 kPa)

$[CH_4] = 5.5 \times 10^{-6}\,\mathrm{mol\,L^{-1}}$

C016: *Methanobacterium bryantii* M.o.H

$H_2 + 0.25\,CO_2 \rightarrow 0.25\,CH_4 + 0.5\,H_2O$

Data from Lovley [106]. $S_{\min}$ (H_2) estimated, from substrate depletion curve, to be $5.0 \times 10^{-8}\,\mathrm{mol\,L^{-1}}$.

$T = 39°C$

pH = 6.9

$[H_2]$ varied

$[CO_2] = 5.4 \times 10^{-2}\,\mathrm{mol\,L^{-1}}$ (the gas phase contained 20% CO_2, pressurised to 230 kPa)

$[CH_4] = 5.5 \times 10^{-6}\,\mathrm{mol\,L^{-1}}$

C017: *Methanospirillum hungatei* JF-1

$H_2 + 0.25\,CO_2 \rightarrow 0.25\,CH_4 + 0.5\,H_2O$

Data from Lovley [106]. $S_{\min}$ (H_2) estimated, from substrate depletion curve, to be $6.9 \times 10^{-8}\,\mathrm{mol\,L^{-1}}$.

$T = 39°C$

pH = 6.9

$[H_2]$ varied

$[CO_2] = 5.4 \times 10^{-2}\,\mathrm{mol\,L^{-1}}$ (the gas phase contained 20% CO_2, pressurised to 230 kPa)

$[CH_4] = 5.5 \times 10^{-6}\,\mathrm{mol\,L^{-1}}$

C018: *Methanobrevibacter* spp. 10-18B, RMB-1, RMB-2, RMB-3, and RMB-4

$H_2 + 0.25\,CO_2 \rightarrow 0.25\,CH_4 + 0.5\,H_2O$

Data from Lovley [105]. $S_{\min}$ (H_2) estimated, from substrate depletion curves, to be: $8.7 \times 10^{-8}\,\mathrm{mol\,L^{-1}}$ for strain 10-18B; $5.6 \times 10^{-8}\,\mathrm{mol\,L^{-1}}$ for strain RMB-1; $5.5 \times 10^{-8}\,\mathrm{mol\,L^{-1}}$ for strain RMB-2; $5.9 \times 10^{-8}\,\mathrm{mol\,L^{-1}}$ fpr strain RMB-3; and $7.2 \times 10^{-8}\,\mathrm{mol\,L^{-1}}$ for strain RMB-4.

$T = 39°C$

pH = 6.9

$[H_2]$ varied

$[CO_2] = 5.4 \times 10^{-2}\,\mathrm{mol\,L^{-1}}$ (the gas phase contained 20% CO_2, pressurised to 230 kPa)

$[CH_4] = 1.6 \times 10^{-5}\,\mathrm{mol\,L^{-1}}$

C019: *Desulfovibrio* sp. G-11 and DG2

$H_2 + 0.25\,SO_4^{2-} \rightarrow 0.25\,HS^- + H_2O$

Data from Warikoo *et al.* [180]. K_S (H_2) estimated, by fitting to substrate depletion curves, to be $1.2 \times 10^{-6}\,\mathrm{mol\,L^{-1}}$ for strain G-11 and $1.4 \times 10^{-6}\,\mathrm{mol\,L^{-1}}$ for strain DG2.

$T = 35°C$

pH = 7.0

$[H_2]$ varied

$[SO_4^{2-}] = 2.0 \times 10^{-3}\,\mathrm{mol\,L^{-1}}$

$[HS^-] = 1.6 \times 10^{-5}\,\mathrm{mol\,L^{-1}}$

C020: *Eubacterium limosum* SA11

$H_2 + 0.5\,CO_2 \rightarrow 0.25\,\mathrm{acetate^-} + 0.5\,H_2O + 0.25\,H^+$

Data from Kelly *et al.* [87] and Henderson and Janssen (unpublished). S_{min} (H_2) estimated, from substrate depletion curves, to be $2.2 \times 10^{-6}\,\mathrm{mol\,L^{-1}}$.

$T = 39°C$

pH = 6.5

$[H_2]$ varied

$[CO_2] = 6.2 \times 10^{-2}\,\mathrm{mol\,L^{-1}}$ (the gas phase contained 100% CO_2)

$[\mathrm{acetate}] = 1.2 \times 10^{-3}\,\mathrm{mol\,L^{-1}}$

C021: *Methanospirillum hungatei* M1h

$H_2 + 0.25\,CO_2 \rightarrow 0.25\,CH_4 + 0.5\,H_2O$

Data from Seitz *et al.* [161]. S_{min} (H_2) estimated, from substrate depletion curve, to be $1.9 \times 10^{-8}\,\mathrm{mol\,L^{-1}}$.

$T = 28°C$

pH = 7.1

$[H_2]$ varied

$[CO_2] = 4.3 \times 10^{-2}\,\mathrm{mol\,L^{-1}}$ (the gas phase contained 20% CO_2)

$[CH_4] = 3.2 \times 10^{-5}\,\mathrm{mol\,L^{-1}}$

C022: *Acetobacterium bakii* Z-4391

$H_2 + 0.5\,CO_2 \rightarrow 0.25\,\text{acetate}^- + 0.5\,H_2O + 0.25\,H^+$

Data from Kotsyurbenko *et al.* [90]. K_S (H_2) estimated, by fitting to growth curve, to be 3.7×10^{-6} mol L^{-1}.

$T = 25°C$

pH = 7.0

[H_2] varied

[CO_2] = 2.2×10^{-2} mol L^{-1} (the gas phase contained 12% CO_2)

[acetate] = 1.2×10^{-2} mol L^{-1}

C023: *Methanosarcina* sp. CALS-1

$\text{Acetate}^- + H^+ \rightarrow CH_4 + CO_2$

Data from Min and Zinder [122]. S_{min} (acetate) estimated, from substrate depletion curve, to be 8.0×10^{-4} mol L^{-1}.

$T = 58°C$

pH = 6.8

[acetate] varied

[CH_4] = 1.8×10^{-5} mol L^{-1}

[CO_2] = 1.9×10^{-2} mol L^{-1} (the gas phase contained 30% CO_2)

C024: *Methanosaeta* sp. CALS-1

$\text{Acetate}^- + H^+ \rightarrow CH_4 + CO_2$

Data from Min and Zinder [122]. S_{min} (acetate) estimated, from substrate depletion curve, to be 1.8×10^{-5} mol L^{-1}.

$T = 58°C$

pH = 6.8

[acetate] varied

[CH_4] = 1.8×10^{-5} mol L^{-1}

[CO_2] = 1.9×10^{-2} mol L^{-1} (the gas phase contained 30% CO_2)

C025: *Sporomusa termitidis* JSN-2

$H_2 + 0.5\,CO_2 \rightarrow 0.25\,\text{acetate}^- + 0.5\,H_2O + 0.25\,H^+$

Data from Breznak *et al.* [21]. K_S (H_2) estimated, by fitting to substrate depletion curve, to be 6.0×10^{-6} mol L^{-1}.

$T = 30°C$

pH = 7.0

[H_2] varied

[CO_2] = 4.1×10^{-2} mol L^{-1} (the gas phase contained 24% CO_2)

[acetate] = 4.4×10^{-3} mol L^{-1}

C026: *Acetobacterium carbinolicum* HP4

$H_2 + 0.5\ CO_2 \rightarrow 0.25\ acetate^- + 0.5\ H_2O + 0.25\ H^+$

Data from Conrad and Wetter [34]. S_{min} (H_2) estimated, from substrate depletion curves, to be: 3.7×10^{-9} mol L^{-1} at $T = 4°C$ with [CO_2] = 7.5×10^{-2} mol L^{-1}; 5.2×10^{-9} mol L^{-1} at $T = 10°C$ with [CO_2] = 7.0×10^{-2} mol L^{-1}; 8.4×10^{-9} mol L^{-1} at $T = 15°C$ with [CO_2] = 6.6×10^{-2} mol L^{-1}; 1.2×10^{-8} mol L^{-1} at $T = 20°C$ with [CO_2] = 6.1×10^{-2} mol L^{-1}; and 2.3×10^{-8} mol L^{-1} at $T = 25°C$ with [CO_2] = 5.6×10^{-2} mol L^{-1}.

pH = 7.05

[H_2] varied

[CO_2] calculated at different temperatures (the gas phase contained 20% CO_2 at 140 kPa)

[acetate] = 4.4×10^{-3} mol L^{-1}

C027: *Methanobacterium bryantii* Bab1

$H_2 + 0.25\ CO_2 \rightarrow 0.25\ CH_4 + 0.5\ H_2O$

Data from Conrad and Wetter [34]. S_{min} (H_2) estimated, from substrate depletion curves, to be: 2.0×10^{-9} mol L^{-1} at $T = 25°C$ with [CO_2] = 5.6×10^{-2} mol L^{-1} and [CH_4] = 5.1×10^{-6} mol L^{-1}; 2.3×10^{-9} mol L^{-1} at $T = 30°C$ with [CO_2] = 5.2×10^{-2} mol L^{-1} and [CH_4] = 4.7×10^{-6} mol L^{-1}; and 4.4×10^{-9} mol L^{-1} at $T = 40°C$ with [CO_2] = 4.3×10^{-2} mol L^{-1} and [CH_4] = 4.0×10^{-6} mol L^{-1}.

pH = 7.05

[H_2] varied

[CO_2] calculated at different temperatures (the gas phase contained 20% CO_2 at 140 kPa)

[acetate] calculated at different temperatures

C028: *Methanothermobacter marburgensis* Marburg

$H_2 + 0.25\,CO_2 \rightarrow 0.25\,CH_4 + 0.5\,H_2O$

Data from Conrad and Wetter [34]. $S_{\min}$ (H_2) estimated, from substrate depletion curves, to be: 3.2×10^{-9} mol L^{-1} at $T = 30°C$ with $[CO_2] = 5.2\times10^{-2}$ mol L^{-1} and $[CH_4] = 4.7\times10^{-6}$ mol L^{-1}; 2.4×10^{-8} mol L^{-1} at $T = 40°C$ with $[CO_2] = 4.3\times10^{-2}$ mol L^{-1} and $[CH_4] = 4.0\times10^{-6}$ mol L^{-1}; 3.6×10^{-8} mol L^{-1} at $T = 50°C$ with $[CO_2] = 3.4\times10^{-2}$ mol L^{-1} and $[CH_4] = 3.6\times10^{-6}$ mol L^{-1}; and 1.4×10^{-7} mol L^{-1} at $T = 60°C$ with $[CO_2] = 2.7 \times 10^{-2}$ mol L^{-1} and $[CH_4] = 3.3 \times 10^{-6}$ mol L^{-1}.

pH = 7.05

$[H_2]$ varied

$[CO_2]$ calculated at different temperatures (the gas phase contained 20% CO_2 at 140 kPa)

[acetate] calculated at different temperatures

C029: *Geobacter sulfurreducens* PCA

$Acetate^- + 4\,Hfumarate^- + 2\,H_2O + H^+ \rightarrow 2\,CO_2 + 4\,Hsuccinate^-$

Data from Esteve-Nuñez *et al.* [45]. K_S (acetate) estimated, from continuous culture, to be 3.0×10^{-5} mol L^{-1}.

$T = 30°C$

pH = 7.0

$[H_2]$ varied

$[CO_2] = 3.4 \times 10^{-2}$ mol L^{-1} (the gas phase contained 20% CO_2)

[fumarate] $= 9.0 \times 10^{-3}$ mol L^{-1}

[succinate] $= 2.1 \times 10^{-2}$ mol L^{-1}

C030: *Methanosarcina barkeri* Fusaro

$Acetate^- + H^+ \rightarrow CH_4 + CO_2$

Data from Fukuzaki *et al.* [50] and Mazumder *et al.* [114]. $S_{\min}$ (acetate) estimated, from substrate depletion curve, to be 6.2×10^{-4} mol L^{-1}.

$T = 37°C$

pH = 6.8

[acetate] varied

$[CH_4] = 3.7 \times 10^{-4}\,\mathrm{mol\,L^{-1}}$

$[CO_2] = 1.0 \times 10^{-3}\,\mathrm{mol\,L^{-1}}$ (the gas phase contained 0.1% CO_2)

C031: *Methanosarcina barkeri* MS, *Methanosarcina* sp. VeA23, and *Methanosaeta* sp. VeAc9

$\mathrm{Acetate^- + H^+ \rightarrow CH_4 + CO_2}$

Data from Großkopf *et al.* [58]. $S_{\min}$ (acetate) estimated, from substrate depletion curves, to be: $8.5 \times 10^{-4}\,\mathrm{mol\,L^{-1}}$ for *Methanosarcina barkeri* MS; $3.1 \times 10^{-4}\,\mathrm{mol\,L^{-1}}$ for *Methanosarcina* sp. VeA23; and $1.0 \times 10^{-5}\,\mathrm{mol\,L^{-1}}$ for *Methanosaeta* sp. VeAc9.

$T = 25°\mathrm{C}$

pH = 7.2

[acetate] varied

$[CH_4] = 1.0 \times 10^{-4}\,\mathrm{mol\,L^{-1}}$

$[CO_2] = 5.5 \times 10^{-2}\,\mathrm{mol\,L^{-1}}$ (the gas phase contained 20% CO_2)

C032: *Methanosaeta soehngenii* Opfikon

$\mathrm{Acetate^- + H^+ \rightarrow CH_4 + CO_2}$

Data from Jetten *et al.* [77]. $S_{\min}$ (acetate) estimated, from substrate depletion curve, to be $7.0 \times 10^{-6}\,\mathrm{mol\,L^{-1}}$.

$T = 37°\mathrm{C}$

pH = 7.6

[acetate] varied

$[CH_4] = 3.3 \times 10^{-6}\,\mathrm{mol\,L^{-1}}$

$[CO_2] = 1.0 \times 10^{-1}\,\mathrm{mol\,L^{-1}}$ (the gas phase contained 20% CO_2)

C033: *Methanosarcina barkeri* Fusaro

$\mathrm{Acetate^- + H^+ \rightarrow CH_4 + CO_2}$

Data from Jetten *et al.* [77] and Scherer and Sahm [151]. $S_{\min}$ (acetate) estimated, from substrate depletion curve, to be $2.4 \times 10^{-4}\,\mathrm{mol\,L^{-1}}$.

$T = 37°\mathrm{C}$

pH = 6.4

[acetate] varied

$[CH_4] = 2.4 \times 10^{-4}\,\mathrm{mol\,L^{-1}}$

$[CO_2] = 1.1 \times 10^{-1}\,\mathrm{mol\,L^{-1}}$ (the gas phase contained 20% CO_2)

C034: *Methanobrevibacter arboriphilus* DH1

$H_2 + 0.25\,CO_2 \rightarrow 0.25\,CH_4 + 0.5\,H_2O$

Data from Junicke *et al.* [82]. K_S (H_2) estimated, by fitting to growth curve, to be $6.0 \times 10^{-7}\,\mathrm{mol\,L^{-1}}$.

$T = 37°C$

pH = 7.1

$[H_2]$ varied

$[CO_2] = 7.3 \times 10^{-4}\,\mathrm{mol\,L^{-1}}$ (the gas phase contained 0.4% CO_2)

$[CH_4] = 2.3 \times 10^{-6}\,\mathrm{mol\,L^{-1}}$

C035: *Methanobacterium formicicum* and *Methanosarcina barkeri*, strains not specified

$H_2 + 0.25\,CO_2 \rightarrow 0.25\,CH_4 + 0.5\,H_2O$

Data from Kral *et al.* [92]. S_{min} (H_2) estimated, from substrate depletion curves, to be $1.7 \times 10^{-8}\,\mathrm{mol\,L^{-1}}$ for *Methanobacterium formicicum* and $1.8 \times 10^{-7}\,\mathrm{mol\,L^{-1}}$ for *Methanosarcina barkeri*.

$T = 37°C$

pH = 7.0

$[H_2]$ varied

$[CO_2] = 4.5 \times 10^{-1}\,\mathrm{mol\,L^{-1}}$ (the gas phase contained 100% CO_2 at 3 atm)

$[CH_4] = 5.7 \times 10^{-6}\,\mathrm{mol\,L^{-1}}$

C036: *Methanococcus maripaludis*, strain not specified

$H_2 + 0.25\,CO_2 \rightarrow 0.25\,CH_4 + 0.5\,H_2O$

Data from Kral *et al.* [92]. S_{min} (H_2) estimated, from substrate depletion curve, to be $4.2 \times 10^{-8}\,\mathrm{mol\,L^{-1}}$.

$T = 25°C$

pH = 6.8

$[H_2]$ varied

$[CO_2] = 3.9 \times 10^{-1}\,\mathrm{mol\,L^{-1}}$ (the gas phase contained 100% CO_2 at 3 atm)

$[CH_4] = 7.0 \times 10^{-6}\,\mathrm{mol\,L^{-1}}$

C037: *Methanthermobacter wolfei*, strain not specified

$H_2 + 0.25\,CO_2 \rightarrow 0.25\,CH_4 + 0.5\,H_2O$

Data from Kral *et al.* [92]. S_{min} (H_2) estimated, from substrate depletion curve, to be $4.7 \times 10^{-8}\,\mathrm{mol\,L^{-1}}$.

$T = 55°C$

pH = 7.0

$[H_2]$ varied

$[CO_2] = 3.0 \times 10^{-1}\,\mathrm{mol\,L^{-1}}$ (the gas phase contained 100% CO_2 at 3 atm)

$[CH_4] = 4.6 \times 10^{-6}\,\mathrm{mol\,L^{-1}}$

C038: *Methanobrevibacter arboriphilus* AZ

$H_2 + 0.25\,CO_2 \rightarrow 0.25\,CH_4 + 0.5\,H_2O$

Data from Kristjansson *et al.* [93]. K_{S} (H_2) estimated, by fitting to substrate depletion curve, to be $6.6 \times 10^{-6}\,\mathrm{mol\,L^{-1}}$.

$T = 35°C$

pH = 6.9

$[H_2]$ varied

$[CO_2] = 2.6 \times 10^{-2}\,\mathrm{mol\,L^{-1}}$ (the gas phase contained 20% CO_2)

$[CH_4] = 1.7 \times 10^{-5}\,\mathrm{mol\,L^{-1}}$

C039: *Desulfovibrio vulgaris* Marburg

$H_2 + 0.25\,SO_4^{2-} \rightarrow 0.25\,HS^- + H_2O$

Data from Kristjansson *et al.* [93]. K_{S} (H_2) estimated, by fitting to substrate depletion curve, to be $1.3 \times 10^{-6}\,\mathrm{mol\,L^{-1}}$.

$T = 35°C$

pH = 6.9

$[H_2]$ varied

$[SO_4^{2-}] = 4.0 \times 10^{-3}\,\mathrm{mol\,L^{-1}}$

$[HS^-] = 1.8 \times 10^{-5}\,\mathrm{mol\,L^{-1}}$

C040: *Acetobacterium psammolithicum* CN-E

$H_2 + 0.5\,CO_2 \rightarrow 0.25\,\text{acetate}^- + 0.5\,H_2O + 0.25\,H^+$

Data from Krumholz *et al.* [94]. $S_{\min}$ (H_2) estimated, from substrate depletion curve, to be 4.1×10^{-7} mol L^{-1}.

$T = 30°C$

pH = 6.8

[H_2] varied

[CO_2] = 2.4×10^{-2} mol L^{-1} (the gas phase contained 20% CO_2)

[acetate] = 2.5×10^{-3} mol L^{-1}

C041: *Desulfomicrobium hypogeium* CN-A

$H_2 + 0.25\,SO_4^{2-} \rightarrow 0.25\,HS^- + H_2O$

Data from Krumholz *et al.* [94]. $S_{\min}$ (H_2) estimated, from substrate depletion curve, to be 2.1×10^{-9} mol L^{-1}.

$T = 30°C$

pH = 6.8

[H_2] varied

[SO_4^{2-}] = 7.6×10^{-3} mol L^{-1}

[HS^-] = 2.5×10^{-3} mol L^{-1}

C042: *Acetobacterium woodii* WB1

$H_2 + 0.5\,CO_2 \rightarrow 0.25\,\text{acetate}^- + 0.5\,H_2O + 0.25\,H^+$

Data from Le Van *et al.* [99]. $S_{\min}$ (H_2) estimated, from substrate depletion curve, to be 2.8×10^{-7} mol L^{-1}.

$T = 30°C$

pH = 7.4

[H_2] varied

[CO_2] = 1.2×10^{-1} mol L^{-1} (the gas phase contained 31.8% CO_2)

[acetate] = 3.9×10^{-2} mol L^{-1}

C043: *Sporomusa termitida* JSN-2

$H_2 + 0.5\,CO_2 \rightarrow 0.25\,\text{acetate}^- + 0.5\,H_2O + 0.25\,H^+$

$S_{\min}$ (H_2) estimated, from substrate depletion curve, to be 6.6×10^{-7} mol L^{-1}.

$T = 30°C$

pH = 7.1

[H_2] varied

[CO_2] = 6.6×10^{-2} mol L^{-1} (the gas phase contained 31.8% CO_2)

[acetate] = 3.9×10^{-2} mol L^{-1}

C044: *Methanobrevibacter* sp. 10-16B

$H_2 + 0.25\,CO_2 \rightarrow 0.25\,CH_4 + 0.5\,H_2O$

Data from Le Van *et al.* [99] and Bryant and Burkey [25]. S_{min} (H_2) estimated, from substrate depletion curve, to be 9.3×10^{-8} mol L^{-1}.

$T = 38°C$

pH = 6.6

[H_2] varied

[CO_2] = 2.3×10^{-2} mol L^{-1} (the gas phase contained 31.8% CO_2)

[CH_4] = 1.7×10^{-6} mol L^{-1}

C046: *Methanobrevibacter smithii* PS

$H_2 + 0.25\,CO_2 \rightarrow 0.25\,CH_4 + 0.5\,H_2O$

Data from Pavlostathis *et al.* [139]. K_S (H_2) estimated, from continuous culture, to be 1.3×10^{-6} mol L^{-1}.

$T = 37°C$

pH = 6.6

[H_2] varied

[CO_2] = 5.9×10^{-2} mol L^{-1} (the gas phase contained 0.798 atm CO_2)

[CH_4] = 2.3×10^{-4} mol L^{-1}

C047: *Desulfovibrio vulgaris* Madison

$H_2 + 0.25\,SO_4^{2-} \rightarrow 0.25\,HS^- + H_2O$

Data from Phelps *et al.* [142]. S_{min} (H_2) estimated, from substrate depletion curve, to be 2.0×10^{-8} mol L^{-1}.

$T = 37°C$

pH = 7.0

$[H_2]$ varied

$[SO_4^{2-}] = 1.9 \times 10^{-2}\,\mathrm{mol\,L^{-1}}$

$[HS^-] = 1.4 \times 10^{-3}\,\mathrm{mol\,L^{-1}}$

C048: *Desulfovibrio vulgaris* Madison

$H_2 + 0.25\,SO_4^{2-} \rightarrow 0.25\,HS^- + H_2O$

Data from Phelps *et al.* [142]. $S_{\min}$ (H_2) estimated, from substrate depletion curve, to be $2.2 \times 10^{-8}\,\mathrm{mol\,L^{-1}}$.

$T = 37°C$

pH = 7.0

$[H_2]$ varied

$[SO_4^{2-}] = 1.9 \times 10^{-2}\,\mathrm{mol\,L^{-1}}$

$[HS^-] = 3.2 \times 10^{-3}\,\mathrm{mol\,L^{-1}}$

C049: *Desulfovibrio vulgaris* Madison

$H_2 + 0.25\,SO_4^{2-} \rightarrow 0.25\,HS^- + H_2O$

Data from Phelps *et al.* [142]. $S_{\min}$ (H_2) estimated, from substrate depletion curve, to be $1.2 \times 10^{-8}\,\mathrm{mol\,L^{-1}}$.

$T = 37°C$

pH = 7.0

$[H_2]$ varied

$[SO_4^{2-}] = 1.8 \times 10^{-2}\,\mathrm{mol\,L^{-1}}$

$[HS^-] = 1.6 \times 10^{-3}\,\mathrm{mol\,L^{-1}}$

C050: *Desulfovibrio vulgaris* Madison

$H_2 + 0.25\,SO_4^{2-} \rightarrow 0.25\,HS^- + H_2O$

Data from Phelps *et al.* [142]. $S_{\min}$ (H_2) estimated, from substrate depletion curve, to be $1.1 \times 10^{-8}\,\mathrm{mol\,L^{-1}}$.

$T = 37°C$

pH = 7.0

$[H_2]$ varied

$[SO_4^{2-}] = 1.8 \times 10^{-2}\,\mathrm{mol\,L^{-1}}$

$[HS^-] = 2.2 \times 10^{-3}\,\mathrm{mol\,L^{-1}}$

C051: *Acetobacterium woodii*, strain not specified

$H_2 + 0.5\,CO_2 \rightarrow 0.25\,\mathrm{acetate^-} + 0.5\,H_2O + 0.25\,H^+$

Data from Poehlein *et al.* [145] and Imkamp *et al.* [70]. $S_{\min}$ (H_2) estimated from substrate depletion curve, to be $1.9 \times 10^{-6}\,\mathrm{mol\,L^{-1}}$.

$T = 30°C$

pH = 7.1

$[H_2]$ varied

$[CO_2] = 4.1 \times 10^{-2}\,\mathrm{mol\,L^{-1}}$ (the gas phase contained 20% CO_2)

$[\mathrm{acetate}] = 1.3 \times 10^{-2}\,\mathrm{mol\,L^{-1}}$

C052: *Desulfovibrio desulfuricans*, *Desulfovibrio vulgaris*, *Desulfovibrio* sp. DG2, *Desulfovibrio* sp. G-11, and *Desulfovibrio* sp. PS1

$H_2 + 0.25\,SO_4^{2-} \rightarrow 0.25\,HS^- + H_2O$

Data from Robinson and Tiedje [147]. K_S (H_2) estimated, by fitting to substrate depletion curves, to be: $1.8 \times 10^{-6}\,\mathrm{mol\,L^{-1}}$ for *Desulfovibrio desulfuricans* (strain not specified); $1.9 \times 10^{-6}\,\mathrm{mol\,L^{-1}}$ for *Desulfovibrio vulgaris* (strain not specified); $1.4 \times 10^{-6}\,\mathrm{mol\,L^{-1}}$ for *Desulfovibrio* sp. DG2; $1.1 \times 10^{-6}\,\mathrm{mol\,L^{-1}}$ for *Desulfovibrio* sp. G-11; and $7.0 \times 10^{-7}\,\mathrm{mol\,L^{-1}}$ for *Desulfovibrio* sp. PS1.

$T = 37°C$

pH = 6.7

$[H_2]$ varied

$[SO_4^{2-}] = 2.4 \times 10^{-2}\,\mathrm{mol\,L^{-1}}$

$[HS^-] = 1.3 \times 10^{-4}\,\mathrm{mol\,L^{-1}}$

C053: *Methanospirillum hungatei* JF-1, *Methanospirillum* sp. PM 1, and *Methanospirillum* sp. PM 2

$H_2 + 0.25\,CO_2 \rightarrow 0.25\,CH_4 + 0.5\,H_2O$

Data from Robinson and Tiedje [147]. K_S (H_2) estimated, by fitting to substrate depletion curves, to be: $5.0 \times 10^{-6}\,\mathrm{mol\,L^{-1}}$ for *Methanospirillum hungatei* JF-1; $2.5 \times 10^{-6}\,\mathrm{mol\,L^{-1}}$ for *Methanospirillum* sp. PM 1; and $4.1 \times 10^{-6}\,\mathrm{mol\,L^{-1}}$ for *Methanospirillum* sp. PM 2.

$T = 37°C$

pH = 6.7

[H_2] varied

[CO_2] = 8.7×10^{-2} mol L^{-1} (the gas phase contained 100% CO_2)

[CH_4] = 5.3×10^{-6} mol L^{-1}

C054: *Methanosarcina barkeri* Fusaro

$Acetate^- + H^+ \rightarrow CH_4 + CO_2$

Data from Schönheit *et al.* [156]. K_S (acetate) estimated, by fitting to substrate depletion curve, to be 3.0×10^{-3} mol L^{-1}.

$T = 30°C$

pH = 6.9

[acetate] varied

[CH_4] = 2.0×10^{-6} mol L^{-1} (estimated, headspace flushed with N_2/CO_2 mixture)

[CO_2] = 2.8×10^{-2} mol L^{-1} (the gas phase contained 20% CO_2)

C055: *Methanospirillum hungatei* JF-1

$H_2 + 0.25\ CO_2 \rightarrow 0.25\ CH_4 + 0.5\ H_2O$

Data from Scholten and Conrad [155]. S_{min} (H_2) estimated, from substrate depletion curve, to be 1.1×10^{-8} mol L^{-1}.

$T = 37°C$

pH = 6.9

[H_2] varied

[CO_2] = 4.2×10^{-2} mol L^{-1} (the gas phase contained 20% CO_2 at 172 kPa)

[CH_4] = 3.9×10^{-7} mol L^{-1}

C056: *Propionibacterium freudenreichii* 53-W

$Lactate^- \rightarrow 0.333\ acetate^- + 0.666\ propionate^- + CO_2 + H_2O$

Data from Seeliger *et al.* [158] and Seeliger [157]. K_S (lactate) estimated, from continuous culture, to be 1.4×10^{-4} mol L^{-1}.

$T = 32.5°C$

pH = 7.1

[lactate] varied

$[CO_2] = 4.0 \times 10^{-2}$ mol L^{-1} (the gas phase contained 20% CO_2)

[acetate] $= 3.3 \times 10^{-3}$ mol L^{-1}

[propionate] $= 6.9 \times 10^{-3}$ mol L^{-1}

C057: *Veillonella parvula* Te3

$Lactate^- \rightarrow 0.333\ acetate^- + 0.666\ propionate^- + CO_2 + H_2O$

Data from Seeliger *et al.* [158]. K_S (lactate) estimated, from continuous culture, to be 2.9×10^{-4} mol L^{-1}.

$T = 32.5°C$

pH = 7.1

[lactate] varied

$[CO_2] = 4.0 \times 10^{-2}$ mol L^{-1} (the gas phase contained 20% CO_2)

[acetate] $= 5.3 \times 10^{-3}$ mol L^{-1}

[propionate] $= 1.0 \times 10^{-2}$ mol L^{-1}

C059:*Desulfobulbus propionicus* Lindhorst

$Ethanol + 0.5\ SO_4^{2-} \rightarrow acetate^- + 0.5\ HS^- + H_2O + 0.5\ H^+$

Data from Szewzyk and Pfennig [170]. K_S (ethanol) estimated, from continuous culture, to be 5.3×10^{-6} mol L^{-1}.

$T = 28°C$

pH = 7.1

[ethanol] varied

$[SO_4^{2-}] = 1.0 \times 10^{-2}$ mol L^{-1}

[acetate] $= 2.0 \times 10^{-7}$ mol L^{-1}

$[HS^-] = 1.0 \times 10^{-3}$ mol L^{-1}

C060: *Methanosarcina barkeri* 227

$Acetate^- + H^+ \rightarrow CH_4 + CO_2$

Data from Westermann *et al.* [183]. S_{min} (acetate) estimated, from substrate depletion curve, to be 1.2×10^{-3} mol L^{-1}.

$T = 37°C$

pH = 7.0

[acetate] varied

$[CH_4] = 4.8 \times 10^{-5}$ mol L^{-1}

$[CO_2] = 4.5 \times 10^{-2}$ mol L^{-1} (the gas phase contained 30% CO_2)

C061: *Methanosarcina mazei* S-6 $Acetate^- + H^+ \rightarrow CH_4 + CO_2$

Data from Westermann *et al.* [183]. S_{min} (acetate) estimated, from substrate depletion curve, to be 4.0×10^{-4} mol L^{-1}.

$T = 37°C$

pH = 7.0

[acetate] varied

$[CH_4] = 3.9 \times 10^{-5}$ mol L^{-1} $[CO_2] = 4.5 \times 10^{-2}$ mol L^{-1} (the gas phase contained 30% CO_2)

C062: *Methanosaeta* sp. Los Angeles River

$Acetate^- + H^+ \rightarrow CH_4 + CO_2$

Data from Westermann *et al.* [183]. S_{min} (acetate) estimated, from substrate depletion curve, to be 6.9×10^{-5} mol L^{-1}.

$T = 37°C$

pH = 7.0

[acetate] varied

$[CH_4] = 6.0 \times 10^{-5}$ mol L^{-1}

$[CO_2] = 4.5 \times 10^{-2}$ mol L^{-1} (the gas phase contained 30% CO_2)

C063: *Methanobrevibacter* sp. 229/11, *Methanobrevibacter* sp. AbM4, *Methanobrevibacter ruminantium* M1, *Methanobrevibacter* sp. SM9, *Methanobrevibacter* sp. D5, *Methanobacterium formicicum* BRM9, and *Methanobacterium* sp. YCM1

$H_2 + 0.25\, CO_2 \rightarrow 0.25\, CH_4 + 0.5\, H_2O$

Data from Kim [88]. S_{min} (H_2) estimated, from substrate depletion curves, to be: 1.8×10^{-8} mol L^{-1} for *Methanobrevibacter* sp. 229/11 with $[CH_4] = 5.5 \times 10^{-7}$ mol L^{-1}; 3.1×10^{-8} mol L^{-1} for *Methanobrevibacter* sp. AbM4 with $[CH_4] = 6.1 \times 10^{-7}$ mol L^{-1}; 3.3×10^{-8} mol L^{-1} for *Methanobrevibacter ruminantium* M1 with $[CH_4] = 5.5 \times 10^{-7}$ mol L^{-1}; 3.4×10^{-8} mol L^{-1} for *Methanobrevibacter* sp. SM9 with $[CH_4] = 5.0 \times 10^{-7}$ mol L^{-1}; 3.1×10^{-8} mol L^{-1} for

Methanobrevibacter sp. D5 with $[CH_4] = 5.5\times10^{-7}$ mol L^{-1}; 1.5×10^{-8} mol L^{-1} for *Methanobacterium formicicum* BRM9 with $[CH_4] = 5.0\times10^{-7}$ mol L^{-1}; and 8.7×10^{-9} mol L^{-1} for *Methanobacterium* sp. YCM1 with $[CH_4] = 6.1 \times 10^{-7}$ mol L^{-1}.

$T = 39°C$

pH = 6.5

$[H_2]$ varied

$[CO_2] = 6.2 \times 10^{-2}$ mol L^{-1} (the gas phase contained 100% CO_2)

C064: *Acetobacterium carbinolicum* WoProp1, *Acetobacterium woodii* NZva16, and *Sporomusa termitida* JSN-2

$H_2 + 0.5\,CO_2 \rightarrow 0.25\,\text{acetate}^- + 0.5\,H_2O + 0.25\,H^+$

Data from Cord-Ruwisch *et al.* [36]. $S_{\min}$ (H_2) estimated, from substrate depletion curves, to be: 7.2×10^{-7} mol L^{-1} for *Acetobacterium carbinolicum* WoProp1; 4.0×10^{-7} mol L^{-1} for *Acetobacterium woodii* NZva16; and 6.3×10^{-7} mol L^{-1} for *Sporomusa termitida* JSN-2.

$T = 30°C$

pH = 7.2

$[H_2]$ varied

$[CO_2] = 5.1 \times 10^{-2}$ mol L^{-1} (the gas phase contained 20% CO_2)

$[\text{acetate}] = 1.3 \times 10^{-2}$ mol L^{-1}

C065: *Desulfovibrio desulfuricans* Essex 6

$H_2 + 0.25\,SO_4^{2-} \rightarrow 0.25\,HS^- + H_2O$

Data from Cord-Ruwisch *et al.* [36]. $S_{\min}$ (H_2) estimated, from substrate depletion curve, to be 6.9×10^{-9} mol L^{-1}.

$T = 30°C$

pH = 7.2

$[H_2]$ varied

$[SO_4^{2-}] = 2.9 \times 10^{-2}$ mol L^{-1}

$[HS^-] = 1.1 \times 10^{-2}$ mol L^{-1}

C066: *Methanobacterium formicium* MF, *Methanobrevibacter arboriphilus* AZ, *Methanobrevibacter smithii* PS, *Methanococcus voltae* SB, and *Methanospirillum hungatei* JF-1

$H_2 + 0.25\,CO_2 \rightarrow 0.25\,CH_4 + 0.5\,H_2O$

Data from Cord-Ruwisch *et al.* [36]. $S_{\min}$ (H_2) estimated, from substrate depletion curves, to be: 2.1×10^{-8} mol L^{-1} for *Methanobacterium formicium* MF; 6.9×10^{-8} mol L^{-1} for *Methanobrevibacter arboriphilus* AZ; 7.6×10^{-8} mol L^{-1} for *Methanobrevibacter smithii* PS; 5.7×10^{-8} mol L^{-1} for *Methanococcus voltae* SB; and 2.3×10^{-8} mol L^{-1} for *Methanospirillum hungatei* JF-1.

$T = 30°C$

pH = 7.2

[H_2] varied

[CO_2] = 5.1×10^{-2} mol L^{-1} (the gas phase contained 20% CO_2)

[CH_4] = 3.2×10^{-6} mol L^{-1}

C067: *Methanogenium frigidum* Ace-2

$H_2 + 0.25\,CO_2 \rightarrow 0.25\,CH_4 + 0.5\,H_2O$

Data from Chong *et al.* [31]. $S_{\min}$ (H_2) estimated, from substrate depletion curve, to be 4.4×10^{-9} mol L^{-1}.

$T = 25°C$

pH = 7.0

[H_2] varied

[CO_2] = 5.6×10^{-2} mol L^{-1} (the gas phase contained 30% CO_2)

[CH_4] = 1.4×10^{-6} mol L^{-1}

C068: *Desulforhabdus amnigenus* ASRB1 and *Desulfobacca acetoxidans* ASRB2

$Acetate^- + SO_4^{2-} + 2\,H^+ \rightarrow 2\,CO_2 + HS^- + 2\,H_2O$

Data from Oude Elferink *et al.* [138], Oude Elferink *et al.* [137], and Stams *et al.* [165]. K_S (acetate) estimated, by fitting to substrate depletion curve, to be 6.0×10^{-4} mol L^{-1}.

$T = 30°C$

pH = 7.0

[acetate] varied

[SO_4^{2-}] = 7.0×10^{-3} mol L^{-1}

[CO_2] = 5.1×10^{-2} mol L^{-1} (the gas phase contained 20% CO_2 at 1.72 atm)

[HS^-] = 5.0×10^{-3} mol L^{-1}

C069: *Acetitomaculum ruminis* 139B and *Acetitomaculum ruminis* 190A4

$H_2 + 0.5\,CO_2 \rightarrow 0.25\,acetate^- + 0.5\,H_2O + 0.25\,H^+$

Data from Le Van *et al.* [99]. S_{min} (H_2) estimated, from substrate depletion curves, to be 3.4×10^{-6} mol L^{-1} for Acetitomaculum ruminis 139B and 2.9×10^{-6} mol L^{-1} for Acetitomaculum ruminis 190A4.

$T = 38°C$

pH = 7.4

[H_2] varied

[CO_2] = 1.1×10^{-1} mol L^{-1} (the gas phase contained 31.8% CO_2)

[acetate] = 3.9×10^{-2} mol L^{-1}

C070: *Methanosarcina barkeri* Fusaro

$Acetate^- + H^+ \rightarrow CH_4 + CO_2$

Data from Fukuzaki *et al.* [50] and Mazumder *et al.* [114]. K_S (acetate) estimated, by fitting to substrate depletion curve, to be 5.7×10^{-3} mol L^{-1}.

$T = 37°C$

pH = 6.5

[acetate] varied

[CH_4] = 3.7×10^{-4} mol L^{-1}

[CO_2] = 1.0×10^{-3} mol L^{-1} (the gas phase contained 1.5% CO_2)

C072: *Acetobacterium woodii* NZva16

$H_2 + 0.5\,CO_2 \rightarrow 0.25\,acetate^- + 0.5\,H_2O + 0.25\,H^+$

Data from Conrad and Wetter [34]. S_{min} (H_2) estimated, from substrate depletion curves, to be: 1.2×10^{-8} mol L^{-1} at $T = 15°C$ with [CO_2] = 6.6×10^{-2} mol L^{-1}; 2.0×10^{-8} mol L^{-1} at $T = 25°C$ with [CO_2] = 5.6×10^{-2} mol L^{-1}; and 4.1×10^{-8} mol L^{-1} at $T = 30°C$ with [CO_2] = 5.2×10^{-2} mol L^{-1}.

pH = 7.05

[H_2] varied

[CO_2] calculated at different temperatures (the gas phase contained 20% CO_2 at 140 kPa)

[acetate] = 2.0×10^{-3} mol L^{-1}

C073: *Clostridium homopropionicum* LuHBu1

$\text{Lactate}^- \rightarrow 0.333\,\text{acetate}^- + 0.666\,\text{propionate}^- + CO_2 + H_2O$

Data from Seeliger *et al.* [158] and Seeliger [157]. K_S (lactate) estimated, from continuous culture, to be $5.6 \times 10^{-4}\,\text{mol}\,\text{L}^{-1}$.

$T = 32.5°\text{C}$

$\text{pH} = 7.1$

[lactate] varied

$[CO_2] = 4.0 \times 10^{-2}\,\text{mol}\,\text{L}^{-1}$ (the gas phase contained 20% CO_2)

$[\text{acetate}] = 3.0 \times 10^{-3}\,\text{mol}\,\text{L}^{-1}$

$[\text{propionate}] = 5.9 \times 10^{-3}\,\text{mol}\,\text{L}^{-1}$

Bibliography

1. Aceti, D. J. & Ferry, J. G. Purification and characterization of acetate kinase from acetate-grown *Methanosarcina thermophila*. Evidence for regulation of synthesis. *The Journal of Biological Chemistry* **263,** 15444–15448 (1988).

2. Agarwal, A., Adams, R., Castellani, G. C. & Shouval, H. Z. On the precision of quasi steady state assumptions in stochastic dynamics. *Journal of Chemical Physics* **137,** 044105. `https://www.ncbi.nlm.nih.gov/pmc/articles/PMC3416873/` (2012).

3. Aklujkar, M. *et al.* The genome of *Pelobacter carbinolicus* reveals surprising metabolic capabilities and physiological features. *BMC genomics* **13,** 690 (2012).

4. Aledo, J. Metabolic pathways: does the actual Gibbs free-energy change affect the flux rate? *Biochemistry and Molecular Biology Education* **29,** 142–143 (2008).

5. Amend, J. P. & Helgeson, H. C. Calculation of the standard molal thermodynamic properties of aqueous biomolecules at elevated temperatures and pressures. Part1 L-α-Amino acids. *Journal of the Chemical Society, Faraday Transactions* **93,** 1927–1941. `https://pubs.rsc.org/en/content/articlelanding/1997/ft/a608126f` (1997).

6. Bader, F. G. Analysis of double-substrate limited growth. *Biotechnology and Bioengineering* **20,** 183–202 (1978).

7. Bader, F. G. *Kinetics of double-substrate limited growth* in *Microbial Population Dynamics* (ed Bazin, M. J.) pp. 1-32 (CRC Press, Boca Raton, Fla., 1982).

8. Badziong, W. & Thauer, R. K. Growth yields and growth rates of *Desulfovibrio vulgaris* (Marburg) growing on hydrogen plus sulfate and hydrogen plus thiosulfate as the sole

energy sources. *Archives of Microbiology* **117,** 209–214. https://doi.org/10.1007/BF00402310 (1978).

9. Bar-Even, A. *et al.* The moderately efficient enzyme: evolutionary and physicochemical trends shaping enzyme parameters. *Biochemistry* **50,** 4402–4410. https://doi.org/10.1021/bi2002289 (2011).

10. Battino, R. The Ostwald coefficient of gas solubility. *Fluid Phase Equilibria* **15,** 231–240. https://www.sciencedirect.com/science/article/pii/0378381284870090 (1984).

11. Bengelsdorf, F. R., Poehlein, A., Schiel-Bengelsdorf, B., Daniel, R. & Dürre, P. Genome sequence of the acetogenic bacterium *Butyribacterium methylotrophicum* DSM 3468^{T}. *Genome Announcements* **4,** e01338–16. https://www.ncbi.nlm.nih.gov/pmc/articles/PMC5137411/ (2016).

12. Bennett, B. D. *et al.* Absolute metabolite concentrations and implied enzyme active site occupancy in *Escherichia coli*. *Nature Chemical Biology* **5,** 593–599. https://www.nature.com/articles/nchembio.186 (2009).

13. Berg, H. C. & Purcell, E. M. Physics of chemoreception. *Biophysical Journal* **20,** 193–219. https://www.ncbi.nlm.nih.gov/pmc/articles/PMC1473391/ (1977).

14. Bertolazzi, E. A combination formula of Michaelis-Menten-Monod type. *Computers & Mathematics with Applications* **50,** 201–215. https://www.sciencedirect.com/science/article/pii/S0898122105002439 (2005).

15. Bertsch, J., Siemund, A. L., Kremp, F. & Müller, V. A novel route for ethanol oxidation in the acetogenic bacterium *Acetobacterium woodii*: the acetaldehyde/ethanol dehydrogenase pathway. *Environmental Microbiology* **18,** 2913–2922 (2016).

16. Beyenal, H., Chen, S. N. & Lewandowski, Z. The double substrate growth kinetics of *Pseudomonas aeruginosa*. *Enzyme and Microbial Technology* **32,** 92–98 (2003).

17. Blackman, F. F. Optima and limiting factors. *Annals of Botany* **19,** 281–296. https://doi.org/10.1093/oxfordjournals.aob.a089000 (1905).

18. Blanch, H. W. & Clark, D. S. *Biochemical Engineering* (Marcel Dekker, New York, NY, 1997).

19. Brandis-Heep, A., Gebhardt, N. A., Thauer, R. K., Widdel, F. & Pfennig, N. Anaerobic acetate oxidation to CO_2 by *Desulfobacter postgatei*: I. Demonstration of all enzymes required for the operation of the citric acid cycle. *Archives of Microbiology* **136,** 222–229. https://ui.adsabs.harvard.edu/abs/1983ArMic.136..222B (1983).

20. Bratbak, G. & Dundas, I. Bacterial dry matter content and biomass estimations. *Applied and Environmental Microbiology* **48,** 755–757 (1984).

21. Breznak, J. A., Switzer, J. M. & Seitz, H. .-. *Sporomusa termitida* sp. nov., an H_2/CO_2-utilizing acetogen isolated from termites. *Archives of Microbiology* **150,** 282–288 (1988).

22. Briggs, G. E. & Haldane, J. B. S. A note on the kinetics of enzyme action. *Biochemical Journal* **19,** 338–339. https://www.ncbi.nlm.nih.gov/pmc/articles/PMC1259181/ (1925).

23. Bright, H. J. & Appleby, M. The pH dependence of the individual steps in the glucose oxidase reaction. *Journal of Biological Chemistry* **244,** 3625–3634. https://www.jbc.org/article/S0021-9258(18)83415-9/abstract (1969).

24. Brune, A. Termite guts: the world's smallest bioreactors. *Trends In Biotechnology* **16,** 16–21 (1998).

25. Bryant, M. P. & Burkey, L. A. Cultural methods and some characteristics of some of the more numerous groups of bacteria in the bovine rumen. *Journal of Dairy Science* **36,** 205–217 (1953).

26. Buckel, W. & Thauer, R. K. Energy conservation via electron bifurcating ferredoxin reduction and proton/Na+ translocating ferredoxin oxidation. *Biochimica et Biophysica Acta* **1827,** 94–113. https://www.sciencedirect.com/science/article/pii/S0005272812009760 (2013).

27. Bungay, H. R. Growth rate expressions for two substrates one of which is inhibitory. *Journal of Biotechnology* **34,** 97–100. https://www.sciencedirect.com/science/article/pii/0168165694901708 (1994).

28. Butler, J. E. *et al.* Genetic characterization of a single bifunctional enzyme for fumarate reduction and succinate oxidation in *Geobacter sulfurreducens* and engineering of fumarate reduction in *Geobacter metallireducens*. *Journal of Bacteriology* **188,** 450–455 (2006).

29. Chang, R. *Physical chemistry: with applications to biological systems* (Macmillan, 1981).

30. Chang, R. *Physical chemistry for the biosciences* 1st edition (University Science Books, Sansalito, Calif, 2005).

31. Chong, S. C., Liu, Y., Cummins, M., Valentine, D. L. & Boone, D. R. *Methanogenium marinum* sp. nov., a H_2-using methanogen from Skan Bay, Alaska, and kinetics of H_2 utilization. *Antonie Van Leeuwenhoek* **81,** 263–270 (2002).

32. Cleland, W. W. The kinetics of enzyme-catalyzed reactions with two or more substrates or products: I. Nomenclature and rate equations. *Biochimica et Biophysica Acta* **67,** 104–137 (1963).

33. Collins, M. D. *et al.* The phylogeny of the genus *Clostridium*: proposal of five new genera and eleven new species combinations. *International Journal of Systematic Bacteriology* **44,** 812–826 (1994).

34. Conrad, R. & Wetter, B. Influence of temperature on energetics of hydrogen metabolism in homoacetogenic, methanogenic, and other anaerobic bacteria. *Archives of Microbiology* **155,** 94–98 (1990).

35. Contois, D. E. Kinetics of bacterial growth: relationship between population density and specific growth rate of continuous cultures. *Journal of General Microbiology* **21,** 40–50 (1959).

36. Cord-Ruwisch, R., Seitz, H.-J. & Conrad, R. The capacity of hydrogenotrophic anaerobic bacteria to compete for traces of hydrogen depends on the redox potential of the terminal electron acceptor. *Archives of Microbiology* **149,** 350–357. `https://doi.org/10.1007/BF00411655` (1988).

37. Dabes, J. N., Finn, R. K. & Welke, C. R. Equations of substrate-limited growth: the case for Blackman kinetics. *Biotechnology and Bioengineering* **15,** 1159–1177 (1973).

38. Davidi, D. *et al.* Global characterization of *in vivo* enzyme catalytic rates and their correspondence to *in vitro* k_{cat} measurements. *Proceedings of the National Academy of Sciences* **113,** 3401–3406. https://www.pnas.org/content/113/12/3401 (2016).

39. Desmond-Le Quéméner, E. & Bouchez, T. A thermodynamic theory of microbial growth. *ISME journal* **8,** 1747–1751 (2014).

40. Dimroth, P. & Hilbi, H. Enzymic and genetic basis for bacterial growth on malonate. *Molecular Microbiology* **25,** 3–10 (1997).

41. Dimroth, P., Kaim, G. & Matthey, U. Crucial role of the membrane potential for ATP synthesis by F(1)F(o) ATP synthases. *The Journal of Experimental Biology* **203,** 51–59 (2000).

42. Dörner, C. & Schink, B. *Clostridium homopropionicum* sp. nov., a new strict anaerobe growing with 2-, 3-, or 4-hydroxybutyrate. *Archives of Microbiology* **154,** 342–348 (1990).

43. Drew, S. W. *Liquid culture* in *Manual of Methods for General Bacteriology* (ed Gerhardt, P.) pp. 151-178 (American Society for Microbiology, Washington, DC, 1981).

44. Eichler, B. & Schink, B. Oxidation of primary aliphatic alcohols by *Acetobacterium carbinolicum* sp. nov., a homoacetogenic anaerobe. *Archives of Microbiology* **140,** 147–152. http://link.springer.com/10.1007/BF00454917 (1984).

45. Esteve-Núñez, A., Rothermich, M., Sharma, M. & Lovley, D. Growth of *Geobacter sulfurreducens* under nutrient-limiting conditions in continuous culture. *Environmental Microbiology* **7,** 641–648 (2005).

46. Fersht, A. *Enzyme structure and mechanism* (W H Freeman & Co, New York, 1985).

47. Flach, E. & Schnell, S. Use and abuse of the quasi-steady-state approximation. *Systems Biology* **153,** 187–191. https://www.ncbi.nlm.nih.gov/pmc/articles/PMC2265107/ (2006).

48. Fowler, R. H. A statistical derivation of Langmuir's adsorption isotherm. *Mathematical Proceedings of the Cambridge Philosophical Society* **31,** 260–264. https://www.cambridge.org/core/journals/mathematical-proceedings-of-the-cambridge-

philosophical-society/article/statistical-derivation-of-langmuirs-adsorption-isotherm/866A71D466CE0EABF6C82A7D8BD5B3E1 (1935).

49. Fritz, M. *et al.* An intermediate step in the evolution of ATPases – a hybrid F_0–V_0 rotor in a bacterial Na^+ F_1F_0 ATP synthase. *The FEBS Journal* **275,** 1999–2007. https://onlinelibrary.wiley.com/doi/abs/10.1111/j.1742-4658.2008.06354.x (2008).

50. Fukuzaki, S., Nishio, N. & Nagai, S. Kinetics of the methanogenic fermentation of acetate. *Applied and Environmental Microbiology* **56,** 3158–3163 (1990).

51. Galushko, A. & Schink, B. Oxidation of acetate through reactions of the citric acid cycle by *Geobacter sulfurreducens* in pure culture and in syntrophic coculture. *Archives of microbiology* **174,** 314–321 (2000).

52. Garg, L. C. & Maren, T. H. The rates of hydration of carbon dioxide and dehydration of carbonic acid at 37. *Biochimica et Biophysica Acta (BBA)-General Subjects* **261,** 70–76 (1972).

53. Gerber, M. & Span, R. An analysis of available mathematical models for anaerobic digestion of organic substances for production of biogas. *Proc. IGRC, Paris* (2008).

54. Gesztelyi, R. *et al.* The Hill equation and the origin of quantitative pharmacology. *Archive for History of Exact Sciences* **66,** 427–438. https://doi.org/10.1007/s00407-012-0098-5 (2012).

55. Gibbons, B. H. & Edsall, J. T. Rate of hydration of carbon dioxide and dehydration of carbonic acid at 25 degrees. *Journal of Biological Chemistry* **238,** 3502–3507 (1963).

56. Gonze, D., Coyte, K. Z., Lahti, L. & Faust, K. Microbial communities as dynamical systems. *Current Opinion in Microbiology. Microbiota* **44,** 41–49 (2018).

57. Gottschalk, G. *Bacterial Metabolism* 2nd edition (Springer-Verlag, New York, New York, USA, 1986).

58. Großkopf, R., Janssen, P. H. & Liesack, W. Diversity and structure of the methanogenic community in anoxic rice paddy soil microcosms as examined by cultivation and direct

16S rRNA gene sequence retrieval. *Applied and Environmental Microbiology* **64,** 960–969 (1998).

59. Großkopf, T. & Soyer, O. S. Microbial diversity arising from thermodynamic constraints. *The ISME journal* **10,** 2725–2733 (2016).

60. Guan, N. *et al.* Microbial response to environmental stresses: from fundamental mechanisms to practical applications. *Applied Microbiology and Biotechnology* **101,** 3991–4008 (2017).

61. Harned, H. S. & Davis, R. The ionization constant of carbonic acid in water and the solubility of carbon dioxide in water and aqueous salt solutions from 0 to 50°. *Journal of the American Chemical Society* **65,** 2030–2037 (1943).

62. Harned, H. S. & Scholes, S. R. The ionization constant of HCO_3^- from 0 to 50°. *Journal of the American Chemical Society* **63,** 1706–1709 (1941).

63. Harold, F. M. *The vital force: Study of bioenergetics* (W.H.Freeman & Co Ltd, New York, NY, 1986).

64. Harris, D. A. *Bioenergetics at a glance* 1st edition (Wiley-Blackwell, Hoboken, 1995).

65. Herzog, E. *et al.* Hydrogen-bonded networks along and bifurcation of the E-pathway in quinol:fumarate reductase. *Biophysical Journal* **103,** 1305–1314 (2012).

66. Hilpert, W. & Dimroth, P. On the mechanism of sodium ion translocation by methylmalonyl-CoA decarboxylase from *Veillonella alcalescens*. *European Journal of Biochemistry* **195,** 79–86 (1991).

67. Hoh, C. Y. & Cord-Ruwisch, R. A practical kinetic model that considers endproduct inhibition in anaerobic digestion processes by including the equilibrium constant. *Biotechnology and Bioengineering* **51,** 597–604 (1996).

68. Howell, J. A. & Atkinson, B. Influence of oxygen and substrate concentrations on the ideal film thickness and the maximum overall substrate uptake rate in microbial film fermenters. *Biotechnology and Bioengineering* **18,** 15–35. `https://onlinelibrary.wiley.com/doi/abs/10.1002/bit.260180103` (1976).

69. Hsu, S. B. Limiting behavior for competing species. *SIAM Journal on Applied Mathematics* **34,** 760–763 (1978).

70. Imkamp, F., Biegel, E., Jayamani, E., Buckel, W. & Müller, V. Dissection of the caffeate respiratory chain in the acetogen *Acetobacterium woodii*: Identification of an Rnf-type NADH dehydrogenase as a potential coupling site. *Journal of Bacteriology* **189,** 8145–8153 (2007).

71. Ingvorsen, K., Zehnder, A. J. & Jørgensen, B. B. Kinetics of sulfate and acetate uptake by *Desulfobacter postgatei*. *Applied and Environmental Microbiology* **47,** 403–408 (1984).

72. Izallalen, M. *et al. Geobacter sulfurreducens* strain engineered for increased rates of respiration. *Metabolic Engineering* **10,** 267–275 (2008).

73. Janssen, P. H. Growth of enterobacteria on malonate under strictly anaerobic conditions. *Systematic and Applied Microbiology* **14,** 94–97 (1991).

74. Jeong, J. *et al.* Energy conservation model based on genomic and experimental analyses of a carbon monoxide-utilizing, butyrate-forming acetogen, *Eubacterium limosum* KIST612. *Applied and Environmental Microbiology* **81,** 4782–4790. `https://www.ncbi.nlm.nih.gov/pmc/articles/PMC4551209/` (2015).

75. Jetten, M. S., Fluit, T. J., Stams, A. J. & Zehnder, A. J. A fluoride-insensitive inorganic pyrophosphatase isolated from *Methanothrix soehngenii*. *Archives of Microbiology* **157,** 284–289 (1992).

76. Jetten, M. S., Stams, A. J. & Zehnder, A. J. Isolation and characterization of acetyl-coenzyme A synthetase from *Methanothrix soehngenii*. *Journal of Bacteriology* **171,** 5430–5435 (1989).

77. Jetten, M. S. M., Stams, A. J. M. & Zehnder, A. J. B. Acetate threshold values and acetate activating enzymes in methanogenic bacteria. *FEMS Microbiology Letters* **73,** 339–344 (1990).

78. Jiang, W., Hermolin, J. & Fillingame, R. H. The preferred stoichiometry of c subunits in the rotary motor sector of *Escherichia coli* ATP synthase is 10. *Proceedings of the*

National Academy of Sciences **98,** 4966–4971. https://www.pnas.org/doi/10.1073/pnas.081424898 (2001).

79. Jin, Q. & Bethke, C. M. The thermodynamics and kinetics of microbial metabolism. *American Journal of Science* **307,** 643–677. https://www.ajsonline.org/content/307/4/643 (2007).

80. Johnson, K. A. A century of enzyme kinetic analysis, 1913 to 2013. *FEBS letters* **587,** 2753–2766 (2013).

81. Johnson, K. A. & Goody, R. S. The original Michaelis constant: Translation of the 1913 Michaelis–Menten paper. *Biochemistry* **50,** 8264–8269. https://doi.org/10.1021/bi201284u (2011).

82. Junicke, H., Feldman, H., van Loosdrecht, M. C. M. & Kleerebezem, R. Impact of the hydrogen partial pressure on lactate degradation in a coculture of *Desulfovibrio* sp. G11 and *Methanobrevibacter arboriphilus* DH1. *Applied Microbiology and Biotechnology* **99,** 3599–3608 (2015).

83. Kanehisa, M., Sato, Y., Kawashima, M., Furumichi, M. & Tanabe, M. KEGG as a reference resource for gene and protein annotation. *Nucleic Acids Research* **44,** D457–D462. https://doi.org/10.1093/nar/gkv1070 (2016).

84. Kang, H.-W., KhudaBukhsh, W. R., Koeppl, H. & Rempała, G. A. Quasi-steady-state approximations derived from the stochastic model of enzyme kinetics. *Bulletin of Mathematical Biology* **81,** 1303–1336. https://doi.org/10.1007/s11538-019-00574-4 (2019).

85. Kaster, A.-K. *Energiestoffwechsel von Cytochrom-freien methanogenen Archaea bei Wachstum auf* H_2 *und* CO_2 PhD thesis (Philipps-Universität Marburg, Germany, 2011).

86. Kaster, A.-K., Moll, J., Parey, K. & Thauer, R. K. Coupling of ferredoxin and heterodisulfide reduction via electron bifurcation in hydrogenotrophic methanogenic archaea. *Proceedings of the National Academy of Sciences* **108,** 2981–2986. https://www.pnas.org/doi/full/10.1073/pnas.1016761108 (2011).

87. Kelly, W. J. *et al.* The complete genome sequence of *Eubacterium limosum* SA11, a metabolically versatile rumen acetogen. *Standards in Genomic Sciences* **11,** 26 (2016).

88. Kim, C. C.-h. *Identification of rumen methanogens, characterization of substrate requirements and measurement of hydrogen thresholds* PhD thesis (Massey University, 2012).

89. Kleerebezem, R. & van Loosdrecht, M. C. M. A generalized method for thermodynamic state analysis of environmental systems. *Critical Reviews in Environmental Science and Technology* **40,** 1–54. https://doi.org/10.1080/10643380802000974 (2010).

90. Kotsyurbenko, O. R., Glagolev, M. V., Nozhevnikova, A. N. & Conrad, R. Competition between homoacetogenic bacteria and methanogenic archaea for hydrogen at low temperature. *FEMS Microbiology Ecology* **38,** 153–159 (2001).

91. Kovárová-Kovar, K. & Egli, T. Growth kinetics of suspended microbial cells: from single-substrate-controlled growth to mixed-substrate kinetics. *Microbiology and Molecular Biology Reviews: MMBR* **62,** 646–666 (1998).

92. Kral, T. A., Brink, K. M., Miller, S. L. & McKay, C. P. Hydrogen consumption by methanogens on the early Earth. *Origins of Life and Evolution of the Biosphere: The Journal of the International Society for the Study of the Origin of Life* **28,** 311–319 (1998).

93. Kristjansson, J. K., Schönheit, P. & Thauer, R. K. Different K_S values for hydrogen of methanogenic bacteria and sulfate reducing bacteria: An explanation for the apparent inhibition of methanogenesis by sulfate. *Archives of Microbiology* **131,** 278–282 (1982).

94. Krumholz, L. R., Harris, S. H., Tay, S. T. & Suflita, J. M. Characterization of two subsurface H_2-utilizing bacteria, *Desulfomicrobium hypogeium* sp. nov. and *Acetobacterium psammolithicum* sp. nov., and their ecological roles. *Applied and Environmental Microbiology* **65,** 2300–2306 (1999).

95. Kuivila, K. M., Murray, J. W., Devol, A. H. & Novelli, P. C. Methane production, sulfate reduction and competition for substrates in the sediments of Lake Washington. *Geochimica et Cosmochimica Acta* **53,** 409–416 (1989).

96. Laanbroek, H. J., Geerligs, H. J., Sijtsma, L. & Veldkamp, H. Competition for sulfate and ethanol among *Desulfobacter*, *Desulfobulbus*, and *Desulfovibrio* species isolated from intertidal sediments. *Applied and Environmental Microbiology* **47,** 329–334 (1984).

97. Laidler, K. J. & Bunting, P. S. *The Chemical Kinetics of Enzyme Action* 2nd ed. `http://ezproxy.massey.ac.nz/login?url=http://search.ebscohost.com/login.aspx?direct=true&db=cat00245a&AN=massey.b1020564&site=eds-live&scope=site&authtype=ip,sso&custid=s3027306` (Clarendon Press, 1973).

98. Larowe, D. E. & Helgeson, H. C. Quantifying the energetics of metabolic reactions in diverse biogeochemical systems: electron flow and ATP synthesis. *Geobiology* **5,** 153–168. `https://onlinelibrary.wiley.com/doi/abs/10.1111/j.1472-4669.2007.00099.x` (2007).

99. Le Van, T. D. *et al.* Assessment of reductive acetogenesis with indigenous ruminal bacterium populations and *Acetitomaculum ruminis*. *Applied and Environmental Microbiology* **64,** 3429–3436 (1998).

100. Liu, C. L. & Peck, H. D. Comparative bioenergetics of sulfate reduction in *Desulfovibrio* and *Desulfotomaculum* spp. *Journal of Bacteriology* **145,** 966–973 (1981).

101. Liu, Y. A simple thermodynamic approach for derivation of a general Monod equation for microbial growth. *Biochemical Engineering Journal* **31,** 102–105. `https://www.sciencedirect.com/science/article/pii/S1369703X06001367` (2006).

102. Liu, Y. Overview of some theoretical approaches for derivation of the Monod equation. *Applied Microbiology and Biotechnology* **73,** 1241–1250. `https://doi.org/10.1007/s00253-006-0717-7` (2007).

103. Liu, Y., Lin, Y.-M. & Yang, S.-F. A thermodynamic interpretation of the Monod equation. *Current Microbiology* **46,** 233–234 (2003).

104. Louca, S., Mazel, F., Doebeli, M. & Parfrey, L. W. A census-based estimate of Earth's bacterial and archaeal diversity. *PLOS Biology* **17,** e3000106. `https://journals.plos.org/plosbiology/article?id=10.1371/journal.pbio.3000106` (2019).

105. Lovley, D. R., Greening, R. C. & Ferry, J. G. Rapidly growing rumen methanogenic organism that synthesizes coenzyme M and has a high affinity for formate. *Applied and Environmental Microbiology* **48,** 81–87 (1984).

106. Lovley, D. R. Minimum threshold for hydrogen metabolism in methanogenic bacteria. *Applied and Environmental Microbiology* **49,** 1530–1531 (1985).

107. Lovley, D. R. & Klug, M. J. Sulfate reducers can outcompete methanogens at freshwater sulfate concentrations. *Applied and Environmental Microbiology* **45,** 187–192 (1983).

108. Lynch, T. A., Wang, Y., van Brunt, B., Pacheco, D. & Janssen, P. H. Modelling thermodynamic feedback on the metabolism of hydrogenotrophic methanogens. *Journal of Theoretical Biology* **477,** 14–23. `https://www.sciencedirect.com/science/article/pii/S0022519319302164` (2019).

109. Lynd, L. H. & Zeikus, J. G. Metabolism of H_2-CO_2, methanol, and glucose by *Butyribacterium methylotrophicum*. *Journal of Bacteriology* **153,** 1415–1423 (1983).

110. Majer, V., Sedlbauer, J., Hnedkovsky, L. & Wood, R. H. Thermodynamics of aqueous acetic and propionic acids and their anions over a wide range of temperatures and pressures. *Physical Chemistry Chemical Physics* **2,** 2907–2917. `https://pubs.rsc.org/en/content/articlelanding/2000/cp/b000593m` (2000).

111. Mankad, T. & Bungay, H. R. Model for microbial growth with more than one limiting nutrient. *Journal of Biotechnology* **7,** 161–166. `https://www.sciencedirect.com/science/article/pii/0168165688900624` (1988).

112. Matthies, D. *et al.* High-resolution structure and mechanism of an F/V-hybrid rotor ring in a Na^+-coupled ATP synthase. *Nature Communications* **5,** 5286 (2014).

113. Mayer, F. & Müller, V. Adaptations of anaerobic archaea to life under extreme energy limitation. *FEMS microbiology reviews* **38,** 449–472 (2014).

114. Mazumder, T. K., Nishio, N., Fukuzaki, S. & Nagai, S. Effect of sulfur-containing compounds on growth of *Methanosarcina barkeri* in defined medium. *Applied and Environmental Microbiology* **52,** 617–622 (1986).

115. McInerney, M. J. & Wofford, N. Q. Enzymes involved in crotonate metabolism in *Syntrophomonas wolfei*. *Archives of Microbiology* **158,** 344–349 (1992).

116. Megee, R. D., Drake, J. F., Fredrickson, A. G. & Tsuchiya, H. M. Studies in intermicrobial symbiosis. *Saccharomyces cerevisiae* and *Lactobacillus casei*. *Canadian Journal of Microbiology* **18,** 1733–1742 (1972).

117. Meier, T., Faraldo-Gómez, J. D. & Börsch, M. *ATP synthase, a paradigmatic molecular machine* in *Molecular Machines in Biology* (ed Frank, J.) pp. 208-238 (Cambridge University Press, 2011).

118. Meier, T., Ferguson, S. A., Cook, G. M., Dimroth, P. & Vonck, J. Structural investigations of the membrane-embedded rotor ring of the F-ATPase from Clostridium paradoxum. *Journal of Bacteriology* **188.** Publisher: American Society for Microbiology, 7759–7764. `https://journals.asm.org/doi/10.1128/JB.00934-06` (2006).

119. Merchuk, J. C. & Asenjo, J. A. The Monod equation and mass transfer. *Biotechnology and Bioengineering* **45,** 91–94. `https://onlinelibrary.wiley.com/doi/abs/10.1002/bit.260450113` (1995).

120. Michaelis, L. & Menten, M. L. Die Kinetik der Invertinwirkung. *Biochem. Z* **49,** 333–369 (1913).

121. Miller, J. H., Rajapakshe, K. I., Infante, H. L. & Claycomb, J. R. Electric field driven torque in ATP synthase. *PLOS ONE* **8,** e74978 (2013).

122. Min, H. & Zinder, S. H. Kinetics of acetate utilization by two thermophilic acetotrophic methanogens: *Methanosarcina* sp. strain CALS-1 and *Methanothrix* sp. strain CALS-1. *Applied and Environmental Microbiology* **55,** 488–491. `https://www.ncbi.nlm.nih.gov/pmc/articles/PMC184136/` (1989).

123. Möller, D., Schauder, R., Fuchs, G. & Thauer, R. K. Acetate oxidation to CO_2 via a citric acid cycle involving an ATP-citrate lyase: a mechanism for the synthesis of ATP via substrate level phosphorylation in *Desulfobacter postgatei* growing on acetate and sulfate. *Archives of Microbiology* **148,** 202–207. `https://doi.org/10.1007/BF00414812` (1987).

124. Monod, J. *Recherches sur la Croissance des Cultures Bactériennes* (Hermann et cie, 1942).

125. Monod, J. The growth of bacterial cultures. *Annual Review of Microbiology* **3,** 371–394. https://doi.org/10.1146/annurev.mi.03.100149.002103 (1949).

126. Morris, J. G. *A Biologist's Physical Chemistry* (Edward Arnold, 1974).

127. Moser, H. *The Dynamics of Bacterial Populations Maintained in the Chemostat* (Carnegie Institution of Washington, 1958).

128. Muñoz-Tamayo, R. *et al.* Hydrogenotrophic methanogens of the mammalian gut: Functionally similar, thermodynamically different—A modelling approach. *PLOS ONE* **14,** e0226243. https://journals.plos.org/plosone/article?id=10.1371/journal.pone.0226243 (2019).

129. Murray, J. D. *Mathematical biology: I. An introduction* (Springer Science & Business Media, 2002).

130. Nagarajan, K., Ni, C. & Lu, T. Agent-based modeling of microbial communities. *ACS Synthetic Biology* **11,** 3564–3574. (2025) (2022).

131. Nanninga, H. J., Drent, W. J. & Gottschal, J. C. Fermentation of glutamate by Selenomonas acidaminophila sp. nov. *Archives of Microbiology* **147,** 152–157. https://doi.org/10.1007/BF00415276 (1987).

132. Nanninga, H. J., Drent, W. J. & Gottschal, J. C. Major differences between glutamate-fermenting species isolated from chemostat enrichments at different dilution rates. *FEMS Microbiology Ecology* **2,** 321–329. https://doi.org/10.1111/j.1574-6968.1986.tb01744.x (1986).

133. Nethe-Jaenchen, R. & Thauer, R. K. Growth yields and saturation constant of *Desulfovibrio vulgaris* in chemostat culture. *Archives of Microbiology* **137,** 236–240. https://doi.org/10.1007/BF00414550 (1984).

134. Nicholls, D. G. Mitochondrial membrane potential and aging. *Aging Cell* **3,** 35–40 (2004).

135. Nicholls, D. G. & Ferguson, S. J. *Bioenergetics 2* (Academic Press, London ; San Diego, 1992).

136. Orellana, R. *Physiological models of Geobacter sulfurreducens and Desulfobacter postgatei to understand uranium remediation in subsurface systems* PhD thesis (University of Massachusetts, Amherst, Massachusetts, USA, 2014). `https://scholarworks.umass.edu/dissertations_2/278/`.

137. Oude Elferink, S. J., Maas, R. N., Harmsen, H. J. & Stams, A. J. *Desulforhabdus amnigenus* gen. nov. sp. nov., a sulfate reducer isolated from anaerobic granular sludge. *Archives of Microbiology* **164,** 119–124 (1995).

138. Oude Elferink, S. J. W. H. O., Luppens, S. B. I., Marcelis, C. L. M. & Stams, A. J. M. Kinetics of acetate oxidation by two sulfate reducers isolated from anaerobic granular sludge. *Applied and Environmental Microbiology* **64,** 2301–2303 (1998).

139. Pavlostathis, S. G., Miller, T. L. & Wolin, M. J. Cellulose fermentation by continuous cultures of *Ruminococcus albus* and *Methanobrevibacter smithii*. *Applied Microbiology and Biotechnology* **33,** 109–116 (1990).

140. Perry, J. J., Staley, J. T. & Lory, S. *Microbial Life* (Sinauer Associates Inc, Sunderland, Mass, 2002).

141. Peters, V., Janssen, P. & Conrad, R. Efficiency of hydrogen utilization during unitrophic and mixotrophic growth of *Acetobacterium woodii* on hydrogen and lactate in the chemostat. *FEMS Microbiology Ecology* **26,** 317–324 (1998).

142. Phelps, T. J., Conrad, R. & Zeikus, J. G. Sulfate-dependent interspecies H_2 transfer between *Methanosarcina barkeri* and *Desulfovibrio vulgaris* during coculture metabolism of acetate or methanol. *Applied and Environmental Microbiology* **50,** 589–594 (1985).

143. Pirt, S. J. *Principles of Microbe and Cell Cultivation* (Blackwell Scientific, Oxford, 1975).

144. Platen, H., Janssen, P. H. & Schink, B. Fermentative degradation of acetone by an enrichment culture in membrane-separated culture devices and in cell suspensions. *FEMS Microbiology Letters* **122,** 27–32. `https://doi.org/10.1111/j.1574-6968.1994.tb07138.x` (1994).

145. Poehlein, A. *et al.* An ancient pathway combining carbon dioxide fixation with the generation and utilization of a sodium ion gradient for ATP synthesis. *PLOS ONE* **7.** Publisher: Public Library of Science, e33439. https://journals.plos.org/plosone/article?id=10.1371/journal.pone.0033439 (2012).

146. Prosser, J. I. & Martiny, J. B. H. Conceptual challenges in microbial community ecology. *Philosophical Transactions of the Royal Society B: Biological Sciences* **375,** 20190241. https://royalsocietypublishing.org/doi/10.1098/rstb.2019.0241 (2020).

147. Robinson, J. A. & Tiedje, J. M. Competition between sulfate-reducing and methanogenic bacteria for H_2 under resting and growing conditions. *Archives of Microbiology* **137,** 26–32 (1984).

148. Ryder, D. N. & Sinclair, C. G. Model for the growth of aerobic microorganisms under oxygen limiting conditions. *Biotechnology and Bioengineering* **14,** 787–798 (1972).

149. Sander, R. Compilation of Henry's law constants (version 4.0) for water as solvent. *Atmospheric Chemistry and Physics* **15,** 4399–4981 (2015).

150. Schauer, M. & Heinrich, R. Analysis of the quasi-steady-state approximation for an enzymatic one-substrate reaction. *Journal of Theoretical Biology* **79,** 425–442. https://www.sciencedirect.com/science/article/pii/0022519379902352 (1979).

151. Scherer, P. & Sahm, H. Influence of sulphur-containing compounds on the growth of *Methanosarcina barkeri* in a defined medium. *European Journal of Applied Microbiology and Biotechnology* **12,** 28–35. https://doi.org/10.1007/BF00508115 (1981).

152. Schink, B. Energetics of syntrophic cooperation in methanogenic degradation. *Microbiology and Molecular Biology Reviews* **61,** 262–280 (1997).

153. Schink, B., Kremer, D. R. & Hansen, T. A. Pathway of propionate formation from ethanol in *Pelobacter propionicus*. *Archives of Microbiology* **147,** 321–327. https://doi.org/10.1007/BF00406127 (1987).

154. Schnell, S. & Maini, P. K. Enzyme kinetics at high enzyme concentration. *Bulletin of Mathematical Biology* **62,** 483–499 (2000).

155. Scholten, J. C. M. & Conrad, R. Energetics of syntrophic propionate oxidation in defined batch and chemostat cocultures. *Applied and Environmental Microbiology* **66,** 2934–2942. https://www.ncbi.nlm.nih.gov/pmc/articles/PMC92094/ (2000).

156. Schönheit, P., Kristjansson, J. K. & Thauer, R. K. Kinetic mechanism for the ability of sulfate reducers to out-compete methanogens for acetate. *Archives of Microbiology* **132,** 285–288 (1982).

157. Seeliger, S. *Energetik und Kinetik der Propionatgärung* PhD thesis (University of Konstanz, Germany, 1993).

158. Seeliger, S., Janssen, P. H. & Schink, B. Energetics and kinetics of lactate fermentation to acetate and propionate via methylmalonyl-CoA or acrylyl-CoA. *FEMS Microbiology Letters* **211,** 65–70. https://doi.org/10.1111/j.1574-6968.2002.tb11204.x (2002).

159. Segel, L. A. On the validity of the steady state assumption of enzyme kinetics. *Bulletin of Mathematical Biology* **50,** 579–593. https://www.sciencedirect.com/science/article/pii/S0092824088800570 (1988).

160. Segel, L. A. & Slemrod, M. The quasi-steady-state assumption: A case study in perturbation. *SIAM Review* **31,** 446–477. https://www.jstor.org/stable/2031405 (1989).

161. Seitz, H.-J., Schink, B. & Conrad, R. Thermodynamics of hydrogen metabolism in methanogenic cocultures degrading ethanol or lactate. *FEMS Microbiology Letters* **55,** 119–124 (1988).

162. Sharak Genthner, B. R. & Bryant, M. P. Additional characteristics of one-carbon-compound utilization by *Eubacterium limosum* and *Acetobacterium woodii*. *Applied and Environmental Microbiology* **53,** 471–476. https://www.ncbi.nlm.nih.gov/pmc/articles/PMC203690/ (1987).

163. Shock, E. L. Organic acids in hydrothermal solutions: standard molal thermodynamic properties of carboxylic acids and estimates of dissociation constants at high temperatures and pressures. *American Journal of Science* **295,** 496–580 (1995).

164. Shock, E. L. & Helgeson, H. C. Calculation of the thermodynamic and transport properties of aqueous species at high pressures and temperatures: Standard partial molal properties of organic species. *Geochimica et Cosmochimica Acta* **54,** 915–945 (1990).

165. Stams, A. J., Van Dijk, J. B., Dijkema, C. & Plugge, C. M. Growth of syntrophic propionate-oxidizing bacteria with fumarate in the absence of methanogenic bacteria. *Applied and Environmental Microbiology* **59,** 1114–1119 (1993).

166. Stenstrom, M. K. & Poduska, R. A. The effect of dissolved oxygen concentration on nitrification. *Water Research* **14,** 643–649 (1980).

167. Stewart, H. A. *et al.* Dual substrate limitation modeling and implications for mainstream deammonification. *Water Research* **116,** 95–105 (2017).

168. Stouthamer, A. H. *The search for correlation between theoretical and experimental growth yields* Pages: 1-48 Publication Title: Microbial Biochemistry. `https://eurekamag.com/research/029/418/029418933.php` (1979).

169. Szewzyk, R. *Untersuchungen zur Konkurrenz zwischen sulfatreduzierenden und garenden Bakterien um gemeinsame Substrate* PhD thesis (University of Konstanz, Germany, 1987).

170. Szewzyk, R. & Pfennig, N. Competition for ethanol between sulfate-reducing and fermenting bacteria. *Archives of Microbiology* **153,** 470–477. `https://doi.org/10.1007/BF00248429` (1990).

171. Tan, Y., Wang, Z.-X., Schneider, R. & Marshall, K. C. Modelling microbial growth: A statistical thermodynamic approach. *Journal of Biotechnology* **32,** 97–106. `https://www.sciencedirect.com/science/article/pii/0168165694901732` (1994).

172. Thauer, R. K., Jungermann, K. & Decker, K. Energy conservation in chemotrophic anaerobic bacteria. *Bacteriological Reviews* **41,** 100–180 (1977).

173. Thauer, R. K., Kaster, A.-K., Seedorf, H., Buckel, W. & Hedderich, R. Methanogenic archaea: ecologically relevant differences in energy conservation. *Nature Reviews Microbiology* **6,** 579–591. `https://www.nature.com/articles/nrmicro1931` (2008).

174. van Bodegom, P. Microbial maintenance: A critical review on its quantification. *Microbial Ecology* **53,** 513–523. `https://www.ncbi.nlm.nih.gov/pmc/articles/PMC1915598/` (2007).

175. Van den Berg, E. M., Boleij, M., Kuenen, J. G., Kleerebezem, R. & van Loosdrecht, M. C. M. DNRA and denitrification coexist over a broad range of acetate/$N-NO_3^-$ ratios, in a chemostat enrichment culture. *Frontiers in Microbiology* **7.** Publisher: Frontiers (2016).

176. van Lingen, H. J. *et al.* Thermodynamic driving force of hydrogen on rumen microbial metabolism: A theoretical investigation. *PLOS ONE* **11,** e0161362. `https://journals.plos.org/plosone/article?id=10.1371/journal.pone.0161362` (2016).

177. Wallrabenstein, C. & Schink, B. Evidence of reversed electron transport in syntrophic butyrate or benzoate oxidation by Syntrophomonas wolfei and Syntrophus buswellii. *Archives of Microbiology* **162,** 136–142. `https://doi.org/10.1007/BF00264387` (1994).

178. Wang, Y. *Microbial co-existence and stable equilibria in a mechanistic model of enteric methane production* PhD thesis (Massey University, 2016). `http://hdl.handle.net/10179/12617`.

179. Wang, Y., Janssen, P. H., Lynch, T. A., Brunt, B. v. & Pacheco, D. A mechanistic model of hydrogen–methanogen dynamics in the rumen. *Journal of Theoretical Biology* **393,** 75–81. `https://www.sciencedirect.com/science/article/pii/S0022519316000333` (2016).

180. Warikoo, V., McInerney, M. J., Robinson, J. A. & Suflita, J. M. Interspecies acetate transfer influences the extent of anaerobic benzoate degradation by syntrophic consortia. *Applied and Environmental Microbiology* **62,** 26–32 (1996).

181. Welte, C., Kröninger, L. & Deppenmeier, U. Experimental evidence of an acetate transporter protein and characterization of acetate activation in aceticlastic methanogenesis of *Methanosarcina mazei*. *FEMS Microbiology Letters* **359,** 147–153 (2014).

182. Welte, C. & Deppenmeier, U. Bioenergetics and anaerobic respiratory chains of aceticlastic methanogens. *Biochimica Et Biophysica Acta* **1837,** 1130–1147 (2014).

183. Westermann, P., Ahring, B. K. & Mah, R. A. Threshold acetate concentrations for acetate catabolism by aceticlastic methanogenic bacteria. *Applied and Environmental Microbiology* **55,** 514–515 (1989).

184. Wilhelm, E., Battino, R. & Wilcock, R. J. Low-pressure solubility of gases in liquid water. *Chemical Reviews* **77.** Publisher: American Chemical Society, 219–262. `https://doi.org/10.1021/cr60306a003` (1977).

185. Wilson, A. H. *Thermodynamics and Statistical Mechanics* (Cambridge University Press, 1957).

186. Woldringh, C. L. & Nanninga, N. *Structure of nucleoid and cytoplasm in the intact cell* in *Molecular Cytology of Escherichia coli.* (ed Nanninga, N.) pp. 161-197 (Academic Press, 1985).